



*kinetic and mechanistic studies of
fading of fluorescent dyes and
application in vital fields*

Eman Amer Husein Alwattar

**A thesis submitted for Degree of Doctor of Philosophy
School of Chemistry
Cardiff University.**

December 2020

Summary

This thesis is divided into six Chapters.

Chapter 1 introduces general information about forensic chemistry, dyes and pigments, light, and its effect in chemistry.

The second chapter describes the development of a LED device, with support from Dr. Joe Beames, that allows us to generate reproducible kinetic data on photofading reactions by irradiating a sample with high intensity white light.

The third chapter shows that thiazole orange (TO) shows increased fading with increased intensity of light. Additionally, we investigated the effect of oxygen within the solution. Many other factors may also play a role in the fading process, for example, temperature, type of buffer, buffer concentration, pH, and the presence of additives. We examine each of these in turn and show that this provides new kinetic insights into the mechanism of fading of thiazole orange. Mass spectroscopy suggests that the product may be formed following reaction of the photoexcited species with a molecule of oxygen. The fading of dyes such as thiazole orange (which is a known DNA binder) may have implications for typical studies of DNA binders.

The fourth chapter presents analyses of the kinetics of the fading process of 3,3'-diethyloxadicarbocyanine iodide (DODC) when exposed to light, determining that it is irradiation itself that drives the colour change. Another factor is the presence of O₂ with limiting oxygen concentrations limiting the observed reaction rate constant. Many other factors may also play a role in the fading process, for example, temperature, type of buffer, buffer concentration, pH and the presence of additives. We examined each of these in turn. Mass spectroscopy suggests that the product may be formed following reaction of the photoexcited species with a molecule of oxygen.

Finally, the fifth Chapter describes the effects of biomacromolecules and serum on fading of TO and DODC. DNA is found to have little effect of fading of TO but to retard fading of DODC. Serum is found to strongly retard fading of TO and DODC. Similarly, added ethanol and DMSO also strongly retard the kinetics of fading.

Overall conclusions, future outlooks, remarks and suggestions can be found in Chapter 6.

I contributed to a publication during my PhD, but this work is not included in this thesis: “Targeted cell imaging properties of a deep red luminescent iridium(iii) complex conjugated with a c-Myc signal peptide” – *Chem. Sci.*, **2020**, 11, 1599-1606; DOI: 10.1039/c9sc05568a.

Acknowledgements

I would like to thank my supervisor, Dr Niek Buurma, for his invaluable teaching, guidance and support. I feel I have brother and friend, not just supervisor and I am glad I had a chance to work with him.

I would also like to thank Dr Joseph Beames for his bright and brilliant support.

A huge thanks to the university members who helped me during my work namely Dr. Mahmoud Akhtar, Prof. Simon Pope, George Summers and may Allah mercy soul of Moira for her support and guide.

Special thanks also go to the present and past students in POC especially Thomas Stonelake, Nathan Watson, Adam Khan and lovely sisters Deemah Alenazy, Haleema Otaif, Mashael Alharbi.

Huge thanks also to all members in IT, PGR and all parts in Cardiff university who support, help us without any excuse.

Thanks to the Iraqi Government / Ministry of Higher Education for funding my scholarship.

More importantly, a very special thanks to my parents may Allah save their life, supportive brother Ahmed, lovely sister Marwa and my lonely boy, AL Mustafa for their love and endless support throughout my life. Thank you all for giving me the strength to chase my dreams.

Last but not least, thanks to everyone who taught and helped me during my life, even by one word.

List of abbreviations and symbols

K obs	Observed rate constant
pH	$-\log [H^+]$
ϵ	extinction coefficient (or Molar absorptivity)
A	Absorbance
λ	Wavelength
t	Time
T	Temperature
M	Molar
mM	Milimolar
μ M	Micromolar
L	Liter
mL	Milliliter
$^{\circ}$ C	Degree Celsius
NMR	Nuclear Magnetic Resonance
TA	transient absorption
S0	ground state
S1	singlet excited states
S2	singlet excited states (no unpaired electrons, one electron has been excited but still has the same spin)
T1	triplet excited state (two unpaired electrons, one electron flipped its spin).
PMT	The photomultiplier tubes
I.C.C	image-converter camera
D ₂ O	Deuterated water
DMSO	Dimethyl sulfoxide
g	Grams
I	Ionic strength
LED	light-emitting diode
r.t	Room temperature
nm	Nanometre
Vis	Visible
DNA	Deoxyribonucleic acid
RNA	Ribonucleic acid
BSA	Bovine Serum Albumin
HSA	Human Serum Albumin
CSA	Calf Serum Albumin
Thiazole orange (TO)	

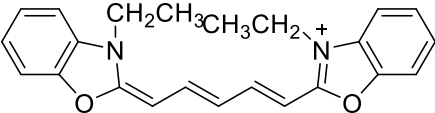
<p>3,3'-Diethyloxadicarbocyanine iodide (DODC)</p>	<p style="text-align: center;">I^-</p> 

Table of Contents	Page Number
Summary	I
Acknowledgements	III
List of abbreviations and symbols	IV
Chapter 1	
Introduction	
General introduction.	2
1.1 Forensic chemistry	2
1.2 Techniques of Evidence Collected at Scenes	5
Luminol to identify blood.	5
Lateral flow test for human blood.	6
Kastle-Meyer and Hemastix tests for blood.	7
Crime scene analysis using alternate light sources.	8
Chemical visualisation of latent print evidence.	10
Detection by fluorescence	10
Semen detection	11
Saliva detection	12
1.3 Organic dyes	12
1.4 Fluorescence and phosphorescence	15
1.5 Dye aggregation	17
1.6 DNA and DNA-binding dyes	19
1.6.1 The structure of DNA	19
1.6.2 DNA binders	22
1.6.2.1 Electrostatic interaction	23
1.6.2.2 Intercalation and intercalators	23
1.6.2.3 Major and minor groove binding	24
1.7 Interaction of cyanine dyes with DNA	24
1.8 Thiazole orange	25
1.9 DODC	27
1.10 Fading of dyes.	29
1.10.1 Overview	29
1.10.2 Photochemical reactions involving singlet or triplet oxygen or ozone.	30
1.11 Kinetics and mechanisms in aqueous solutions	36
1.11.1 (Pseudo) First-order reactions	36
1.11.2 Acid and base catalysis.	38
1.12 Aims	41
1.13 References	42

Chapter Two	
Development of a LED device for kinetic studies of photochemical reactions	
Summary	61
2.1 Introduction	62
2.1.1 Flash-photolysis	62
2.1.2 Brief Aims Statement	65
2.2. Results and discussion	66
2.2.1 Daylight induced fading of common organic dyes.	66
2.2.2 Kinetics experiments by using a battery driven irradiation device (First LED Device)	67
2.2.3 Kinetics experiments by using a commercial tuneable power supply with 2nd version LED irradiation device.	70
2.2.4 Kinetics experiments by using lenses in 3rd version LED device.	77
- Limitation and obstacles with the LED device.	87
2.2.5 Kinetics experiments performed using the fourth (4 th) revision of the LED based device	87
- The last version of LED (4th)-Before setting	88
- The last version of LED (4th)-After setting	91
2.3 conclusion	94
2.4 experimental conditions	95
2.4.1 Buffer preparation	95
2.4.2 Filters for solutions	95
2.4.3 Equipment.	95
2.4.4 Kinetic measurement using UV-Visible spectroscopy.	95
2.4.5 Incubator	96
2.4.6 IKA Big Squid (Ocean) Magnetic Stirrer.	96
2.4.7 Compounds.	96
2.4.8 Software	97
2.5 References	98
Chapter Three	
Kinetic study of fading of thiazole orange	
Summary	102
3.1 Introduction	103
3.1.1 Thiazole orange	103
3.1.2 Fading of thiazole orange by Oxygen and light	104

3.1.3 Aim and purpose	105
3.2 results and discussion	106
3.2.1 Kinetic studies of fading of TO.	106
a) Effect of light	106
b) Effect of pH	108
c) Effect of buffer concentration.	110
d) Effect of ionic strength.	111
e) Different temperature	112
f) Effect of water source	113
g) Kinetic isotope effect (KIE)	113
h) Effect of the nature of the buffer	114
i) Effect of oxygen	115
j) Effects of buffer additives	116
k) Effect of light intensity.	119
3.2.2 product analysis	122
3.2.3 Proposed mechanism	126
3.3 conclusion	127
3.4 Experimental	128
3.4.1 Buffer preparation	128
3.4.2 Preparation of TO solutions for kinetic experiments	128
3.4.3 UV-Visible spectroscopy	128
3.4.4 Reaction temperature control	129
3.4.5 Magnetic Stirrer	129
3.4.6 Compounds	129
3.4.7 Power supply	129
3.4.8 Nuclear Magnetic Resonance (NMR)	129
3.4.9 Mass spectrometry.	129
3.4.10 Software	130
3.5 References	131
Chapter Four	
Kinetic studies of photochemical fading of 3,3'-diethyloxadicyanine iodide (DODC)	
Summary	134
4.1 Introduction of DODC.	135
4.1.1 Spectroscopic properties of DODC.	135
4.1.2 The dynamics of photoisomerization of cyanine dyes	136
4.1.3 mechanisms of reaction of DODC with $^1\text{O}_2$	137
4.1.4 Aims and purpose.	140
4.2 Results and discussion	141

4.2.1 Kinetic studies	141
a) light	141
b) Effect of oxygen	143
c) effect of pH	144
d) effect of buffer concentration.	146
e) Ionic strength	147
f) Effect of temperature	148
g) Water source	149
h) Solvent kinetic isotope effect (SKIE)	150
i) Fading of DODC in tap water	152
j) Effects of buffer choice	154
k) Effect of buffer additives	155
i) Light intensity	156
4.2.2 product analysis	157
4.3 conclusion	161
4.4 Experimental	162
4.5 References	165
Chapter Five	
Interaction of cyanine dyes with biological samples and the effects on fading	
5.1 Introduction	171
5.1.2 serum, plasma and serum albumin	173
5.1.3 Cyanine dye interaction with serum albumins	174
5.1.4 Effects of solvents on behaviour of dyes	175
5.1.5 Aim and purpose	176
5.2 Result and discussion	177
5.2.1 Effects of biomacromolecules on fading of TO	177
5.2.1a Fading of TO in the presence of fish-sperm DNA.	177
5.2.1b Fading of TO in the presence of BSA	178
5.2.1c Fading of TO in human serum	180
5.2.1d Fading of TO in calf serum	181
5.2.1e Fading of TO in the presence of DMSO.	181
5.2.1f Fading of TO in the presence of ethanol.	182
5.2.2 Effects of biomacromolecules on fading of DODC.	183
5.2.2a Fading of DODC in the presence of fish-sperm DNA	183
5.2.2b Fading of DODC in the presence of BSA.	185
5.2.2c Fading of DODC in human serum.	187
5.2.2d Fading of DODC in calf serum.	188
5.2.2e Fading of DODC in the presence of DMSO.	189

5.2.3 Effect of TO and DODC on integrity of DNA samples	190
5.3 Experimental	191
5.4 References	197
Chapter six	
Overall conclusions, future work and outlook	
Summary	207
6. Introduction	208
6.1 DNA Forensics in Criminal Cases	208
6.2 Preliminary studies of forensic applications	208
6.2.1 Visual changes in solution when adding DNA	210
6.2.2 Visually detected colour changes when spraying or swabbing the dyes	210
6.3 Experimental	213
General conclusions	214
Suggestions for future work	215
Appendix	
Appendix-chapter 2	216
Appendix-chapter 3	218
Appendix-chapter 4	233
Appendix-chapter 5	244

Chapter One

Introduction

General introduction.

It is well known that DNA can be left behind on a crime scene surface by contact, providing potentially valuable trace evidence. However, few methods for detecting it *in situ* have been developed. Collecting DNA samples can be problematic because the DNA is often targeted rather than the likely biological samples, resulting in many samples being submitted to a forensic laboratory. For use in the laboratory, a variety of dyes that bind to DNA with great specificity are available, and we report on the use of these dyes to detect latent DNA on diverse substrates and within biological materials.

Of particular interest are fluorescent dyes, also known as fluorophores, which are chemicals that absorb light at one wavelength and release light at a different wavelength. Organic dyes (e.g., fluorescein), biological fluorophores (green fluorescent protein), and quantum dots are examples of these fluorophores.

Biologists and forensic chemists alike can now choose from a wide range of fluorescent dyes. The variety of options allows for greater flexibility as well as more possibilities in terms of what may be observed and analysed in research applications like fluorescence microscopy and flow cytometry but also potentially in crime scenes. As an example, to enhance latent prints created with superglue fuming, fluorescent colours are utilized.

Although useful in applications requiring high sensitivity, many fluorescent dyes are also known to be susceptible to photofading. Photofading itself may also be sensitive to the presence of biological macromolecules. It is therefore clear that an improved understanding of the mechanisms of photofading of dyes and the effect of biological macromolecules on this reaction is of interest.

1.1 Forensic chemistry

Forensic science is a combination of two distinct Latin words: *forénsis* and *scientia*. The first, *forénsis*, referred to a discussion or examination which was achieved in public. The second, *scientia*, is extracted from the Latin word for 'knowledge'. Forensic science uses scientific methods and transactions in crime solving. ^(1,2,3)

Forensic chemistry is a field of chemistry that analyses products that may be used in a crime, or to solve crime. Substances that can damage others may also be evaluated by a forensic chemist. For example, anthrax powder sent in the mail could be analysed. ⁽⁴⁾

Tv programs like CSI were watched by ordinary viewers who saw chemists

examine and recognize microscopic amounts of blood or tissue and a range of other substances. For example, if investigators in the crime scene suspect that drugs may be present, a chemist can analyse the presence of specific drugs through all materials taken from a crime scene. These experts could evaluate different samples, such as fibres, from clothing or carpet.⁽⁵⁾

The function of the Crime Scene Centre in any police station or interior ministry is to advise the requesting agency on pre-arrival techniques of securing the crime scene; to document the scene with photograph, video and diagrams; and to ensure that the physical evidence found on the scene is properly identified, handled, collected and packaged and perform specialty examinations to help reconstruct the events of the crime. The laboratory crime scene team will typically react to; homicides, tentative homicides, abductions, death investigations, officer involved shootings, clandestine grave body recovery, burglaries, sex crimes and assaults.^(6,7)

A wide range of approaches and techniques are available to experts in this area to help identify unidentified substances. These include high-performance liquid chromatography, gas spectrometry, analysis of atomic absorption, Fourier transform infrared spectroscopy, and chromatography.⁽⁸⁾ Due to the destructive nature of certain tools and the number of potentially unknown materials found on the scene, the range of different methods is relevant. Forensic scientists prefer first to use non-destructive methods to preserve evidence, and identify destructive methods that work best.⁽⁹⁾

In cases involving assault, and in cases involving paternity, forensic biochemists perform blood typing and enzyme tests on body fluids. Only small samples of blood, saliva, or semen can be isolated by electrophoresis and enzymatically analysed. In the case of rape, signs of semen found on clothes or on individuals are essential evidence; the composition of semen varies from person to person. Some individuals excrete enzymes such as acid phosphatase and other proteins that are seldom present outside seminal fluid, and their semen samples are distinguished by these chemical substances. The presence of semen can be confirmed by microscopic analyses for the existence of spermatozoa or by a positive prostate-specific antigen examination. ⁽¹⁰⁾

1984 saw the earliest use of DNA. This was developed by Sir Alec Jeffreys who discovered that variations in the genetic code could be used to identify individuals. Jeffreys used the first DNA profiles in a double killing case at Narborough, Leicestershire, a small English town. ⁽¹¹⁾ DNA profiling (also called DNA fingerprinting) is the method of determining the DNA properties of a person. DNA research intended to classify a species is called barcoding DNA,

rather than an entity. DNA profiling is a forensic method in criminal investigations, comparing the profiles of suspects with DNA evidence to determine the probability that they may be involved in the crime. ⁽¹²⁾

This is also used in parentage verification, in assessing eligibility for citizenship, and in genealogical and medical studies. DNA testing was also used in the study of populations of animals and plants in the zoological, botanical and agricultural fields. In cases of sexual abuse, tiny samples of DNA may be contained in the blood, semen, skin, or hair found on the victim, and the amount of DNA may be increased by using the polymerase chain reaction (PCR) to obtain amounts that are large enough for examination. Since DNA is as unique to an individual as fingerprints, the matching of an offender's DNA with a sample found on a victim is considered evidence of contact. ⁽¹³⁾

In criminal instances, DNA forensics is used to match an individual's DNA with that of body cells remaining in a crime scene, such as skin cells, hair, semen, and blood. In such instances, The DNA center uses STR-analysis commonly. Chemists take DNA samples from crime scene fields with STR-analysis. These are then compared to individual DNA profiles booked in a large database called CODIS to identify suspects. ^(14,15)

In other crime scenes, there may be a need to identify trace amounts of blood. The most famous test for blood is the luminol test. Iron present in the blood haemoglobin catalyses oxidation. This creates 3-aminophthalate in an excited state (Figure 1). Blue light is produced when energy is released when the electrons return to the ground state. ^(16,17) The response to luminol chemiluminescence is accountable for light stick glow. Criminologists use the response to detect blood traces at crime scenes. Luminol powder ($C_8H_7O_3N_3$) is combined with hydrogen peroxide (H_2O_2) and hydroxide (KOH, for example), in a spray bottle.

The luminol solution is sprayed anywhere blood can be found. The haemoglobin iron in the blood acts as a trigger for the chemiluminescence reaction that causes compound 4 and 5 from luminol to shine finally in compound 6 (figure 1). So that when the blood solution is sprayed, a blue glow is produced. To catalyze the reaction, only a small amount of iron is required. The blue glow lasts about 30 seconds before it disappears, which is enough time to take pictures of the fields so that they can be more carefully researched. ⁽¹⁸⁾

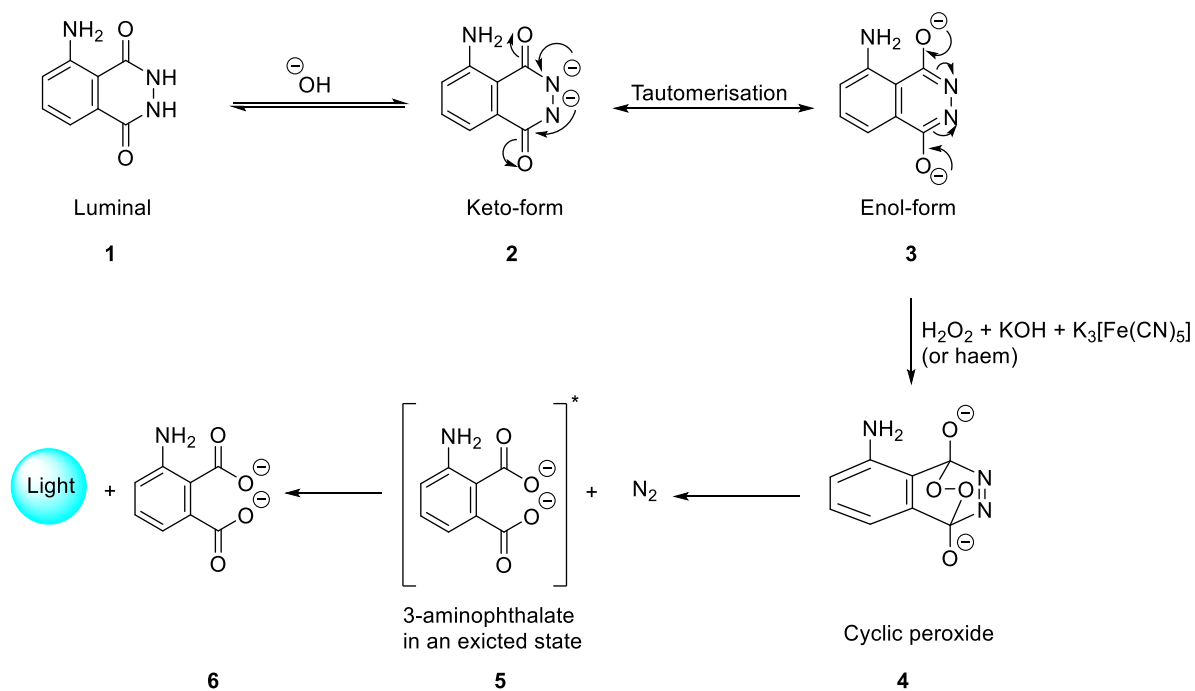


Figure 1 Oxidation of luminol

Unfortunately, luminol is not always useful because other chemicals, such as bleach, can generate the same fluorescence to produce fake results. Moreover, further problems with the use of luminol in crime scenes include 1) health concerns, although these are disputed if suitable protective equipment, i.e. goggles, respirators, gloves and protective clothes, are worn during spraying of luminol and the area investigated is aerated after luminol application, 2) visualisation using luminol needs to be carried out in the dark and photos have to be taken before the chemiluminescence of luminol is finished 3) visualisation using luminol may affect usability of DNA present in the crime scene for later analysis, 4) extensive equipment is required. Problems with the use of spectroscopic techniques include the requirement for extensive and expensive equipment on the crime scene. (19, 20)

1.2 Techniques of Evidence Collection at crime scenes

Luminol to identify blood

The search for blood in a crime scene is usually performed through close visual examination. There is a chance, however, that blood may be too small to see with the naked eye, or that the blood on the scene has been "washed" before the crime scene team arrived. (21) Only in a darkened room can the luminescence be seen, and the glow lasts for seconds to minutes. Luminescence is caused by the reaction of luminol with a peroxide, which is catalysed by blood components.

Scientists can use the luminol response to identify potentially undetectable blood through visual examination. In addition to being helpful in finding minute blood quantities, the luminescent pattern found on surfaces could show things like; the way out of the crime scene, drag marks in the blood, or an attempt to clean up blood. (22)

The sensitivity of luminol-based approaches has gotten a lot of press recently. (23, 24) With case studies showing that blood could be detected after months outside in Iraq and Afghanistan (25) and under numerous layers of paint, luminol has a high sensitivity. There have been false positives investigated. (26)

Copper or copper-containing chemical compounds, certain bleaches, horseradish sauce, via the enzyme horseradish peroxidase, small amounts of blood present in urine (i.e. animals' urine may be a false positive), faecal matter, and excessive smoke in an enclosed space can all cause luminol chemiluminescence. (20)



Figure 2 blood trace under luminol application

Lateral flow test for human blood

For the qualitative indication of human blood, the crime scene team utilizes an immunochromatographic operation (Figure 3). Such testing is designed for selective use in crime scenes when the human origin of suspected bloodstains is dubious and/or when determining the human origin indication is time-sensitive. (27)



Figure 3 The left test strip showed a positive reaction for human blood where both control and sample line are visible while the right test strip is an example of a negative test where only the control line is visible.

This test is designed for use on stains that have been positively evaluated using the phenolphthalein test. Limited sample size may prevent use of this test to allow future DNA testing. ⁽²⁸⁾

Kastle-Meyer and Hemastix tests for blood

The Kastle-Meyer or Phenolphthalein test is a presumptive test that responds to the blood-borne heme molecule. It is a two-step response where one drop of phenolphthalein reagent is added to the presumed blood sample, followed by addition of hydrogen peroxide. ⁽²⁹⁾ A positive result results in a pink colour change. Although blood stains tend to appear red-brown in colour, substrate colour or stain age can affect the appearance or visibility of the stain which illustrated in figure 4.

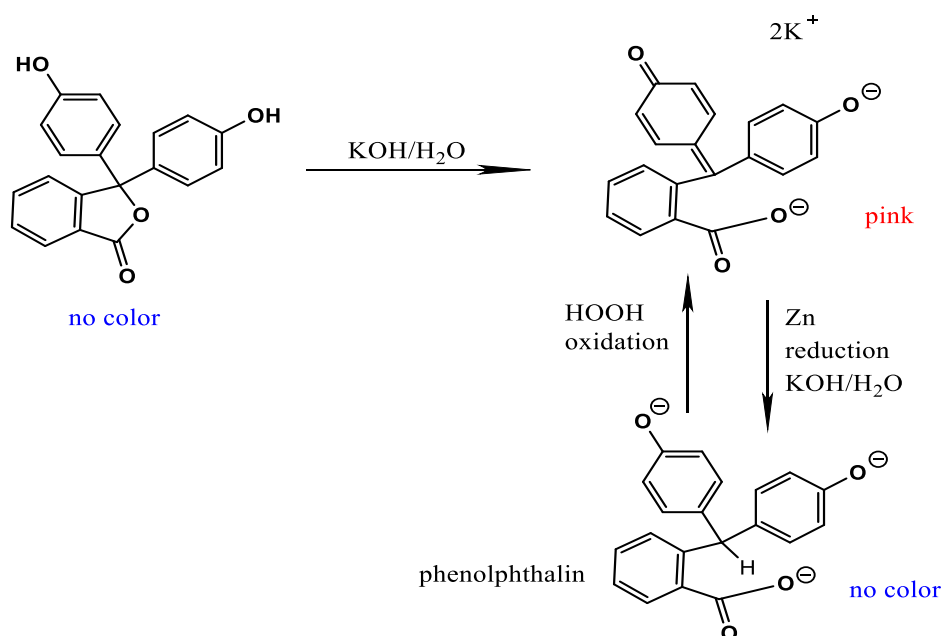


Figure 4 The figure shows chemical reaction of the phenolphthalein test.

Typically, phenolphthalein tests are performed prior to collection on suspected bloodstains. While a positive reaction to phenolphthalein indicates blood, it is only a presumptive test, and it is feasible to have false positives. Furthermore, the response is not specific for human blood. ⁽³⁰⁾ The swab in Figure 5 shows the colour of a positive reaction with the phenolphthalein test, indicating the presence of blood.

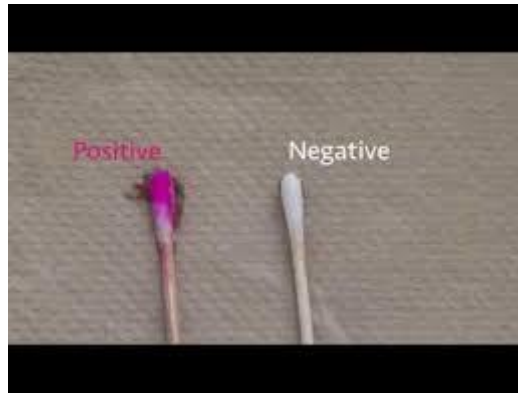


Figure 5 The image shows a positive test (pink) in the right swab while the negative test (clear) in the left swab with the phenolphthalein test.

Similar to the Kastle-Meyer test, Hemastix is also a standardised catalytic test for a specific strip where the blood sample is used and a positive result leads to a change in dark green colour. Originally, the Takayama Crystal Assay or an immunochromatographic test is used for confirmatory testing. ⁽³¹⁾ The Takayama Crystal Assay, which forms a ring of ferro protoporphyrin through a response between the heme group's pyridine and iron atom. A presumptive blood sample is introduced to a slide with the Takayama reagent. ⁽³²⁾ After adding the Takayama reagent, the flap is dried at 115 degrees Celsius. It is then put under a microscope and the visualization of dark red, feathery crystals is a positive result. It works analogous to a pregnancy test in which antigens in the blood are identified and a positive result is a band at the test site and control site for the immune chromatographic test. An analyst can verify the existence of blood after performing the multiple experiments and proceed to develop a DNA profile with downstream apps such as DNA extraction, polymerase chain reaction (PCR), capillary electrophoresis (CE). ⁽³³⁾

Crime scene analysis using alternate light sources.

Crime scenes can be examined using monochromatic light sources, also called alternate light sources, to help locate and identify prospective proof. This sort of testing uses the intrinsic luminescent characteristics of materials subjected to monochromatic light (biological fluids, fibres, latent prints). ^(34, 35)



Figure 6 Various stains on fabric from various biological fluids



Figure 7 shirt as viewed in normal lighting (left) and a semen stain on the pocket (right), as seen using ALS.

Visible light sources were used over many years during most searches for crime scenes. While some forensic investigators sometimes used ultraviolet light to investigate evidence for the crime scene, the key was white light. ⁽³⁶⁾ However, in the 1970s, the Royal Canadian Mounted Police developed the use of argon-ion lasers. The use of these expensive, cumbersome, bulky devices in crime scenes was impractical, thus restricting their use to the criminal laboratory. ⁽³⁷⁾ The 1980s saw the appearance on the market of portable lasers, but their usefulness was limited to a single colour of light for the most part. In the 1990s, the availability of high-intensity incandescent lamps slowly revolutionised alternative light source evaluation of physical evidence as these devices weighed much less than 20 pounds. They can provide a powerful beam of light that can be passed through several visible filters of blue, green, yellow and red light. Using these colours has improved the ability to expose an abundance of invisible facts. ⁽³⁸⁾ While blood does not glow in the visible spectrum, it has a distinctive wavelength in which the darkening of the bloodstain increases its contrast by about four times.

This is the most efficient way to photograph blood prints because of the improved contrast. Oblique or parallel lighting will show tiny particles such as hair and fibres for collection, such as a ground or carpet with a strong white light (the more powerful the better). Secondly, some hair and fibres also shine under UV or Blue light and for collection will stand out heavily. ^(39, 40)

Forensic light sources of bruises / bite marks / pattern wounds may show bruise and patterned wound information that are invisible under ordinary white light illumination. In a suspect palm, details of a bruise pattern may link a suspect to a weapon. In addition, details of a victim's bruise, such as a bite mark or a shoe mark, may link a suspect to the victim. Multiple frequencies are essential because distinct colours pierce distinct depths of the skin and therefore the wavelength of the tool varies based on the size of the scar or wound. ^(41, 42, 43)

Deep injuries may involve sufficient infrared light to penetrate the skin. Questioned Documents Inks have various formulations, even within the same sort of colour that is evident, visible. A tuneable Forensic Light Source can be used

to assess small variations in the ink type by analysing ink reactions as the light colour is changed across the visible and infrared spectrum. ⁽⁴⁴⁾

Chemical visualisation of latent print evidence

Latent print evidence can be visualised using many chemicals like amido black, fingerprint powder, Leucocrystal violet, cyanoacrylate (superglue) fuming, and titanium dioxide. ^(45,46)

Detection by fluorescence

The following may be revealed by alternative sources of UV light: seminal fluid, saliva and urine stains. Some narcotics will also fluoresce like pieces of bone and teeth. ⁽⁴⁷⁾ Fluorescent latent printing powders can produce the latent residue on a fluorescent surface. The advantage here is that the ridges fluoresce brightly, and a multi-coloured or confused background can be minimized when photographed to the stage where it does not appear in pictures. Fluorescent liquids are used on porous surfaces such as paper and carton to create latent prints. ^(48,49)

Using superglue fuming, fluorescent colours are used to improve latent prints. Using alternative sources of light offers an extremely practical and effective way to locate physical evidence in crime scenes. Light Emitting Diodes (LEDs) invention and perfection has further developed evidence retrieval as even 1 and 3watt LEDs can be mounted in tiny handheld flashlights and it is noteworthy their performance ^(50, 51) Because body fluids such as semen, saliva, and vaginal fluids are naturally fluorescent, using a light source provides a distinctive way to locate them. ⁽⁵²⁾

Instead of testing whole, big pieces of proof such as a mattress, a carpet, a sheet, a clothing article, etc., a criminal scene researcher can narrow down the places of stains for collection. The dried body fluids will shine under the illumination of the light source. ⁽⁵³⁾ While body fluids will fluoresce under normal UV black light, many items you would find them on, including clothing and sheets will also shine and hinder the detection of proof. Therefore, to eliminate background interference (background rejection) it is essential to adjust longer wavelengths. ⁽⁵⁴⁾

Considering that one may be searching for high-profile body fluids in capital crime cases, the more body fluid evidence that can be revealed the better. This has been aided by the advent and availability of DNA typing systems. The stronger your source of light and the more wavelengths you have, the more proof you will find. ⁽⁵⁵⁾

Semen detection

Semen is a colourless liquid, but an Alternative Light Source (ALS) can be used in the initial detection of semen. Researchers can see the collection of samples from a crime scene under UV light. The semen detection test for Acid Phosphatase (AP) is a common presumptive test.⁽⁵⁶⁾ The AP test detects the phosphatase enzyme acid which is secreted from the prostate gland. However, this test may be positive due to the presence of acid phosphatase in other body fluids. A drop of sodium alpha-naphthyl phosphate reagent is applied to the suspected stain in order to perform the experiment, followed by a drop of Quick Blue B. A positive test result of this test is a change in colour to dark violet which shown in figure 8. ⁽⁵⁷⁾

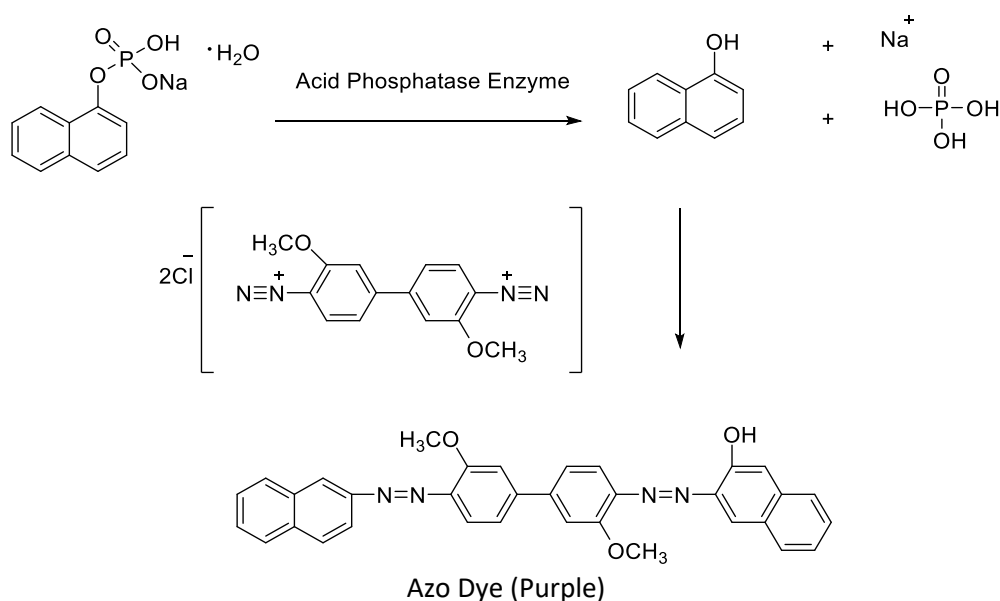


Figure 8 The figure shows the chemical reaction of AP test.

Suspected semen stains, generally discovered using an alternative light source, can be tested at the crime scene using the reagent BCIP (5-bromo-4-chloro-3-indolyl phosphate). In this analysis, the BCIP reagent reacts in the presence of prostatic acid phosphatase, a component of the semen, to produce a purple or aqua-coloured response. A transformation in colour is a positive response and is indicative of the presence of semen (Figure 9). ⁽⁵⁸⁾



Figure 9 The image shows a positive BCIP test on the left and a negative test on the right.

Saliva detection

The presumptive test for detecting saliva is the alpha-amylase test also known as the Phadebas test. This detection method is based on the activity of the alpha-amylase enzyme, which breaks starches from food into smaller molecules of oligosaccharides, beginning digestion in the mouth. ⁽⁵⁹⁾ The saliva sample is introduced using a petri dish gel and permitted to spread overnight through the gel. Visualization is done by adding iodine to the gel that stains the starch in the blue gel. ⁽⁶⁰⁾ If saliva is present, then the starch is broken down by the alpha-amylase, producing a transparent coloured circle around where the sample was placed. There was not as much study conducted for confirmatory exams compared to blood and semen. RSID tests were conducted to detect alpha-amylase, however, they are not always accurate because there can be many false positives. ⁽⁶¹⁾

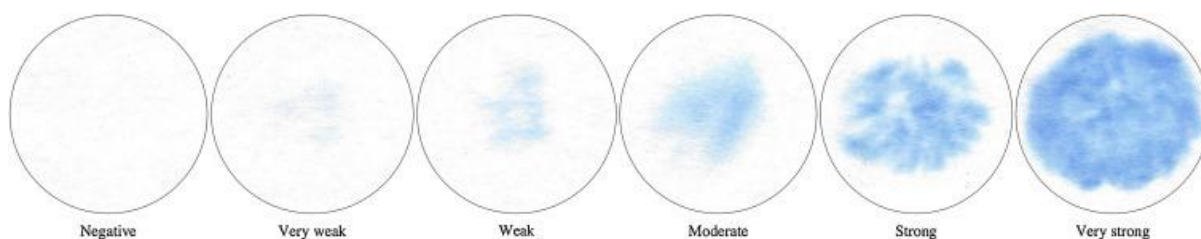


Figure 10 presumptive Phadebas test

1.3 Organic dyes

Organic dyes are compounds which can provide materials such as fabrics and paper with colour. Dyes are distinguished from pigments which are finely ground solids that are diffused or mixed with other compounds in liquids such as paint or ink. Dyes are soluble colourants, pigments are insoluble, many dye molecules are

carbon based, which makes them organic compounds, but pigments typically are inorganic compounds and exhibit lighter colours. ⁽⁷⁹⁾

Unlike most organic compounds, dyes have colour because they absorb light in the visible spectrum between 400 and 700 nm. Dyes have at least one chromophore and this is typically a conjugated structure. [The part of a molecule that gives it colour is called a chromophore. The colour we see is the one that is not absorbed by our eyes within a specific wavelength range of visible light. The chromophore is a part of the molecule where the energy difference between two molecular orbitals is within the visible spectrum's range].⁽⁸⁰⁾ The colour of a compound is lost if these qualities are not present in the molecular structure. Most dyes will contain “colour helpers” known as auxochromes. Auxochromes are functional groups such as carboxylic acids, amines, hydroxyls, and sulfonic acids. Auxochromes are not responsible for the colour, but their presence can change the colour of the dye and also affects the solubility of the dye. ⁽⁸¹⁾ [When attached to a chromophore, an auxochrome is a functional group of atoms with one or more lone pairs of electrons that changes the wavelength and intensity of absorption]⁽⁸²⁾ An example of a chromophore with an auxochrome is given in Fig.13

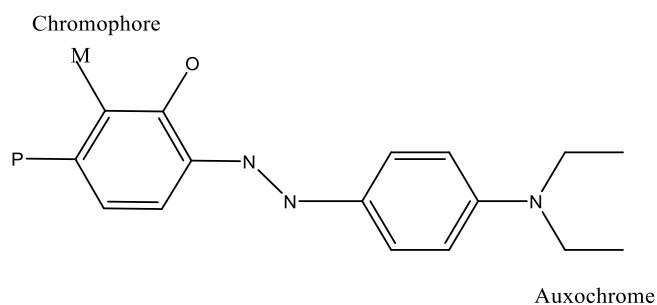


Figure 13 Chromophore with auxochrome ⁽⁸³⁾

There are more than 25 common categories of dyes, with natural dyes falling into the following eight groups: anthraquinones, hydroxy cations, carotenoids, naphthoquinones, flavonoids, flavones and flavonols ⁽⁸⁴⁾

The type of dye is defined either by its use or by its chemical structure. To ensure that the emphasis is placed on the composition of the colors, a program is used that catalogues coloring by chemical structure. ⁽⁸⁵⁾ Although not comprehensive, the following outline refers to those dyes that are of the greatest chemical and economic significance other than azo or phthalocyanine. The anthraquinone colorings, second only to azo coloring, are commonly used in terms of commercial importance. ⁽⁸⁶⁾ Also important are vat dyes, which are colors of any chemical class that are applied through a vat dyeing process.

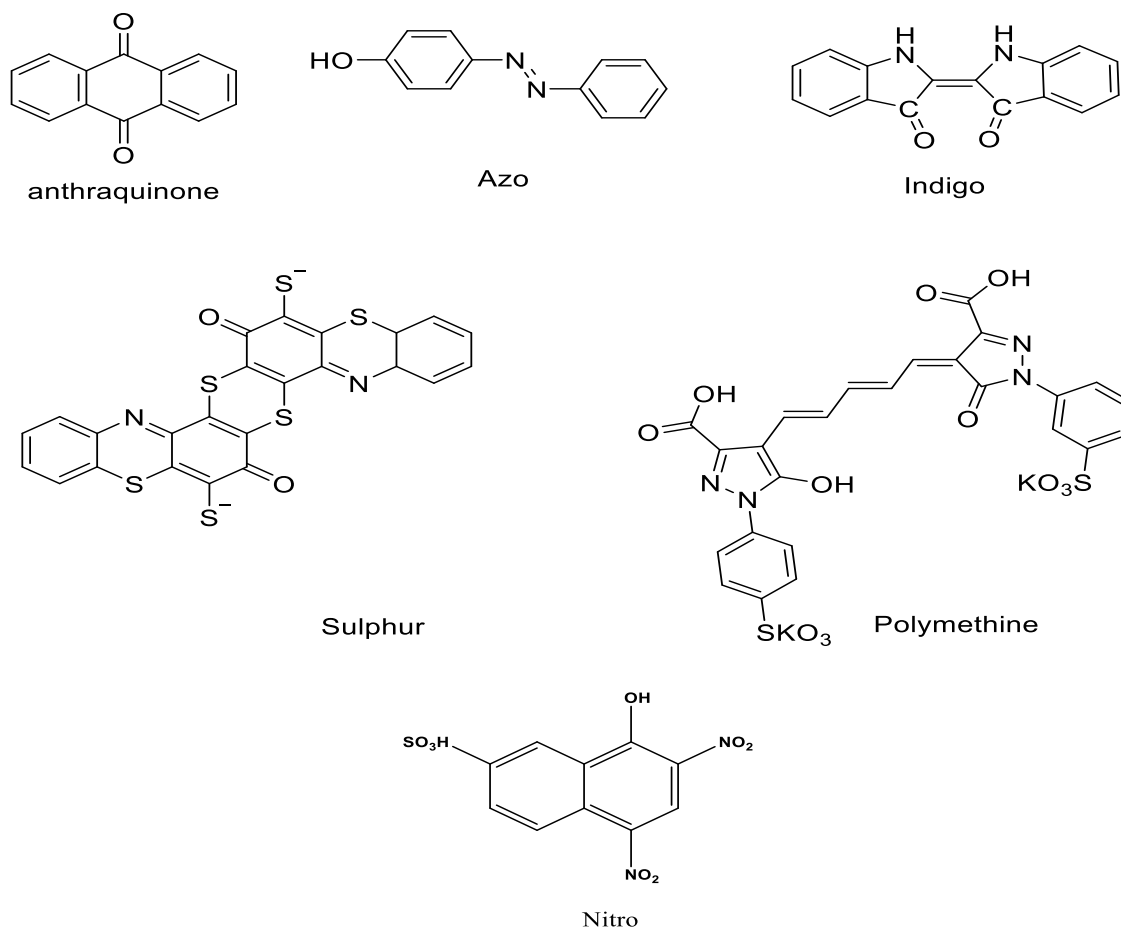


Figure 14 Some examples of commercial dyes.

The method of vatting involves treating the insoluble dyes in an alkaline medium with a reduction agent to give the reduced, or leuco, form. ⁽⁸⁷⁾ The process is reversed after applying the dye's leuco form to the fiber and the colored dye is formed by oxidation.

Indigoid coloring is often treated separately from other vat coloring due to its value as a member of a distinct group of colored compounds, exclusive to the rest of the vat coloring. Di and tri-aryl carbonium dyes are the oldest class of synthetic dye; this group contains mauveine. Historically, nitro dyes are important as picric acid was the first synthetic compound commercially used to colour substrates, there are finally the sulphur and polymethine colors which illustrated in figure 14. ⁽⁸⁸⁾

1.4 Fluorescence and phosphorescence

Fluorescence is a type of photoluminescence that occurs when an electron is excited by absorbing energy, and subsequently relaxes to its ground state by emitting energy in photon form. Generally, these emitted photons have a longer wavelength than the absorbed light, meaning that they have less energy. The reason for this is vibrational relaxation in the different electronic states ⁽⁸⁹⁾, as shown in a Jablonski diagram (Figure 15).

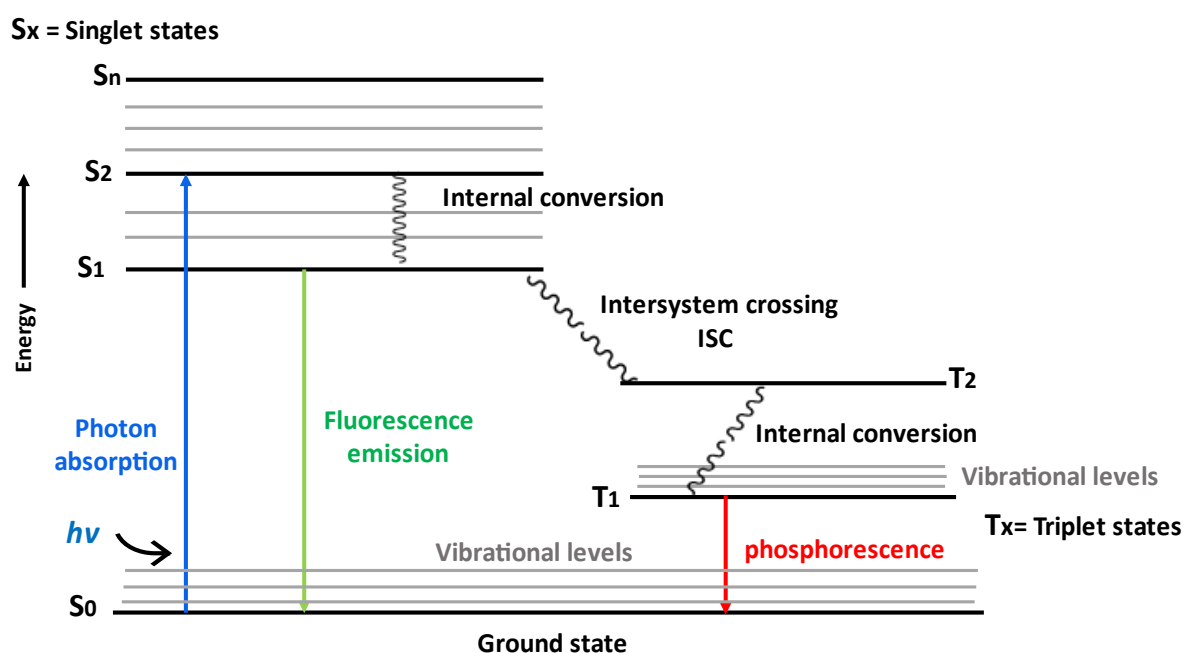


Figure 15 **Jablonski Diagram** ⁽⁹⁰⁾

A Jablonski diagram illustrates the processes that occur between absorption and light emission. In Figure 15, the singlet ground, first, and second electronic states, respectively, are represented by S₀, S₁, and S₂. At each of these electronic energy levels, there may be fluorophores in a variety of vibrational energy levels, represented by 0, 1, 2. ⁽⁹¹⁾ The transitions between states are shown in this Jablonski diagram as vertical lines to demonstrate the instantaneous nature of light absorption because transitions occur in a time too short for major nuclei displacement. This idea is the basis for the Franck Condon principle. ^(92, 93)

When speaking of fluorescence, the fluorescence life span and the fluorophore's quantum yield are important parameters. The fluorescence lifetime is the average time the fluorophore spends in its excited state, normally around 10 nanoseconds, and the quantum yield is the number of photons emitted compared to the number of photons absorbed, meaning that it can have a maximum value of 1 and a minimum value of zero. ⁽⁹⁴⁾

Scintillation is the light emission from any material that emerges from electronically excited states. Depending on the nature of the excited state, luminescence is classified into two groups, viz. fluorescence and phosphorescence. If the electron in the excited state is paired with the second electron in the ground state, this is a singlet excited state. ⁽⁹⁵⁾ In a singlet excited state, a return to the ground state with emission of a photon is an allowed process. Phosphorescence, on the contrary, is the emission of light from triplet excited states where the electron in the excited orbit has the same rotational direction as the electron in the ground state. ⁽⁹⁶⁾ The transition from the triplet excited state to the singlet ground state is forbidden, so the lifetime of phosphorescence is generally milliseconds to seconds.

There are many examples of luminophore. Fluorescein is an organic fluorescent dye. Fluorescein is a fluorophore commonly utilized in microscopy, in dye lasers, in forensics and serology to detect latent blood stains, and in dye tracing. Fluorescein has a maximum absorption of 494 nm, and a maximum emission of 512 nm (in water). Rhodamine derivatives, coumarin, and cyanine are historically common fluorophores. ^(97,98) Fluorophores usually comprise multiple aromatic groupings, or planar or cyclic moieties with multiple π bonds. New generations of fluorophore, many of which are patented, often perform better, being more light-stable, brighter, and/or less pH-sensitive than conventional excited pigments with comparable emissions. The absorbed wavelengths, the efficiency of energy transfer, and the time before emission depend on the fluorophore structure and its chemical environment. Total absorption wavelengths (excitation) and emissions (e.g. absorption / emission = 485 nm/517 nm) are common terms used to refer to a specific fluorophore, but it may be important to consider the entire spectrum. ⁽⁹⁹⁾

We will be illustrated here some information about thiazole orange and DODC dyes (figure 16) which experimented in the next chapters (chapter 3 and 4).

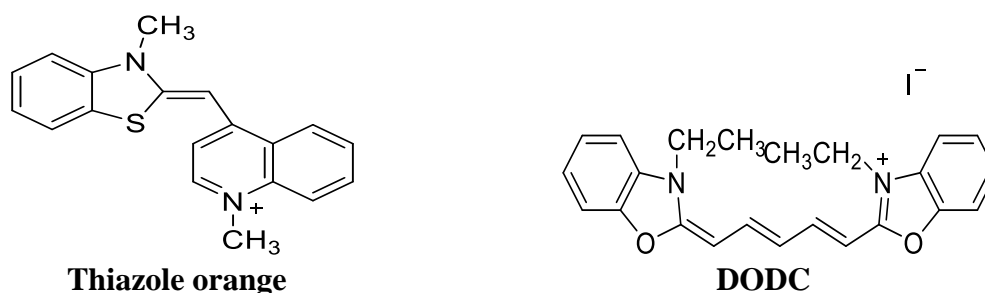


Figure 16 **Thiazole orange and DODC**

1.5 Dye aggregation

Most dyes aggregate in aqueous solution under certain conditions. Dye density, concentration of electrolytes, and temperature are the main factors affecting aggregation. Increases in the first two and a decline in the third encourage aggregation.^(100, 101) There are many methods used to study the degree of dye aggregation including conductivity, light dispersion, diffusion, and spectrophotometry. UV-Vis spectroscopy can be used to investigate aggregation with the help of Beer's law.⁽¹⁰²⁾ When a dye's degree of aggregation varies with concentration, the system shows an obvious deviation from the law of Beer, in which a plot of absorption versus concentration is not linear. It is also important at this point to remember that, for instance, an isosbestic point may be present when comparing the absorption spectra at varying concentration or temperature.⁽¹⁰³⁾ This means that the two species, monomer and dimer, or monomer and aggregate, are present which shown in the figure 17 below.

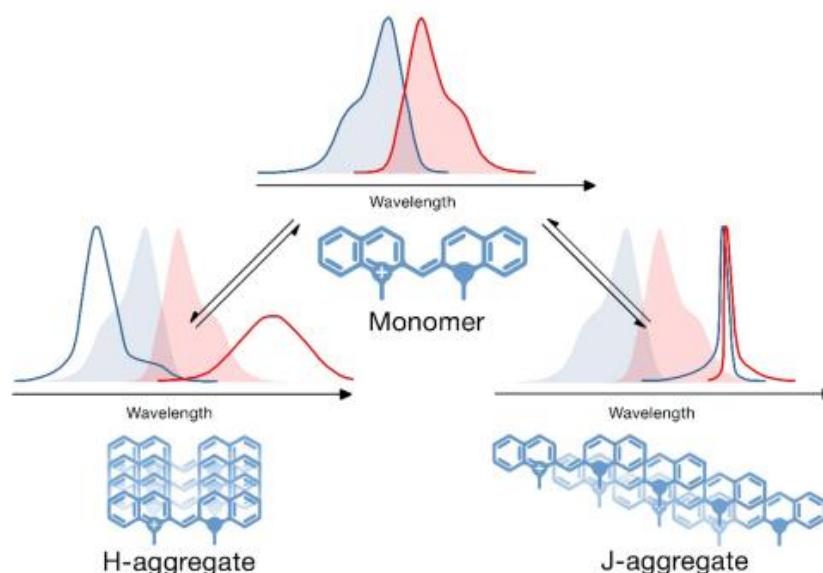


Figure 17 aggregation of cyanine dye⁽¹⁰⁴⁾

Dyes are well known to aggregate in aqueous solution. The π stacking of the conjugated systems of the dyes is favored based on both the hydrophobicity and polarizability of the dye.⁽¹⁰⁵⁾ The presence of aggregates in dye solutions may considerably influence their photo-physical behaviour. UV-vis absorption spectroscopy is one of the most suitable methods for quantitative study of the aggregation properties of dyes as a function of concentration, since in the concentration range used (10^{-6} – 10^{-3} M) monomer-dimer equilibrium mainly exists. To date, the best description of the aggregation behavior of dye

chromophores is based on the exciton-splitting theory. ⁽¹⁰⁶⁾ The aggregation of a dye leads to a strong coupling of the molecular transition dipoles, i.e. the electrostatic interaction between molecular transition dipoles of the chromophores causes the splitting of energy levels of the excited states of the molecules. ⁽¹⁰⁷⁾ Kasha's rule notes that photon emission (fluorescence or phosphorescence) occurs in significant output only from the lowest excited state of a given multiplicity. The energy diagram displays excitation pathways (relative to the monomer) for the J-dimer, H-dimer, and oblique dimer which shown in figure 18. ⁽¹⁰⁸⁾

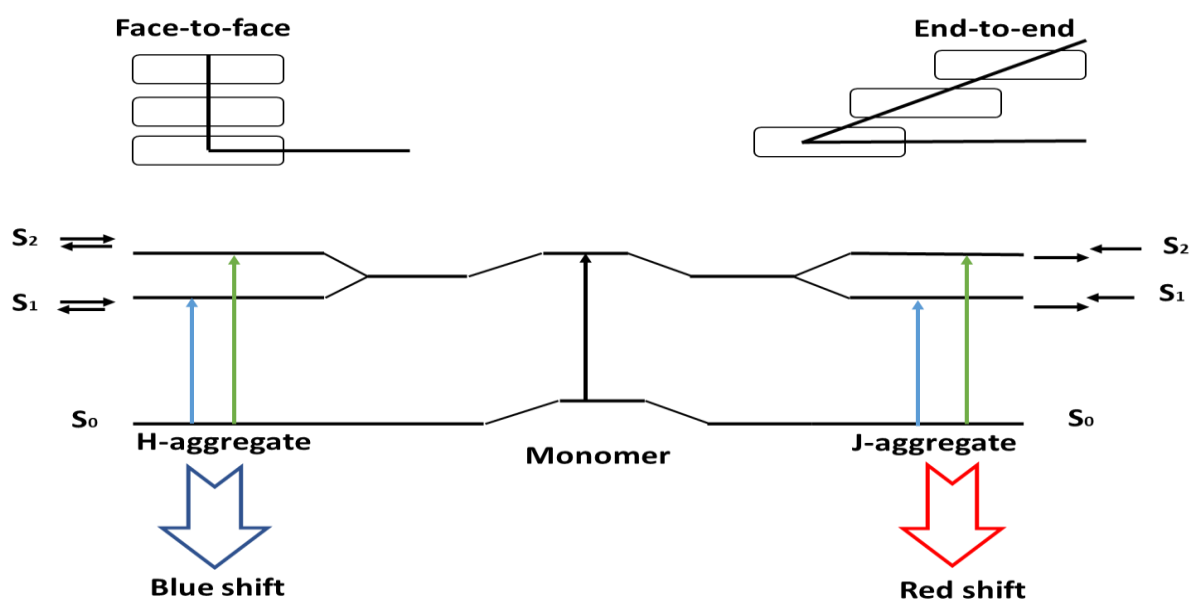


Figure 18 model showing spectral shift based upon aggregate structure.

Thiazole orange occurs predominantly as a monomer in aqueous medium, where its fluorescence is small due to intramolecular movements. At low concentrations, TO forms H-dimer and H-aggregates (Figure 19). The nonfluorescent TO (monomer) form starts to fluoresce in aggregated or dimeric forms. ⁽¹⁰⁹⁾

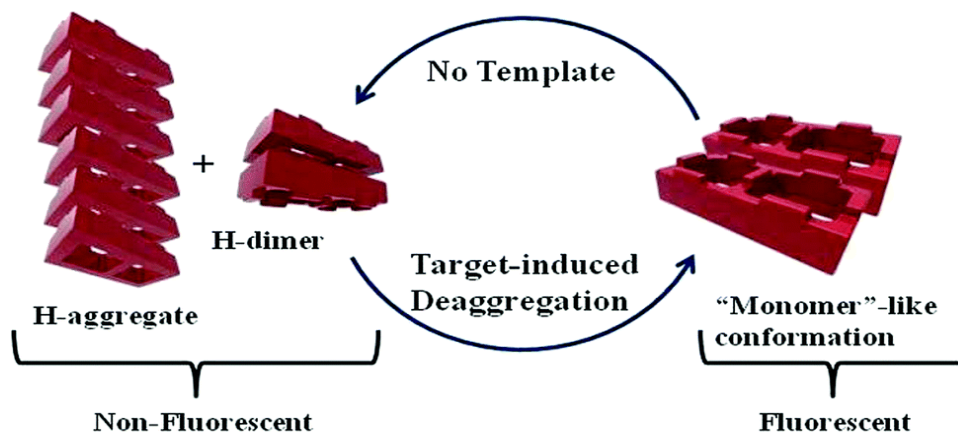


Figure 19 Template-free H-dimer and H-aggregate formation by dimeric carbocyanine dyes

It is known that there are many chromophores in solution at higher concentration or in viscous medium that are present as a dimers and higher aggregates along with the monomeric form. ⁽¹¹⁰⁾ Aggregation limits the dye's free movement with far-reaching consequences. Many applications in optics, solar cells, nonlinear optical devices semiconductors, and organic photovoltaic cells have been identified for the self-aggregation of dyes. ⁽¹¹¹⁾

1.6 DNA and DNA-binding dyes

1.6.1 The structure of DNA

Nucleic acids are one of the biomacromolecules of greatest importance. They are vital for all known life forms. With the exception of cells such as red blood cells, all living cells contain both DNA and RNA, while viruses contain either DNA or RNA. Nucleic acids have the function of encoding, storing, transmitting and expressing genetic information to the cell itself and ultimately passing the information on to the next generation of each organism. ^(112, 113)

Extensive interest in nucleic acids in the 1940-1950s resulted in it being unambiguously shown that DNA is the carrier of genetic information. ⁽¹¹⁴⁾ This resulted in the development of the now famous model of the three-dimensional DNA structure, which Watson and Crick developed using X-ray diffraction photographs taken by Franklin and Wilkins. Nucleic acids are biopolymers that are linear. Their monomers are nucleotides, hence their other name of polynucleotides. Each nucleotide consists of three components: a nitrogen base (also known as a nucleobase or simply as a base), a pentose (5-carbon) sugar (ribose in RNA and deoxyribose in DNA) and a phosphate group associated with acidic nucleic acid characteristics (Figure 20). ⁽¹¹⁵⁾

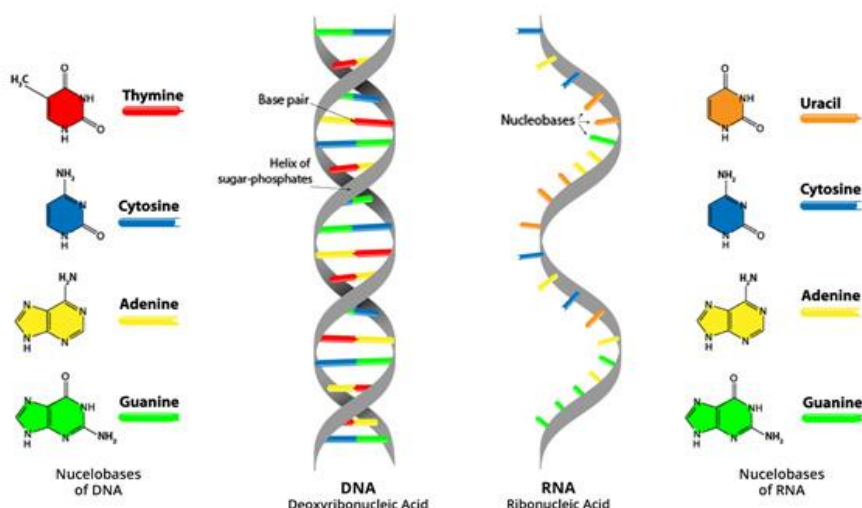


Figure 20 Comparison of DNA and RNA nucleotides (116)

DNA contains β D 2'-deoxyribose sugar, a pentose sugar. One oxygen atom at the 2' carbon is missing hence the name 2'-deoxy as shown in Figure 21. Deoxyribose sugar exists in the ring form in the composition of DNA. Each numbered carbon on the sugar is followed by a prime mark, so DNA is connected through the 5 prime or 3 prime carbon. (117)

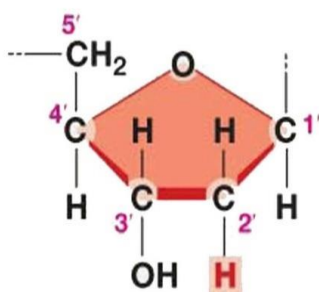


Figure 21 pentose sugar

The bases in DNA can be classified into two main organic bases groups (figure 22), viz. pyrimidines and purines.

A six-membered pyrimidine ring exists in pyrimidine bases which is like the benzene ring except that it contains nitrogen in a place of carbon at the positions of 1 and 3. Three pyrimidine derivatives are uracil, thymine and cytosine. They are abbreviated by three capital letters U, T and C, respectively. Cytosine and thymine are found in DNA, while cytosine and uracil are found in RNA. Thymine is replaced by uracil in RNA. (118)

Thymine is present in DNA because thymine guarantees stability of the genetic message. Otherwise, uracil would result in mispairing and mutagenesis on subsequent replication. Pyrimidine bases have a standard keto- oxygen at position 2. In cytosine, an amino group (-NH₂) in location 4. A keto-oxygen is present at position 4 of uracil, while thymine contains a keto-oxygen at position 4 and a methyl group (CH₃) at position 5. the pyrimidine bases have a hydrogen atom at the position 1 which it shares in their linkage with carbon 1 of pentose sugar. ⁽¹¹⁹⁾

Purine is composed of a pyrimidine ring and a five-membered imidazole ring which are fused. ⁽¹²⁰⁾ Adenine (A) and guanine (G) are two purine compounds found in DNA (Figure 21). There is an amino group (-NH₂) at the 6 position in adenine, while there are a keto group and an amino group at the 6 and 2 positions of carbon in guanine. A (β-N) glucosidic bond in the base attaches to the pentose sugar. The bases absorb ultraviolet light at 260 nm. ⁽¹²¹⁾ This feature is beneficial in the identification and analysis of DNA and chromatographic or electrophoretic methods easily separated pyrimidine and purine bases.

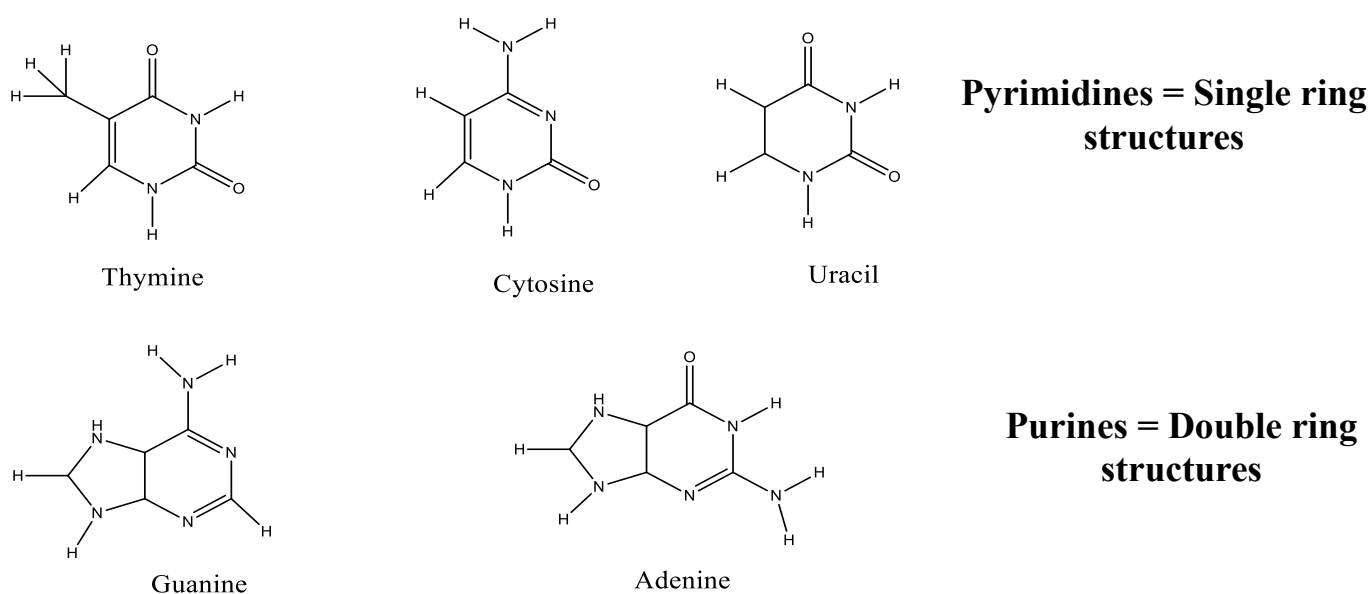


Figure 22 purines and pyrimidines

The three-dimensional model of DNA structure was discovered by Watson and Crick in 1953. ⁽¹²²⁾ The Watson-Crick model of DNA structure shows that two right-handed polydeoxyribonucleotide strands are coiled in a helical way around the same axis, which forms a double helix. The two strands are oriented as antiparallel; for example, if one strand is oriented in the p-3' → 5'-p direction, the second strand is oriented in the p-5' → 3'-p direction. Hydrogen bonds and stacking interactions hold the two strands together, facing each other. ⁽¹²³⁾

Two nucleotides connected by hydrogen bonds on opposite complementary DNA strands are called a base pair. ⁽¹²⁴⁾ Adenine forms a base pair with thymine and cytosine with guanine. A GC base pair shows three intermolecular hydrogen bonds while an AT base pair shows two intermolecular hydrogen bonds (Figure 23). ⁽¹²⁵⁾

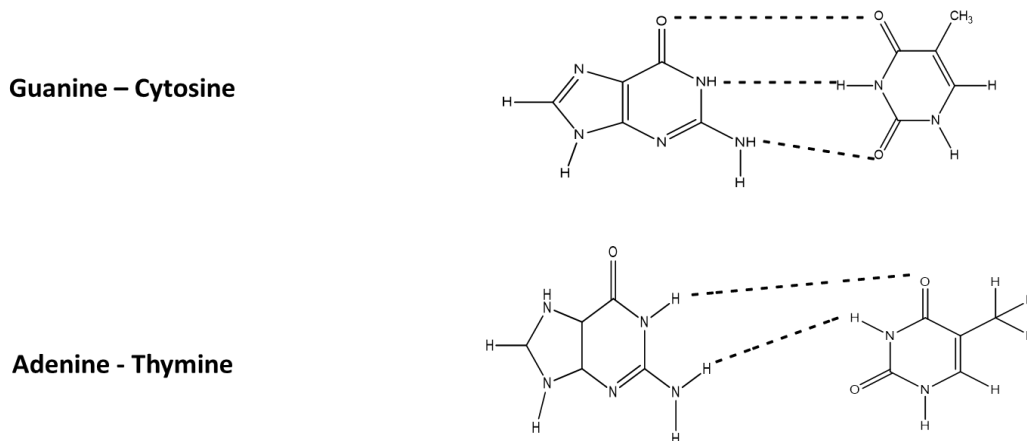


Figure 23 intermolecular hydrogen bond between base pair

1.6.2 DNA binders

Most molecules, including proteins, interact with DNA through various interaction modes. In addition, molecules can reversibly or irreversibly interact with DNA. Typically, irreversible binding requires non-specific covalent binding to the DNA backbone's phosphate or sugar portion. ^(126, 127) This typically the distortion or breakage of DNA. For example cisplatin, an anticancer drug, acts exactly in this way when it binds within DNA bases to nitrogen atoms (Figure 24). ⁽¹²⁸⁾

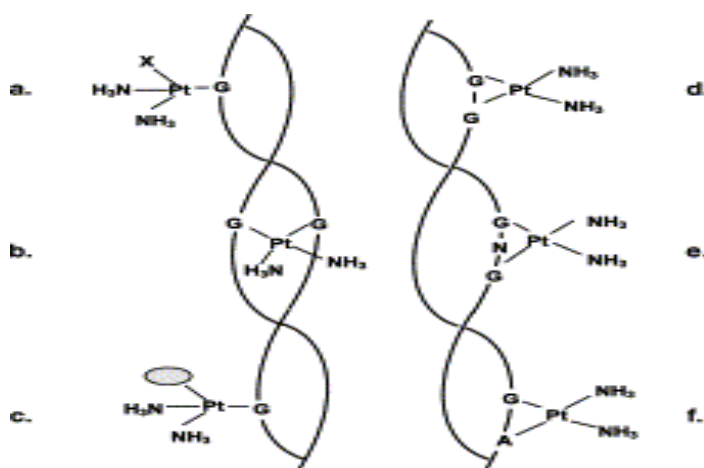


Figure 24 Cisplatin interactions with DNA. ⁽¹²⁹⁾

Molecules can reversibly bind to DNA through a number of binding modes. Reversible DNA binders interact with DNA through (a) electrostatic (b) groove binding (major and minor) interactions (c).⁽¹²⁹⁾ On the backbone of the DNA there are electrostatic interactions. Groove binding or intercalation between the base pairs are shown in Figure 25.

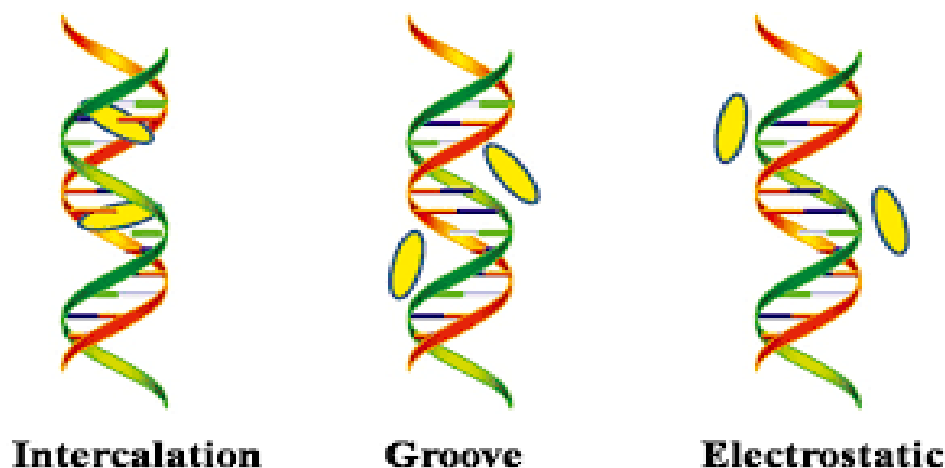


Figure 25 Examples of different reversible interactions between molecules and DNA.
(130)

1.6.2.1 Electrostatic interaction

Electrostatic interactions are usually non-specific and occur along the external surface of the DNA double helix. Because the nucleic acid structural structure is made by alternating phosphate and sugar groups, the backbone of DNA is negatively charged. This negative charge enables electrostatic interactions between DNA and cationic molecules.⁽¹³¹⁾ The size of the ligand, the charge on the ligand and the ligand hydrophobicity will influence this mode of interaction. Normally, electrostatic interactions play a significant role in DNA stability. However, non-specific interaction with, for example, Na^+ or Mg^{2+} leads to partial neutralisation of the charge of the phosphate backbone. Binding small molecules to DNA is therefore dependent on the medium's ionic strength.⁽¹³²⁾

1.6.2.2 Intercalation and intercalators

In 1961, Lerman proposed the intercalation principle. Planar (flat and rigid) molecules slip between the base pairs in this binding process. Intercalators are typically not flexible and generally have a conjugated aromatic system. Intercalation takes place between DNA base pairs.⁽¹³³⁾ The driving force in this event is the stacking interaction between the planar aromatic molecule and the base pairs of DNA and Van der Waals interactions. Intercalators are molecules such as methylene blue, ethidium bromide and coralyne. These are all flat and rigid molecules.⁽¹³⁴⁾

1.6.2.3 Major and minor groove binding

Groove binding involves molecules in the major groove or the minor groove interacting with DNA. Major groove binding by proteins plays a major role in transcription and replication, as the major groove provides a binding region that allows DNA-binding proteins to interact sequentially. The major groove is wide, which allows large biomolecules such as proteins to bind to the major groove predominantly through recognition of hydrogen bond donating and accepting sites. ⁽¹³⁵⁾ Small molecules, on the other hand, are often minor groove binders. Minor groove binders have several features, for example they are usually long and flexible. Minor groove binders are often charged positively, and interaction between the DNA binder and the DNA's anionic phosphate backbone can therefore also occur. Moreover, these molecules also interact with the hydrophobic interior as well as with donors and acceptors in the groove through hydrogen bonding. ⁽¹³⁶⁾

1.7 Interaction of cyanine dyes with DNA

Cyanine dyes are among the oldest classes of synthetic compounds but continue to find applications in different fields. In colour photography, and then in high-energy lasers and digital image storage, cyanine dyes found their first application. However, the greater interest in cyanine dyes is related to its biological and biomedical where they are used as molecular probes. ⁽¹³⁷⁾

The majority of fluorescent dyes widely used for DNA visualisation assays nowadays belong to the cyanine family as these molecules display high affinity for double-stranded nucleic acid, strong absorption in the visible spectrum range, and sharp increase in fluorescence emission when interacting with DNA. ⁽¹³⁸⁾ Cyanine dyes display negligible fluorescence when free in solution and very strong fluorescence when bound to DNA (essentially through intercalation), making them useful to detect DNA at a sensitivity comparable to that of radioactive labels. ^(139, 140)

If their first use is DNA sequencing and fluorescence microscopy, cyanine dyes can also be very usefully used through fluorescence energy transfer for conformational studies. Cyanine dyes can interact with DNA through intercalation, but also through groove-binding as seen in figure 26. ⁽¹⁴¹⁾

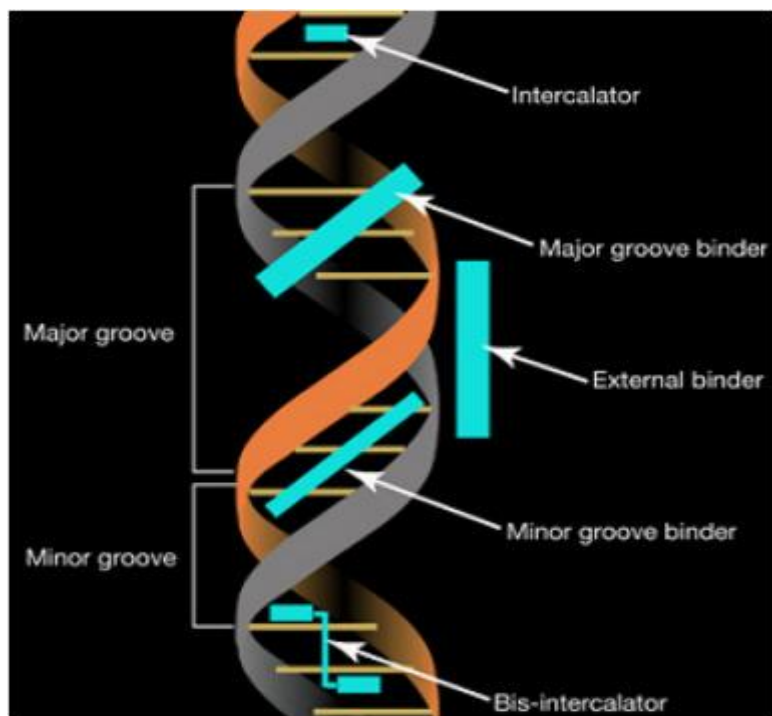


Figure 26 the interactions between cyanine dye and ds DNA

Apart from simply binding the dye as a monomer, some dyes form well-defined helical aggregates using DNA as a template. Although these dyes are typically achiral, the aggregates show induced chirality due to the right-hand helical structure of the DNA template underlying them.

1.8 Thiazole orange, TO.

The fluorescence quantum yield of TO has been reported to increase 18,900 times upon binding to DNA.⁽¹⁴²⁾ In figure 27 below, the chemical structure of TO. However, by intercalating DNA or other oligomers such as peptide nucleic acids between the nitrogenous bases, the rotation is limited, thus closing an important channel of non-radiative decay.⁽¹⁴³⁾

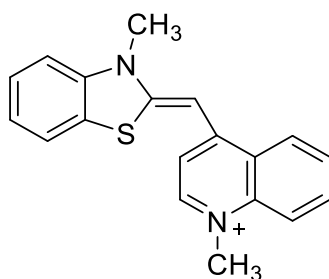


Figure 27 Thiazole orange

TO's quantum fluorescence yield bound to nucleic acids is temperature dependent. When the temperature rises from 5 to 50 °C, the quantum yield decreases by 3–4-fold. ⁽¹⁴⁴⁾ TO's quantum yield increases by 50–2000 times when bound to nucleic acids, depending on the sequence, structure, and temperature. This is most likely due to increased DNA thermal motion, allowing for more internal rotation in the TO bond. ⁽¹⁴⁵⁾ The significant difference in the quantum yield between the free and bound forms is due to the fact that the non-radiative relaxation, caused by isomerization across the internal bridge between the benzoxazole or benzothiazole unit and the quinoline unit in the free form, is impeded by intercalation of the molecule in DNA. Such a decay mechanism that governs the free dye's excited-state lifetime is a common feature of cyanine dyes and has been the subject of many investigations. ⁽¹⁴⁶⁾ The two aromatic rings of TO are conjugated only when the rings are coplanar. Because of free rotation in the excited state leading to quenching, the dye shows negligible fluorescence in aqueous solution. However, by intercalating between the nitrogenous bases of DNA or other oligomers, such as peptide nucleic acids, rotation becomes restricted, thus closing an important nonradiative decay channel. ⁽¹⁴⁷⁾ Thus, this property provides a convenient means for screening candidate oligomer duplexes for stability. Because of their fluorogenic behavior, unsymmetrical cyanine dyes are widely used in biomolecular detection, whereby fluorescence quantum yields can be very low in fluid solution but are significantly enhanced in conformally restricted environments. ⁽¹⁴⁸⁾ The cationic unsymmetrical cyanines such as TO are best known for their fluorogenic behavior in the presence of DNA and RNA. Thiazole orange serves as an ideal scaffold for these conjugates because it is highly fluorescent when bound to DNA. For example, it may be linked with a peptide nucleic acid (PNA) to detect a target nucleic acid in homogeneous solution. ^(149, 150)

A common use of thiazole orange is to measure the formation of DNA duplexes. TO binds to DNA both as a monomer and as a dimer. The monomer stacks between the bases of DNA and is the dominant interaction mode with ds DNAs and with poly(dA). It binds with high affinity, and the binding is accompanied by high quantum yield fluorescence. ⁽¹⁵¹⁾ Dimeric binding dominates with single-stranded polypyrimidines and is characterized by low affinity and low quantum yields for fluorescence. To poly (dG) TO binds both as a monomer and a dimer, and both are fluorescent species. The greatest fluorescence is observed for poly(dG)-bound TO. For both the monomer and the dimer, the quantum yield is about 0.40. ⁽¹⁵²⁾

Another example is its use as a dye for reticulocyte analysis which depends on its biological staining characteristics [Reticulocytes are immature red blood cells

(RBCs) that are created in the bone marrow and discharged into the bloodstream, where they grow into RBCs in 1 to 2 days. When it comes to anemias and bone marrow dysfunction, a rise or decrease in reticulocyte count might be a sign of erythropoiesis activity or failure, [The percentage of immature blood cells in the reticulocyte population is a diagnostic sign of erythropoietic activity].⁽¹⁵³⁾ Thiazole orange is commonly used to stain the residual RNA of blood cells in reticulocyte analysis or to stain DNA in agarose gels and capillary electrophoresis, (it is a non-precipitating dye and can permeate through the membranes of live cells.⁽¹⁵⁴⁾ TO may therefore also be used to stain live bacteria (gram-positive and gram-negative). TO is concentrated in the nucleus in live yeast but the staining is cytoplasmic after fixation. Thiazole orange initially stains mitochondria in live mammalian cells, and then redistributes to the nucleus and cytoplasm.⁽¹⁵⁵⁾

1.9 3,3'-Diethyloxycarbocyanine iodide/ DODCI.

3,3'-Diethyloxycarbocyanine iodide (DODC) in figure 28, binds primarily as dimers to the minor groove of duplex DNA, and the dimers can form higher-order structures. DODC interacts preferentially with AT- rich regions of duplex DNA,⁽¹⁵⁶⁾ this preference for AT- rich sequences is common for minor groove binders. The interactions between the dye in the minor groove's chiral environment result in an induced CD spectrum when the dyes bind to duplex DNA.⁽¹⁵⁷⁾

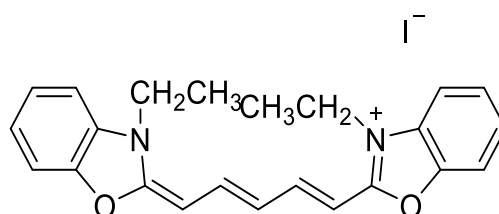


Figure 28 chemical structure of DODC

Single-molecule force spectroscopy studies have provided binding kinetics, affinity, and type. From these studies, it was found there are 3 modes of binding, viz. major-groove binding, minor-groove binding and intercalation.⁽¹⁵⁸⁾

To distinguish groove binding (either major or minor) from intercalation, energy transfer from DNA bases to the bound dye is used as indirect evidence for intercalation.⁽¹⁵⁹⁾ DNA can serve as a template and promote dimerisation and aggregation of the DODC binding to duplex DNA. Dimerisation and aggregation result in increased absorbance at shorter wavelengths, indicating straight stacking dimerization.⁽¹⁶⁰⁾ When in the presence of an aggregation template, such as duplex DNA, carbocyanine dyes can form face-to-face dimers.⁽¹⁶¹⁾ Whether the

two molecules are offset or not, the formation of a dimer may cause a wavelength shift of the main visible absorption band in either direction, depending on the dimer's conformation. The observation of a red shift of the absorption of DODC is consistent with offset aggregation, or "J aggregation" ⁽¹⁶²⁾, shown in Figure 18 above in (1.6 – Dye aggregation.)

Studies have shown that DODC also binds to quadruplex DNA. Upon interaction with quadruplex DNA, DODC shows an increase in fluorescence and an induced circular dichroism (ICD). ⁽¹⁶³⁾

DODC has been shown to interact differently with G-quadruplexes compared with interactions with single-stranded or duplex DNA. Binding modes with quadruplexes are shown in figure 29. The binding modes are external stacking, intercalating and groove binding. ⁽¹⁶⁴⁾

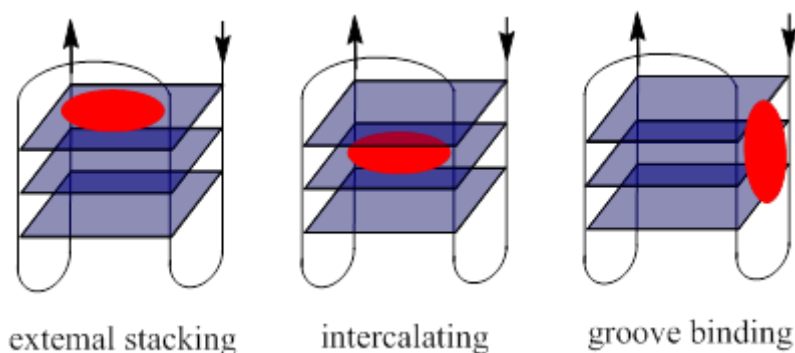


Figure 29 binding modes of DODC with G-quadruplex DNA

DODC has been found to interact differently with different quadruplex structures. Because the dG tetramers themselves are very similar among the various quadruplex DNA structures, it is possible that the dyes are binding between the DNA loops, which show a high degree of variation. It has been shown that DODC binds to quadruplex DNA in ways that rely on both the dye and the quadruplex. ⁽¹⁶⁵⁾ The data suggest that the use of DODC as reporter molecules for quadruplex DNA binding would be possible in a competition assay. A quadruplex-binding assay would then involve monitoring DODC absorption as an indicator that another molecule is competitively binding to the quadruplex, removing DODC. ⁽¹⁶⁶⁾

DODC is also used in the photosensitization of mitochondria and endoplasmic reticulum; ⁽¹⁶⁷⁾ as a conjugate for labelling cells in cytofluorometry and for imaging of carbon nanotubes (CNTs) using fluorescence microscopy. ⁽¹⁶⁸⁾ Through its staining ability, DODC can also be used in flow cytometric quantification and viability assays of spermatozoa. ⁽¹⁶⁹⁾

1.10 Fading of dyes

1.10.1 Overview

Organic colour fading is typically due to the oxidation of the chromophores within the molecules, but when nitrogen dioxide is present, the nitrosation of the organic colour usually causes the colour of the coloured material to display a more yellowish colour. Blue dyes, as well as some violets and reds, tend to be more influenced by this form of fading. This may be because of the amino groups in the molecule that move the light absorption band to longer wavelengths. ⁽¹⁷⁰⁾ Organic dyes are predominately affected by photochemical fading. The presence of oxygen, the effects of alkaline fading, the effects of sulphur dioxide and nitrogen dioxide will affect the rate constant for fading. ⁽¹⁷¹⁾ Photochemical reactions involving ultraviolet radiation and visible light are the foremost way for organic dyes to fade. The reason for the presence of a dye is for visual purposes, so photochemical fading cannot be fully excluded. Nevertheless, it has been found that there are techniques that can be used to minimise light damage and decolouration. ⁽¹⁷²⁾

Electrons are excited to a higher state as dye molecules absorb photons. In the excited state, the dyes have the ability to undergo photochemical reactions, allowing covalent bonds to be broken or allowing irreversible reactions with other molecules. As a result of these reactions, the structure of the molecules will be altered, also changing the absorption properties. ⁽¹⁷³⁾ For example, if breaking of a double bond disturbs the conjugated system, the absorbance will change to shorter wavelengths and potentially out the visible region, so a faded colour is observed. For reasonable colour-fast dyes, most of the excited molecules will either de-excite and only give off heat instead of fluorescing. The photochemical process will therefore not occur most of the time. The lower the chances of a photochemical reaction starting from the excited state, the lower the fading kinetics and the dye will continue to absorb photons until it eventually breaks down. ⁽¹⁷⁴⁾

Ultraviolet radiation (UV) is the most important factor in fading, but visible light and many other factors also play a role in the fading process. When an object is struck by UV light, the energy can break chemical bonds. This process decreases the object's vividness and intensity and is irreversible. Photofading is the name for this phenomenon. As examples, upon light exposure TF1, methylene blue, thiazole orange and 3,3'-diethylthiacyanine iodide (DODC) have all been found to fade. ⁽¹⁷⁵⁾

When a molecule absorbs a photon, it is elevated to an excited state. Before it has time to return to the ground state, the excited molecule can react with another

molecule. Such a reaction is called a bimolecular photochemical reaction. Unimolecular photochemical reactions are of importance when there is no second molecule to react with. Several factors may affect the ultimate photostability of a dye, including the nature of the light source, the dye's absorption characteristics, the lifetime of the S₁ and T states, intersystem crossing efficiency, the solvent and the presence or absence of air or humidity. ^(176,177) The theory is that the longer the molecule spends in the excited state, the greater the chance of participation in photochemical processes. Photofading reactions may be directly related to the absorption of the dye or indirect and caused by another molecule that has been photoexcited.

To avoid fading, the energy of the excited dye molecule should be dissipated before it could react, which means one needs to decrease the lifetime of the excited state. One factor to consider is water. Water has an influence that is not yet fully understood, but in nature it is assumed to be chemical. Water plays a role in oxidative fading as it can facilitate the hydrogen peroxide generation that can lead to photooxidation. ⁽¹⁷⁸⁾

1.10.2 Photochemical reactions involving singlet or triplet oxygen or ozone.

Photochemical change is governed by two basic rules: ⁽¹⁷⁹⁾

- 1) Grotthus – Draper Law, which states that only the radiation absorbed by the reacting system is effective in producing chemical change.
- 2) The Stark Einstein law, which states that each molecule taking part in a chemical reaction induced by exposure to light absorbs one quantity of light energy or one photon. ⁽¹⁸⁰⁾

We can reasonably speculate that when a photon impinges on the dye molecule, it is excited from the ground state (S₀) to a singlet excited state. The excited molecule may also undergo a process of inter system crossing (ISC) in which population is transferred from a singlet (S_n) to triplet (A_n) state which shown in figure 30 below. ⁽¹⁸¹⁾

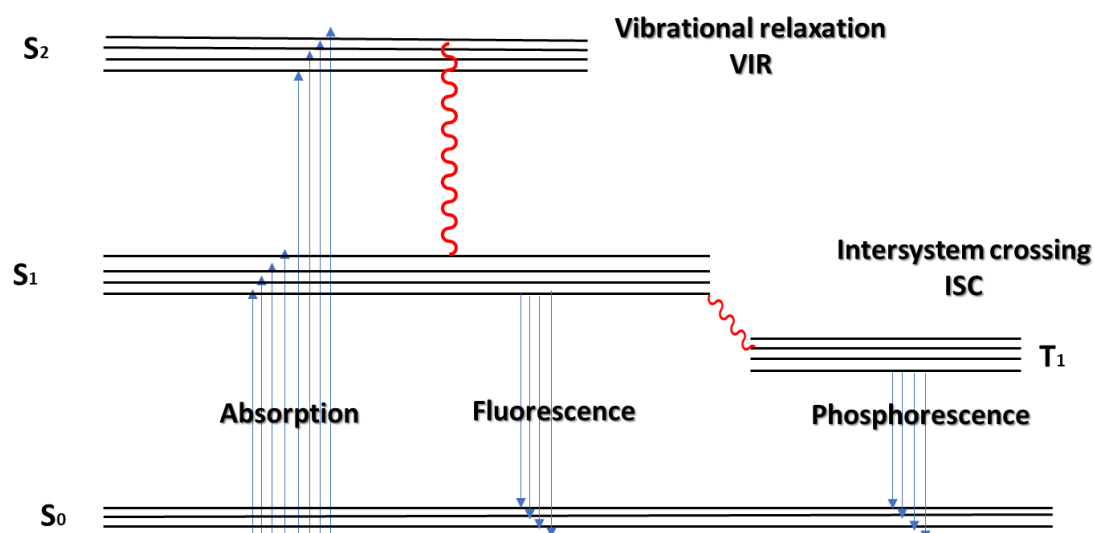


Figure 30 Scheme shows energy transfer for the cyanine dye.

The presence of oxygen in our environment can affect the fading of organic dyes. Photochemical fading of many dyes can be prevented when the air or solution surrounding the dye is oxygen-free. Oxygen-free conditions do not fully avoid fading, which may be due to the fact that oxygen-free does not always mean being fully oxygen free, allowing residual oxygen reactions. ⁽¹⁸²⁾ Nevertheless, it has been shown that eliminating oxygen and decreasing light intensity can suppress photobleaching. ⁽¹⁸³⁾

Oxygen can be involved in photochemical reactions in a variety of forms, viz. ground state triplet oxygen, singlet oxygen and ozone. In principle, both the $^1\Delta_g$ and the $^1\Sigma_g^+$ excited states can be formed (Figure 31 below) but only the $^1\Delta_g$ state has a sufficient lifetime to play a role in chemical reactions in solution. The $^1\Delta_g$ state is commonly referred to as singlet oxygen and, in the following, we follow this convention. ⁽¹⁸⁴⁾

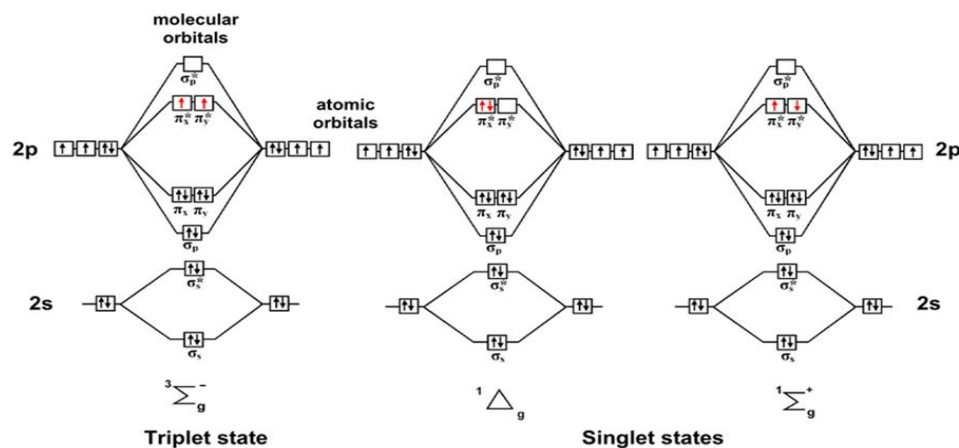


Figure 31 showed the scheme explain the triplet and singlet states of oxygen. (185)

Photosensitized generation is a process for generating $^1\text{O}_2$ from $^3\text{O}_2$ requiring only oxygen, light of a suitable wavelength, and a photosensitizer capable of absorbing and using the energy to excite oxygen to its singlet state. (186) The excitation of the sensitizer is typically accomplished through a single-photon transition from the ground state (S_0) to a singlet excited state S_n . S_n -state relaxation via internal conversion and other relaxation process yields the sensitizer S_1 state, the lowest excited singlet state. (187) The process of intersystem crossing then generates the triplet sensitizer state ($S_1 \rightarrow T_1$). Due to symmetry selection rules, the $T_1 \rightarrow S_0$ relaxation pathway is formally forbidden, thus the T_1 state exhibits a longer lifetime than that of the S_1 state (ns). This longer lifetime facilitates the ability of the triplet excited state to react in one of two ways, defined as Types I and II mechanisms. (188)

Singlet oxygen can be produced indirectly through irradiation of an organic dye sensitizers such as rose Bengal or methylene blue. In experiments where photosensitized generation of singlet oxygen is undesirable (for example in control experiments for photochemical fading), singlet oxygen can also be produced from hydrogen peroxide disproportionation catalysed by molybdate ions. (189)

One of the challenges in identifying photochemical reactivity is that excited triplet sensitizer may be subjected to radical reactions (Type I process) or may produce singlet oxygen (Type II process). The formation of superoxide (another type of reactive oxygen species) is also possible but is uncommon. Type II processes are generally preferred at low concentrations of substrates and high concentrations of oxygen (Figure 32). (190)

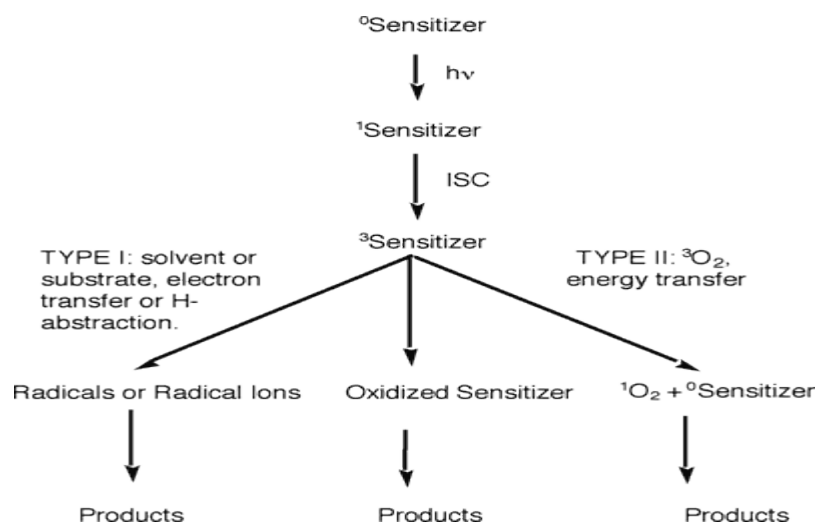


Figure 32 Possible reaction outcomes from excitation of a sensitizer.

Quenching singlet oxygen requires deactivating the excited state of the molecule. Either physical or chemical quenching can accomplish deactivation.

Physical quenching leads only to the deactivation of singlet oxygen to its ground state without oxygen consumption or product formation. ⁽¹⁹¹⁾

Physical quenching:



Here, interaction with A leads only to deactivation of singlet oxygen with no O₂ consumption or product formation. An example of physical quenching involves physical quenching of singlet oxygen by H₂O. ⁽¹⁹²⁾

Here, K_p is the equilibrium constant determined from a reaction equation's partial pressures. It is a mathematical expression for the relationship between product and reactant pressures. Although it connects the stresses, it is a unitless number. ⁽¹⁹³⁾

In chemical quenching, singlet oxygen reacts with quencher R to create RO₂.

Chemical quenching:

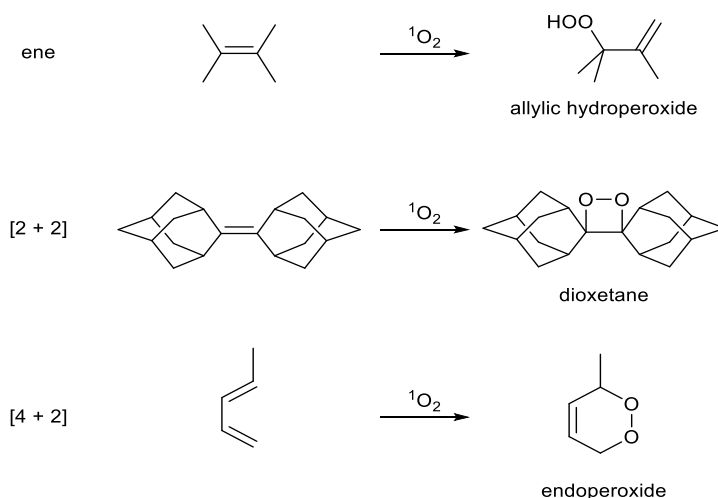


Here, K_c is the ratio of equilibrium component concentrations to equilibrium reactant concentrations increased to the power of their stoichiometric coefficients. ⁽¹⁹³⁾

To explore whether singlet oxygen is involved in a reaction, sodium azide is often used as a quencher. NaN_3 acts mainly as a physical quencher of $^1\text{O}_2$. However, NaN_3 is not specific towards $^1\text{O}_2$; it also reacts with hydroxyl radical OH , forming the azidyl radical. The N_3 -radical appears to be one of the most important one-electron oxidants used in fast-kinetic studies and in the reaction of N_3^- with OH . ⁽¹⁹⁴⁾ It is produced at a diffusion-controlled rate. The rate constants for the oxidation of a wide variety of organic substrates with azidyl radical are generally higher than those with other radicals, which indicates that azidyl radical is a very strong oxidant. When using NaN_3 as a quencher of $^1\text{O}_2$. The kinetic study revealed that N_3 quenches the reaction between nitrones and $^1\text{O}_2$ with specific rate constant k and this quenching is considered to proceed through a charge-transfer complex. ⁽¹⁹⁵⁾

Another test for the involvement of singlet oxygen in a reaction in aqueous solutions is to substitute H_2O with D_2O . The lifetime of singlet oxygen is an order of magnitude longer in D_2O than in H_2O . Reactions involving singlet oxygen in D_2O therefore proceed faster because singlet oxygen decay is less competitive with reactions with substrates. ⁽¹⁹⁶⁾

Singlet oxygen can act as a reactive intermediate and is highly electrophilic. Singlet oxygen has been found to participate in several reactions with organic molecules. The fundamental reaction types of singlet oxygen (Scheme 1) are 1) the ene-reaction, 2) the 2 + 2 cycloaddition and 3) the Diels-Alder reaction and many more. ⁽¹⁹⁷⁾



Scheme 1 ⁽¹⁹⁷⁾

In general, if a reaction is established to be a photochemical reaction. Several main potential pathways will need to be explored. If the reaction proceeds to completion even in the absence of oxygen, pathways may include type 1 reactions including attack of the solvent on the excited state or reactions with a second equivalent of the dye. If the reaction requires oxygen to proceed, the key mechanisms to explore involve generation of singlet oxygen or electron transfer reactions. ⁽¹⁹⁸⁾ Ground state triplet oxygen is unlikely to react with singlet state dyes because such a reaction would involve a triplet state transition state which would be very high in energy.

An investigation into the stability of cyanine dyes addressed the question whether these react with singlet oxygen or with other reactive oxygen species (Figure 33).

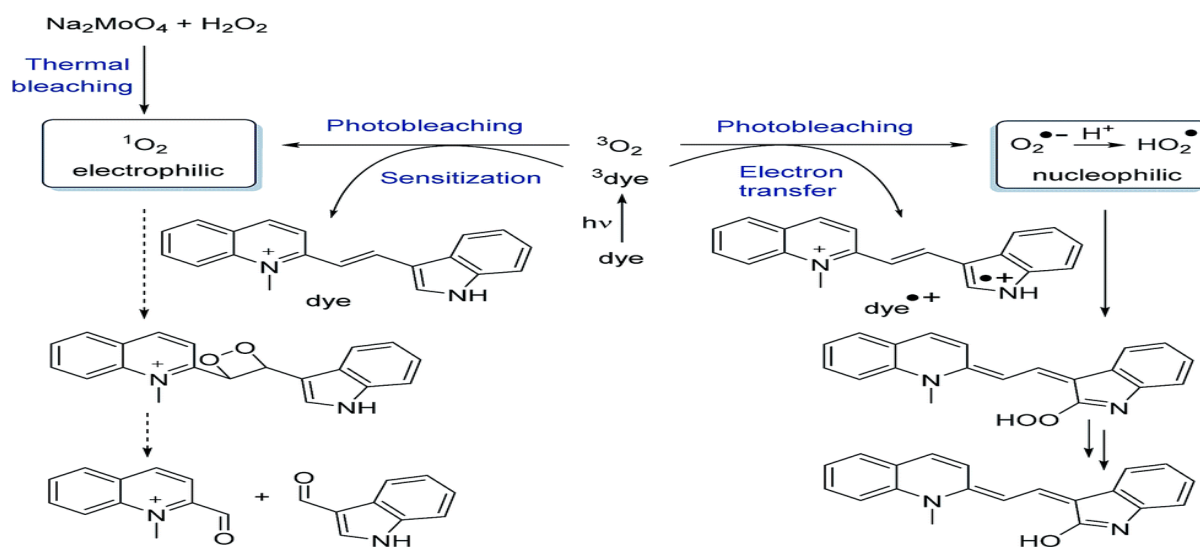


Figure 33 Quenching and proposed photodegradation pathways.
(199)

The conclusion was that type I reactions with oxygen were primary photobleaching pathways, especially by the highly reactive perhydroxyl radicals.

Similarly, the fading reactions of YO [Oxazole yellow is a DNA-binding fluorescent cyanine dye that is used to detect apoptotic cells.] and its dimer YOYO were studied. ⁽²⁰⁰⁾ The authors concluded that photofading of YO involved reactive oxygen species potentially deriving from electron transfer from excited state YO to oxygen to form $\text{O}_2^{\bullet-}$. This type of electron transfer had previously been observed by others as well. ⁽²⁰¹⁾ Photofading of YOYO was suggested to take place through reaction with singlet oxygen, however.

Polyfluorination of a cyanine dye resulted in reduced reactivity with singlet oxygen and reduced photofading.⁽²⁰²⁾ Similarly, meso-substituted thiazole orange was significantly less sensitive to singlet oxygen and to photobleaching.⁽²⁰³⁾

A very different mechanism in which reactions involving light and oxygen take place is when ultraviolet light hits oxygen molecules in the atmosphere. This process induces a photochemical reaction which separates the two oxygen atoms in O₂ which then collide with other oxygen molecules, allowing the formation of ozone (O₃).⁽²⁰⁴⁾ Since ozone is a very strong oxidising agent, it can cause dyes to fade by breaking down the molecule's conjugated system. Figure 34 shows the oxidation reaction of indigo dye (blue in colour) to isatin sulfonic acid (ISA-yellow in colour) by ozone.⁽²⁰⁵⁾

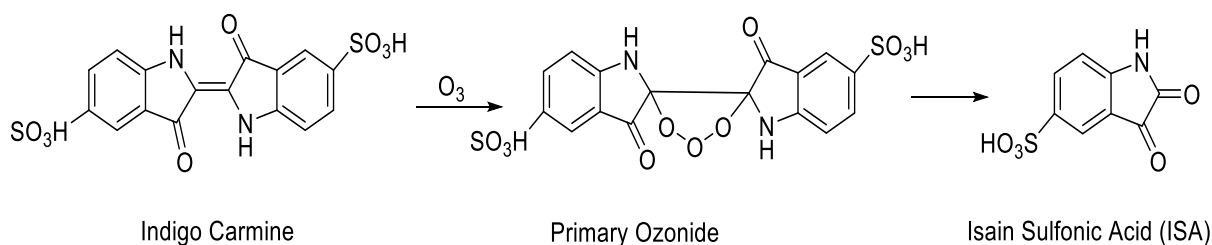


Figure 34 Reaction of Indigo oxidation by Ozone.

1.11 kinetics and mechanisms in aqueous solutions

1.11.1(Pseudo) first-order reactions

Ideally, kinetic experiments are carried out under (pseudo) first-order conditions. Pseudo first-order conditions make data analysis simpler and avoid the need to precisely know the concentration of the reaction component under study – in this thesis the reaction component under study will be the fading dye.⁽²⁰⁶⁾

In pseudo first-order kinetics, the concentration of the reaction component of interest, as well as a measurable physical property that is linear with the concentration, varies with time as given by Equation 1.⁽²⁰⁷⁾

$$signal_t = signal_{t=0} + \Delta signal \cdot (1 - e^{-k \cdot t}) \quad \text{Equation 1.}$$

In equation 1, signal_t is the measured property at time t , $\text{signal}_{t=0}$ is the signal at the start of the experiment, Δsignal is the change in the property from start to the end of the experiment, k is the observed rate constant and t is time.

The rate constant k itself depends on temperature and potentially on concentrations for other reactants if the reaction is carried out under pseudo-first-order conditions.

For the case that the reaction is first order and describes a single elementary reaction step, the observed rate constant's dependence on temperature is predicted by the Eyring equation (Equation 2).

$$k = \frac{k_B \cdot T}{h} \cdot e^{-\frac{\Delta H^{\ddagger}}{R \cdot T}} \cdot e^{\frac{\Delta S^{\ddagger}}{R}} \quad \text{Equation 2}$$

Where ΔH^{\ddagger} and ΔS^{\ddagger} are the standard molar enthalpy and standard molar entropy of activation, respectively. For higher order reactions carried out under pseudo first-order conditions, the rate constants have to be corrected for the concentration(s) of other reactant(s) before using the Eyring equation. ⁽²⁰⁸⁾

For photochemical reactions of fluorescent dyes, as studied in this thesis, the minimum kinetic scheme is shown in Figure 35.

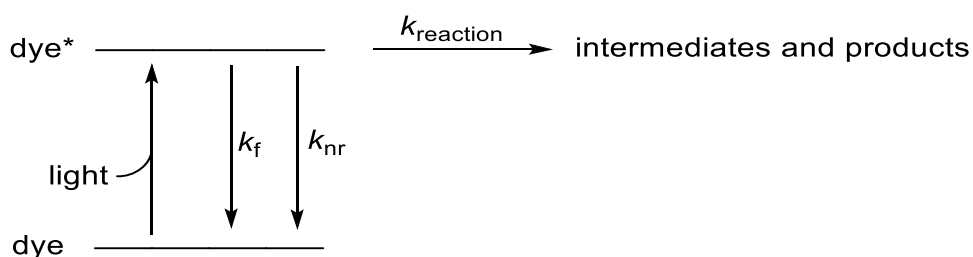


Figure 35 Minimum kinetic scheme for photofading of fluorescent dyes.

In Figure 35, the dye is excited to form the excited state dye*. This reaction step will depend on the intensity of the irradiation. The mechanistic rate constant k_{reaction} is for the reaction step towards products. This step is in competition with fluorescence and non-radiative decay with rate constants k_f and k_{nr} , respectively. As a result, the observed rate constant for the reaction will depend on the competition between the various processes. For example, if changing reaction conditions lead to increasing non-radiative decay without a concomitant increase in k_{reaction} , the observed rate constant will decrease.

1.11.2 Acid and base catalysis

In acid-base catalysis, an acid or a base is added to accelerate the chemical reaction, and the acid or base itself is not consumed in the reaction. Transfer of protons is the most common reaction mediated by enzymes. Donors and acceptors of protons, i.e. acids and base, can donate and accept protons to stabilise the developing charges in the transition state.

Acid and base catalysis usually have the effect of either activating nucleophile and electrophile groups, or stabilising leaving groups. Many biochemical catalytic acid-base reactions involve histidine because it has a pK_a close to 7 which allows it to act as both acid and a base. ⁽²⁰⁹⁾ Under physiological conditions, i.e. near pH 7, chemical reactions are usually at their slowest. For example, *in vitro*, reactive compounds are readily hydrolysed with the addition of strong acid or base. This is obviously not a practical proposition for an enzyme: in the presence of strong acid or base, proteins are denatured. ⁽²¹⁰⁾ Nevertheless, the way we think of enzyme catalysis is based on our *in-vitro* understanding of acid – base catalysis. Chemical reactions in near-neutral aqueous solutions, including photochemical reaction, involving (de)protonation processes show similar acid-base catalysis as seen in enzymes.

The pH-rate profiles shown in Figure 36 illustrate acid-base catalysis. The three plots are representative of the behaviour of most types of substrates undergoing typical reactions in water. The lower curve (I) represents the reaction of a typical unreactive compound: it only shows acid- and base-catalysed reactions, and the reaction is at least very slow near pH 7. ⁽²¹¹⁾ Curve II similarly shows acid and base catalysis but also a pH-independent region where the un catalysed reaction with water is faster than the acid- and base-catalysed reactions. Curve III is the pH-rate profile for a typical enzyme-catalysed reaction: it is much faster than the others, and it is also very different in efficiency, as the rate now reaches a maximum close to pH 7. Enzymes are 'designed' to operate close to pH 7, typically showing pH optima in this region, with rates dropping at higher and lower pH. ^(212, 213)

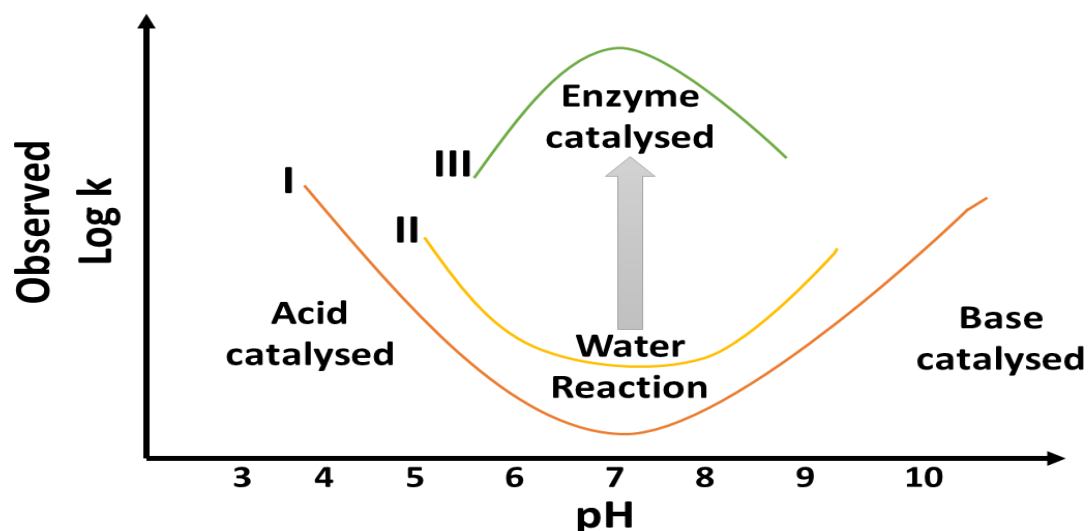
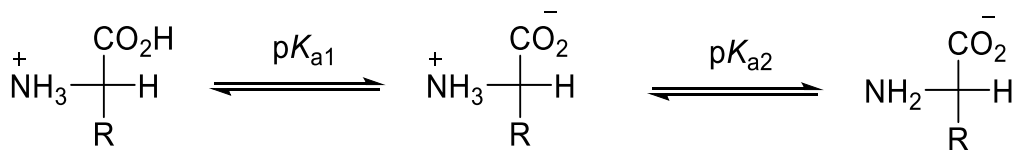


Figure 36 **The acid- and base-catalysed reactions** ⁽²¹⁴⁾

If the substrate material is sufficiently reactive (electrophilic), activation by protonation is not necessary, and the rate of attack by water on the neutral molecule near pH 7 suffices for reaction. ⁽²¹⁵⁾ Formally this produces both a positive and a negative charge, and as the reaction proceeds these will be "delocalized" through the hydrogen bond network into the surrounding solvent. A water molecule is of course the nucleophile in a hydrolysis reaction. As the new C – O bond forms, the positive charge on the nucleophilic oxygen increases, and the attached OH protons become increasingly acidic until they can be moved to solvent water, formally acting as a general base (gb). ⁽²¹⁶⁾ The negative charge that forms on, e.g., the carbonyl oxygen in an ester being hydrolysed can be similarly transferred to another water molecule through hydrogen bond or protonation. In this case, water or a weak acid acts as a general acid (ga). ⁽²¹⁷⁾

An acid or a base involved in catalysing a reaction plays a very specific role and can therefore be assumed to be present in a particular form, i.e. protonated or deprotonated. This means that reactivity will depend on pH. When two (or more) catalytic molecules are involved, it is normal for one to be active in a protonated form as a general acid and the other as a general base or nucleophile and therefore as a general base. ⁽²¹⁸⁾ The reaction's pH-rate profile then reflects the fraction of the system in the active ionic form of both groups. For example, for amino acids a single species is present at both high and low pH, as the free base or as a fully protonated form. But the fraction of the intermediate zwitterionic form between the two pK_a s increases to a maximum at a pH-halfway. If this zwitterion is the

reactive form, then the pH – rate profile at this pH should indicate a maximum.
(219)



Scheme 2 the acid-base catalysed reaction with a pH optimum.

The typical interpretations of acid and base catalysis in aqueous solutions in terms of mechanistic reaction steps are summarised in Figure 37.

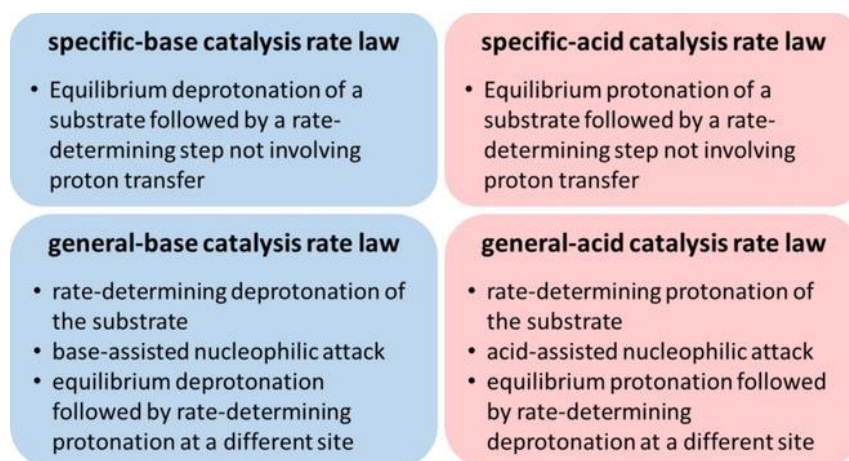


Figure 37 Typical reaction mechanisms for the different rate laws for acid and base catalysis. (220)

1.12 Aims

The aims of this thesis are to develop an experimental approach to generate reproducible kinetic data for photofading of dyes and to use this approach to study photofading of selected DNA-binding dyes.

Applications of these dyes in forensic chemistry will then be explored.

1.13 References

1. Chambers, G. K., Curtis, C., Millar, C. D., Huynen, L. & Lambert, D. M. DNA fingerprinting in zoology: past, present, future. *Investig. Genet.* **5**, 1–11 (2014).
2. Mohan, A. Fabrication of a Fiber Scanning Multiphoton Microendoscope. (2019).
3. Budowle, B., Moretti, T. R., Niezgoda, S. J. & Brown, B. L. CODIS and PCR-based short tandem repeat loci: law enforcement tools. in *Second European Symposium on Human Identification* vol. 7388 (Promega Corporation, Madison, Wisconsin, 1998).
4. Bjerkeng, B. Chromatographic analysis of synthesized astaxanthin—a handy tool for the ecologist and the forensic chemist? *Progress. Fish-Culturist* **59**, 129–140 (1997).
5. James, S. H., Nordby, J. J. & Bell, S. Forensic science: An introduction to scientific and investigative techniques: Fourth edition. *Forensic Sci. An Introd. to Sci. Investig. Tech. Fourth Ed.* 1–586 (2014) doi:10.1201/b16445.
6. Duwe, G. To what extent does civil commitment reduce sexual recidivism? Estimating the selective incapacitation effects in Minnesota. *J. Crim. Justice* **42**, 193–202 (2014).
7. Gefrides, L. & Welch, K. Forensic biology: serology and DNA. in *The forensic laboratory handbook procedures and practice* 15–50 (Springer, 2011).
8. Harper, L., Powell, J. & Pijl, E. M. An overview of forensic drug testing methods and their suitability for harm reduction point-of-care services. *Harm Reduct. J.* **14**, 1–13 (2017).
9. Drugs, U. N. O. on, Drugs, U. N. O. on, Laboratory, C. & Section, S. *Crime scene and physical evidence awareness for non-forensic personnel.* (United Nations Publications, 2009).
10. Magalhães, T., Dinis-Oliveira, R. J., Silva, B., Corte-Real, F. & Nuno Vieira, D. Biological evidence management for DNA analysis in cases of sexual assault. *Sci. World J.* **2015**, (2015).

11. Khan, P. *et al.* Luminol-based chemiluminescent signals: clinical and non-clinical application and future uses. *Appl. Biochem. Biotechnol.* **173**, 333–355 (2014).
12. Irobalieva, R. N. *et al.* Structural diversity of supercoiled DNA. *Nat. Commun.* **6**, 1–11 (2015).
13. Ogden, R. Forensic science, genetics and wildlife biology: getting the right mix for a wildlife DNA forensics lab. *Forensic Sci. Med. Pathol.* **6**, 172–179 (2010).
14. Goulka, J. E. *Toward a comparison of DNA profiling and databases in the United States and England.* (Rand Corporation, 2010).
15. Baechtel, F. S., Brown, J. & Terrell, L. D. Presumptive screening of suspected semen stain in situ using cotton swabs and bromochloroindolyl phosphate to detect prostatic acid phosphatase activity. *J. Forensic Sci.* **32**, 880–887 (1987).
16. Albrecht, C. Joseph R. Lakowicz: Principles of fluorescence spectroscopy. (2008).
17. Sheppard, N. Hydrogen bonding. *Nature* **234**, 491–492 (1971).
18. Quickenden, T. I. & Creamer, J. I. A study of common interferences with the forensic luminol test for blood. *Luminescence* **16**, 295–298 (2001).
19. Barni, F., Lewis, S. W., Berti, A., Miskelly, G. M. & Lago, G. Forensic application of the luminol reaction as a presumptive test for latent blood detection. *Talanta* **72**, 896–913 (2007).
20. <https://en.wikipedia.org/wiki/Luminol>. (*accessed 13 November 2019*).
21. Proescher, F. & Moody, A. M. Detection of blood by means of chemiluminescence. *J Lab Clin Med* **24**, 1183–1189 (1939).
22. James, S. H., Kish, P. E. & Sutton, T. P. *Principles of bloodstain pattern analysis: theory and practice.* (CRC press, 2005).
23. Patel, G. & Hopwood, A. An evaluation of luminol formulations and their effect on DNA profiling. *Int. J. Legal Med.* **127**, 723–729 (2013).
24. Polacco, S., Wilson, P., Illes, M. & Stotesbury, T. Quantifying chemiluminescence of the forensic luminol test for ovine blood in a dilution and time series. *Forensic Sci. Int.* **290**, 36–41 (2018).

25. Gardner, E. T. Ability of Bluestar Forensics and Luminol to Reveal Latent Bloodstains Exposed to Extreme Outdoor Conditions. *J. Forensic Identif.* **67**, (2017).
26. Sorum, E. D. Identifying a false positive reaction from Bluestar on nonporous surfaces. *J. Forensic Identif.* **63**, 660 (2013).
27. Houck, M. M. & Siegel, J. A. *Fundamentals of forensic science*. (Academic Press, 2009).
28. Dutelle, A. W. & Becker, R. F. *Criminal Investigation*. (Jones & Bartlett Learning, 2018).
29. Lee, J. B., Levy, M. & Walker, A. Use of a forensic technique to identify blood contamination of emergency department and ambulance trauma equipment. *Emerg. Med. J.* **23**, 73–75 (2006).
30. Crowe, G., Moss, D. & Elliot, D. The effect of laundering on the detection of acid phosphatase and spermatozoa on cotton t-shirts. *Can. Soc. Forensic Sci. J.* **33**, 1–5 (2000).
31. Virkler, K. & Lednev, I. K. Analysis of body fluids for forensic purposes: from laboratory testing to non-destructive rapid confirmatory identification at a crime scene. *Forensic Sci. Int.* **188**, 1–17 (2009).
32. Lichtman, J. W. & Conchello, J.-A. Fluorescence microscopy. *Nat. Methods* **2**, 910–919 (2005).
33. Gaensslen, R. E. *Sourcebook in forensic serology, immunology, and biochemistry*. (US Department of Justice, National Institute of Justice Washington, DC, 1983).
34. Viner, T. C., Kagan, R. A. & Johnson, J. L. Using an alternate light source to detect electrically singed feathers and hair in a forensic setting. *Forensic Sci. Int.* **234**, e25–e29 (2014).
35. Nelson, D. G. & Santucci, K. A. An alternate light source to detect semen. *Acad. Emerg. Med.* **9**, 1045–1048 (2002).
36. Marin, N. & Buszka, J. M. *Alternate light source imaging: forensic photography techniques*. (Routledge, 2013).
37. Pollanen, M. S. Forensic Science in Canada: Report of a Multidisciplinary Discussion. *Can. J. Pathol.* **6**, (2014).

38. Carter-Snell, C. & Soltys, K. Forensic ultraviolet lights in clinical practice: evidence for the evidence. *Can. J. Police Secur. Serv.* **3**, 79–85 (2005).
39. Hetheridge, M. J. An evaluation of the environmental fate of reactive dyes. (2001).
40. Johari, D. P. Studies in the light fading of dyes. (1967).
41. Fähnrich, K. A., Pravda, M. & Guilbault, G. G. Recent applications of electrogenerated chemiluminescence in chemical analysis. *Talanta* **54**, 531–559 (2001).
42. Huntress, E., Stanley, L. & Parker, A. The preparation of 3-aminophthalhydrazide for use in the demonstration of chemiluminescence. *J. Am. Chem. Soc.* **56**, 241–242 (1934).
43. Pollitt, E. N. *et al.* Alternate light source findings of common topical products. *J. Forensic Nurs.* **11**, 97 (2016).
44. Mamedov, S., Goldey, J., Whitley, A. & Vezard, N. Forensics applications of X-ray fluorescence spectroscopy in combination with advanced light source sample discovery. *Spectrosc. THEN EUGENE THEN DULUTH-* **22**, 9 (2007).
45. Kasper, S. P. *Latent print processing guide*. (Academic Press, 2015).
46. Penven, D. Latent Blood Prints—Methods For Chemical Enhancement. *No Rec. Crime Scene Investig. Netw.* **22**, (2013).
47. Eckert, W. G. & James, S. H. *Interpretation of bloodstain evidence at crime scenes*. (CRC press, 1998).
48. Kobus, H. J., Stoilovic, M. & Warrenner, R. N. A simple luminescent post-ninhydrin treatment for the improved visualisation of fingerprints on documents in cases where ninhydrin alone gives poor results. *Forensic Sci. Int.* **22**, 161–170 (1983).
49. Hazarika, P. & Russell, D. A. Advances in fingerprint analysis. *Angew. Chemie Int. Ed.* **51**, 3524–3531 (2012).
50. Kanjanawarut, R., Yuan, B. & XiaoDi, S. UV-vis spectroscopy and dynamic light scattering study of gold nanorods aggregation. *Nucleic Acid Ther.* **23**, 273–280 (2013).
51. Bumbrah, G. S. Cyanoacrylate fuming method for detection of latent

- fingermarks: a review. *Egypt. J. forensic Sci.* **7**, 1–8 (2017).
52. An, J.-H., Shin, K.-J., Yang, W.-I. & Lee, H.-Y. 88. Hetheridge, M. J. (2001). An evaluation of the environmental fate of reactive dyes. *BMB Rep.* **45**, 545–553 (2012).
 53. Baxter Jr, E. *Complete crime scene investigation handbook*. (CRC press, 2015).
 54. Shah, B. C. Novel fingerprint development techniques. (2013).
 55. Guastalli, H. Training of Law Enforcement and Crime Scene Personnel in the field of Latent Prints; ability to identify ridge detail may help reduce backlog within the public crime laboratory system. (2016).
 56. Sato, I., Hamabe, T., Yamazaki, K. & Watanabe, Y. A new method for the determination of the ABO blood type of semen by immunoblotting using anti-ABH antibodies following immunoprecipitation. *J. Immunol. Methods* **188**, 229–237 (1995).
 57. Li, R. Forensic serology. *Forensic Chem. handbook. 1st ed. Hoboken, NJ John Wiley Sons* 269–290 (2012).
 58. Finnis, J., Lewis, J. & Davidson, A. Comparison of methods for visualizing blood on dark surfaces. *Sci. Justice* **53**, 178–186 (2013).
 59. Mittal, S., Bansal, V., Garg, S. K., Atreja, G. & Bansal, S. The diagnostic role of saliva: a review. (2011).
 60. Wong, D. T. Salivary diagnostics powered by nanotechnologies, proteomics and genomics. *J. Am. Dent. Assoc.* **137**, 313–321 (2006).
 61. Gröschl, M. Current status of salivary hormone analysis. in *Annales de biologie clinique* vol. 67 493–504 (2009).
 62. Yousif, E. & Haddad, R. Photodegradation and photostabilization of polymers, especially polystyrene. *Springerplus* **2**, 1–32 (2013).
 63. Weinstein, L. A. Electromagnetic waves. *Radio i svyaz', Moscow* (1988).
 64. [Http://hyperphysics.phy-astr.gsu.edu/hbase/ems1.html](http://hyperphysics.phy-astr.gsu.edu/hbase/ems1.html). hyperphysics.
 65. Pirogova, E., Vojisavljevic, V. & Cosic, I. Biological effects of electromagnetic radiation. *Biomed. Eng. (NY)*. 87–106 (2009).
 66. Sliney, D. H., Bitran, M. & Murray, W. Infrared, Visible, and Ultraviolet Radiation. *Patty's Toxicol.* 169–208 (2001).

67. Elert, G. The Electromagnetic Spectrum, The Physics Hypertextbook. *Hypertextbook. com* (1998).
68. Radebner, J. *et al.* Tetraacylgermanes: highly efficient photoinitiators for visible-light-induced free-radical polymerization. *Angew. Chemie Int. Ed.* **56**, 3103–3107 (2017).
69. Trypsteen, M. F. M. & Walker, R. *Spectroscopy for amateur astronomers: recording, processing, analysis and interpretation.* (Cambridge University Press, 2017).
70. Council, N. R. Background Information and Scientific Principles. in *Health Effects of Exposure to Low Levels of Ionizing Radiation: Beir V* (National Academies Press (US), 1990).
71. Haugland, R. P. *Handbook of fluorescent probes and research chemicals.* (Molecular Probes, 1992).
72. Martin, J. E. *Physics for radiation protection.* (Wiley Online Library, 2013).
73. Barrett, J. *Atomic structure and periodicity.* vol. 9 (Royal Society of Chemistry, 2002).
74. Harris, D. C. & Bertolucci, M. D. *Symmetry and spectroscopy: an introduction to vibrational and electronic spectroscopy.* (Courier Corporation, 1989).
75. Braude, E. A. & Nachod, F. C. *Determination of organic structures by physical methods.* (Elsevier, 2013).
76. Wiese, W. L., Smith, M. W. & Glennon, B. M. Atomic transition probabilities. volume i. hydrogen through neon. (1966).
77. Potekhin, A. Y. Structure and radiative transitions of the hydrogen atom moving in a strong magnetic field. *J. Phys. B At. Mol. Opt. Phys.* **27**, 1073 (1994).
78.

https://www.api.simply.science/images/content/chemistry/structure_of_matter/atomic_structure/conceptmap/Hydrogen_Spectra.html. vol. 64 816–820 (2006).
79. Shindy, H. Basics in colors, dyes and pigments chemistry: A review. *Chem. Int* **2**, 2016 (2016).

80. Chem 2223b Intersession 2008 : Colours and Chromophores. 1–23 (2008).
81. Cancer, I. A. for R. on. *Some aromatic amines, organic dyes, and related exposures*. vol. 99 (IARC Press, International Agency for Research on Cancer, 2010).
82. Tewari, K. S. & Vishnoi, N. K. *A textbook of organic chemistry*. (Vikas Publishing House, 1976).
83. Gürses, A., Açıkyıldız, M., Güneş, K. & Gürses, M. S. Dyes and pigments: their structure and properties. in *Dyes and Pigments* 13–29 (Springer, 2016).
84. Shahid, M. & Mohammad, F. Recent advancements in natural dye applications: a review. *J. Clean. Prod.* **53**, 310–331 (2013).
85. Bien, H., Stawitz, J. & Wunderlich, K. Anthraquinone dyes and intermediates. *Ullmann's Encycl. Ind. Chem.* (2000).
86. El Harfi, S. & El Harfi, A. Classifications, properties and applications of textile dyes: A review. *Appl. J. Environ. Eng. Sci.* **3**, 0–3 (2017).
87. Goodwin, J. *Dyer's manual*. (1982).
88. Booth, G., Zollinger, H., McLaren, K., Sharples, W. G. & Westwell, A. Dyes, general survey. *Ullmann's Encycl. Ind. Chem.* (2000).
89. Itoh, T. Fluorescence and phosphorescence from higher excited states of organic molecules. *Chem. Rev.* **112**, 4541–4568 (2012).
90. Chan, B. Biomedical Applications of Photochemistry. *Tissue Eng. Part B. Rev.* **16**, 509–522 (2010).
91. Mataga, N. & Kubota, T. Molecular interactions and electronic spectra. (1970).
92. Jaffé, H. H. & Miller, A. L. The fates of electronic excitation energy. *J. Chem. Educ.* **43**, 469 (1966).
93. Priestley, E. B. & Haug, A. Phosphorescence spectrum of pure crystalline naphthalene. *J. Chem. Phys.* **49**, 622–629 (1968).
94. Berezin, M. Y. & Achilefu, S. Fluorescence lifetime measurements and biological imaging. *Chem. Rev.* **110**, 2641–2684 (2010).

95. Shinde, K. N., Dhoble, S. J., Swart, H. C. & Park, K. Basic mechanisms of photoluminescence. in *Phosphate Phosphors for Solid-State Lighting* 41–59 (Springer, 2012).
96. Eftink, M. R. Fluorescence quenching: theory and applications. in *Topics in fluorescence spectroscopy* 53–126 (Springer, 2002).
97. Wang, L., Liu, D., He, N., Jacques, S. L. & Thomsen, S. L. Biological laser action. *Appl. Opt.* **35**, 1775–1779 (1996).
98. Budowle, B., Leggitt, J. L., Defenbaugh, D. A., Keys, K. M. & Malkiewicz, S. F. The presumptive reagent fluorescein for detection of dilute bloodstains and subsequent STR typing of recovered DNA. *J. forensic Sci.* **45**, 1090–1092 (2000).
99. Patil, J. B., Kenny, R. S., Chindarkar, N. R. & Mashelkar, U. C. Synthesis and fluorescence studies of benzothiazole and 4, 5-diarylimidazole substituted 2H-1-benzo/naphthopyran-2-one. (2016).
100. Zhang, J., Chen, A., Wang, L., Li, X. & Huang, W. Striving toward visible light photocatalytic water splitting based on natural silicate clay mineral: the interface modification of attapulgite at the atomic-molecular level. *ACS Sustain. Chem. Eng.* **4**, 4601–4607 (2016).
101. Clark, M. *Handbook of Textile and Industrial Dyeing: Volume 2: Applications of Dyes*. (Elsevier, 2011).
102. Clarke, R. M. *et al.* Electronic Structure Description of a Doubly Oxidized Bimetallic Cobalt Complex with Proradical Ligands. *Inorg. Chem.* **55**, 762–774 (2016).
103. Ziarani, G. M., Moradi, R., Lashgari, N. & Kruger, H. G. *Metal-free synthetic organic dyes*. (Elsevier, 2018).
104. Bricks, J. L., Slominskii, Y. L., Panas, I. D. & Demchenko, A. P. Fluorescent J-aggregates of cyanine dyes: basic research and applications review. *Methods Appl. Fluoresc.* **6**, 12001 (2017).
105. Elmorsi, T. M., Riyad, Y. M., Mohamed, Z. H. & Abd El Bary, H. M. H. Decolorization of Mordant red 73 azo dye in water using H₂O₂/UV and photo-Fenton treatment. *J. Hazard. Mater.* **174**, 352–358 (2010).
106. AlHamedi, F. H., Rauf, M. A. & Ashraf, S. S. Degradation studies of Rhodamine B in the presence of UV/H₂O₂. *Desalination* **239**, 159–166 (2009).

107. Kasha, M. Characterization of electronic transitions in complex molecules. *Discuss. Faraday Soc.* **9**, 14–19 (1950).
108. McNaught, A. D. & Wilkinson, A. Compendium of chemical terminology. IUPAC recommendations. (1997).
109. Festa, G. *et al.* Aggregation states of A β 1–40, A β 1–42 and A β p3–42 amyloid beta peptides: A SANS study. *Int. J. Mol. Sci.* **20**, 4126 (2019).
110. Das, S. & Purkayastha, P. Modulating Thiazole Orange Aggregation in Giant Lipid Vesicles: Photophysical Study Associated with FLIM and FCS. *ACS omega* **2**, 5036–5043 (2017).
111. Oh, J.-W. *et al.* Ultrafast energy transfer in J-aggregate on AgBr microcrystals: its dependence on dye coverage. *Chem. Phys. Lett.* **352**, 357–362 (2002).
112. Mashaghi, A. & Katan, A. A physicist's view of DNA. *arXiv Prepr. arXiv1311.2545* (2013).
113. Venter, J. C. *et al.* The sequence of the human genome. *Science* (80-.). **291**, 1304–1351 (2001).
114. Dahm, R. Friedrich Miescher and the discovery of DNA. *Dev. Biol.* **278**, 274–288 (2005).
115. Olby, R. C. *The path to the double helix: the discovery of DNA*. (Courier Corporation, 1994).
116. <https://sciencenotes.org/dna-vs-rna-similarities-and-differences/>. DNA figure.
117. Rashid, N., Imanaka, H., Fukui, T., Atomi, H. & Imanaka, T. Presence of a novel phosphopentomutase and a 2-deoxyribose 5-phosphate aldolase reveals a metabolic link between pentoses and central carbon metabolism in the hyperthermophilic archaeon *Thermococcus kodakaraensis*. *J. Bacteriol.* **186**, 4185–4191 (2004).
118. Lagoja, I. M. Pyrimidine as constituent of natural biologically active compounds. *Chem. Biodivers.* **2**, 1–50 (2005).
119. Frank-Kamenetskii, M. D. DNA and RNA, Biophysical Aspects. (2005).
120. Steenken, S. Purine bases, nucleosides, and nucleotides: aqueous solution redox chemistry and transformation reactions of their radical cations and e- and OH adducts. *Chem. Rev.* **89**, 503–520 (1989).

121. Berens, R. L., Krug, E. C. & Marr, J. J. Purine and pyrimidine metabolism. in *Biochemistry and molecular biology of parasites* 89–117 (Elsevier, 1995).
122. Rodgers, M. H. Discovery of the Structure of DNA. *Sci. Technol. Soc. A Student-Led Explor.* (2020).
123. Pray, L. Discovery of DNA structure and function: Watson and Crick. *Nat. Educ.* **1**, (2008).
124. Dickerson, R. E. *et al.* The anatomy of a-, b-, and z-dna. *Science* (80-.). **216**, 475–485 (1982).
125. Schweitzer, B. A. & Kool, E. T. Hydrophobic, non-hydrogen-bonding bases and base pairs in DNA. *J. Am. Chem. Soc.* **117**, 1863–1872 (1995).
126. Luzzati, V., Masson, F. & Lerman, L. S. Interaction of DNA and proflavine: a small-angle x-ray scattering study. *J. Mol. Biol.* **3**, 634–639 (1961).
127. Wanunu, M. & Tor, Y. *Methods for studying nucleic acid/drug interactions.* (CRC Press, 2011).
128. Tsai, C.-C., Jain, S. C. & Sobell, H. M. Drug—nucleic acid interaction: X-ray crystallographic determination of an ethidium—dinucleoside monophosphate crystalline complex, ethidium: 5-iodouridylyl (3'-5') adenosine. *Philos. Trans. R. Soc. London. B, Biol. Sci.* **272**, 137–146 (1975).
129. Onoa, G. B., Cervantes, G., Moreno, V. & Prieto, M. J. Study of the interaction of DNA with cisplatin and other Pd (II) and Pt (II) complexes by atomic force microscopy. *Nucleic Acids Res.* **26**, 1473–1480 (1998).
130. Sha, Y., Chen, X., Niu, B. & Chen, Q. The interaction mode of groove binding between quercetin and calf thymus DNA based on spectrometry and simulation. *Chem. Biodivers.* **14**, e1700133 (2017).
131. Lodish, H. *et al.* *Molecular cell biology.* (Macmillan, 2008).
132. Zhou, H.-X. & Pang, X. Electrostatic interactions in protein structure, folding, binding, and condensation. *Chem. Rev.* **118**, 1691–1741 (2018).
133. Hendry, L. B., Mahesh, V. B., Bransome Jr, E. D. & Ewing, D. E. Small molecule intercalation with double stranded DNA: implications for normal gene regulation and for predicting the biological efficacy and genotoxicity of drugs and other chemicals. *Mutat. Res. Mol. Mech. Mutagen.* **623**, 53–

- 71 (2007).
134. Faddeeva, M. D. & Beliaeva, T. N. DNA intercalators: their interaction with DNA and other cell components and their use in biological research. *Tsitologiia* **33**, 3–31 (1991).
 135. Rohs, R. *et al.* Origins of specificity in protein-DNA recognition. *Annu. Rev. Biochem.* **79**, 233–269 (2010).
 136. Berger, M. F. *et al.* Variation in homeodomain DNA binding revealed by high-resolution analysis of sequence preferences. *Cell* **133**, 1266–1276 (2008).
 137. Biver, T., De Biasi, A., Secco, F., Venturini, M. & Yarmoluk, S. Cyanine dyes as intercalating agents: kinetic and thermodynamic studies on the DNA/Cyan40 and DNA/CCyan2 systems. *Biophys. J.* **89**, 374–383 (2005).
 138. Diwu, Z., Zhang, C., Klaubert, D. H. & Haugland, R. P. Fluorescent molecular probes VI: The spectral properties and potential biological applications of water-soluble DapoxylTM sulfonic acid. *J. Photochem. Photobiol. A Chem.* **131**, 95–100 (2000).
 139. Carreon, J. R., Mahon, K. P. & Kelley, S. O. Thiazole orange–peptide conjugates: sensitivity of DNA binding to chemical structure. *Org. Lett.* **6**, 517–519 (2004).
 140. Norman, D. G., Grainger, R. J., Uhrin, D. & Lilley, D. M. J. Location of cyanine-3 on double-stranded DNA: importance for fluorescence resonance energy transfer studies. *Biochemistry* **39**, 6317–6324 (2000).
 141. Rye, H. S. *et al.* Stable fluorescent complexes of double-stranded DNA with bis-intercalating asymmetric cyanine dyes: properties and applications. *Nucleic Acids Res.* **20**, 2803–2812 (1992).
 142. Liang, M. *et al.* A convenient thiazole orange fluorescence assay for the evaluation of DNA duplex hybridization stability. *Mol. imaging Biol.* **11**, 439 (2009).
 143. Svanvik, N., Westman, G., Wang, D. & Kubista, M. Light-up probes: thiazole orange-conjugated peptide nucleic acid for detection of target nucleic acid in homogeneous solution. *Anal. Biochem.* **281**, 26–35 (2000).
 144. Zhu, C.-Q. *et al.* Fluorescence enhancement method for the determination of nucleic acids using cationic cyanine as a fluorescence probe. *Analyst* **129**, 254–258 (2004).

145. Daniel, D. C., Thompson, M. & Woodbury, N. W. Fluorescence intensity fluctuations of individual labeled DNA fragments and a DNA binding protein in solution at the single molecule level: a comparison of photobleaching, diffusion, and binding dynamics. *J. Phys. Chem. B* **104**, 1382–1390 (2000).
146. Walsh, S. & Brown, T. Glen Report 32.11: Thiazole Orange as a Fluorogenic Reporter in Oligonucleotide Probes.
147. Schwechheimer, C., Rönicke, F., Schepers, U. & Wagenknecht, H.-A. A new structure–activity relationship for cyanine dyes to improve photostability and fluorescence properties for live cell imaging. *Chem. Sci.* **9**, 6557–6563 (2018).
148. Bohländer, P. R. & Wagenknecht, H.-A. Synthesis and evaluation of cyanine–styryl dyes with enhanced photostability for fluorescent DNA staining. *Org. Biomol. Chem.* **11**, 7458–7462 (2013).
149. Tomoike, F. & Abe, H. RNA imaging by chemical probes. *Adv. Drug Deliv. Rev.* **147**, 44–58 (2019).
150. Santangelo, P. J., Alonas, E., Jung, J., Lifland, A. W. & Zurla, C. Probes for intracellular RNA imaging in live cells. *Methods Enzymol.* **505**, 383–399 (2012).
151. Fang, W.-J. *et al.* A DNA minor groove binder shows high effectiveness as a quencher for FRET probes. *Bioorg. Med. Chem. Lett.* **24**, 3956–3960 (2014).
152. Lubitz, I., Zikich, D. & Kotlyar, A. Specific high-affinity binding of thiazole orange to triplex and G-quadruplex DNA. *Biochemistry* **49**, 3567–3574 (2010).
153. Lee, L. G., Chen, C.-H. & Chiu, L. A. Thiazole orange: A new dye for reticulocyte analysis. *Cytometry* **7**, 508–517 (1986).
154. Lee, L. G., Chen, C. & Chiu, L. A. Thiazole orange: a new dye for reticulocyte analysis. *Cytom. J. Int. Soc. Anal. Cytol.* **7**, 508–517 (1986).
155. <https://biotium.com/product/thiazole-orange-10-mm-in-dmsol/>.
156. Silva, G. L., Ediz, V., Yaron, D. & Armitage, B. A. Experimental and Computational Investigation of Unsymmetrical Cyanine Dyes: Understanding Torsionally Responsive Fluorogenic Dyes. *J. Am. Chem. Soc.* **129**, 5710–5718 (2007).

157. Cao, R., Venezia, C. F. & Armitage, B. A. Investigation of DNA binding modes for a symmetrical cyanine dye trication: effect of DNA sequence and structure. *J. Biomol. Struct. Dyn.* **18**, 844–857 (2001).
158. Holmgaard List, N. *et al.* Origin of DNA-Induced Circular Dichroism in a Minor-Groove Binder. *J. Am. Chem. Soc.* **139**, 14947–14953 (2017).
159. Zhang, S. *et al.* A bright red fluorescent cyanine dye for live-cell nucleic acid imaging, with high photostability and a large Stokes shift. *J. Mater. Chem. B* **2**, 2688–2693 (2014).
160. Sovenyhazy, K. M., Bordelon, J. A. & Petty, J. T. Spectroscopic studies of the multiple binding modes of a trimethine-bridged cyanine dye with DNA. *Nucleic Acids Res.* **31**, 2561–2569 (2003).
161. Kellett, A., Molphy, Z., Slator, C., McKee, V. & Farrell, N. P. Molecular methods for assessment of non-covalent metallodrug–DNA interactions. *Chem. Soc. Rev.* **48**, 971–988 (2019).
162. Cannon, B. L. *et al.* Coherent exciton delocalization in a two-state DNA-templated dye aggregate system. *J. Phys. Chem. A* **121**, 6905–6916 (2017).
163. Sengupta, B., Pahari, B., Blackmon, L. & Sengupta, P. K. Prospect of bioflavonoid fisetin as a quadruplex DNA ligand: a biophysical approach. *PLoS One* **8**, e65383–e65383 (2013).
164. Xiong, Y.-X., Huang, Z.-S. & Tan, J.-H. Targeting G-quadruplex nucleic acids with heterocyclic alkaloids and their derivatives. *Eur. J. Med. Chem.* **97**, 538–551 (2015).
165. Cocco, M. J., Hanakahi, L. A., Huber, M. D. & Maizels, N. Specific interactions of distamycin with G-quadruplex DNA. *Nucleic Acids Res.* **31**, 2944–2951 (2003).
166. Chen, Q., Kuntz, I. D. & Shafer, R. H. Spectroscopic recognition of guanine dimeric hairpin quadruplexes by a carbocyanine dye. *Proc. Natl. Acad. Sci.* **93**, 2635–2639 (1996).
167. Garoff, R. A., Litzinger, E. A., Connor, R. E., Fishman, I. & Armitage, B. A. Helical aggregation of cyanine dyes on DNA templates: Effect of dye structure on formation of homo- and heteroaggregates. *Langmuir* **18**, 6330–6337 (2002).

168. Novo, D., Perlmutter, N. G., Hunt, R. H. & Shapiro, H. M. Accurate flow cytometric membrane potential measurement in bacteria using diethyloxycarbocyanine and a ratiometric technique. *Cytom. J. Int. Soc. Anal. Cytol.* **35**, 55–63 (1999).
169. Gallon, F., Marchetti, C., Jouy, N. & Marchetti, P. The functionality of mitochondria differentiates human spermatozoa with high and low fertilizing capability. *Fertil. Steril.* **86**, 1526–1530 (2006).
170. BEEK, H. C. A. V. A. N. & Heertjes, P. M. Fading by light of organic dyes on textiles and other materials. *Stud. Conserv.* **11**, 123–132 (1966).
171. Berrie, B. H. & Strumfels, Y. Change is permanent: thoughts on the fading of cochineal-based watercolor pigments. *Herit. Sci.* **5**, 1–9 (2017).
172. Forster, A. L., Bitter, J. L., Rosenthal, S., Brooks, S. & Watson, S. S. Photofading in cotton fibers dyed using red, yellow, and blue direct dyes during examination with microspectrophotometry (MSP). *Forensic Chem.* **5**, 72–78 (2017).
173. Hu, X., McFadden, M. E., Barber, R. W. & Robb, M. J. Mechanochemical Regulation of a Photochemical Reaction. *J. Am. Chem. Soc.* **140**, 14073–14077 (2018).
174. Menzel, R. *Photonics: linear and nonlinear interactions of laser light and matter*. (Springer Science & Business Media, 2013).
175. Scarlett, W. L. Ultraviolet radiation: sun exposure, tanning beds, and vitamin D levels. What you need to know and how to decrease the risk of skin cancer. *J. Am. Osteopath. Assoc.* **103**, 371–375 (2003).
176. Kimura, S. *et al.* A luminescent organic radical with two pyridyl groups: high photostability and dual stimuli-responsive properties, with theoretical analyses of photophysical processes. *Chem. Sci.* **9**, 1996–2007 (2018).
177. Ji, Y. *et al.* LED-Illuminated NMR Spectroscopy: A Practical Tool for Mechanistic Studies of Photochemical Reactions. *ChemPhotoChem* **3**, 984–992 (2019).
178. Glusac, K. What has light ever done for chemistry? *Nat. Chem.* **8**, 734–735 (2016).
179. Iii, U. & Introduction, P. Lecture - Photochem & Spectroscopy. (2000).
180. Beeler, A. B. Introduction: Photochemistry in organic synthesis. *Chem. Rev.* **116**, 9629–9630 (2016).

181. Wardle, B. *Principles and applications of photochemistry*. (John Wiley & Sons, 2009).
182. Arney, J. S., Jacobs, A. J. & Newman, R. The influence of oxygen on the fading of organic colorants. *J. Am. Inst. Conserv.* **18**, 108–117 (1979).
183. Bernas, T., Zarębski, M., Cook, R. R. & Dobrucki, J. W. Minimizing photobleaching during confocal microscopy of fluorescent probes bound to chromatin: Role of anoxia and photon flux. *J. Microsc.* **215**, 281–296 (2004).
184. Clennan, E. L. New mechanistic and synthetic aspects of singlet oxygen chemistry. *Tetrahedron* **47**, 9151–9179 (2000).
185. Scholz, M. *Methods of Study of Photosensitizer-Photophysics with Application on Thiazolyl-porphyrins*. (2011). doi:10.13140/RG.2.1.2052.7768.
186. Krishna, M. M. G. & Periasamy, N. Spectrally constrained global analysis of fluorescence decays in biomembrane systems. *Anal. Biochem.* **253**, 1–7 (1997).
187. Vysniauskas, A. *Molecular rotors as sensors of microscopic viscosity and temperature*. (2016).
188. Herman, B., Lakowicz, J. R., Murphy, D. B., Fellers, T. J. & Davidson, M. W. *Fluorescence excitation and emission fundamentals*. 2008). <http://www.olympusfluoview.com/theory/fluoroexciteemit.html> (2009).
189. Boehme, K. & Brauer, H. D. Generation of singlet oxygen from hydrogen peroxide disproportionation catalyzed by molybdate ions. *Inorg. Chem.* **31**, 3468–3471 (1992).
190. Ni, J., Wang, Y., Zhang, H., Sun, J. Z. & Tang, B. Z. Aggregation-Induced Generation of Reactive Oxygen Species: Mechanism and Photosensitizer Construction. *Molecules* **26**, 268 (2021).
191. Lovell, J. F. *et al.* FRET quenching of photosensitizer singlet oxygen generation. *J. Phys. Chem. B* **113**, 3203–3211 (2009).
192. Aramendia, P. F., Negri, R. M. & Roman, E. S. Temperature dependence of fluorescence and photoisomerization in symmetric carbocyanines. Influence of medium viscosity and molecular structure. *J. Phys. Chem.* **98**, 3165–3173 (1994).

193. De Nevers, N. *Physical and chemical equilibrium for chemical engineers*. (Wiley Online Library, 2012).
194. Bancirova, M. Sodium azide as a specific quencher of singlet oxygen during chemiluminescent detection by luminol and Cypridina luciferin analogues. *Luminescence* **26**, 685–688 (2011).
195. Skotnicki, K. *et al.* Spectral probe for electron transfer and addition reactions of azide radicals with substituted quinoxalin-2-ones in aqueous solutions. *Int. J. Mol. Sci.* **22**, 633 (2021).
196. Merkel, P. B., Nilsson, R. & Kearns, D. R. Deuterium effects on singlet oxygen lifetimes in solutions. New test of singlet oxygen reactions. *J. Am. Chem. Soc.* **94**, 1030–1031 (1972).
197. Clennan, E. & Pace, A. *Advances in singlet oxygen chemistry*. (2005).
198. Doizi, D. & Mialocq, J. C. Photosensitized electron-transfer reaction in the first excited singlet state of the polymethine-cyanine dye DODCI. *J. Phys. Chem.* **91**, 3524–3530 (1987).
199. Luo, J., Tang, L., Zhang, Y., Ding, W. & Lai, T. Photodegradation of Scopoletin in Organic Solvents and Aqueous Solutions: Kinetics and Degradation Pathways. *Water, Air, Soil Pollut.* **229**, 1–15 (2018).
200. Schneegans, O. *et al.* Conducting probe-mediated electrochemical nanopatterning of molecular materials. *J. Am. Chem. Soc.* **123**, 11486–11487 (2001).
201. Clapp, P. J., Armitage, B. A. & O'Brien, D. F. Two-dimensional polymerization of lipid bilayers: Visible-light-sensitized photoinitiation. *Macromolecules* **30**, 32–41 (1997).
202. Renikuntla, B. R., Rose, H. C., Eldo, J., Waggoner, A. S. & Armitage, B. A. Improved photostability and fluorescence properties through polyfluorination of a cyanine dye. *Org. Lett.* **6**, 909–912 (2004).
203. Guan, L. *et al.* Nonplanar monocymanines: Meso-Substituted thiazole orange with high photostability and their synthetic strategy as well as a cell association study. *J. Org. Chem.* **81**, 6303–6313 (2016).
204. Lo, J.-I. *et al.* Thresholds of photolysis of O₂ and of formation of O₃ from O₂ dispersed in solid neon. *Phys. Chem. Chem. Phys.* **20**, 13113–13117 (2018).

205. Yano, T. *et al.* Decolorization of indigo carmine solution using nanosecond pulsed power. *IEEE Trans. Dielectr. Electr. Insul.* **16**, 1081–1087 (2009).
206. Corbett, J. F. Pseudo first-order kinetics. *J. Chem. Educ.* **49**, 663 (1972).
207. Hubbe, M. A., Azizian, S. & Douven, S. Implications of apparent pseudo-second-order adsorption kinetics onto cellulosic materials: A review. *BioResources* **14**, 7582–7626 (2019).
208. Chmyrov, A. Photo-induced dark states in fluorescence spectroscopy—investigations & applications. (2010).
209. Bevilacqua, P. C. Mechanistic considerations for general acid–base catalysis by RNA: Revisiting the mechanism of the hairpin ribozyme. *Biochemistry* **42**, 2259–2265 (2003).
210. Drabkin, D. L. Action of Urea Upon Hemoglobin. Spectrophotometric Study of Progress of a Protein Denaturation. *Proc. Soc. Exp. Biol. Med.* **41**, 225–227 (1939).
211. Eigen, M. Proton transfer, acid-base catalysis, and enzymatic hydrolysis. Part I: elementary processes. *Angew. Chemie Int. Ed. English* **3**, 1–19 (1964).
212. Jencks, W. P. General acid-base catalysis of complex reactions in water. *Chem. Rev.* **72**, 705–718 (1972).
213. Thompson, J. E. & Raines, R. T. Value of general acid-base catalysis to ribonuclease A. *J. Am. Chem. Soc.* **116**, 5467–5468 (1994).
214. Kirby, A. J. Acid–Base Catalysis by Enzymes. *e LS* (2001).
215. Swain, C. G. Concerted Displacement Reactions. V. The Mechanism of Acid-Base Catalysis in Water Solution¹. *J. Am. Chem. Soc.* **72**, 4578–4583 (1950).
216. Soderberg, T. *Organic chemistry with a biological emphasis*. (University of Minnesota Morris Morris, Minnesota, 2016).
217. Yus, M., González-Gómez, J. C. & Foubelo, F. Diastereoselective allylation of carbonyl compounds and imines: application to the synthesis of natural products. *Chem. Rev.* **113**, 5595–5698 (2013).

218. Thomas, S. S. & Bohne, C. Determination of the kinetics underlying the pK_a shift for the 2-aminoanthracenium cation binding with cucurbit [7] uril. *Faraday Discuss.* **185**, 381–398 (2015).
219. Yan, J., Springsteen, G., Deeter, S. & Wang, B. The relationship among pK_a, pH, and binding constants in the interactions between boronic acids and diols—it is not as simple as it appears. *Tetrahedron* **60**, 11205–11209 (2004).
220. Ballard, A. *et al.* Frontispiece: Racemisation in Chemistry and Biology. *Chem. Eur. J.* **26**, (2020).

Chapter Two

Development of a LED device for kinetic studies of photochemical reactions

Summary

We have developed a device for high intensity irradiation of solution-phase samples yielding reproducible kinetics for photofading reactions.

2.1 Introduction

2.1.1 Flash-photolysis

Flash-photolysis is one of the important methods in modern photochemistry and photophysics. The purpose of the approach is to use a brief light flash to perturb a system being examined or initiate a chemical process, and subsequently to follow the photo-reaction or perturbation pathway by measuring the system's absorption properties after the flash ⁽¹⁾.

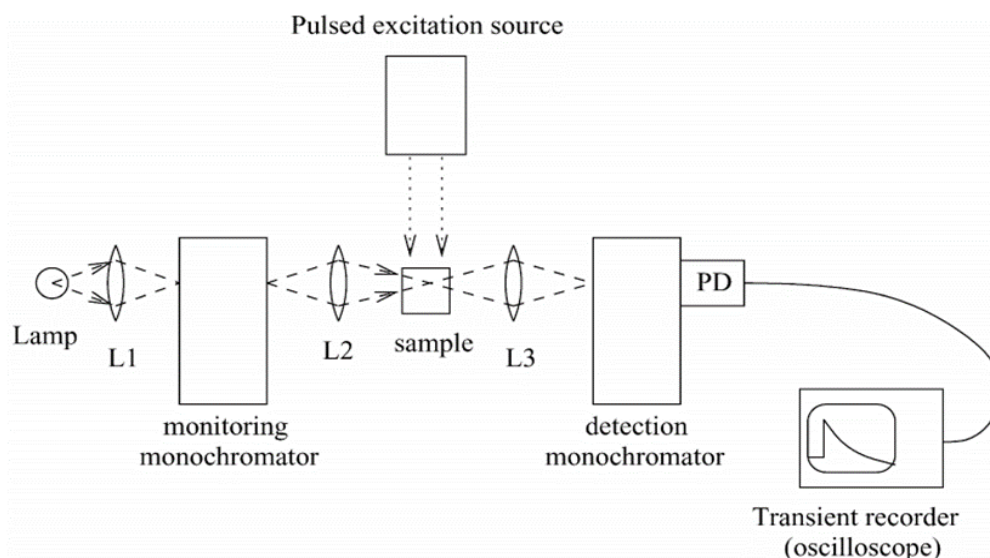


Figure 1 Scheme of a simple flash-photolysis spectrometer. PD is a photo detector and L1, L2 and L3 are lenses. ⁽²⁾

Figure 1 shows a typical experimental setup for a flash photolysis instrument. The excitation (pump) beam crosses the control beam (probe) at right angles within the sample. For liquid samples, this is a common design, and it is also called a T-scheme. The samples are prepared in cuvettes with 4 optically transparent faces, often found in a 1 cm fluorescence cuvette (fluorescence is also typically collected perpendicular to the pump beam). ⁽³⁾

A flash photolysis system's basic components are light sources, which serve as an optical pump and probe, a monochromator (a prism-like device which affords wavelength dependent optical refraction/defraction), and a detector. An example commercial instrument, the Edinburgh Instruments LP980, contains all these components in one instrument, and is shown in figure 2 ⁽⁴⁾. The PMT detector, monitor, and oscilloscope models may be selected to suit the application's spectral range and time resolution. Data averaging can be performed either through the oscilloscope or during post processing ⁽⁵⁾.

Let us now consider how a dye molecule might behave in a spectrometer like this. The dye molecules are typically fully solvated under normal room temperature conditions which means that the electronic subsystem is typically in its lowest electronic state, the ground state ⁽⁶⁾. The absorption of a photon by a molecule lifts one of its electrons to a higher orbital and increases the molecule's internal energy. The excited molecule can relax back to the ground state either radiatively or non-radiatively. This can occur via one or more intermediate electronic states, such as additional excited singlet and triplet states. Alternatively, the system can use this internal energy to engage in a reaction (photo-reaction), such as a charge transfer or isomerisation ⁽⁶⁾. Using a time resolved UV-Visible spectrometer, which is analogous to a flash-photolysis spectrometer, we can attempt to monitor the progress of this energy disposal.

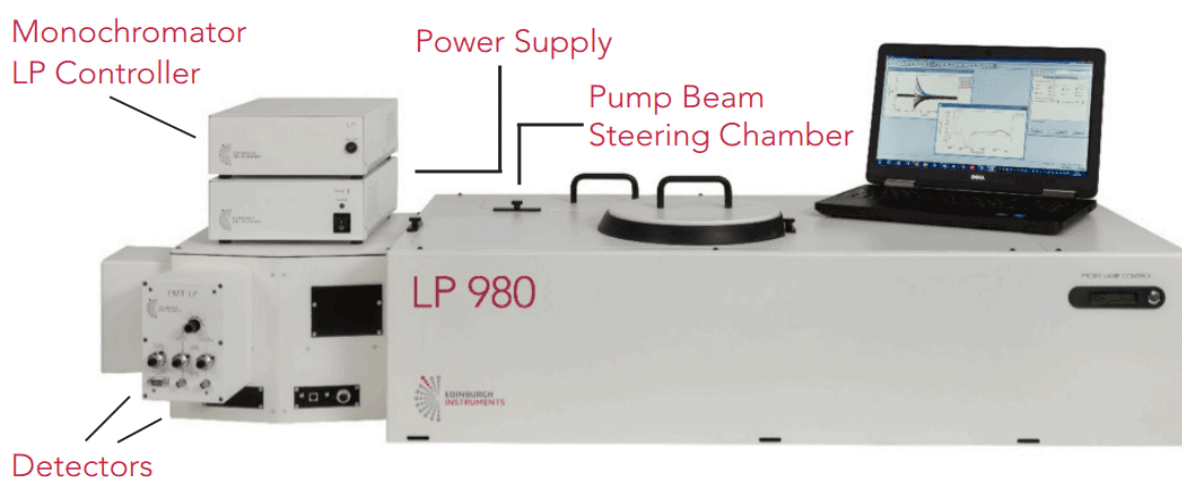


Figure 2 Flash Photolysis-The LP980 Spectrometer made by Edinburgh Instruments (Figure missing the light source) ⁽⁷⁾

We will look at the example of an excited triple state to understand what happens in a TA (transient absorption) experiment – again this is very similar to the flash photolysis cases described above, with the only significant difference being that in this case no bonds are formed or broken after the light-induced perturbation. ⁽⁸⁾

The lifetime of the excited singlet/triplet states may be estimated from their lifetime of fluorescence/phosphorescence; however, if luminescence cannot be observed, instead, TA can be used. For example, one can monitor the change in absorbance of T_0 as a function of time, reported by monitoring the probe beam at the wavelength of transition T_0-T_n ⁽⁹⁾. The TA absorptions, shown in red in the figure above, are observed as an increase in optical density of the system. As the population of the T_0 state declines from T_0 to S_0 , this absorption band decreases.

The mechanism of excited-state-absorption (ESA) requires the sequential absorption of pump photons by a single dye molecule due to a simple multilevel system's ladder-like structure ⁽¹⁰⁾.

Any molecules removed from the ground state by the pump pulse are moved to an excited state. This means that the concentration of molecules in the ground state reduces and part of the absorption signal of the ground state disappears ⁽¹¹⁾. Therefore, the absorption difference becomes negative at the wavelengths of ground state absorption. This negative contribution's spectral form is similar to the spectrum of ground state absorption measured by a spectrophotometer (this is what is missing, since certain molecules are now in the excited state) ⁽¹²⁾. Over time, this signal persists until all the excited molecules return to the original ground state from which they were excited. This contribution to the difference absorption signal is called ground state bleaching (GSB) ⁽¹³⁾.

Despite the increasing interest in flash photolysis, the high cost of UV lasers and the complexity of implementing the technique have hindered this technique's widespread implementation ⁽¹⁴⁾. A light-emitting diode (LED) may be an alternative UV light source for flash photolysis, as recent developments in the semiconductor industry have seen a system being developed that can emit UV light with wavelengths and powers that are theoretically compatible with photolysis ⁽¹⁵⁾.

Upon the use of a traditional UV-Vis spectrometer, the path length for the irradiation beam is 1 cm, and independent of the cuvette's fill height. It must be understood that the LED light passing through the cuvette does not disrupt the UV-Vis spectra detection ⁽¹⁶⁾. Any scattered light from the irradiation source can, however, enter the UV-Vis detector orthogonal to the irradiation beam. Despite this, usually the spectra do not show any distortion at the peak wavelength of the LED. Placing the sample holder on a magnetic stirrer provides the whole solution with homogeneous illumination and provides reproducible conditions for the reaction ⁽¹⁶⁾.

In general, this experimental apparatus affords cost effective and high precision monitoring of photochemical reactions, allowing a chemist to continue in their pursuit of understanding light-matter interactions.

2.1.2 Brief Aims Statement

To develop an LED based device that allows the reproducible irradiation of a sample of a dye in solution to investigate the mechanism of dye fading. This involves the creation of a new LED irradiation device which can hold a liquid phase sample for interrogation, and which can irradiate the solution with light intense enough to provide reproducible fading kinetics without interference from external interference. For clarity, this means the sample must be stable to external fluctuations in temperature and light over the period of the measurement: which is considerably more challenging if the fading process requires substantial time (>hrs). The device must have a consistent and reproducibly controllable light source, which should also be able to drive the photochemical dye fading process.

2.2. Results and discussion

2.2.1 Daylight induced fading of common organic dyes.

We started studying the effect of normal daylight on the fading of DODC. We propose that DODC (in this case acting as a prototypical dye molecule) absorbs a photon of near-UV/visible light and then undergoes a non-reversible photochemical reaction. At present it is unclear whether this is unimolecular or bi(poly)molecular. The fading of DODC (Alfa Aesar / Thermo Fisher Scientific-96%) occurs readily when exposed to ambient light and was studied using UV-visible spectroscopy. The changes in absorption spectra as a function of time exposed to sunlight were measured in buffer (25 mM MOPS pH 7.0, 50 mM NaCl and 1 mM EDTA) at room temperature.

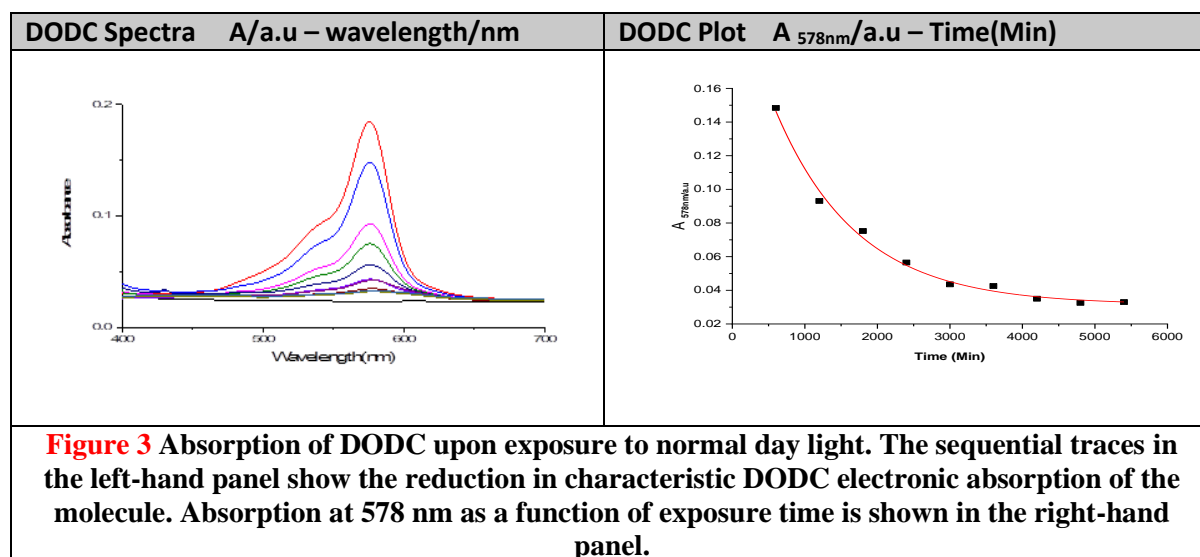


Figure 3 shows an obvious decrease in the absorbance of DODC (which was not filtered or sonicated – *vide infra*) around 578 nm. The reasons for the decrease in absorbance is the destruction of the DODC chromophore, which may be caused by some combination of, amongst other possible factors, exposure to normal daylight, exposure to dissolved O₂, and/or thermal degradation.

This experiment was repeated under the same conditions, i.e. with normal daylight and using a solution of DODC (Alfa Aesar/ Thermo Fisher Scientific-96%) that was not sonicated and filtered and the temperature was not kept constant. However, the composition of the solution was varied, and led to the results displayed in Table 1 (see Appendix for additional experiments performed using daylight conditions).

Table 1. Rate constants for different solutions containing DODC exposed to normal day light at ambient temperature

Components	Without DNA	With DNA (5ul only)	Experimental numbers
Buffer pH=7	$(52 \pm 2.2) \times 10^{-3} \text{min}^{-1}$		26-4-2017
			$(47 \pm 9.3) \times 10^{-3} \text{min}^{-1}$ 27-4-2017
			$(27 \pm 4.6) \times 10^{-3} \text{min}^{-1}$ 2-5-2017
Distilled water	$(15 \pm 1.59) \times 10^{-3} \text{min}^{-1}$		$(5.3 \pm 3.9) \times 10^{-3} \text{min}^{-1}$ 3-5-2017
			26-4-2017
			$(76 \pm 30) \times 10^{-3} \text{min}^{-1}$ 2-5-2017
Distilled water +NaCl	$(32 \pm 5.4) \times 10^{-3} \text{min}^{-1}$		$(82 \pm 26) \times 10^{-3} \text{min}^{-1}$ 3-5-2017
			26-4-2017
			$(39 \pm 7.1) \times 10^{-3} \text{min}^{-1}$ 27-4-2017
Distilled water +MOPS	$(25 \pm 6.1) \times 10^{-3} \text{min}^{-1}$		$(26 \pm 4.8) \times 10^{-3} \text{min}^{-1}$ 4-5-2017
			$(14 \pm 2.43) \times 10^{-3} \text{min}^{-1}$ 4-5-2017
			4-5-2017
Buffer pH=7	$(22 \pm 1.3) \times 10^{-3} \text{min}^{-1}$		$(20 \pm 1.5) \times 10^{-3} \text{min}^{-1}$ 2-5-2017
			$(25 \pm 7.6) \times 10^{-3} \text{min}^{-1}$ 3-5-2017
			25-4-2017
Distilled water	$(17 \pm 1.7) \times 10^{-3} \text{min}^{-1}$		26-4-2017
Distilled water + NaCl only	$(23 \pm 0.73) \times 10^{-3} \text{min}^{-1}$		26-4-2017
Distilled water + MOPs only	$(23 \pm 0.94) \times 10^{-3} \text{min}^{-1}$		25-4-2017

We attempted to analyse these data in terms of a first-order rate law for the photochemical fading reaction, however the results were not reproducible given the variation in possible experimental conditions, by which is meant external/uncontrolled factors that do not include the choice of solutes.

2.2.2 Kinetics experiments using a battery driven irradiation device; the first LED device.

Because of the irreproducibility of the fading kinetics upon exposure to ambient light, we looked for an alternative method of irradiating our samples. With the assistance of the Beames group, we built a battery-operated LED-based setup delivering a more constant intensity of light (Figure 4).

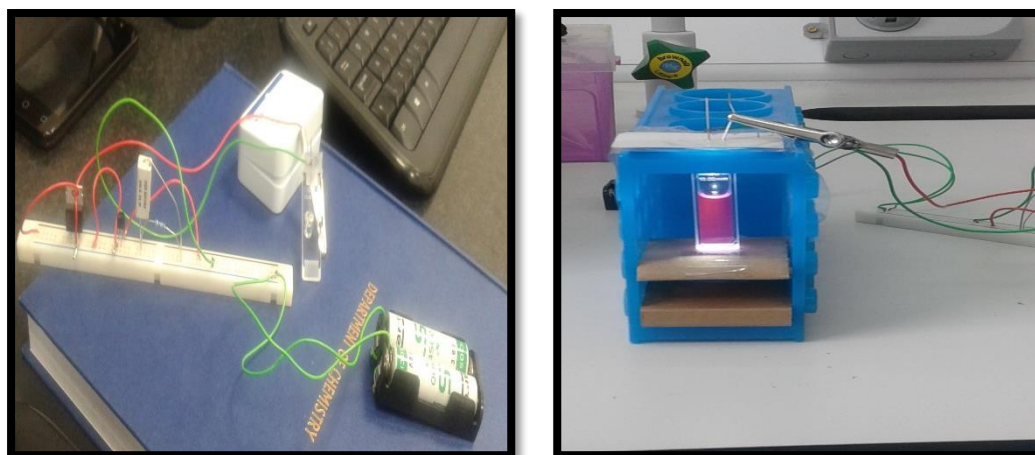


Figure 4 The first design of an LED-based irradiation device

The advantages and disadvantages of this set up are compared in Table 2.

Q	Device components	Advantages	Disadvantages
1	Lithium batteries (3.5-3.6 V)	Easy to handle	Limited lifetime of batteries
2	Simple electric circuit	Low cost	Could not accurately measure the intensity and voltage
3	Basic wiring	Available spare parts	Not particularly long lasting
4	Crocodile clips	Easy to attach to LED/cheap	
5	LEDWE-15 (THORLABS)	Available and cheap Provides reasonable coverage of the visible spectrum (see below). Low external heating.	

The selected LED was a LEDWE-15 from Thorlabs (Figure 5).

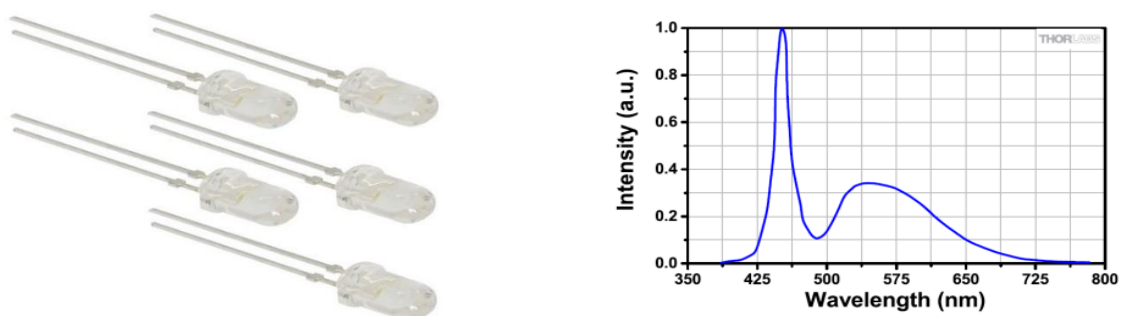


Figure 5 LEDWE-15 (Left) and its output spectrum and radiation distribution measured with a forward current of 20 mA (Right).

LEDs, compared to traditional lighting, generate low amounts of heat due to their high performance. The energy is mostly processed and converted into light (90 % of total), which allows direct human contact with the source of LED lighting without skin burns even after a long period of work and therefore it is also a significantly reduced fire risk ⁽¹⁷⁾. For this reason, LED illumination is favourable for goods or equipment that are extremely sensitive to temperature ⁽¹⁸⁾. This is also relevant in this case where we want to study a reaction at a constant temperature.

In addition, light-emitting diodes (LEDs) are compact, energy-efficient sources of light that can emit light across a wide range of wavelengths. The LEDWE-15 from Thorlabs has a spectral output ranging over the wavelength range $430 \text{ nm} < \lambda < 660 \text{ nm}$. This LED is encapsulated in a clear, circular epoxy case with a diameter of 5 mm ⁽¹⁹⁾. The breadth of the spectrum is good, covering a good proportion of the visible region of the spectrum, and is likely to drive any photochemical reaction that can be promoted with visible light.

When we want to explain the simple electric circuit, it shown in diagram (Figure 6) below.

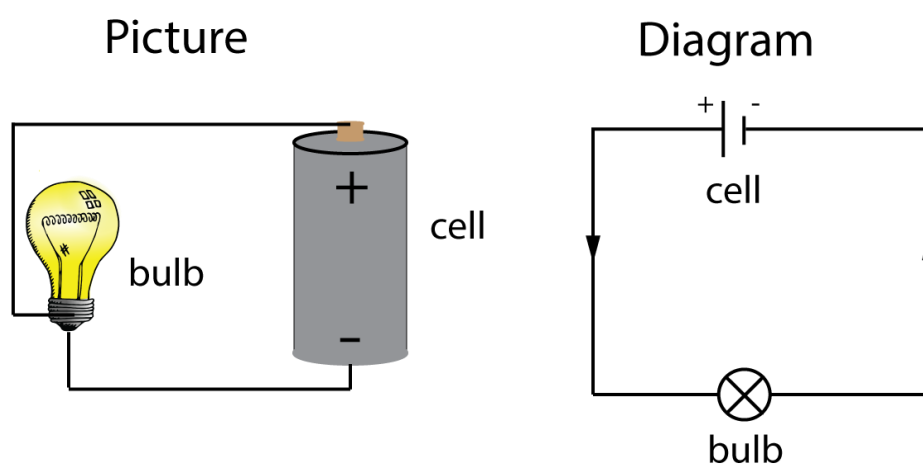


Figure 6 Diagram of simple electric circuit. ⁽²⁰⁾

Table 3 summarises the rate constants for DODC fading upon irradiation with the device in buffer solutions (25 mM MOPS, 50mM NaCl and 1 mM EDTA) with different pH. A buffer solution is an aqueous mixture of a weak acid and its conjugate base, or the other way around. When a small amount of strong acid or base is added to it, the pH changes very little. Buffer solutions are used in a wide range of chemical applications to hold pH at a nearly constant value. ⁽²¹⁾ The chelating agent EDTA (ethylenediaminetetraacetic acid) binds divalent metal ions including calcium and magnesium. EDTA can be used to prevent DNA and RNA degradation as well as inactivate nucleases that need metal ions to work. Metal ion-requiring enzymes may also be inactivated with EDTA. ⁽²²⁾ Has been

shown to have antifungal properties, in preformed biofilms, there was a substantial reduction in fungal metabolic activity. ⁽²³⁾

DODC (Alfa Aesar / Thermo fisher Scientific - 96%) was used in the absence and presence of added DNA, at room temperature and pressure.

Table 3 Rate constants for photolysis in buffer at different pH upon irradiation with the 1st LED device

Q ^a	Conditions	Without DNA	With added DNA (10µl of a 14.8mM stock solution)	Concentration of DNA inside cuvette
1	Buffer pH=7	$(8.9 \pm 0.8) \times 10^{-3} \text{min}^{-1}$		
			$(5.5 \pm 1.1) \times 10^{-3} \text{min}^{-1}$	500 µM
2	Buffer pH=8	$(9.4 \pm 0.7) \times 10^{-3} \text{min}^{-1}$		
			$(5.2 \pm 0.4) \times 10^{-3} \text{min}^{-1}$	500 µM
3	Buffer pH=6	$(7.8 \pm 0.8) \times 10^{-3} \text{min}^{-1}$		
			$(3.02 \pm 1.4) \times 10^{-3} \text{min}^{-1}$	500 µM

Table 3 reports data with a dye which was not filtered prior to the experiment but simply sonicated and the compound was assumed to be dissolved, which led to the inaccurate rate constant. Additional sources of instability in this data were a still somewhat inconsistent irradiation of the sample (due to some presence of sunlight and slightly fluctuating intensity of LED).

2.2.3 Kinetics experiments using a commercial tuneable power supply; the 2nd version of the LED-based irradiation device.

Because we had not been able to obtain reproducible kinetic data, we decided to use a commercially available high-intensity LED with accompanying power supply in combination with a 3D-printed irradiation box (Figure 7) inspired by a custom-built spectrophotometer developed in the Beames group. ⁽²⁴⁾

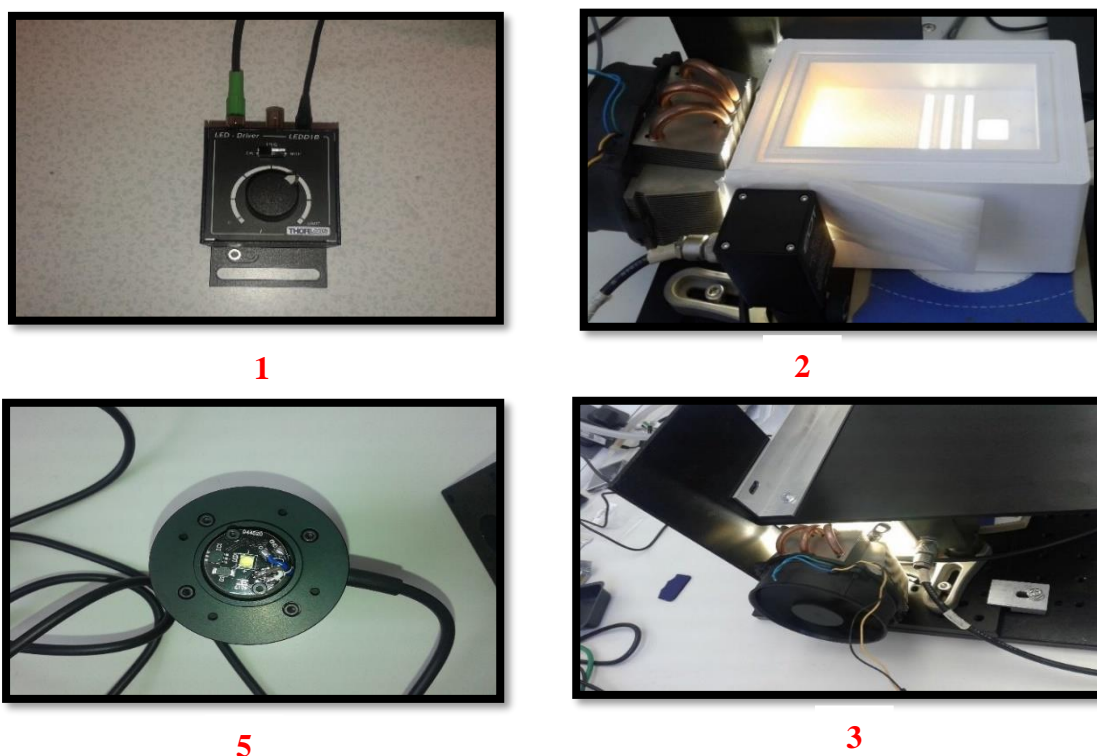


Figure 7 Key components of 2nd LED device

The key components of the revised irradiation setup are listed in Table 4.

Q	Device components	Advantages	Disadvantages
1	Commercial controlable power supply	Reasonably low cost	
2	3D printed cuvette holder	Easy to handle	Limited space (1 cuvette)
3	Fan (commercial CPU fan)	Available spare parts	Difficult to mount to the LED
4	Magnetic stirrer	Consistent solution mixing, removing concentration gradients	
5	MCWHD3 - 6500 K- LED on Metal-Core PCB ⁽²⁵⁾	Good intensity and voltage control	Not intense enough to drive the reaction rapidly

High intensity LEDs use heat sinks to absorb the heat produced by the LED and dissipate it into the surrounding environment. This keeps LEDs from overheating and burning out. Thermal management is typically the single most important factor in an LED's longevity. The higher the temperature at which the LEDs are

operated, the more quickly the LED will degrade, and the shorter the useful life will be ⁽²⁶⁾. In our setup, we have thermally connected the metal-mount of the LED to a heat dissipator equipped with a CPU fan which we recycled from an old computer.

We used the LEDD1B power supply designed for high-brightness LEDs. The compact T-Cube LEDD1B can drive LEDs with a current of up to 1200 mA, the output power can be varied (and modulated with an external trigger signal if needed). The maximum output current is set using the T-Cube front adjuster. This ensures that the output current does not exceed the maximum, regardless of the other settings or the input voltage of the modulation ⁽²⁷⁾. The actual current going through the LED is set manually as a fraction of the maximum current.

To evaluate the performance of this new device, we studied the effect of light on fading of a solution of Thiazole Orange (TO) 90% (Sigma-Aldrich / Merck; CAS No: 107091-89-4).

We first carried out a control experiment. The control solution was sonicated but not filtered in buffer (pH=7, MOPS 25 mM, NaCl 50 mM and EDTA 1 mM) and absorption spectra recorded and analysed in the absence of light (Figure 8).

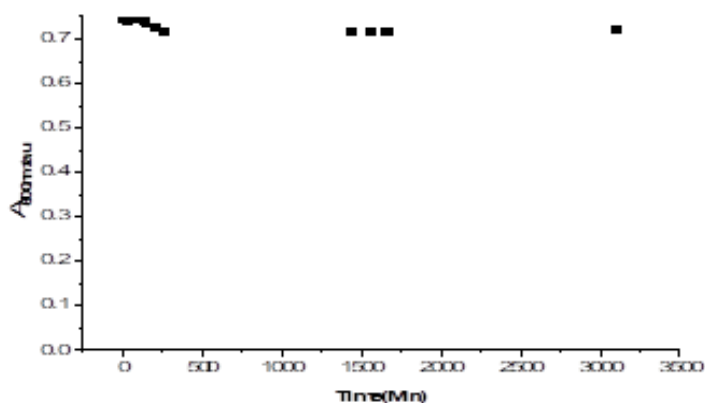
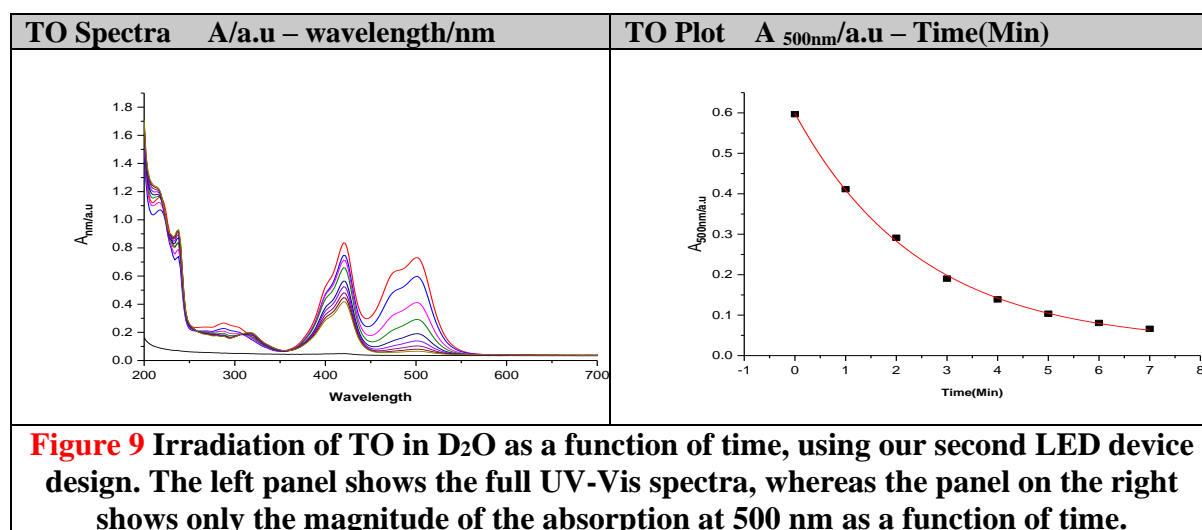


Figure 8 TO absorption at its visible spectrum maximum (500 nm) as a function of time, in buffer solution without irradiation.

Figure 8 shows that negligible fading occurs in the absence of light, as expected.

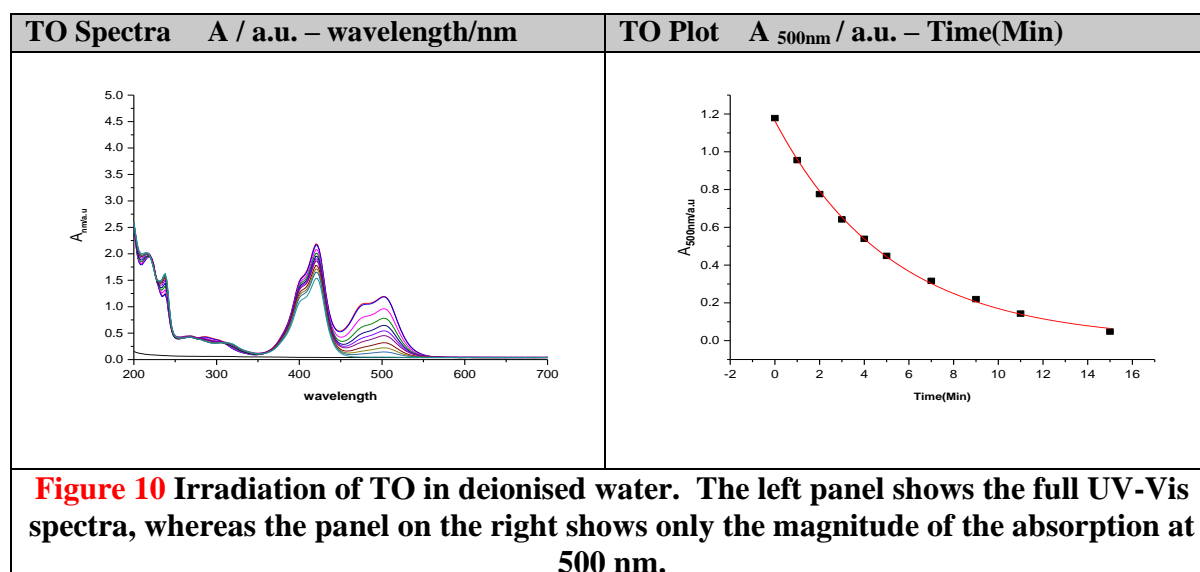
Subsequently, we studied the effect of light (irradiation with the 2nd LED device) on fading of a solution of TO which was sonicated but not filtered in D₂O. These experiments were carried out 3 times (see Appendix) at ambient laboratory temperature (Figure 9 and Table 5).



The decrease in absorbance at 500 nm as a function of time was analysed in terms of a first-order rate law, yielding the rate constants summarised in Table 5.

Table 5. Rate constants of TO fading in D₂O	
original rate constants / min⁻¹	Errors (fit/min⁻¹)
0.40415	0.01494
0.650	0.02495
0.59174	0.01711
Average k / min⁻¹	Average error/ min⁻¹
0.548613333	0.019
standard deviation / min⁻¹	Error margin/ min⁻¹
0.104878794	0.104879

We then changed the experimental conditions and exposed (TO) to light in our device in deionised water, sonicated and without filtration, to light in our device. This experiment was carried 3 times (see Appendix) at ambient laboratory temperature (Figure 10).

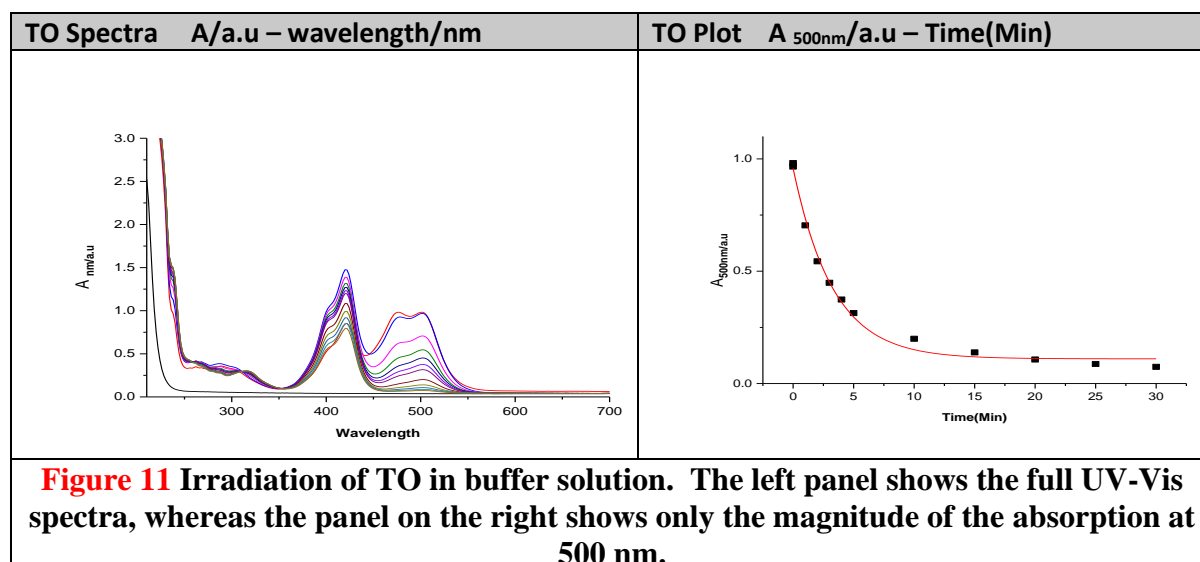


The data were analysed in terms of first-order rate law and the result are summarized in Table 6.

Table 6 Rate constants of TO fading in deionised water upon irradiation with the 2 nd generation device.	
original rate constants / min ⁻¹	original errors (fit/min ⁻¹)
0.19241	0.00753
0.1957	0.00845
0.283	0.01058
Average <i>k</i> / min ⁻¹	Average error / min ⁻¹
0.22358	0.008853333
standard deviation / min ⁻¹	Error margin / min ⁻¹
0.041776252	0.041776

Table 6 shows an estimated error of 20% on the rate constant so we continued to explore sources of error.

We changed the experimental conditions to preparing a solution of TO in buffer (pH=7, 25 mM MOPs, 50 mM NaCl, 1 mM EDTA) through sonication, but still without filtration, with the resulting solution stored for 24 hours in the dark prior to irradiation. These experiments were carried out 3 times (see Appendix) at normal laboratory temperature (Figure 11 and table 7).



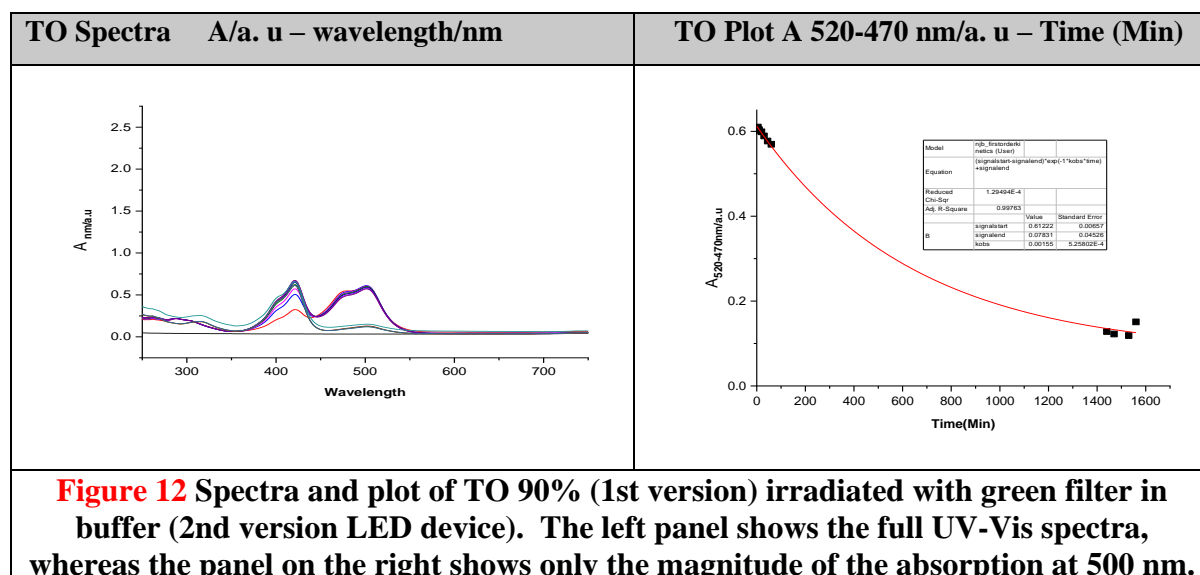
From the experiments, rate constants were determined (Table 7).

Table 7 Rate constants of TO fading in buffer pH=7, 25 mM MOPs, 50 mM NaCl, 1 mM EDTA	
original rate constants/min ⁻¹	original errors (fit/min ⁻¹)
0.3031	0.01956
0.281	0.0214
0.3051	0.01956
Average k /min ⁻¹	Average error/min ⁻¹
0.296406667	0.020173333
standard deviation /min ⁻¹	
0.010910611	

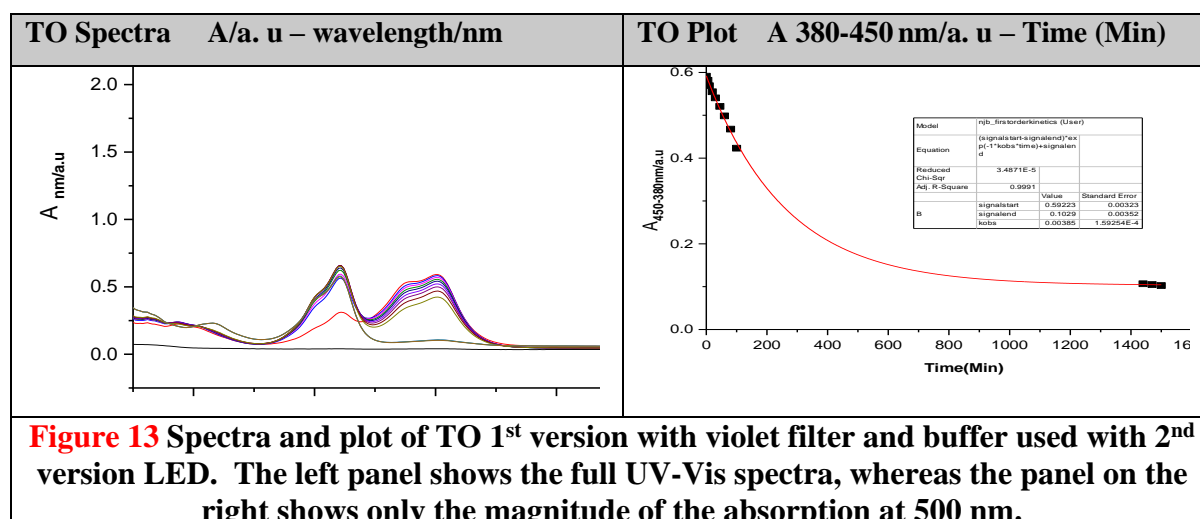
The data from these experiments show that we can now obtain reproducible kinetics from this setup.

The second revision of the irradiation device design included the option to place filters in the light path to explore the irradiation wavelength dependence of the kinetics of fading. One part of the optical spectrum is selected using an optical filter, while rejecting other portions. In general, by adding coloured glasses or dyes, filters either absorb unwanted light or reflect unwanted light by adding interference coatings ⁽²⁸⁾. The amount of energy blocked or rejected by a filter is defined by Optical Density (OD). A high optical density value means low transmission, and high transmission is indicated by low optical density ⁽²⁹⁾. For precision light blocking requirements, such as in Raman spectroscopy or fluorescence microscopy, optical densities of 6 or greater are used. For laser separation and clean-up, machine vision, and chemical detection, optical densities of 3.0-4.0 are optimal, while optical densities of 2.0 or less are ideal for colour sorting and spectral order separation ⁽²⁸⁾.

We incorporated 2 kinds of filter into our 2nd LED device. The first filter we used was green (470-520 nm absorption) and the second filter we used was violet (filter 380-450 nm). Both were used with TO 90% (1st version) dissolved in buffer at 25 °C (Figures 12 and 14).



From Figure 12 it is clear that fading took a long time (more than 26 hours = 1600 min). We identified the cause as the filter, which clearly removes an important wavelength range of light responsible for fading, and thus has an effect on the rate constant of the fading process.



From Figure 13 it is clear that, again, it took a long time (more than 24 hours=1400 min) to finish fading TO and this is again because the filter removes key spectral intensity that drives the fading process.

Overall, we found that using the second version of our setup, we achieved more reproducible kinetics but found a very slow reaction, which made inferring photochemical information from the filter experiments very challenging. This slow reaction could be due to a low intensity of the LED. We therefore tried to increase the intensity in the 3rd version of LED.

2.2.4 Kinetics experiments by using lenses in 3rd version LED device.

In order to increase the irradiation intensity, we designed an irradiation setup that focusses the LED light on our sample cuvette (Figure 14).

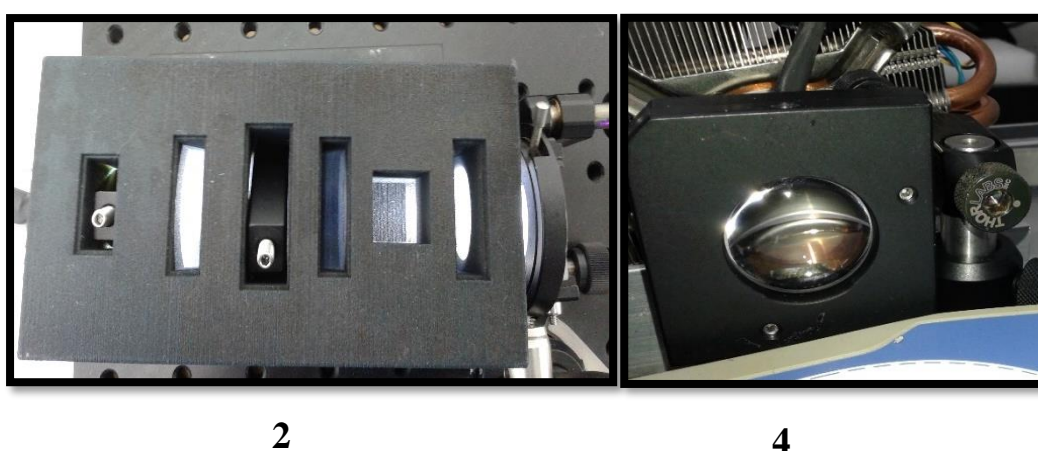


Figure 14 3rd version of our LED sample irradiation device.

The key components of this setup are listed in Table 8.

Table 8 Components of 3 rd version LED device			
Q	Device components	Advantages	Disadvantages
1	Power supply	Relatively low cost	
2	Box for putting cuvette	Easy to handle	Limited space (1 cuvette)
3	MCWHD3 - 6500 K-LED on Metal-Core PCB ⁽²⁵⁾	Good intensity and voltage	
4	Lenses	Greater fluence within the cuvette	

According to the lens equation, we can show the radiation path through the 3rd version LED-device (Table 9) (Figure 15)

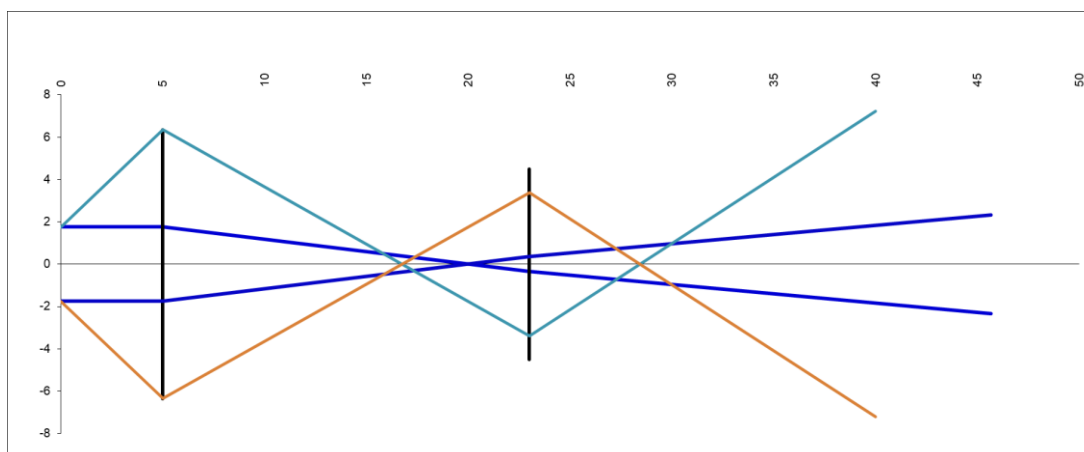


Figure 15 The radiation path through the lenses – thin lens spreadsheet design

In Figure 15, the lenses (black vertical lines) are designed to take the light from the LED (designated at $x = 0$) and focus them such that they fill a 1 cm x 1 cm cuvette window 28 cm downstream from the LED. The dark blue lines indicate collimated light from the LED whereas orange and light blue lines are indicative of the most divergent light from the LED, based on published divergence criteria. Using two different focal length lenses, one can see that we can use all of the LED light to irradiate the sample.

Table 9 The calculated parameters that used lens at 3rd version LED		
Characteristics	calculations for equation	
diameter of LED	3.5 mm (millimetre)	
diameter of 1st lens D1	12.7 mm (millimetre)	
diameter of 2nd lens D2	9 mm (millimetre)	
focal length of 1st lens f1	15 cm (centimetres)	
focal length of 2nd lens f2	12 cm (centimetres)	
distance between LED and 1st lens u	5 cm or mm (centimetres, millimetre)	
distance between 2 lenses d	18 cm (centimetres)	
distance between 2nd lens and final image v'	22.66666667 cm (centimetres)	
Total Magnification M	-1.333333333 (ratio of two lengths, so no units)	
Divergency (in degree)	42.61405597 degrees (°)	
θ_1 (after first lens)	28.40937065 (°)	
vertical distance travelled to the second lens	9.73636856	
θ_2 (after second lens)	31.96054198 (°)	
vertical distance travelled at $x=?$	10.60650725	X40

These calculations and figure are generated according to the guidelines of Dr. Beames and are used in the 3rd version of LED.

We also explored whether the quality/purity of TO we used affected our experiments. We used a new batch of TO which was 80-90% pure obtained from ChemCruz (Figure 16).

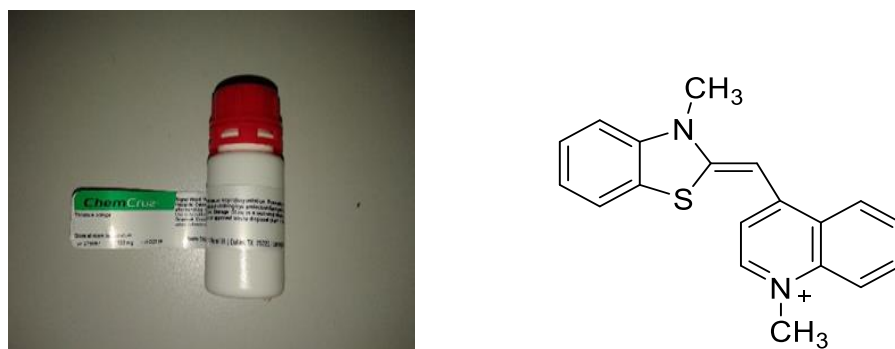


Figure 16 Thiazole orange from alternative source.

We changed the experiments to use TO (80-90% from ChemCruz) which was dissolved in buffer, and then sonicated and filtered (pH=7, 25 mM MOPs, 50 mM NaCl, 1 mM EDTA) and left for 24 hours in the dark. The solution was then removed from the dark environment immediately prior to irradiation. These experiments were carried out 3 times (see Appendix) at 25 °C. figure 17.

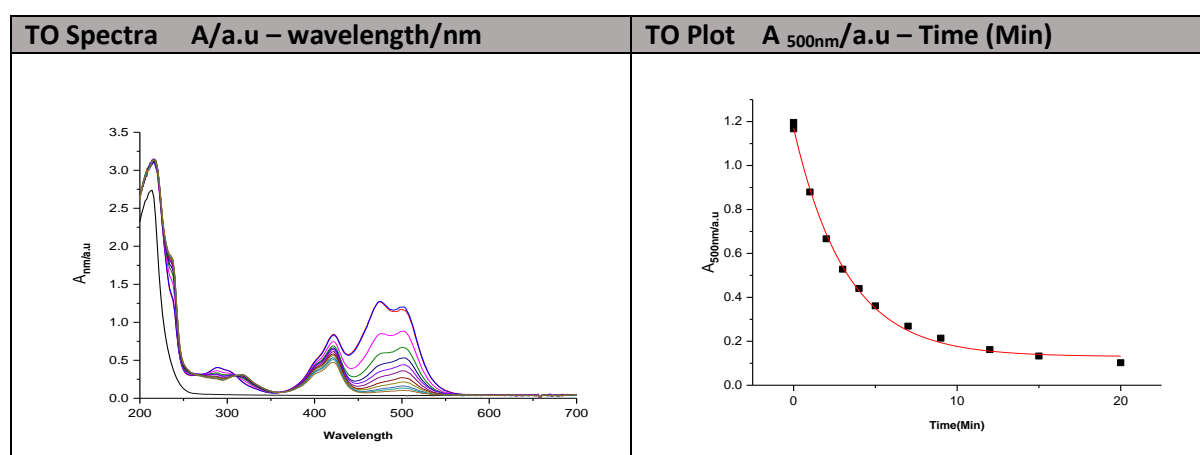
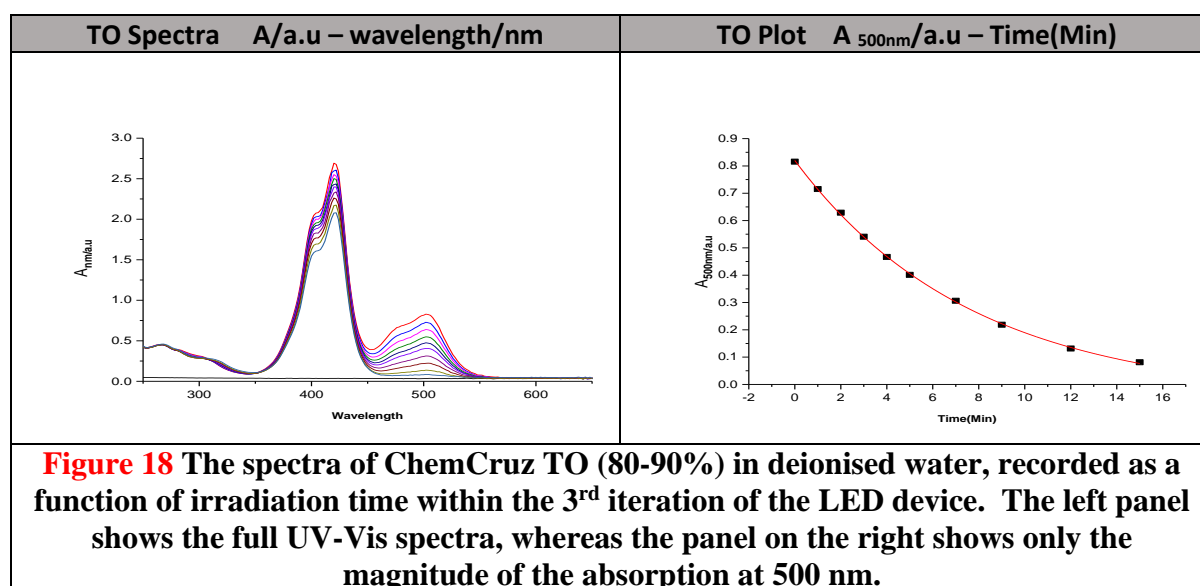


Figure 17 Spectra of ChemCruz TO (80-90%) in buffer solution, recorded as a function of irradiation time within the 3rd iteration of the LED device. The left panel shows the full UV-Vis spectra, whereas the panel on the right shows only the magnitude of the absorption at 500 nm.

The data were analysed in terms of first-order rate law, with rate constants reported in Table 10.

Table 10 Rate constants of TO fading from LED device 3.	
original rate constants/min ⁻¹	original errors/min ⁻¹
0.31099	0.01226
0.37101	0.00563
0.32688	0.01309
Average k/ min ⁻¹	Average error/ min ⁻¹
0.336293333	0.010326667
standard deviation/ min ⁻¹	
0.025391051	

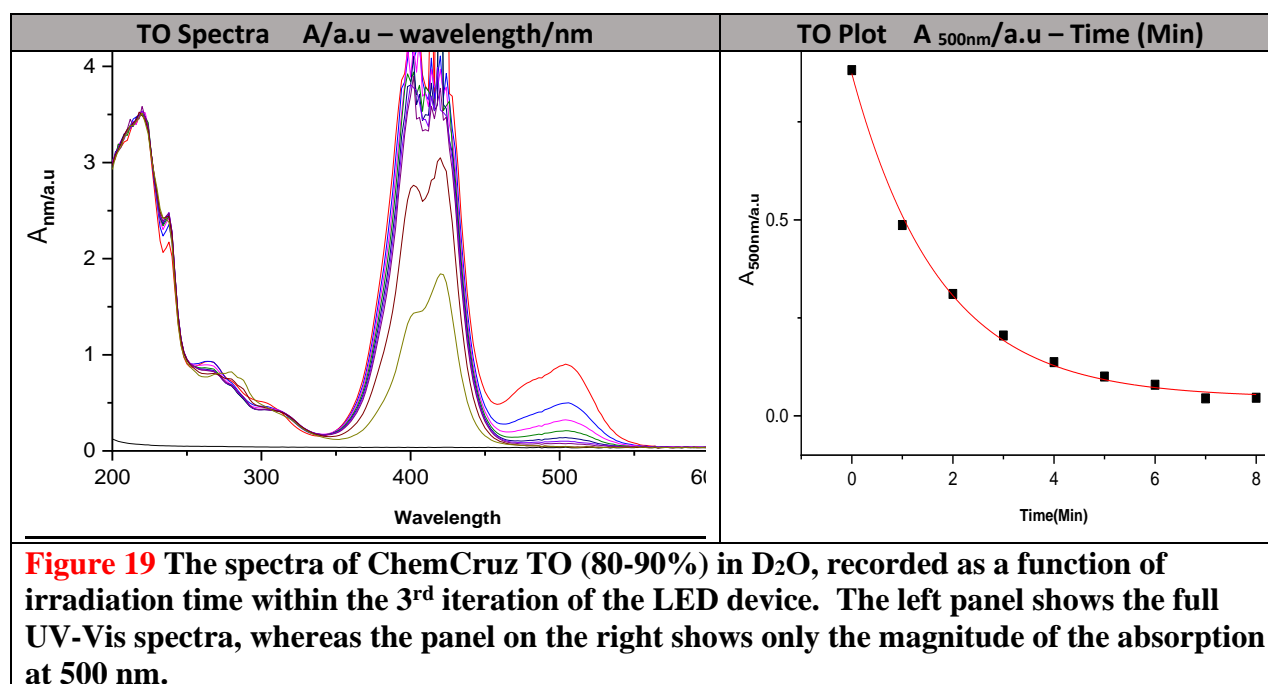
We then used Thiazole orange (80-90% from ChemCruz) dissolved in deionised water and sonicated and filtered at 25 °C. The results are shown in Figure 18 (experiments performed 3 times, see appendix).



The data were analysed in term of a first-order rate law, with rate constants shown in Table 11.

Table 11 Rate constants of TO fading in deionised water.	
original rate constants/ min ⁻¹	original errors/ min ⁻¹
0.13017	0.00343
0.08495	0.00995
0.141	0.00573
Average k/ min ⁻¹	Average error/ min ⁻¹
0.118706667	0.00637
standard deviation/ min ⁻¹	
0.024275593	

Next, we used Thiazole orange (80-90% from ChemCruz) dissolved in D₂O, sonicated and filtered at 25 °C. The results are illustrated in Figure 19 (experiments performed 3 times, see appendix)



The data were analysed in term of first-order rate law, with rate constants shown in Table 12.

Table 12 Rate constants of TO fading in D₂O	
original rate constants/ min⁻¹	original errors/ min⁻¹
0.40388	0.01028
0.54575	0.01725
0.40388	0.01725
Average k/ min⁻¹	Average error/ min⁻¹
0.45117	0.012603333
standard deviation/ min⁻¹	
0.066878159	

The experiments showed stable reaction rate constants because the filtering process reduced the possibility of particulate aggregation, which we have now demonstrated gives instabilities in fading. These experiments were repeated multiple times, and were both more consistent, but also showed greatly reduced fading time thanks to the increased LED light density in the 3rd version of the LED device.

From previous studies, we found that the version of TO which we used was only partially purified. This explains why we have second anomalous peak in the UV-Vis spectrum of the compound at $\lambda \sim 400$ nm. After many fading experiments and NMR tests, we ensure that partially purified compound does not negatively affect the rate of fading of this version of TO.

We then used another new version of TO (3rd source) which was 98% pure from Insight Biotechnology.

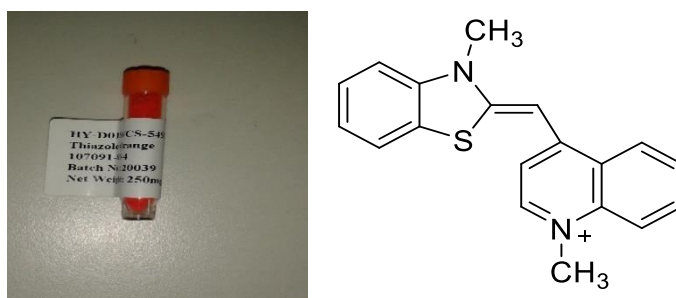
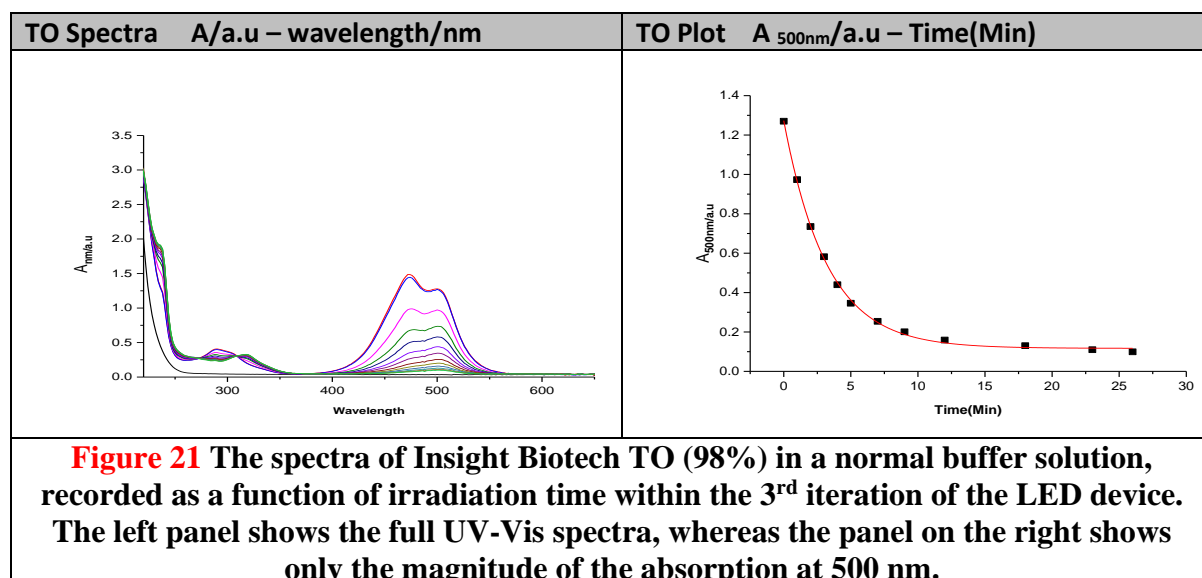


Figure 20 TO structure and sample from Insight Biotechnology

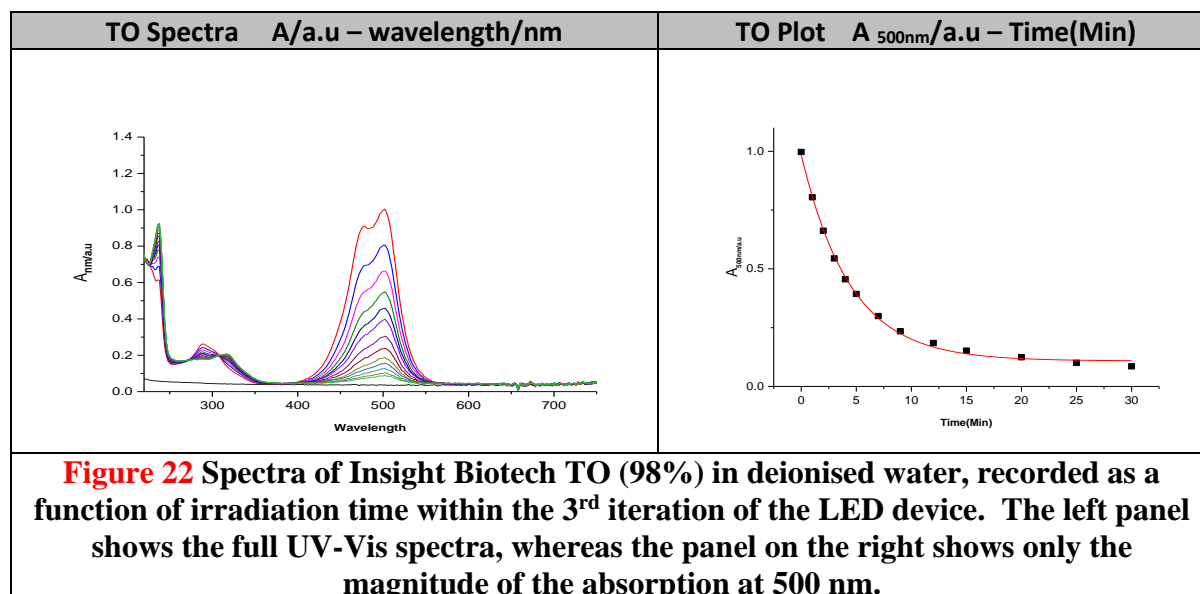
We used Thiazole orange 98% (Insight Biotechnology) dissolved in buffer (pH=7, 25 mM MOPS, 50 mM NaCl and 1mM EDTA), sonicated and filtered and stored overnight at 25 °C (Figure 21) in irradiation experiments (experiments performed 3 times, see appendix).



First of all, Figure 21 shows the absence of the peak around 400 nm which we observed for TO obtained from other suppliers. This suggests that the peak at 400 nm can be attributed to an impurity. The data in Figure 20 were analysed in terms of a first-order rate law (Table 13).

Table 13. Rate constants of TO (98%) fading in buffer solution	
original rate constants/ min ⁻¹	original errors/ min ⁻¹
0.31043	0.007
0.42053	0.01244
0.31567	0.00967
Average k/ min ⁻¹	Average error/ min ⁻¹
0.348876667	0.009703333
standard deviation/ min ⁻¹	
0.050711698	

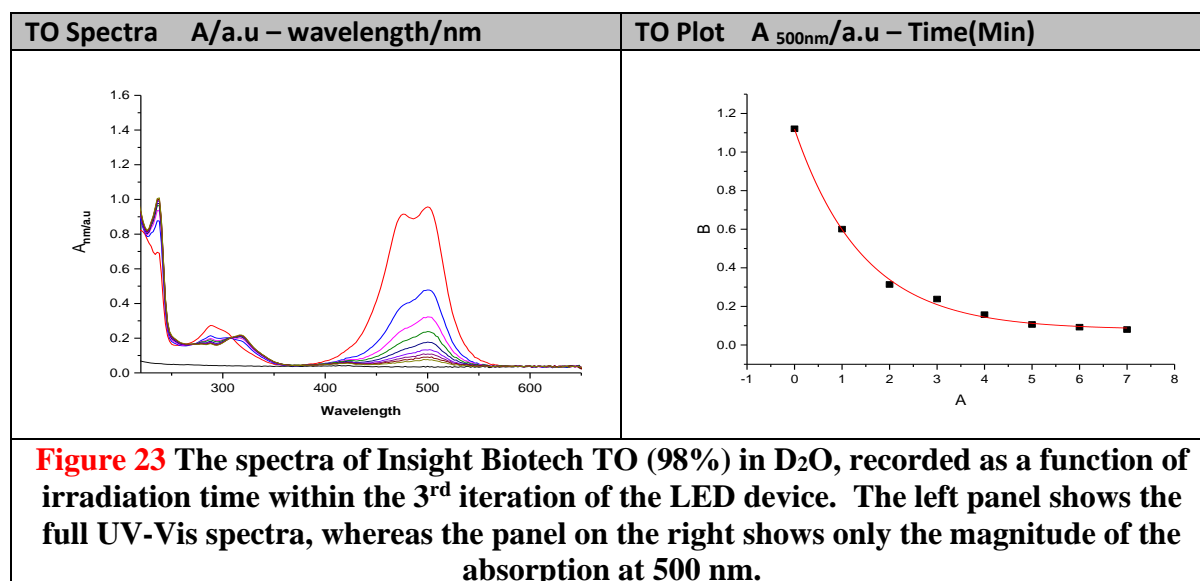
Analogous data were obtained for thiazole orange (98%) dissolved sonicated and filtered in deionised water at 25 °C (Figure 22; experiments performed 3 times, see appendix).



Rate constants for fading were determined by fitting a first-order rate law to the data (Table 14).

Table 14 Rate constants of TO (98%) fading in deionised water	
original rate constants / min ⁻¹	original errors / min ⁻¹
0.22462	0.0071
0.23967	0.00975
0.22989	0.00727
Average <i>k</i> / min ⁻¹	Average error/ min ⁻¹
0.231393333	0.00804
standard deviation/ min ⁻¹	
0.006235417	

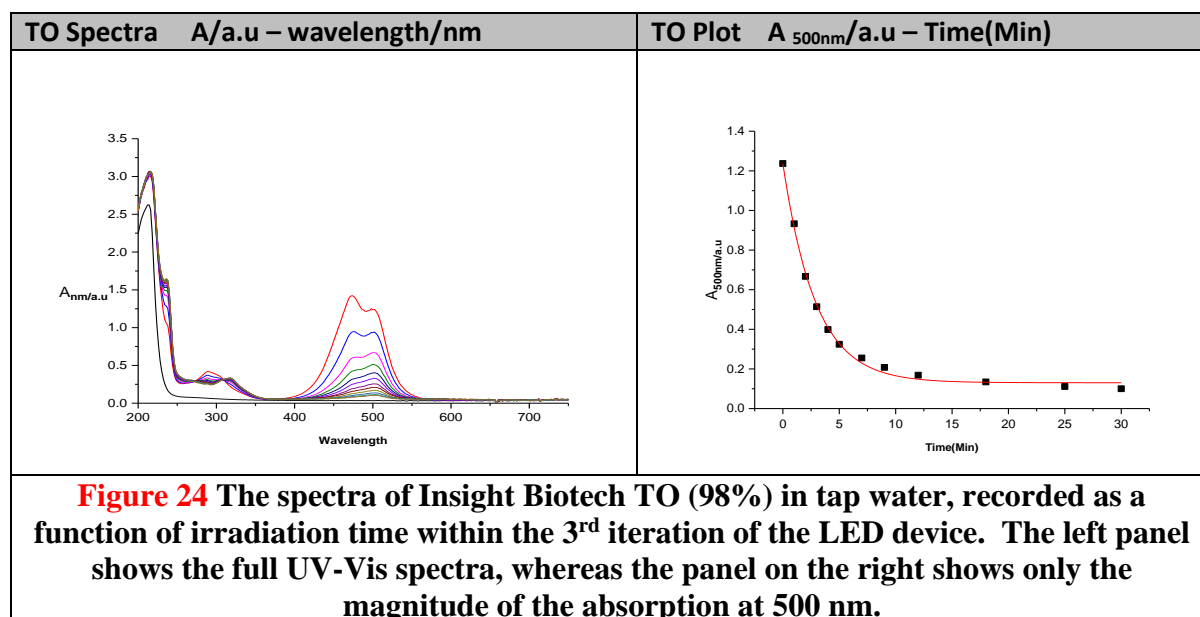
We then used thiazole orange (98%) dissolved in D₂O sonicated and filtered at 25 °C yielding the results illustrated in Figure 23 (experiments performed 3 times, see appendix).



Rate constants for fading were determined by fitting a first-order rate law to the data (Table 15).

Table 15 Rate constants of TO (98%) fading in D ₂ O	
original rate constants/ min ⁻¹	original errors/ min ⁻¹
0.68522	0.06007
0.6944	0.03453
0.55967	0.03014
Average <i>k</i> / min ⁻¹	Average error/ min ⁻¹
0.64643	0.04158
standard deviation/ min ⁻¹	
0.06146295	

Lastly, we studied thiazole orange (98%) dissolved in tap water sonicated and filtered at 25 °C (Figure 24, experiments performed 3 times, see appendix).



Rate constants were determined by fitting a first-order rate law to the absorbance at 500nm (Table 16).

Table 16 Rate constants of TO (98%) fading in tap water	
original rate constants/ min ⁻¹	original errors/ min ⁻¹
0.34448	0.0135
0.30825	0.01052
0.28727	0.01101
Average k/ min ⁻¹	Average error/ min ⁻¹
0.31333333	0.011676667
standard deviation/ min ⁻¹	
0.023630859	

Our initial experiments were performed with TO which was not totally purified and because of that we observed anomalous peaks in the UV-Vis spectra (472 nm & 316 nm). After several experiments and NMR examinations of the solutions, we believe the impurities have little impact upon the TO fading. Regardless, when 3rd version of TO was used, it was clear that the anomalous peaks disappeared because of the high level of purification, affording easier, and more reliable, interpretation of the data.

Through all the experiments it was found that the rate constants and results were more rapid and more reliable using the final LED device, which employs lenses to increase the light fluence. In addition, we have discovered that particulate formation greatly impacts the ability to understand TO photofading, so filtration of solutions is required.

Limitation and obstacles with the LED device

When using the 3rd version of the LED irradiation device, no magnetic stirrer was initially used to homogenise the solution during irradiation. This will have likely affected our data because only part of the cuvette volume is irradiated. As a result, only molecules in the irradiated volume fade. In the absence of stirring, molecules outside the irradiated spot can only fade if they diffuse into the irradiated volume, resulting in biphasic kinetics. Biphasic kinetics were indeed observed by an M. Chem. Student. ⁽²⁴⁾ using an analogous device to study a different photochemical fading reaction without stirring.

We also found a heating issue. When the 3rd version LED device was used in these experiments over longer times, a thermal disconnect occurred leading to local heating from prolonged use, and therefore the frame surrounding the LED started melting.

Because of these obstacles, a final version of the LED (4th) device was designed and 3D-printed.

2.2.5 Kinetics experiments performed using the fourth revision of the LED based device.

After many experiments with the 3rd version of the device, an overheating issue appeared. To avoid overheating we order a new LED (Thorlabs MCWHLP1 Mounted LED, which is the heat-sink-mounted equivalent of MCWHD3) which comes attached to a dedicated cooling element (Figure 25).

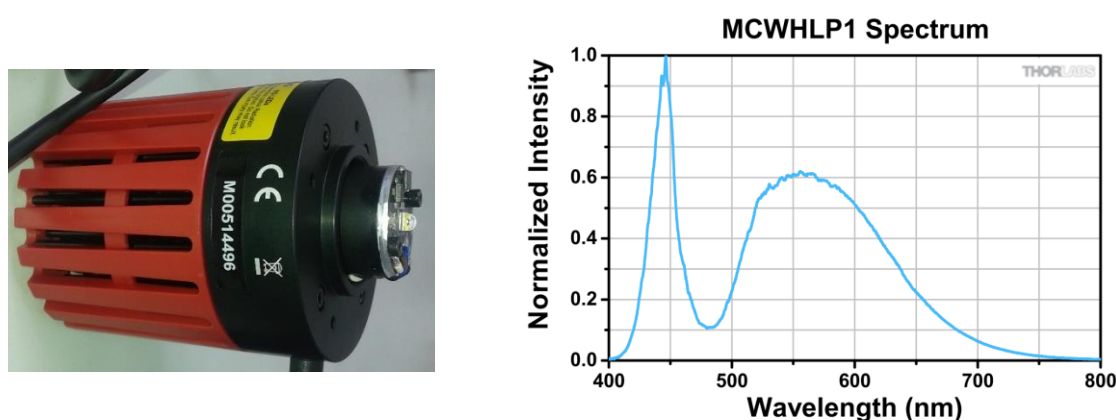


Figure 25 The new LED with attached heatsink and its spectral profile. ⁽³⁰⁾

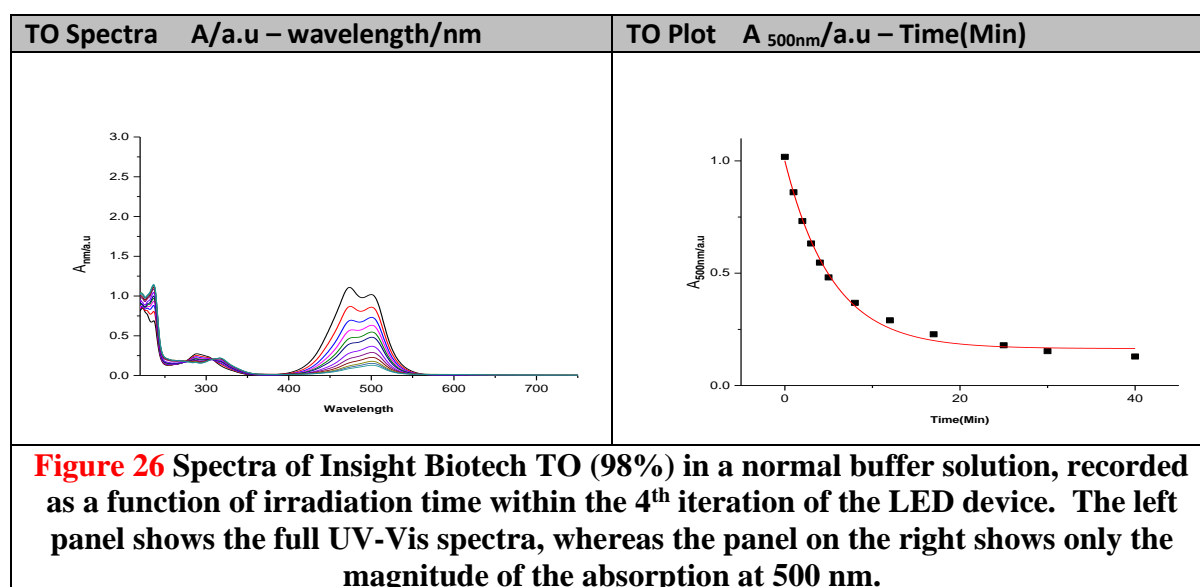
The Thorlabs' MCWHLP1 mounted LED ⁽³¹⁾ has a correlated colour temperature of 6500 K and an output of more than 2350 mW of power and is mounted to the

end of a large Ø57.0 mm heat sink. This LED needs to be supplied with a constant current that must not exceed the maximum current of 700 mA.

This LED gave some challenges in mounting to the cuvette holder (due to problems adjusting the alignment of the LED within the printed box). Therefore, we have multiple datasets in this Chapter and the next, some prior to a more accurate alignment of the LED, labelled "before setting" and some after re-alignment, labelled "after setting".

We have two series of data sets for various conditions. The first series of data sets is with the new LED **before setting**.

TO (98%) sonicated and filtered in buffer (pH=7, 25 mM MOPs, 50 mM NaCl and 1 mM EDTA) irradiated with the new LED before setting with magnetic stirring (Figure 26, experiments performed 3 times, also see appendix).

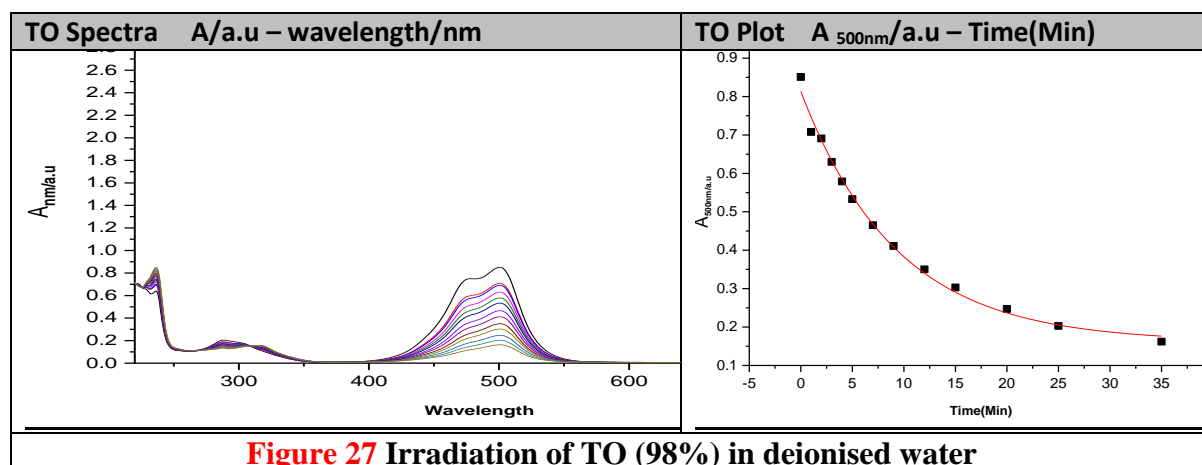


An equation representing a first-order rate law was fitted to the absorbances at 500 nm as a function of time and the resulting rate constants are summarised in Table 17.

Table 17 The rate constant of TO (98%) fading in a normal buffer solution, with the 4th iteration of the LED device.	
original rate constants / min⁻¹	original errors/ min⁻¹
0.18555	0.01088
0.18013	0.0251
0.17492	0.0244
Average k/ min⁻¹	Average error/ min⁻¹
0.1802	0.020126667
standard deviation/ min⁻¹	
0.004339962	

Table 17 shows that the rate constants are highly reproducible but lower than when measured with the third version of the device. We attribute this to slightly different positioning of the LED relative to the optics.

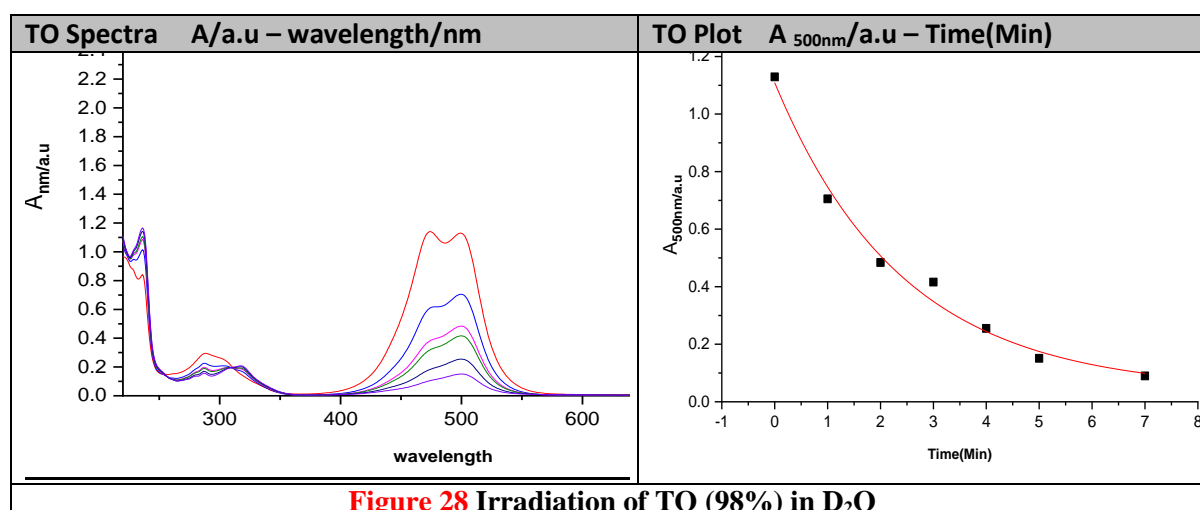
Analogous data for thiazole orange (98%) sonicated and filtered in deionised water, with stirring during irradiation, are illustrated in Figure 27 (experiments carried out 3 times, see appendix).



As before rate constants were determined by analysing the absorbance at 500 nm as a function of time and these are summarised in Table 18.

Table 18 Rate constants for TO (98%) fading in deionised water	
original rate constants/ min ⁻¹	original errors/ min ⁻¹
0.100643721	0.005404877
0.107902406	0.008300359
0.10404	0.00474
Average k/ min ⁻¹	Average error/ min ⁻¹
0.104195376	0.006148412
standard deviation/ min ⁻¹	
0.002965382	

Fading of thiazole orange (98% sonicated and filtered, with stirring during irradiation) was also studied in D₂O (Figure 28, experiments performed 3 times, see appendix).

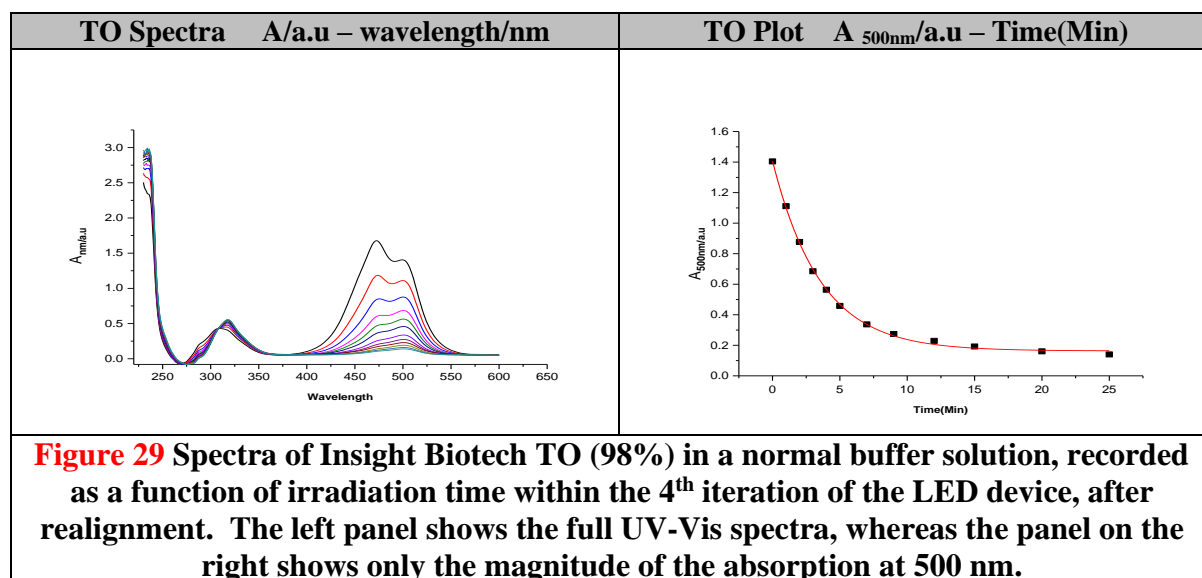


The resulting rate constants are listed in Table 18.

Table 18 Rate constants of TO (98%) fading in D ₂ O	
original rate constants/ min ⁻¹	original errors/ min ⁻¹
0.41385	0.06435
0.54147	0.02649
0.6944	0.03453
Average k/ min ⁻¹	Average error/ min ⁻¹
0.549906667	0.04179
standard deviation/ min ⁻¹	
0.114689315	

We believe the final version of this LED device is the most appropriate for studying photofading kinetics, however we were concerned about the stability of the LED mounted on the 3D-printed housing. We also noted the reduced rate constant with the new LED, which we attributed to poor alignment. Therefore, the housing was slightly altered a final time to make mounting the LED more reproducible. Because this only involved creating space to seat a screw that sticks out from the mounted LED, this is not considered a full design revision.

The fading of TO (98%) was studied with new LED **after setting** [the stability of the LED mounted on the 3D-printed housing was accurate to make the final version of LED- the 4th version] and magnetic stirring. Data for thiazole orange 98% sonicated and filtered with buffer (pH=7, 25 mM MOPS, 50 mM NaCl and 1 mM EDTA) at 25°C, are illustrated in Figure 29 (experiments performed 3 times, see appendix).



The rate constants from fitting the data in Figure 29 in terms of the first-order rate law are reported in Table 19.

Table 19 Rate constants of TO (98%) fading in buffer	
original rate constants/ min ⁻¹	original errors/ min ⁻¹
0.28133	0.00683
0.30496	0.01104
0.29658	0.0104
Average k/ min ⁻¹	Average error/ min ⁻¹
0.29429	0.009423333
standard deviation/ min ⁻¹	Average error/ min ⁻¹
0.009781864	0.032020569

The fading of thiazole orange (98%, sonicated and filtered) in deionised water was also studied using the new LED after setting and with magnetic stirring, yielding the data in figure 30 (experiments performed 3 times, see appendix).

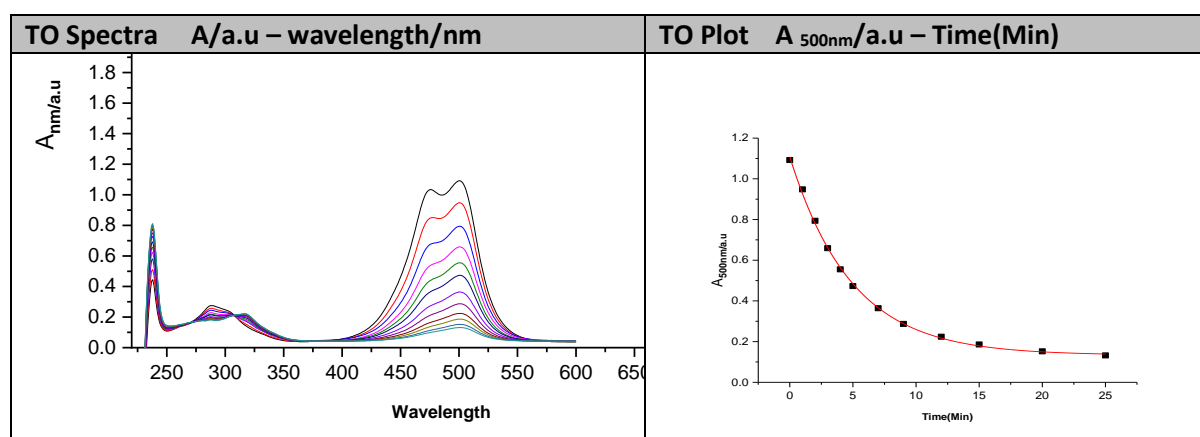
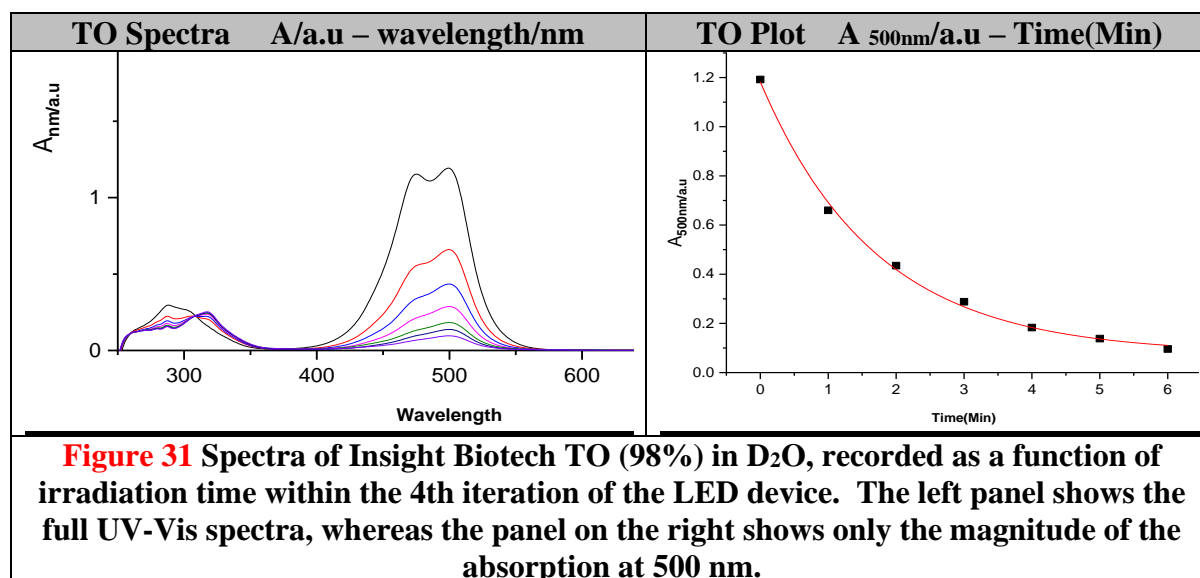


Figure 30 The spectra of Insight Biotech TO (98%) in deionised water, recorded as a function of irradiation time within the 4th iteration of the LED device. The left panel shows the full UV-Vis spectra, whereas the panel on the right shows only the magnitude of the absorption at 500 nm.

The rate constants are listed in Table 20.

Table 20 Rate constant of TO (98%) fading in D.W.	
original rate constants/ min ⁻¹	original errors/ min ⁻¹
0.204364839	0.005521467
0.21124	0.00237
0.27868	0.0111
Average k/ min ⁻¹	Average error/ min ⁻¹
0.23142828	0.006330489
standard deviation/ min ⁻¹	Average error %
0.033529696	0.027354

Finally, we examined fading of TO (98%) with the new LED after setting and with magnetic stirring. Data for thiazole orange sonicated and filtered in D₂O are illustrated in Figure 31 (experiments performed 3 times, see appendix).



The corresponding rate constants reported in Table 21.

Table 21 Rate constants of TO (98%) fading in D ₂ O	
original rate constants/ min ⁻¹	original errors/ min ⁻¹
0.58726	0.0388
0.50817	0.02336
0.67231	0.04772
Average k/ min ⁻¹	Average error/ min ⁻¹
0.589246667	0.036626667
standard deviation/ min ⁻¹	Average error %
0.067024598	0.062158462

2.3 Conclusions

Most of the experiments showed a fairly rapid reaction with the 4th version of our new LED device. This is greatly assisted by increasing the intensity of light through the use of high-end LEDs in combination with lenses. We also see much more reproducible kinetics thanks to the greater purity of the ligand, and thanks to careful filtering and stirring the solution during irradiation. Because of this substantial improvement in the design of the experiment, most of the experiments and data generated have been repeated to get better results and accurate rate constants.

Each experiment was repeated 3 times or more in order to calculate the average rate of the reaction and to evaluate the uncertainty in the measurements.

In comparison to the 1st and 2nd version of LED irradiation device, the obstacles of inconsistent power, insufficient intensity, and overheating of the LED, all of which effect on the result negatively, have been overcome. The last versions of the device, and most reliably device 4, allow us to record a reproducible, stable data and obtain results efficiently. We now observe rapid and consistent rate constants, with reduced standard deviations, for our datasets and fit parameters. We now anticipate that moving forwards, the last LED device allows us to generate highly efficient data and could be adapted for use in parallel to reduce the time cost of the experiments.

2.4 Experimental

2.4.1 Buffer preparation

All experiments were carried out in MOPS buffer. This buffer contained 25 mM MOPS, 50 mM NaCl and 1 mM EDTA, pH 7.0.

MOPS purchased from Melford (CAS 1132-61-2), NaCl was purchased from Fisher Scientific (CAS 7647-14-5), EDTA was purchased from VWR (CAS 60-00-4). The amounts required for 2 litres of buffer were dissolved in approximately 1.5 litres of distilled water with stirring at room temperature until all solids dissolved. A solution of sodium hydroxide (NaOH) was used for adjusting the pH to 7.0 and the buffer was made up to 2 litres in a volumetric flask.

The pH of aqueous solutions was determined using a Hanna microprocessor pH-meter equipped with a VWR 662-1382 glass electrode. Materials were weighed out on a Fisher brand 4-decimal balance. Deionised water was produced using an ELGA (description below) water purifier for all solutions (Ledvina, M,1991).

2.4.2 Filters for solutions

PTFE syringe filters (Thermo Scientific-0.22 and 0.45 μm) were used to filter solutions of dyes.

2.4.3 Equipment

JASCO V630 and V650 UV-Visible spectrophotometers were used to monitor reactions by either time resolved absorption (spectra) or parallel kinetic measurements. Both machines were equipped with a Peltier thermostat cell holder to control the temperature. ^1H NMR spectra were recorded in D_2O on a Bruker spectrometer (400 MHz). Water was purified using an ELGA option-R 7BP. Mass spectra were recorded using Waters Micromass LCT Premier Mass Spectrometer (Perkampus, H.1992).

2.4.4 Kinetic measurement using UV-Visible spectroscopy

Time resolved absorption peak measurements were carried out in 1.00 cm pathlength stoppered quartz cuvettes (Hellma) holding approximately 1.00 cm^3 of headspace (i.e., under aerobic conditions), at 25°C and different temperatures. Peaks are selected for temporal investigation through full UV-Visible time resolved absorption spectral measurements for the reactions. The wavelengths chosen were thiazole orange (500.0 nm) or DODC (580nm). Typically, a total volume of 2.5 ml was used.

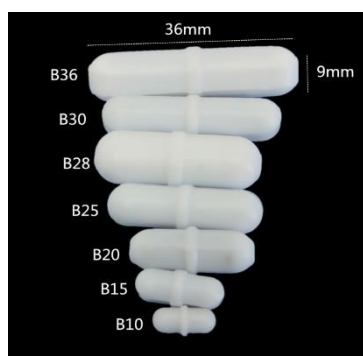
All rate constants are expressed as observed first-order rate constants. Kinetic measurements at fixed wavelengths were performed using the same JASCO V-650 UV-Visible spectrometer at constant temperature following the abovementioned procedure. Effects of the pH, buffer concentration, different NaCl, MOP's concentration and different temperature. were all studied by UV-Visible kinetic measurements. During the course of the project, the JASCO instrument was replaced with an analogous SHIMADZU- UV-1800 (UV-spectrophotometer).

2.4.5 Incubator

The device that we used is an incubator shaker: Heidolph unimax 1010 shaker with incubator. We used the incubator to control the temperature for the reaction.

2.4.6 IKA Big Squid (Ocean) Magnetic Stirrer

The IKA Big Squid is a magnetic stirrer suitable for mixing fluid media up to 1500 ml by using a magnetic bar up to a length of 30 mm. The speed can be adjusted between 0 and 1500 RPM. The dimensions of the device 18 x 17 x 5cm and it weight 0.8 kg and Serial no. 01.346321. We used a magnetic stirrer within this device to mix our solutions during irradiation.



2.4.7 Compounds

Heavy water (deuterium oxide, $^2\text{H}_2\text{O}$, D_2O) was purchased from Sigma-Aldrich.

DODC (H33094 3,3'-diethyloxadicarbocyanine iodide) was purchased from Alfa Aesar and was used in our experiments with last version LED device. The compound choice was highly purified H33094 3,3'-Diethyloxadicarbocyanine iodide, 96% from Alfa Aesar by Thermo Fisher Scientific company.

Early in these experiments we used a new batch of TO which was 80-90% pure obtained from ChemCruz. We then used another new version of TO (3rd) which

was 98% pure from Insight Biotechnology. This version was much purer, and consequently was stored at 4°C and protected from light.

2.4.8 Software

Graphs were constructed and kinetic data were analysed using Originlab Origin 2020 software. Wavelengths for analysis were selected through UV-Visible time resolved absorption spectra measurement for the reaction (for thiazole orange this was 500.0 nm). All rate constants are expressed as observed first-order rate constants resulting from fitting a first-order rate law to the data at 500 nm using Originlab Origin 2020.

Molarity Calculator. GraphPad Prism was used to calculate the molarity (Molar), volume (Milliliter) and formula weight (daltons - g/mol).

<https://www.graphpad.com/quickcalcs/molarityform.cfm>

2.5 References

1. Bigger, S. W. FlashPhotol: Using a Flash Photolysis Apparatus Simulator To Introduce Students to the Kinetics of Transient Species and Fast Reactions. (2016).
2. Tkachenko, N. V. *Optical spectroscopy: methods and instrumentations*. (Elsevier, 2006).
3. Soltis, M. G. Flash photolysis: the technique and its application. (1982).
4. Cosa, G., Focsaneanu, K.-S., McLean, J. R. N., McNamee, J. P. & Scaiano, J. C. Photophysical Properties of Fluorescent DNA-dyes Bound to Single- and Double-stranded DNA in Aqueous Buffered Solution¶]. *Photochem. Photobiol.* (2001) doi:10.1562/0031-8655 (2001) 073 <0585:ppofdd>2.0.co;2.
5. Abbruzzetti, S., Sottini, S., Viappiani, C. & Corrie, J. E. T. Kinetics of proton release after flash photolysis of 1-(2-nitrophenyl) ethyl sulfate (caged sulfate) in aqueous solution. *J. Am. Chem. Soc.* **127**, 9865–9874 (2005).
6. Novak, J. R. & Windsor, M. W. Laser photolysis and spectroscopy: a new technique for the study of rapid reactions in the nanosecond time range. *Proc. R. Soc. London. Ser. A. Math. Phys. Sci.* **308**, 95–110 (1968).
7. Instruments, F. P.-T. L. S. made by E. 48. <https://www.edinst.com/wp-content/uploads/2018/10/Flash-Photolysisusing-the-LP980-Web>.
8. Banderini, A., Sottini, S. & Viappiani, C. Method for acquiring extended real-time kinetic signals in nanosecond laser flash photolysis experiments. *Rev. Sci. Instrum.* **75**, 2257–2261 (2004).
9. Skoog, D. A., Holler, F. J. & Crouch, S. R. *Principles of instrumental analysis*. (Cengage learning, 2017).
10. Penzkofer, A. & Leupacher, W. S0-S1 two photon absorption dynamics of organic dye solutions. *Opt. Quantum Electron.* **19**, 327–349 (1987).
11. Claude Rulliere.2005. Femtosecond laser pulses: principles and experiments / – [2nd ed.]. Library of Congress Cataloging-in-Publication Data (Advanced texts in physics, ISSN 1439-2674).ISBN 3-387-01769-0. Springer Science+Business Media, Inc.
12. Farr, E. P. *et al.* Introduction to time-resolved spectroscopy: Nanosecond transient absorption and time-resolved fluorescence of eosin b. *J. Chem. Educ.* **95**, 864–871 (2018).

13. Walker, Jearl D., "Fundamentals of Physics Extended, 9th ed." (2010). Scholarship Collection. 125.
<https://engagedscholarship.csuohio.edu/scholbks/125>
14. Kou, J. *et al.* Selectivity enhancement in heterogeneous photocatalytic transformations. *Chem. Rev.* **117**, 1445–1514 (2017).
15. Rapp, G. & Güth, K. A low cost high intensity flash device for photolysis experiments. *Pflügers Arch.* **411**, 200–203 (1988).
16. Gombár, M., Józsa, É., Braun, M. & Ósz, K. Construction of a photochemical reactor combining a CCD spectrophotometer and a LED radiation source. *Photochem. Photobiol. Sci.* **11**, 1592–1595 (2012).
17. <https://www.stouchlighting.com/blog/top-15-advantages-of-led-lighting>.
18. Ciugudeanu, C., Buzdugan, M., Beu, D., Campianu, A. & Galatanu, C. D. Sustainable Lighting-Retrofit Versus Dedicated Luminaires-Light Versus Power Quality. *Sustainability* **11**, 7125 (2019).
19. <https://www.thorlabs.com/drawings/383ba730fa8f5990-779CEFF9- & DF98-6C23-0A1112078641E87D/LEDWE-15-SpecSheet>.
20. <https://ggebooks.com/BOOKA/2-electricity/2-1-circuits.php>. The Simple Circuit.
<http://www.regentsprep.org/regents/physics/phys03/bsimplcir/default.htm>.
21. Scorpio, R. *Fundamentals of acids, bases, buffers and their application to biochemical systems*. (Kendall/Hunt Publishing Company, 2000).
22. EDTA. <https://www.takarabio.com/products/protein-research/sds-page-and-western-blotting/buffers-and-powders/edta-powder>.
23. Casalnuovo, I. A., Sorge, R., Bonelli, G. & Di Francesco, P. Evaluation of the antifungal effect of EDTA, a metal chelator agent, on *Candida albicans* biofilm. *Eur. Rev. Med. Pharmacol. Sci.* **21**, 1413–1420 (2017).
24. The Construction of an inexpensive, compact and modular 3D-printed UV-vis spectrometer for the measurement of absorption, emission and kinetics of photo driven reactions. *Ivan Lesnianski*. (2019).
25. LED, 2nd and 3rd device &
<https://www.thorlabs.com/thorproduct.cfm?partnumber=MCWHD3>.
26. Photodiodes.aspx?, H. com/standard-products/ingaa., gclid =
EA1aIQobChMIkKag9ZOA7QIVB- &
3tCh2rRwYrEAAAYASAAEgKHBvD_BwE.

Chapter 2 - Development of a LED device for kinetic studies of photochemical reactions

27. https://www.thorlabs.com/newgrouppage9.cfm?objectgroup_id=2616.
28. <https://www.olympus-lifescience.com/en/microscope-resource/primer/lightandcolor/filtersintro/>.
29. <https://www.edmundoptics.co.uk/knowledge-center/applicationnotes/optics/optical-filters/>.
30. Paper 4Th Version.
https://www.thorlabs.com/newgrouppage9.cfm?objectgroup_id=14242
31. <https://www.thorlabs.com/drawings/6992a0b0a03db2e0-3F145436- & A7C7-3288-C2F59F2FF8EEF4B3/M405LP1-SpecSheet.pdf>.

Chapter Three

Kinetic studies of fading of thiazole orange

Summary

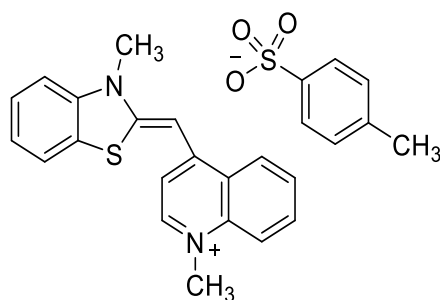
Thiazole orange (TO) is a dye and most of the uses of this molecule are dependent on its vivid colour. However, the colour fades over time, lessening its utility. We have analysed the kinetics of this fading process, determining that it is irradiation with light in the visible region of the spectrum that drives the colour change. We have demonstrated that TO shows increased fading with increased intensity of light, demonstrating that the reaction proceeds via the excited state of TO. Additionally, we investigated the effect of oxygen within the solution because light-driven singlet-oxygen generation is often used to explain photobleaching processes in biological stains. We found that limiting the amount of oxygen [when we de-gas the solution by vacuum degassing or by bubbling N₂ gas through the solution] limited the extent of reaction, although the reduced oxygen concentration has no effect on the observed reaction rate constant.

Other factors may also play a role in the fading process, for example temperature, type of buffer, buffer concentration, pH, and the presence of additives. We examined each of these in turn and show that this provides new kinetic insights into the mechanism of fading of thiazole orange. The composition of different buffers did not affect kinetics; different concentrations of MOPS and different pH all produce similar rate constants. This observation suggests that (de)protonation processes do not play a role in the reaction up to the rate-determining step. Even carrying out the reaction at three different temperatures (25 °C, 35 °C and 45 °C) did not strongly affect the observed kinetics. In fact, the observed rate constant for fading decreases with increasing temperature, suggesting that the fading reaction is in competition with a more temperature-sensitive pathway quenching the excited state of TO. The addition of singlet-oxygen quenchers does not affect the observed kinetics. Mass spectroscopy suggests that the product may be formed following reaction of the photoexcited species with a molecule of oxygen.

3.1 Introduction

3.1.1 Thiazole orange

Thiazole orange (TO) consists of two heterocyclic ring systems, a quinolinium cation connected to a benzothiazole by a methine bridge ⁽¹⁾ (Scheme 1).



Scheme 1.

TO is a fluorescent dye which means that it emits light after excitation ⁽¹⁾. The wavelength of the emitted light is longer than that of the incident light, as usual. The extinction coefficient (ϵ) is $63,000 \text{ M}^{-1} \text{ cm}^{-1}$ at 500 nm ^(2, 3). General spectroscopic characteristics of thiazole orange are summarised in Table 1.

Table 1. Selected spectroscopic properties of thiazole orange.	
Description	Characteristic
Absorption	λ_{max} 500-508 nm
Fluorescence	λ_{ex} 509 nm; λ_{em} 530 nm in 0.1 M phosphate pH 7.0

Fluorescence intensity of TO relies on its conformation ⁽⁴⁾. Computational studies on these dyes showed that twisting the monomethine bridge beyond an interplanar angle of 60 degrees leads to a dark state that non-radiatively decays to the ground state, accounting for the fluorogenic activity observed ⁽⁵⁾. The effects of position and number of fluorine substituents correlate with both observed quantum yield and calculated activation energy for twisting beyond this critical angle ^(5, 6). Cyanine dye fluorescence including (TO) is quenched in the excited state by intramolecular twisting. The interconversion is intrinsic to thiazole orange dye. As the structure twists away from the Franck-Condon region and becomes more displaced, the electronic ground state overlaps with increasingly higher vibrational wave functions. Therefore, twisting motion is leveraged through a

rapidly decreasing effective energy distance between the two electronic states, and internal conversion follows (7,8).

Thiazole orange is subject to protonation events. The resulting cation exhibits long wavelength absorption and a strong fluorescence band when the indole nitrogen atom is protonated (9). In less acidic media, the cation would be deprotonated, resulting in a neutral nitrogen atom that results in a blue-shifted absorption band and decreased fluorescence emission. Most of the pH-sensitive dyes currently used are analogues of well-known cyanines (10).

3.1.2 Fading of thiazole orange by oxygen and light.

Most of the uses of thiazole orange are dependent on its vivid colour and fluorescence, however the colour (and fluorescence) fades over time, lessening its utility; as with other cyanines, thiazole orange suffers from poor photostability (11,12).

The principal photodecomposition process is thought to include reaction with $^1\text{O}_2$ singlet oxygen. Specifically, thiazole orange in its singlet excited state S1 undergoes intersystem crossing to the triplet excited state T1. The dye's T1 state then reacts with triplet oxygen to form singlet oxygen (13,14). Singlet oxygen is then thought to react with the dye.

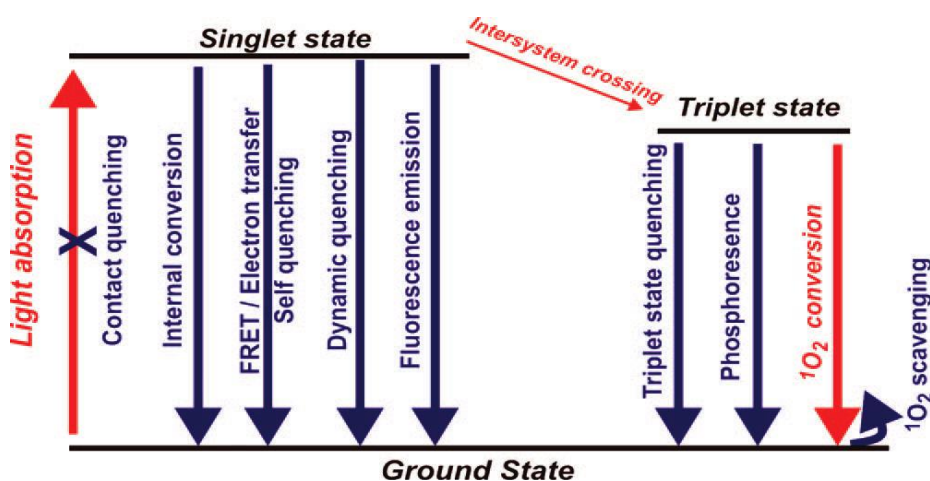


Figure 1 Simplified energy level diagram showing potential singlet oxygen deactivation pathways (10)

Singlet oxygen can be regarded as an electrophile. It should therefore be possible to reduce the dye reactivity towards singlet oxygen by introduction of electron-withdrawing substituents and thus improving photostability. The photostability of thiazole orange-derived dyes has indeed been enhanced when the electron density is decreased by cyano groups at the methine bridge or by fluoro substituents at the aromatic sections of cyanine dyes.⁽¹⁵⁾ For thiazole orange-derived dyes, Armitage et al. have shown that electron-withdrawing substituents lower the HOMO (and LUMO equally) energy, especially at the benzothiazole moiety, while those substituents at the quinolinium part leave the HOMO energy somewhat unaffected (and reduce mainly the LUMO energy)⁽¹⁶⁾.

An alternative mechanism involves type I reactions forming the superoxide radical anion and the perhydroxyl radical as major reactive oxygen species. In this mechanism, excited singlet states are alternatively quenched by photoinduced electron transfer (PET) processes with oxygen. In particular, because of its high oxidation potential, the perhydroxyl radical undergoes electron transfer with centres rich in electrons.⁽¹⁷⁾

3.1.3 Aim and purpose

We will study the kinetics of fading of thiazole orange under different conditions. We will follow fading using the LED irradiation setup that we developed with help of Dr. Joseph Beames (See Chapter 2) and analyse the resulting kinetic data with a focus on elucidating the mechanism of fading of TO.

We will analyse the kinetics of this fading process, determining whether it is irradiation that drives the colour change. Additionally, we investigate the effect of oxygen within the solution: light driven singlet oxygen generation is often used to explain photo bleaching processes in biological stains. Nevertheless, many other factors may also play a role in the fading process, for example temperature, type of buffer, buffer concentration, pH, and the presence of additives. We will examine each of these in turn to provide new kinetic insights into the mechanism of fading of thiazole orange.

3.2. Results and discussion

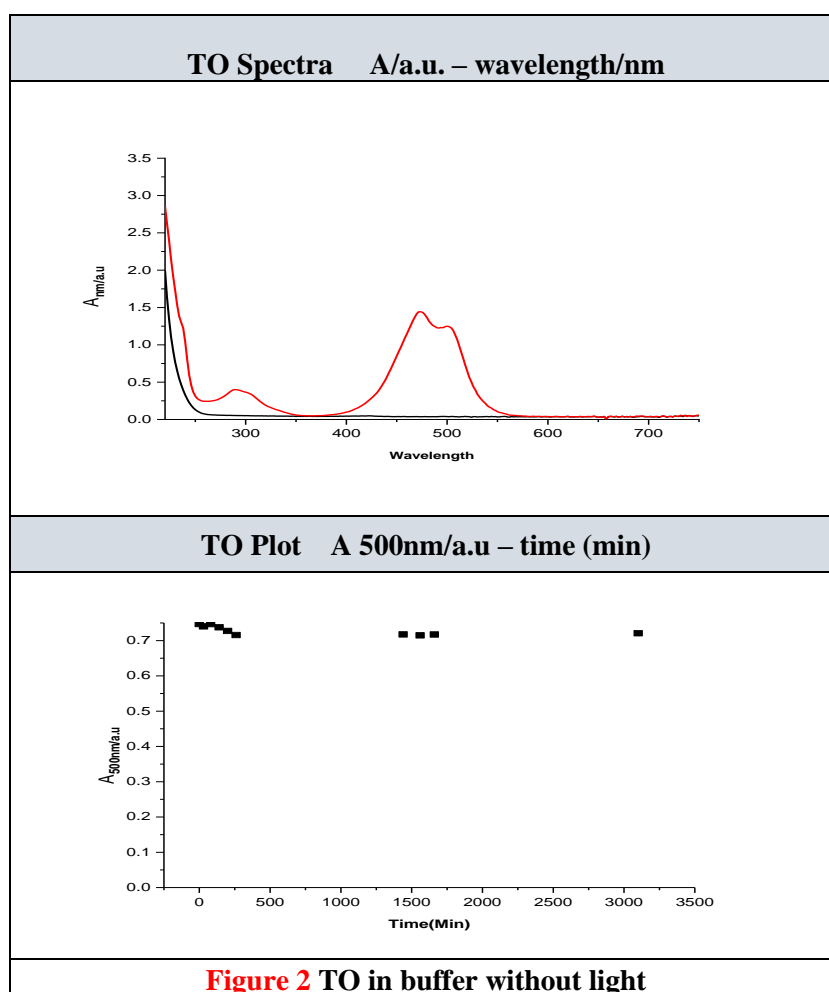
We carried out kinetic and spectroscopic studies and this section starts with the kinetic studies.

3.2.1 Kinetic studies of fading of TO.

We studied the kinetics of fading of TO as a function of absence or presence of light, effect of pH, effect of buffer concentration, and effect of temperature. The results are described in the following subsections.

a) Effect of light.

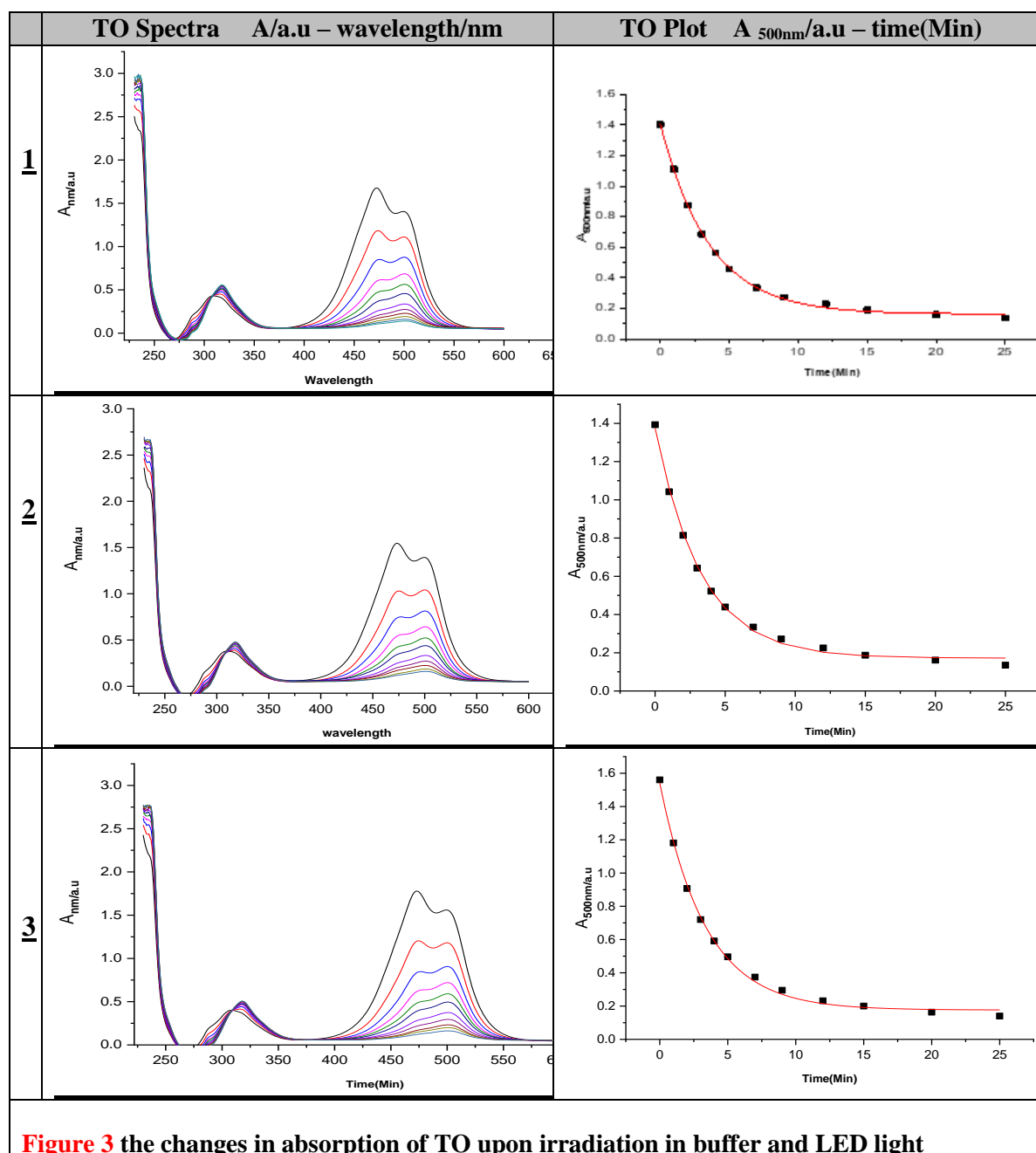
To confirm that fading of TO is driven by light, the stability of TO in the dark was studied first. In this experiment thiazole orange (highly purity sample) was shielded from light. TO was placed in buffer (25 mM MOPS, pH 7.0, 50 mM NaCl and 1 mM EDTA), sonicated and then filtered. The solution was kept in the dark with magnetic stirring at 25 °C (Figure 2).



Chapter Three Kinetic studies of fading of thiazole orange

Figure 2 shows the result of experiments with TO in buffer at 25 °C in the dark. Figure 2 shows that no fading happened.

Figure 3 shows the reaction of TO in buffer upon irradiation using our LED set up (Chapter 2). The changes in absorption upon irradiation were measured in three-fold in buffer (25 mM MOPS pH 7.0, 50 mM NaCl and 1 mM EDTA) with magnetic stirring at 25 °C.



First of all, Figure 3 shows that fading now occurs. This observation confirms that exposure to light is the basic reason for fading and when this reason disappears fading will not occur, as shown by Figure 2.

The spectra show two peaks for TO between 400 and 500 nm. In the literature, the longer wavelength peak is attributed to the monomer and the shorter wavelength peak to the dimer. ⁽¹⁸⁾ Accordingly, the relative peak heights for the two peaks change as fading progresses because the TO concentration decreases, leading to the dimerization equilibrium to shift towards the monomer.

The absorbance at 500 nm was plotted as a function of time and a first-order exponential decay curve was fitted to the data. The resulting rate constants are summarised in **Table 2**.

Table 2 Rate constants for fading of TO^a	
original rate constants	original errors
0.28133 min⁻¹	0.00683
0.30496 min⁻¹	0.01104
0.29658 min⁻¹	0.0104
average <i>k</i>	Average error
0.294 min⁻¹	0.010 min⁻¹
standard deviation	Average error %
0.010 min⁻¹	0.032
<p>a) Upon irradiation of a stirred solution of TO in buffer (25 mM MOPS pH 7.0, 50 mM NaCl and 1 mM EDTA) at 25 °C. Experiment 11-4-2019.</p>	

Table 2 shows that reproducible kinetic data for fading of TO can be obtained giving a rate constant $k = (0.294 \pm 0.010) \text{ min}^{-1}$

b) Effect of pH

We wanted to know the effect of pH of buffer (25 mM MOPS, 50 mM NaCl and 1 mM EDTA) on the kinetics of fading. Buffers were prepared at pH 4.30, 7 and 10.80. The new LED after setting (Chapter 2) was used with magnetic stirring of the solution at 25 °C. The results are summarised in Table 3.

Table 3. fading of TO at different pH ^a				
Description	average k_{obs} / min^{-1}	average error / min^{-1}	standard deviation / min^{-1}	error margin / min^{-1}
pH = 4.3	0.3358	0.0195	0.0351	0.0351
pH = 7.0	0.2943	0.0094	0.0098	0.0098
pH = 10.8	0.3286	0.0095	0.0301	0.0301
a- (with the individual overlay spectra and kinetic traces in the appendix).				

For ease of comparison, rate constants in Table 3 are plotted as a function of pH (Figure 4). We did not create the more usual plot of $\log k$ as a function of pH because changes in k are minimal.

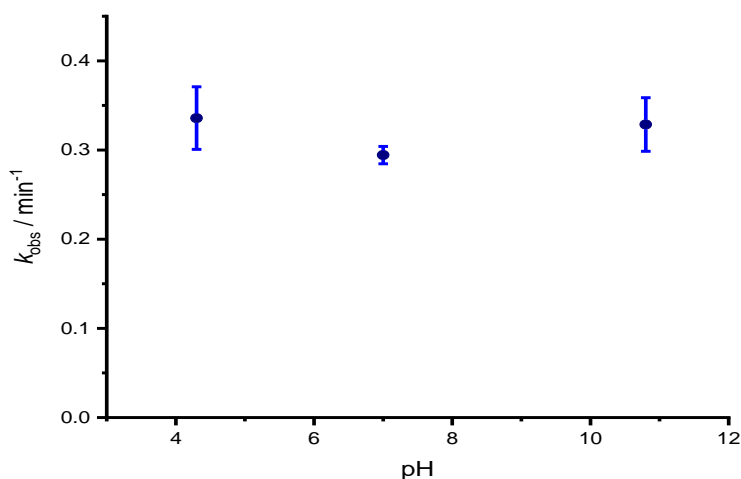


Figure 4 Relation between k for fading of TO and pH of buffer.

Figure 4 shows negligible changes in k with varying pH. This observation suggests that equilibrium (de)protonation processes do not play a significant role in the reaction up to the rate-determining step. We note that pH 4.3 and 10.8 are outside the region of good buffer capacity of MOPS, but the absence of a strong effect is pH is clear regardless.

c) Effect of buffer concentration.

We next studied the effect of buffer concentration on the kinetics of fading to evaluate whether the reaction shows general-acid or general-base catalysis. The reference buffer is 25 mM MOPS, so we used different concentrations (50 mM and 100 mM) of MOPS with other components maintained consistent (Table 4).

Table 4 Effect of buffer concentration on fading of MOPS ^a ,				
Description ^b	Average (k obs.) / min⁻¹	Average error / min⁻¹	Standard deviation / min⁻¹	Error margin / min⁻¹
25 mM	0.2943	0.0094	0.0098	0.0098
50 mM	0.3579	0.0136	0.0220	0.0220
100 mM	0.3364	0.0147	0.0167	0.0167
a- Average of experiments carried out in triplicate.				
b- MOPS concentration				

From the data in Table 4 Figure 5 was constructed.

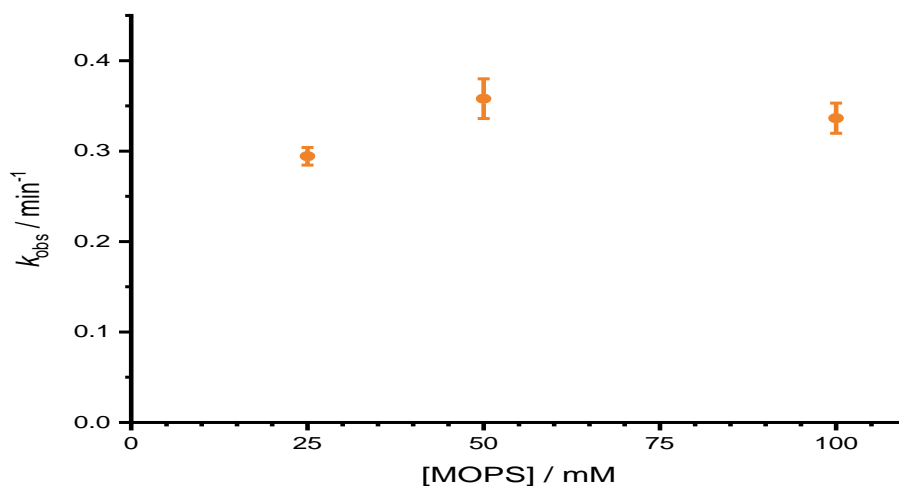


Figure 5. The relation between log k for fading of TO and concentration of MOPS.

Figure 5 illustrates that the different concentrations of MOPS did not affect kinetics. This observation suggests that (de)protonation processes do not play a role in the reaction up to the rate-determining step (Appendix).

d) Effect of ionic strength.

We wanted to know whether ionic strength affects the reaction. The reference buffer involved 50 mM of NaCl, so we used 100 mM and 200 mM NaCl with other buffer components consistent with the reference buffer. The results are summarised in Table 5.

Table 5 Kinetics of fading of TO at varying ionic strength ^a				
Description ^b	Average (k obs.)	Average error	Standard deviation	Error margin
50 mM	0.2943	0.0094	0.0098	0.0098
100 mM	0.2786	0.0141	0.0191	0.0191
200 mM	0.2438	0.0177	0.0232	0.0232
a- Experiments carried out in triplicate.				
b- Concentration of NaCl				

The rate constants in Table 5 are presented in Figure 11.

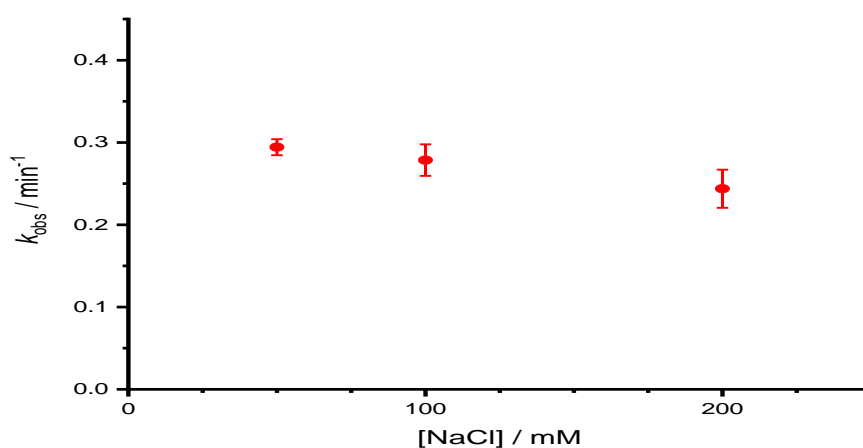


Figure 6 Relation between k for fading of TO and ionic strength.

Figure 6 shows a negligible effect of ionic strength, with at most a small decrease in rate constant with increasing ionic strength. The observation shows that ionic strength doesn't strongly affect the kinetics, suggesting that there is little formation or disappearance of charge up to, and including in, the rate-determining step.

e) Different temperature

We wanted to know the impact of different temperatures on the fading reaction and determine activation parameters. We therefore experimented at 3 different temperatures (25 °C, 35 °C and 45 °C) with the new LED after setting (Chapter 2) and with magnetic stirring in the reference buffer (Table 6).

Table 6 rate constants for fading of TO at different temperatures. ^a				
Description ^b	Average (k_{obs})	Average error	Standard deviation	Error margin
25 °C	0.2943	0.0094	0.0098	0.0098
35 °C	0.2769	0.0112	0.0259	0.0259
45 °C	0.2591	0.0094	0.0420	0.0420
a- Data for experiments carried out in triplicate.				
b- Temperatures determined by incubator temperature control				

An Eyring plot was created using the data in Table 6 (Figure 7).

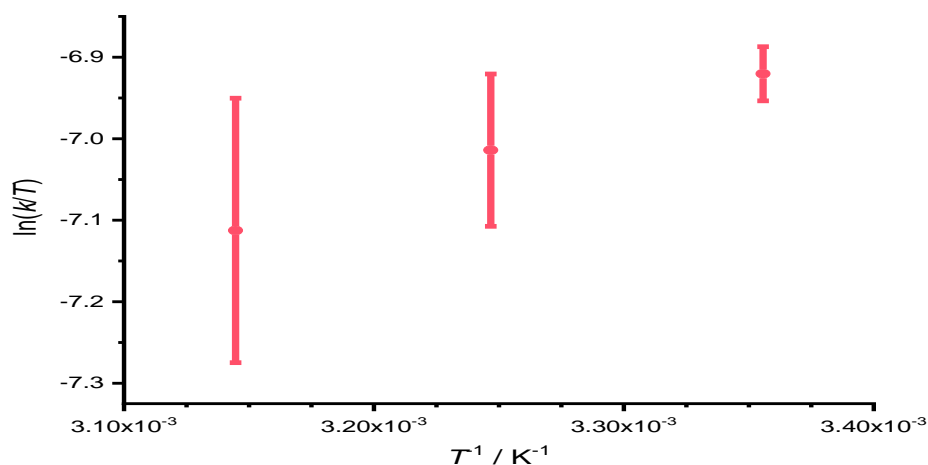


Figure 7 Relation between $\ln k/T$ for fading of TO and inverse temperature.

The Eyring plot suggests a negative standard molar enthalpy of activation, which is unrealistic. This observation suggests that there are no significant thermal barriers up to the transition state of the rate-determining step. This, in turn, suggest that limited molecular reorganisation is involved in reaching the transition state of the rate-determining step after photo-excitation. In addition, the data suggest that there is likely a pathway that quenches the excited state of TO without leading to fading which is temperature sensitive and proceeds faster at higher temperatures. This quenching mechanism allows the TO molecule to

return to its ground state rather than proceeding through the photochemical reaction, decreasing the rate of fading.

f) Effect of water source

The previous sections show that pH, buffer concentration and ionic strength do not affect reaction kinetics. We therefore wondered whether deionised water was required for these kinetics studies, in light of potential applications where deionised water may not be readily available. We changed the water used in our experiments and we got reproducible rate constants again (Table 7).

entry	Description	Rate constant (<i>k</i>)
1	reference buffer pH=7	0.2943 ± 0.0094
2	tap water instead of deionised water in reference buffer pH=7	0.2727 ± 0.0074
3	deionised water	0.2314 ± 0.0063
4	tap water	0.1612 ± 0.0091

The results in Table 7 show that the rate constants in buffered solutions are essentially the same, as expected based on the observation that buffer composition does not affect fading kinetics and the fact that the concentrations of buffer components are significantly higher than concentrations of potential contaminants remaining in tap water. Surprisingly, the rate constants for fading of TO are lower in deionised water alone and in tap water.

We are not sure why this is the case. It may be required to repeat these experiments with different water sources, and at low concentrations of buffer components to understand the differences in rate constants.

g) Solvent kinetic isotope effect (KIE)

We next evaluated the solvent kinetic isotope effect (SKIE) for fading of TO (Table 8).

entry	Description	Rate constant (k)
1	reference buffer	0.2943 ± 0.0094
4	D ₂ O-based buffer	0.4171 ± 0.0261
2	deionised water	0.2314 ± 0.0063
3	D ₂ O (Deuterium oxide)	0.5892 ± 0.0366

Table 8 shows that the reaction is faster in deuterated solvent. Because pH and buffer concentration don't affect the reaction kinetics, there are no protonation processes that can lead to a SKIE. However, it is known that deuterated solvents reduce quenching of singlet oxygen, thus enhancing reactions involving singlet oxygen. The observed SKIE therefore suggests a reaction involving singlet oxygen. There is a possibility that deuterated solvents may also reduce quenching of the excited state of TO and therefore accelerate a photochemical reaction proceeding from the excited state, leading to enhanced fading. However, in light of a recent correlation between fluorescence enhancement upon switching from H₂O to D₂O and absorbance wavelength of fluorescent dyes, ⁽¹⁹⁾ this appears unlikely for TO which has an absorbance maximum around 500 nm.

h) Effect of the nature of the buffer

Amines can be used as sacrificial electron donors in photochemically initiated reactions. Because MOPS contains an amine functional group and might therefore also act as a sacrificial electron donor, it is important to evaluate the effect of buffer choice on the reaction.

We therefore compared the effect of MOPS and phosphate buffer (Na₂HPO₄) on the reaction (Table 9), with all other parameters maintained as in the reference buffer.

	Description	Rate constants (k)
1	reference buffer	0.2943 ± 0.0094
2	Na ₂ HPO ₄ -based buffer	0.4081 ± 0.0229

It's clear there is a significant change in average *k*, with phosphate buffer giving a higher constant rate than MOPS buffer (Appendix). Although we don't have an explanation for the 30% increase in the rate constant upon going from MOPS to

Na_2HPO_4 , it is clear that MOPS doesn't drive the reaction forward in comparison with phosphate. This suggests that donation of an electron by the amine to excited state (if this happens) is more likely to stop the reaction than to support it.

i) Effect of oxygen

We next studied the effect of oxygen on the kinetics of fading. We firstly degassed the buffer by alternate flushing with N_2 and evacuation under vacuum in the dark for 2 hours.

We then added thiazole orange from the filtered and sonicated stock solution and the resulting sample was exposed to LED irradiation under a N_2 atmosphere. The N_2 atmosphere was maintained using a balloon connected to a needle sticking through the stopper of our cuvette. This setup created an environment with limited oxygen, although it is difficult to make it fully oxygen free. The result is shown in **Figure 8**.

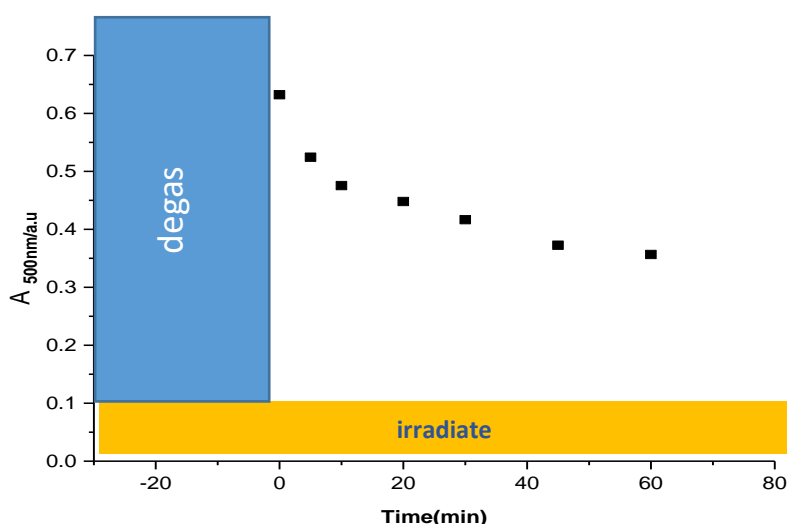


Figure 8. Fading of TO after degassing the sample.

Figure 8 shows that fading occurred, but the higher final absorbance of approximately 0.35 compared to other experiments suggests that the reaction stops before all TO has faded. We interpret this as indicating that there is a small quantity of O_2 , as a result of imperfect degassing, that leads to the chemical reaction to proceed to some extent.

When we fitted a first-order rate law to the data, we found a rate constant of $0.27 \pm 0.0035 \text{ min}^{-1}$. This rate constant is similar to the rate constant found for fading in the reference buffer without degassing.

We wanted to confirm that the reaction had indeed stopped as a result of depleting available oxygen. Figure 9 shows what happened after allowing O₂ into the cuvette, keeping the cuvette open in the dark for 1 hour, and subsequent exposure again to the LED irradiation.

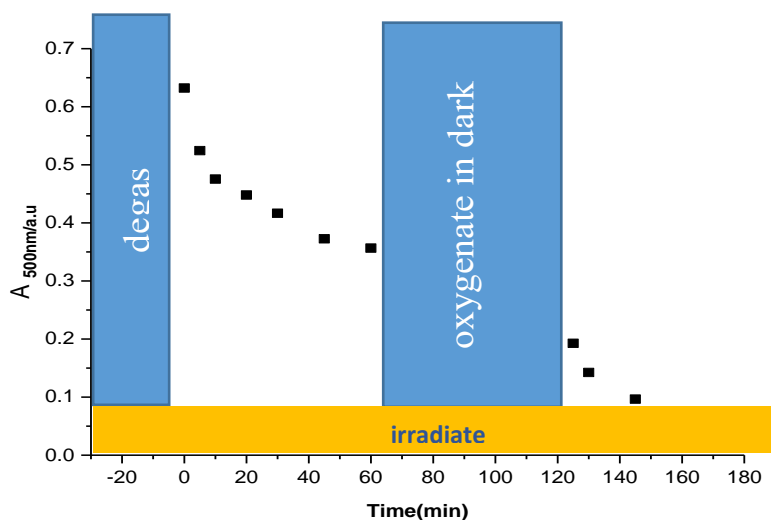


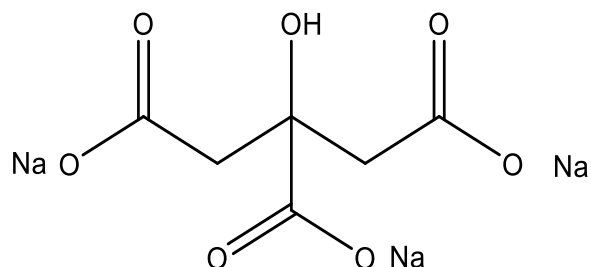
Figure 9 The absorbance of TO as a function of time in an experiment that involved degassing, followed by 60 minutes of irradiation, aeration of the sample in the dark for 60 minutes, followed by further irradiation.

Figure 9 shows that allowing the solution to oxygenate subsequently allows the reaction to go to completion. The fact that the rate constant does not change even though the extent of the reaction is limited by how much oxygen is present suggests that O₂ is not involved in the rate-determining step.

j) Effects of buffer additives

Sodium citrate (Na₃C₆H₅O₇, Scheme 2) was added to the reference buffer to discover its effect on the kinetics of fading. Citrate is used, amongst others, to stabilise serum (See Chapter 5). Sodium citrate is the anticoagulant used during blood collection. Anticoagulant-preservatives are used to prevent the blood from clotting or coagulating after collecting the blood from the donor, and then these materials provide enough nutrients to maintain red blood cell functionality and practicability during transportation and storage⁽²⁰⁾. The final citrate concentration in blood components is highest in plasma product. To allow testing for the

envisaged applications using serum, we therefore need to know whether citrate affects TO fading kinetics when it is used in our reference buffer.



Scheme 2

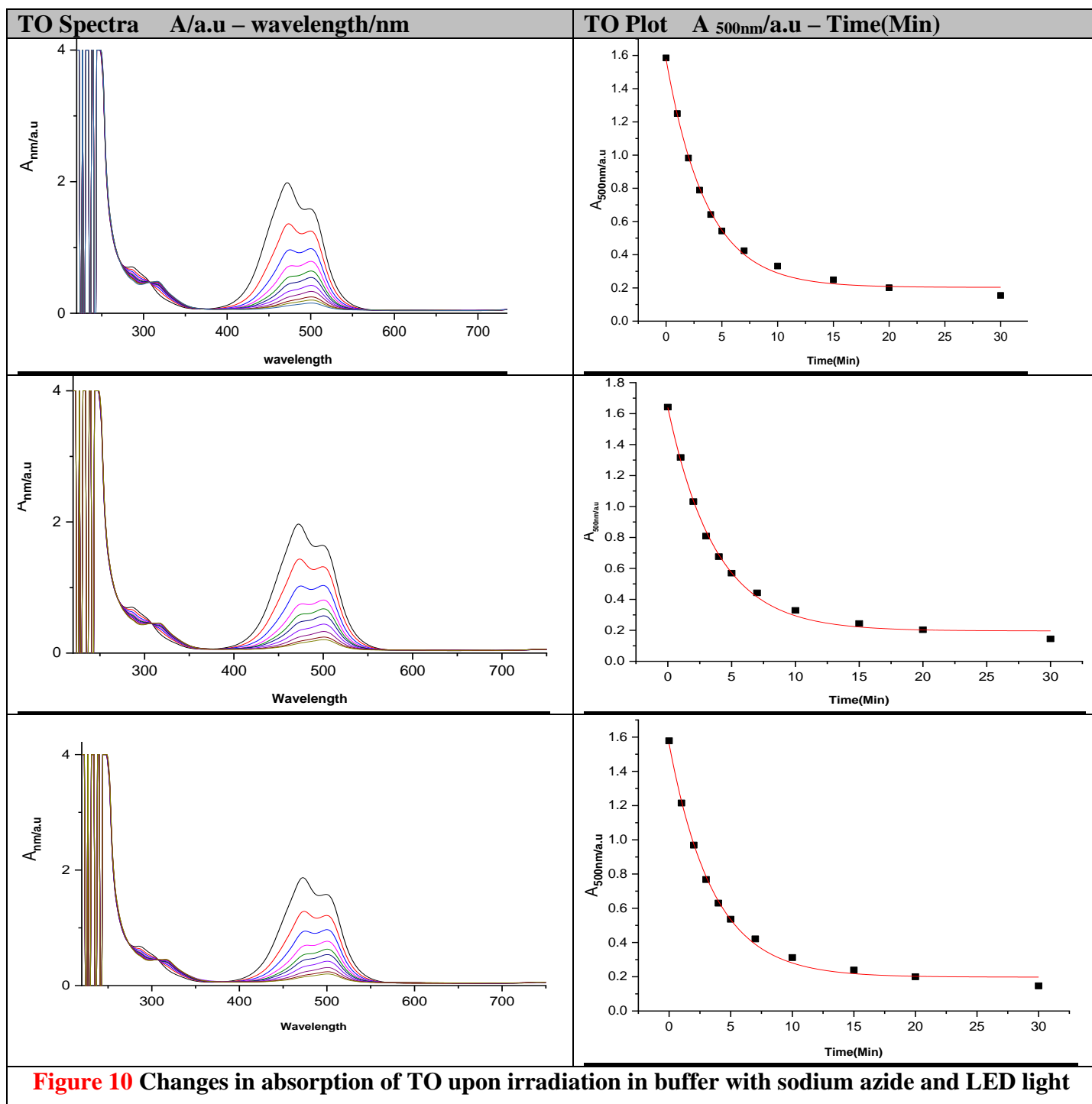
We added 20 mM sodium citrate to the reference buffer that we used before (pH=7, 25 mM MOPs, 50 mM NaCl, 1 mM EDTA) and irradiated a solution of TO with the last version of the LED with magnetic stirring (Appendix). We get the rate constants reported in Table 10.

	Description	Rate constants k / min^{-1}
1	Reference buffer	0.2943 ± 0.0094
2	Reference buffer + $\text{Na}_3\text{C}_6\text{H}_5\text{O}_7$	0.3573 ± 0.0133

From the results in Table 10, there is a change in average k in comparison with reference buffer without sodium citrate. The reason for the increase is not obvious but we note that the increase is relatively small.

We next add sodium azide (NaN_3) to the reference buffer to discover its effect. Sodium azide is used to discover whether the reaction involves singlet oxygen. The indirect tests for singlet oxygen are based on the inhibiting effects of an additive on the rate of a photochemical reaction. For example, azide ion is a useful water-soluble agent. Sodium azide as quencher is widely used for removing O_2^- and $^1\text{O}_2$ from reaction mixtures.

Figure 10 shows the overlay spectra and a plot of absorbance of TO at 500 nm, in the presence of 10 mM sodium azide, with other components as in the reference buffer (pH = 7, 25 mM MOPS, 50 mM NaCl, 1 mM EDTA) using the last version of the LED setup for irradiating and magnetic stirring.



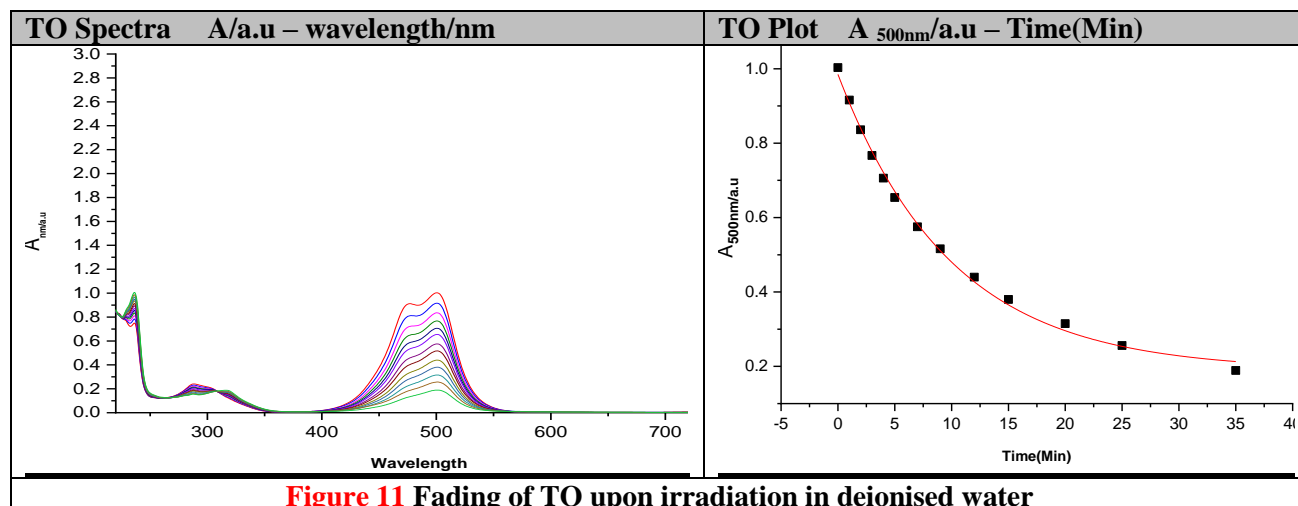
The obtained rate constants are summarised in Table 11.

Table 11 Rate constants for fading of TO in the presence of NaN ₃	
original rate constants	original errors
0.27652 min ⁻¹	0.01171
0.26909 min ⁻¹	0.01144
0.28 min ⁻¹	0.01198
Average k	Average error
0.275	0.012
standard deviation	Average error %
0.005 min ⁻¹	0.043

When we compare the average k in the presence of sodium azide (**Table 11**) and average k without sodium azide (**Table 2**), there is no significant change. This observation suggests that the reaction does not involve singlet oxygen.

k) Effect of light intensity.

We finally changed the power supplied to the LED to discover the effect of intensity of LED irradiation (using the last version of the LED setup but before setting – see Chapter 2) on the kinetics of fading under otherwise the same circumstances. We first irradiated with the full intensity of the LED in deionised water with magnetic stirring at 25 °C (3 times - appendix) see Figure 11.



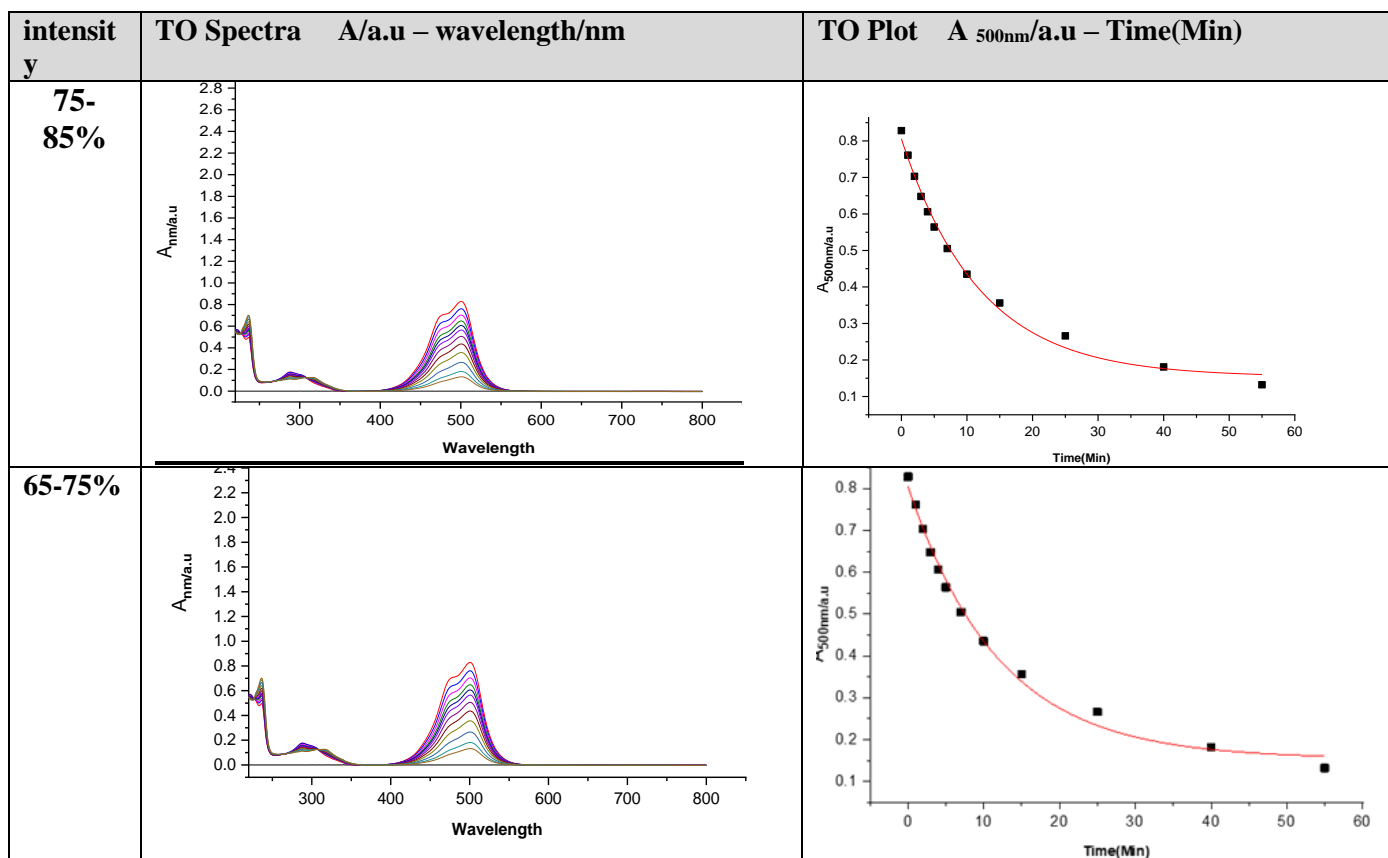
Chapter Three Kinetic studies of fading of thiazole orange

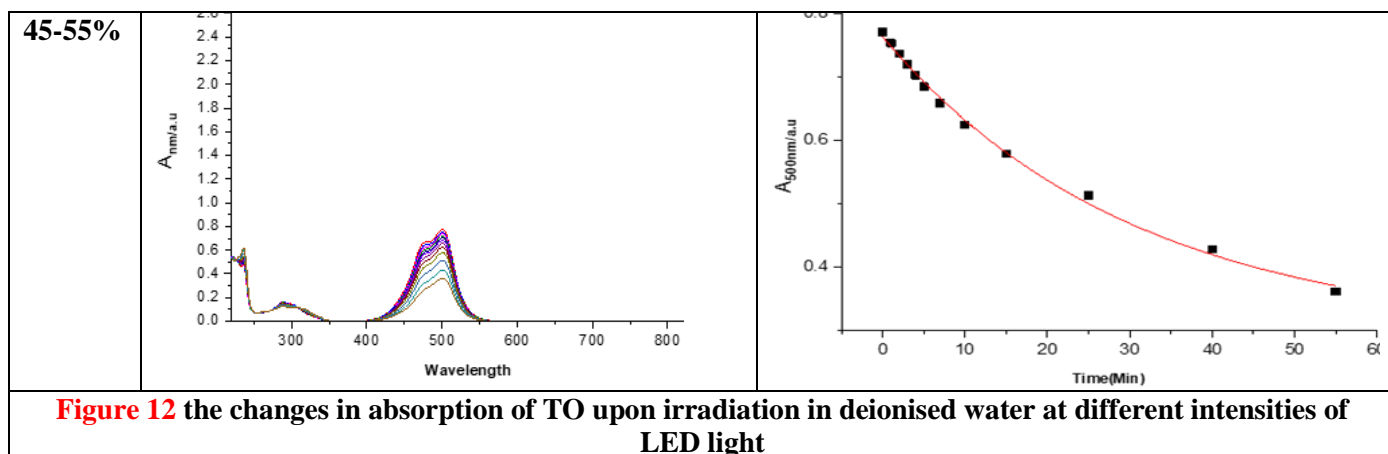
The resulting rate constants are summarised in Table 12.

Table 12 summarised fading TO with D.W and 100% LED in 15-3-2019	
original rate constants	original errors
0.100643721 min⁻¹	0.005404877
0.107902406 min⁻¹	0.008300359
0.10404 min⁻¹	0.00474
Average k	Average error
0.104	0.006
standard deviation	
0.003 min⁻¹	

Please note that the rate constants in Table 12 are lower than those reported elsewhere in this Chapter. The reason for this is that this experiment and the other experiments at varying light intensity in this sub-section were carried out with an earlier version of the irradiation setup.

The experiment was repeated at 75-85%, 65-75% and 45-55% intensity of LED in deionised water at 25 °C (Figure 12).



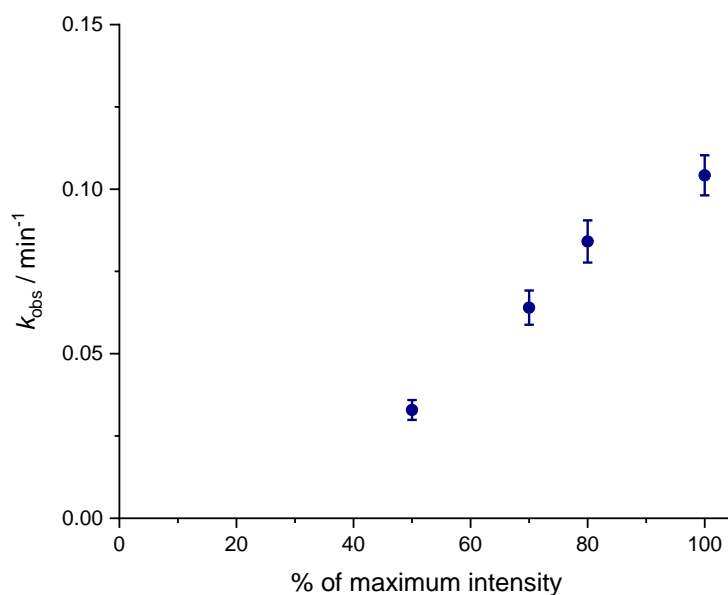


The resulting rate constants are summarised in Table 13.

Table 13 Fading of TO in deionised water at varying LED intensities

Intensity	rate constant	errors
100%	0.1042 min ⁻¹	0.0061 min ⁻¹
75-85%	0.0841 min ⁻¹	0.0064 min ⁻¹
65-75%	0.0640 min ⁻¹	0.0052 min ⁻¹
45-55%	0.0329 min ⁻¹	0.0030 min ⁻¹

The data in Table 13 are plotted in Figure 13.



Chapter Three Kinetic studies of fading of thiazole orange

Figure 13 shows the relation between the intensity and k , which demonstrates that the speed and time of fading is strongly affected by the intensity of LED. The increase is approximately linear, but the graphs does not appear to go through the origin for unknown reasons.

Note: because of COVID-19 lock down, we could not repeat the experiments with the new LED after setting (See Chapter 2).

3.2.2 product analysis

To understand the reaction better, we carried out mass spectrometry for thiazole orange (98%) before and after fading.

Figure 14 shows the positive and negative ions before fading.

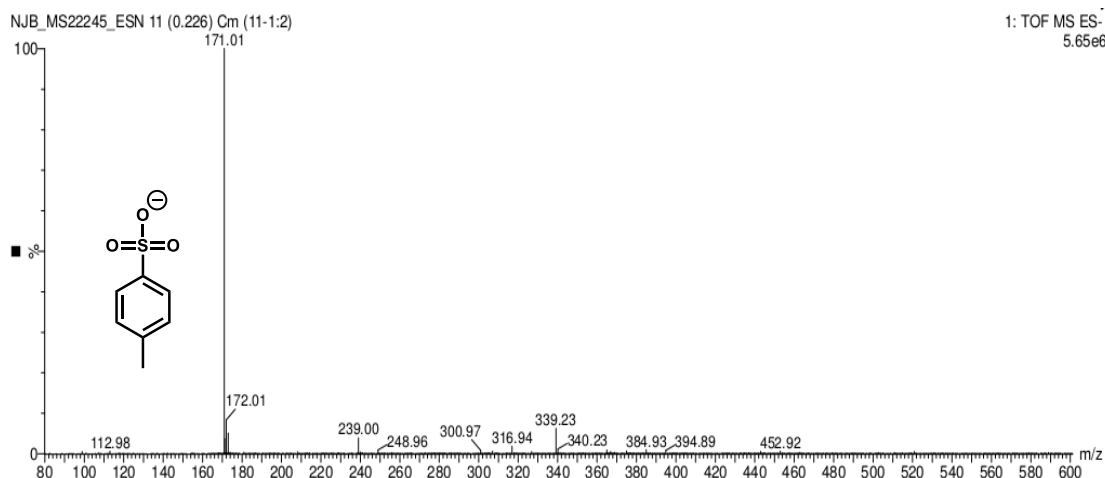
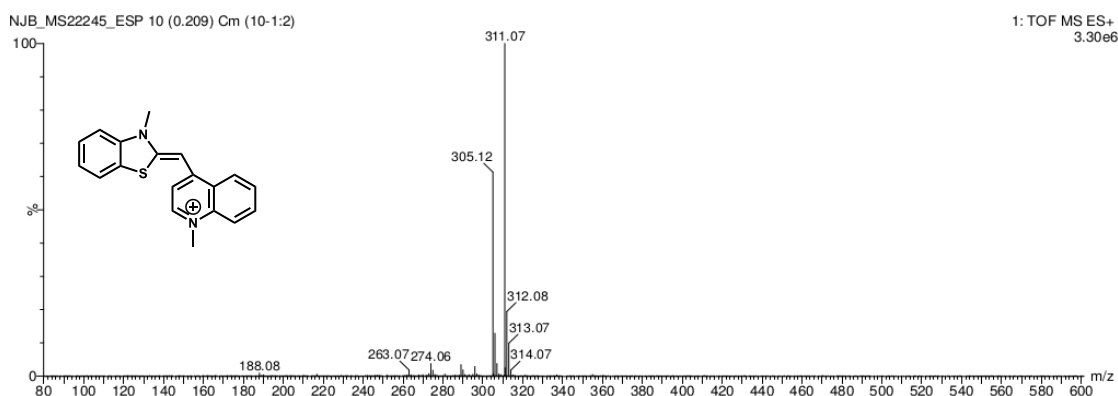


Figure 14 mass spectrum of thiazole orange before fading.

Figure 14 clearly shows the TO cation with major peak at 311.07 amu/z and mass 305.12 amu/z (expected 305.11 amu/z) in positive electrospray. The negative electrospray mass spectrum shows the tosylate anion with mass 171.01 amu/z (expected 171.01 amu/z).

The mass spectrum after fading is shown in Figure 15.

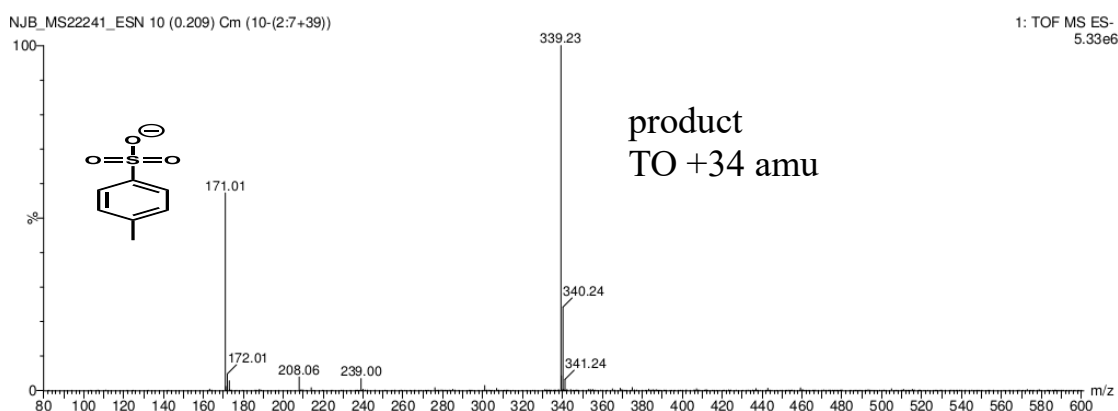
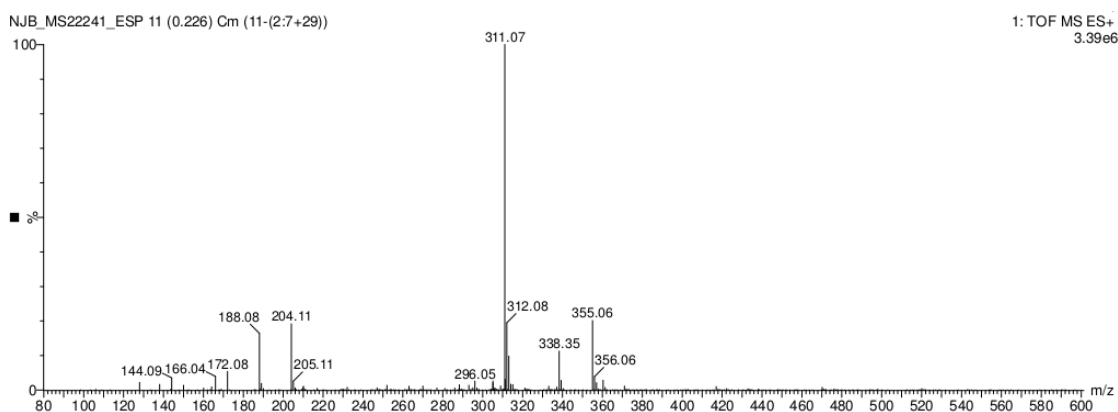


Figure 15 mass spectrum after fading.

Figure 15 shows a product with an increase in mass by 34 amu in negative electrospray mode. This ion could correspond to a compound with two additional hydroxyl groups. The mass spectrum from positive electrospray no longer shows the TO cation and only shows the unidentified compound at 311.07 amu/z.

Chapter Three Kinetic studies of fading of thiazole orange

In general terms, the spectrum shows the features expected on the basis of the predicted spectrum, with the addition of the aromatic AB-system and the singlet around 2.5 ppm for the tosylate anion and the solvent residual peaks near 2.5 and 4.7 ppm. However, there also appear to be some additional signals of unknown origin, e.g., the additional singlets near 4 ppm and between 6 and 6.5 ppm. We attribute these peaks to the unknown impurity in this batch of TO which is not the highest purity available.

The spectrum after fading was similarly recorded (Figure 18).

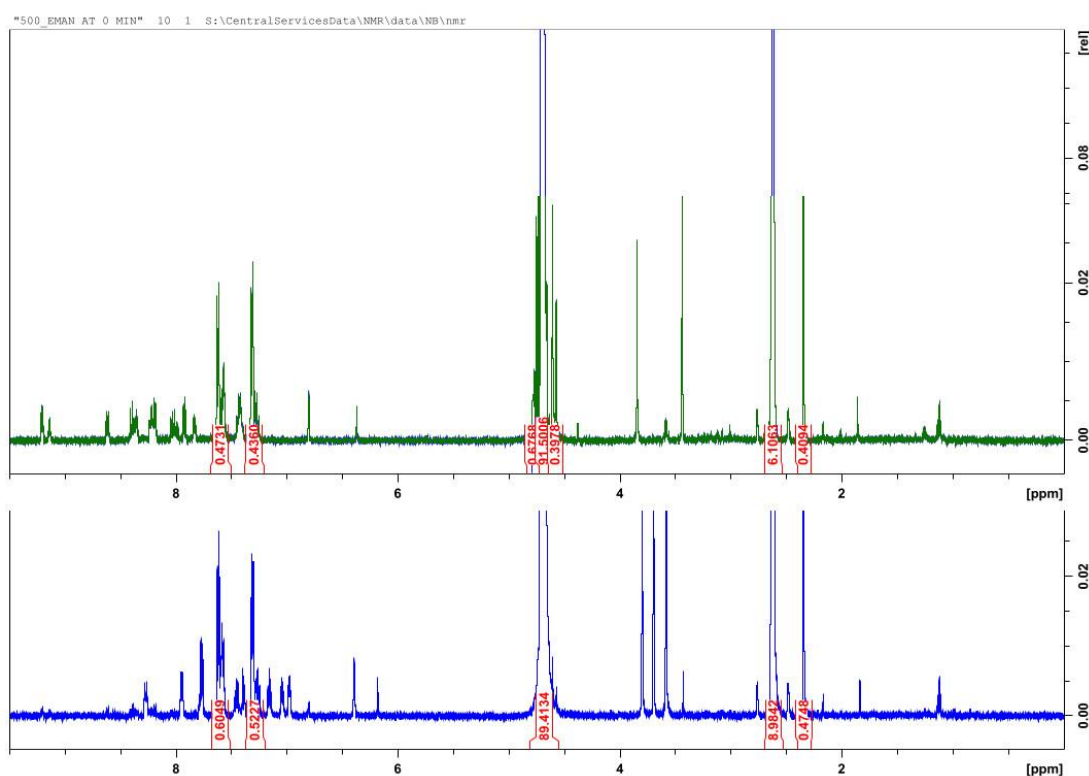


Figure 18. ¹H NMR spectrum for TO before (blue) and after (green) fading.

Figure 18 shows that both methyl groups have changed environment and so have all aromatic protons. One of the two signals that might represent the C=C-H in the thiazole orange cation has also disappeared whereas the other signal has not moved. According to mass spectroscopy, the product may have two additional hydroxyl groups. We therefore also predicted the chemical shifts for a candidate products and product mixtures (Figure 19).

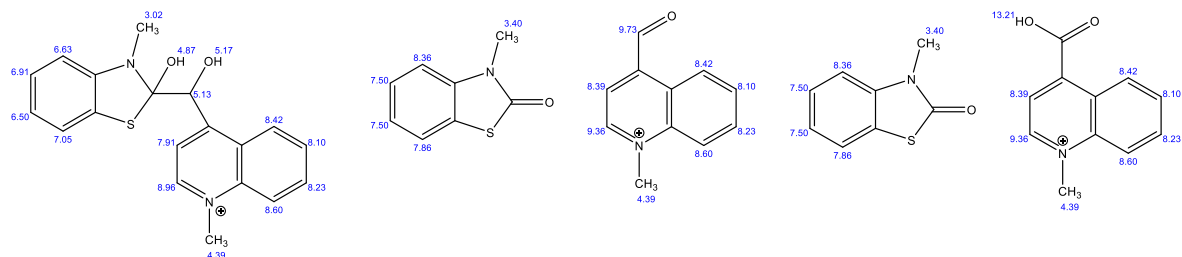
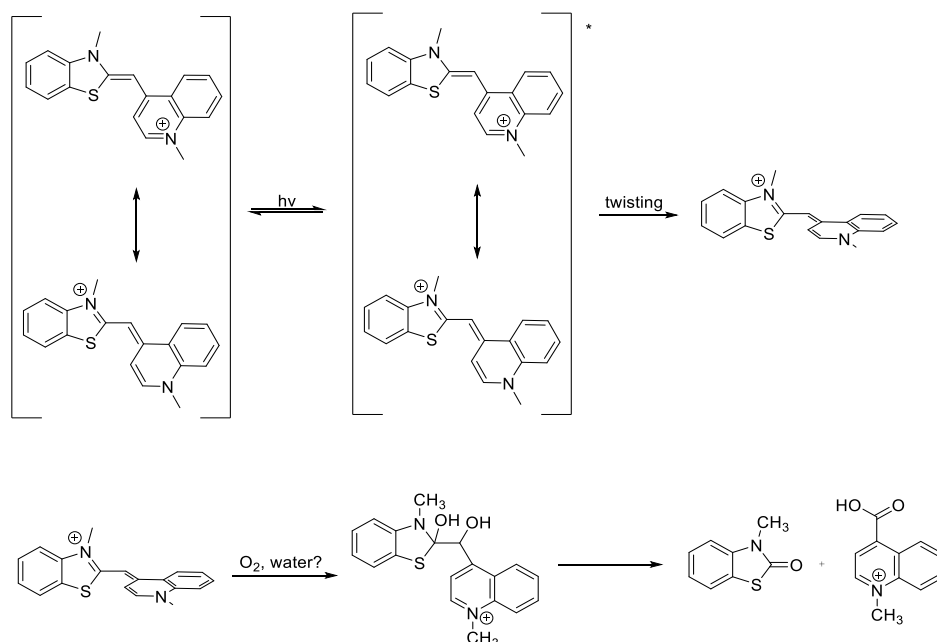


Figure 19. Predicted ^1H NMR spectra for potential photolysis products.

Figure 19 shows that the first potential product, suggested on the basis of mass spectrometry, is unlikely because two new singlets near 3 ppm are predicted and these are not observed. Continued reaction could lead to the two product mixtures also shown in Figure 19. The first of these is unlikely because no aldehyde proton is observed. The aldehyde could oxidise to form the corresponding carboxylic acid, however. The last product mixture therefore does not appear unreasonable for this reaction but should result in peaks in mass spectrometry at 166.03 amu/z ($\text{M}+\text{H}^+$) and at 188.07 amu/z (cation). Both these peaks are indeed observed, albeit small. The fact that these peaks are small may be the result of limited solubility of these compounds in the reaction mixture.

3.2.3 Proposed mechanism

The literature suggests that exposure to light causes TO to twist ⁽²¹⁾. Mass spectroscopy suggests that the product may be formed following reaction of the photoexcited species with a molecule of oxygen and/or water leading to introduction of two hydroxyls. Further analysis of the NMR spectra suggests that this species may be an intermediate which eventually decomposes to form the products shown in Scheme 3.



Scheme 3

The π -conjugation stabilises the planar conformation, entropically oriented dynamics and steric obstacles in favour of twisting structures in the oligomethine chains. These twisted structures are especially pronounced in the electronically excited states where the methine linkers' π -bonding character is reduced ⁽²²⁾. The twisting dynamics and breaking of the π -conjugation provide mechanisms for non-radiative deactivation of excited states causing a dramatic reduction in the quantity of cyanine colour emissions ⁽²³⁾.

3.3 Conclusions

The fading of TO occurs via a mechanism that does not involve proton-transfer processes in the pH range studied. Although oxygen is involved in the reaction, it does not appear to be involved in the rate-determining step. Whether singlet oxygen is involved in the reaction is not fully clear because results from experiments involving D_2O and singlet oxygen quenchers give contradictory results. The rate constant increases linearly with light intensity. Taken together, it may be that the fading of TO involves twisting around double bond as the rate-determining step.

3.4 Experimental

3.4.1 Buffer preparation

All experiments were carried out in MOPS buffer. The reference buffer contained 25 mM MOPS, 50 mM NaCl and 1 mM EDTA, pH 7.0.

MOPS was purchased from Melford (CAS 1132-61-2), NaCl was purchased from Fisher Scientific (CAS 7647-14-5), EDTA was purchased from VWR (CAS 60-00-4). The required amounts of the solids were placed in distilled water and stirred at room temperature until the solids dissolved. A solution of sodium hydroxide (NaOH) was used for adjusting the pH to 7.0 and the buffer was made up to 2 litres in a volumetric flask.

The pH of aqueous solutions was determined using a Hanna microprocessor pH-meter equipped with a VWR 662-1382 glass electrode. Materials were weighed out on a Fisher brand 4-decimal balance. De-ionised water was produced using an ELGA PF3XXXXM1 Water Purification System Type I 2 Lpm for all solutions.

3.4.2 Preparation of TO solutions for kinetic experiments

A stock solution of TO was prepared by placing a small amount of TO in the solvent of interest. The resulting suspension was placed in a sonicator bath and sonicated for 5-10 minutes and then filtered through hydrophilic PTFE syringe filters (Thermo Scientific-0.22 and 0.45 μm). The stock solutions was stored in the dark. For individual experiments, 250 μL of the TO stock solution were added to 2250 μL of buffer in a 1 cm pathlength quartz cuvette (Hellma).

3.4.3 UV-visible spectroscopy

JASCO V630 and V650 UV-Visible spectrophotometers as well as a SHIMADZU- UV-1800 were used to monitor reactions by recording absorption spectra after set amounts of time of irradiation using our irradiation device. Both JASCO machines were equipped with a Peltier thermostat cell holder to control the temperature. Absorption spectra were recorded in 1.00 cm pathlength stoppered quartz cuvettes (Hellma) holding approximately 2.5 cm^3 liquid and 1.00 cm of headspace (i.e. under aerobic conditions), at 25°C and different temperature.

3.4.4 Reaction temperature control

The device that we used for temperature control is a Heidolph unimax 1010 shaker with incubator. We used the incubator in control the temperature for the reaction by placing the complete irradiation setup in the shaker.

3.4.5 Magnetic Stirrer

We used an IKA Big Squid magnetic stirrer placed under our irradiation setup to magnetically stir the solutions during irradiation.

3.4.6 Compounds

Deuterium oxide (Heavy water) was from sigma-Aldrich. TO was 98% pure from Insight Biotechnology. TO was stored at 4°C, protected from light.

3.4.7 Power supply

The LED was powered using a T-Cube LEDD1B with a CAB-LEDD1 LED link cable. The LED used was connected to the supplier to control and manage the intensity of LED. Its stable and knowing voltage and current.

3.4.8 Nuclear Magnetic Resonance (NMR)

¹H-NMR and ¹³C-NMR spectra were recorded on a Bruker DPX 400 (400 MHz) or DPX 500 (500 MHz) spectrometer. Chemical shifts are expressed in parts per million downfield from tetramethylsilane as an internal standard. NMR spectra were recorded in solutions in deuterated-dimethylsulfoxide (DMSO-d₆) or chloroform (CDCl₃).

3.4.9 Mass spectrometry

LCMS experiments were performed using a Waters 2790 liquid chromatography system and a Waters ZQ mass spectrometer. Samples were loaded using a Gilson 232XL auto-sampler. Low-resolution mass spectrometric data were determined using a Fisons VG Platform II quadrupole instrument using electrospray ionisation (ES), unless otherwise stated. High resolution mass spectrometric data were obtained in electrospray (ES) mode unless otherwise reported, on a Waters Q-TOF micro-mass spectrometer.

3.4.10 Software

Graphs were constructed and kinetic data were analysed using Originlab Origin 2020 software. Wavelengths for analysis were selected through UV-Visible time resolved absorption spectra measurement for the reaction (for thiazole orange this was 500.0 nm). All rate constants are expressed as observed first-order rate constants resulting from fitting a first-order rate law to the data at 500 nm using Originlab Origin 2020.

Molarity Calculator. GraphPad Prism was used to calculate the molarity (Molar), volume (Milliliter) and formula weight (daltons - g/mol).

<https://www.graphpad.com/quickcalcs/molarityform.cfm>

3.5 References

1. Sylvie Prodhomme, Jean-Philippe Demaret, Sergeï Vinogradov, Ulysse Asseline, Luc Morin-Allory, P. V. A theoretical and experimental study of two thiazole orange derivatives with single- and double-stranded oligonucleotides, polydeoxyribonucleotides and DNA. *J. Photochem. Photobiol. B Biol.* **V.53**, Pages 60-69 (1999).
2. Sparano, B. A. & Koide, K. A strategy for the development of small-molecule-based sensors that strongly fluoresce when bound to a specific RNA. *J. Am. Chem. Soc.* **127**, 14954–14955 (2005).
3. Rulliere, C. *Femtosecond laser pulses*. (Springer, 2005).
4. Silva, G. L., Ediz, V., Yaron, D. & Armitage, B. A. Experimental and computational investigation of unsymmetrical cyanine dyes: understanding torsionally responsive fluorogenic dyes. *J. Am. Chem. Soc.* **129**, 5710–5718 (2007).
5. Pow, C. L. *et al.* A rainbow of fluoromodules: a promiscuous scFv protein binds to and activates a diverse set of fluorogenic cyanine dyes. *J. Am. Chem. Soc.* **130**, 12620–12621 (2008).
6. Flinders, J. *et al.* Recognition of planar and nonplanar ligands in the malachite green–RNA aptamer complex. *ChemBioChem* **5**, 62–72 (2004).
7. Bordelon, J. A., Feierabend, K. J., Siddiqui, S. A., Wright, L. L. & Petty, J. T. Viscometry and atomic force microscopy studies of the interactions of a dimeric cyanine dye with DNA. *J. Phys. Chem. B* **106**, 4838–4843 (2002).
8. Improta, R. & Santoro, F. A theoretical study on the factors influencing cyanine photoisomerization: the case of thiacyanine in gas phase and in methanol. *J. Chem. Theory Comput.* **1**, 215–229 (2005).
9. Lakowicz, J. R. *Principles of fluorescence spectroscopy*. (Springer science & business media, 2013).
10. Spielmann, H. P., Wemmer, D. E. & Jacobsen, J. P. Solution structure of a DNA complex with the fluorescent bis-intercalator TOTO determined by NMR spectroscopy. *Biochemistry* **34**, 8542–8553 (1995).
11. Walsh, S. & Brown, T. Glen Report 32.11: Thiazole Orange as a Fluorogenic Reporter in Oligonucleotide Probes.
12. Bohländer, P. R. & Wagenknecht, H.-A. Synthesis and evaluation of

- cyanine–styryl dyes with enhanced photostability for fluorescent DNA staining. *Org. Biomol. Chem.* **11**, 7458–7462 (2013).
13. Karunakaran, V., Pérez Lustres, J. L., Zhao, L., Ernsting, N. P. & Seitz, O. Large dynamic Stokes shift of DNA intercalation dye Thiazole Orange has contribution from a high-frequency mode. *J. Am. Chem. Soc.* **128**, 2954–2962 (2006).
 14. Wilkinson, F., Helman, W. P. & Ross, A. B. Quantum yields for the photosensitized formation of the lowest electronically excited singlet state of molecular oxygen in solution. *J. Phys. Chem. Ref. data* **22**, 113–262 (1993).
 15. Rastede, E. E. *et al.* Spectral fine tuning of cyanine dyes: Electron donor-acceptor substituted analogues of thiazole orange. *Photochem. Photobiol. Sci.* **14**, 1703–1712 (2015).
 16. Armitage, B. A. *DNA Binders and related subjects*. vol. 253 (Springer Science & Business Media, 2005).
 17. Rastede, E. E. *et al.* Spectral fine tuning of cyanine dyes: electron donor-acceptor substituted analogues of thiazole orange. *Photochem. Photobiol. Sci.* **14**, 1703–1712 (2015).
 18. Nygren, J., Svanvik, N. & Kubista, M. The interactions between the fluorescent dye thiazole orange and DNA. *Biopolymers* **46**, 39–51 (1998).
 19. Maillard, J. *et al.* Universal quenching of common fluorescent probes by water and alcohols. *Chem. Sci.* **12**, 1352–1362 (2021).
 20. Hardwick, J. Blood storage and transportation. *ISBT Sci. Ser.* **3**, 177–196 (2008).
 21. Boutorine, A. S., Novopashina, D. S., Krasheninina, O. A., Nozeret, K. & Venyaminova, A. G. Fluorescent probes for nucleic acid visualization in fixed and live cells. *Molecules* **18**, 15357–15397 (2013).
 22. Upadhyayula, S. *et al.* Photoinduced dynamics of a cyanine dye: parallel pathways of non-radiative deactivation involving multiple excited-state twisted transients. *Chem. Sci.* **6**, 2237–2251 (2015).
 23. Guarin, C. A., Villabona-Monsalve, J. P., López-Arteaga, R. & Peon, J. Dynamics of the Higher Lying Excited States of Cyanine Dyes. An Ultrafast Fluorescence Study. *J. Phys. Chem. B* **117**, 7352–7362 (2013).

Chapter Four

Kinetic studies of photochemical fading of 3,3'-diethyloxadicyanin iodide (DODC)

Summary

We have studied the kinetics of the fading process of 3,3'-diethyloxadicyanobocyanine iodide (DODC) when exposed to light, determining that it is irradiation that drives the colour change. We have demonstrated that DODC shows increased fading with increased intensity of light. Another factor is the presence of O₂. Limiting oxygen concentrations limits the extent of reaction, although the oxygen concentration has no effect on the observed reaction rate constant.

Other factors may also play a role in the fading process, for example temperature, type of buffer, buffer concentration, pH and the presence of additives. We examined each of these in turn. The composition of different buffers did not affect kinetics; different concentration of MOPS and different pH all produce rate constants that are the same within error margins. This observation suggests that (de)protonation processes do not play a role in the reaction up to the rate-determining step. Even carrying out the reaction at three different temperatures (25 °C, 38 °C and 50 °C) did not strongly affect the observed kinetics. The addition of singlet-oxygen quenchers does not affect the observed kinetics and there is no increase in rate constant upon going from H₂O to D₂O. These observations suggest that the reaction does not involve singlet oxygen.

Mass spectroscopy suggests that the product may be formed following reaction of the photoexcited species with a molecule of oxygen. The sensitivity of the reaction to oxygen concentration suggests that a form of oxygen is involved in the rate-determining step.

Taken together, it may be that the fading of DODC involves a higher order excited state reacting with molecular oxygen in its triplet ground state. An alternative interpretation involves formation of superoxide radicals resulting from electron transfer to oxygen leading to hydroxyl radicals.

4.1 Introduction

3,3'-Diethyloxadicyanine iodide (DODC, CAS no. 14806-50-9, Figure 4.1) is a cyanine dye, also known by the names 3-ethyl-2-[5-(3-ethyl-2-benzoxazolinylidene)-1,3-pentadienyl] benzoxazolium iodide, C5-oxacyanine and oxadicyanine (C5) dye. DODC is suitable for use in histology and haematology. ^(1,2)

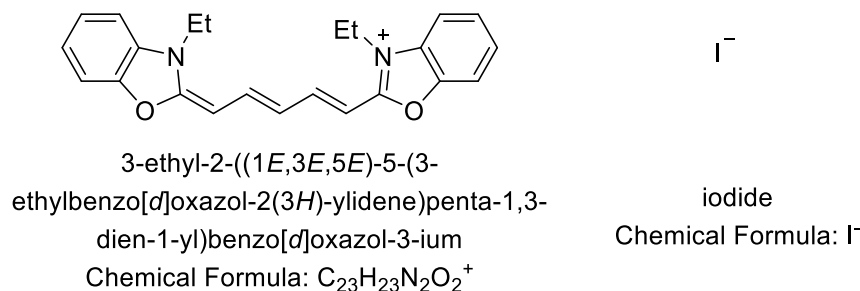


Figure 4.1 DODC

4.1.1 Spectroscopic properties of DODC

DODC is a cationic cyanine dye with an iodide counter anion and is a member of the 1,3-benzoxazole class of dyes. It is a fluorescent compound. ⁽³⁾ The general spectroscopic characteristics of DODC are summarised in Table 1.

Description	Characteristic
Absorption	λ_{\max} 582 nm
Fluorescence	λ_{ex} 582 nm; λ_{em} 603 nm
Absorption coefficient	237000 M ⁻¹ cm ⁻¹ at 582 nm
Fluorescence quantum yield	0.49

The UV-visible spectrum of DODC in our reference buffer (See below) is shown in Figure 4.2.

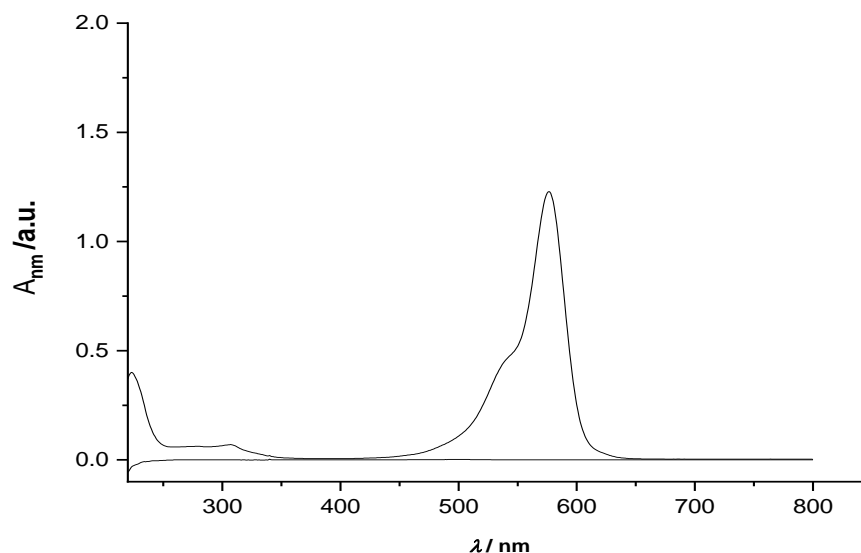


Figure 4.2 UV-visible spectrum of DODC in reference buffer

4.1.2 The dynamics of photoisomerization of cyanine dyes

The first excited singlet state of DODC is dominated by a very rapid isomerisation process. DODC molecules adopt a trans configuration in their ground state, but, due to molecular twisting, DODC forms an initial excited state twisted molecule. ^(5, 6) The twisted molecular configuration of DODC in its excited state is formed by rotation about its carbon-carbon double bonds, this requires the simultaneous molecular rotation about two or three torsional angles. The formed twisted molecule decays to form ground state photoisomers or returns to the thermodynamically stable ground state. ^(7,8)

The dynamics of DODC photoisomerization are governed by medium viscosity and temperature. ⁽⁹⁾

Polymethine dyes, which are cyanine dye analogues, are the most prevalent class of dyes that show rotational isomerisation. One of the main pathways of energy degradation of the cyanine S₁ state in low-viscosity media is usually trans-cis or cis isomerisation, rotating a fragment of the dye molecule around one of the polymethine chain bonds by ~180°. ^(10,11) Internal conversion, vibration and torsion-induced non-radiative transition S₁ → S₀, is also possible. The photophysics of Cy5, a dye related to DODC, has been shown to be rather complex. ⁽¹²⁾ Figure 4.3 shows generalised molecular structures of cyanine dyes' trans and cis isomers.



Figure 4.3 cyanine dyes' trans and cis isomers

The photoisomerization of DODC involves molecular motion.⁽¹³⁾ Isomerisation processes with relatively low activation energies, being close to the activation energy of the solvent's viscous flow (this is usually the case for isomerisation in the S1 state), mean that the rate constant of isomerisation depends heavily on the medium's viscosity.^(14,15) As a result, isomerisation slows sharply with increasing viscosity. A high viscosity solvent inhibits the twisting motion about the DODC double bonds and causes the photoisomerization rate to be drastically retarded. Henrichs and Gross determined the rate constants for the radiative (k_r) and non-radiative (k_{nr}) decay at different temperatures to determine the activation energy for the photoisomerization processes. Overall, a variety of processes is possible and shown in Figure 4.4.^(16,17)

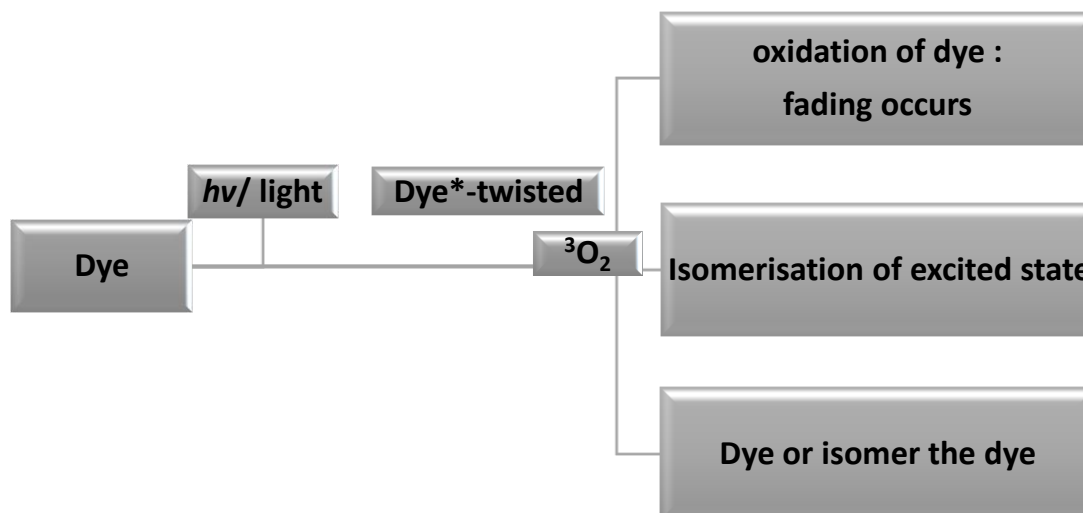


Figure 4.4 Dye excitation allows a variety of possible processes, including isomerisation.

4.1.3 mechanisms of reaction of DODC with $^1\text{O}_2$

Excitation of DODC doesn't only allow photoisomerisation; fading of DODC also appears to be driven by light. Chapter 1 discusses the various mechanisms

by which photochemically induced fading may occur. In this Chapter, we discuss DODC more specifically.

In terms of the quenching mechanisms of singlet oxygen presented in Chapter 1, here the quencher is DODC which reacts with singlet oxygen to give a new product. Cyanine dyes have singlet-oxygen quenching constants which approach the diffusion-controlled limit as is the case with carotenoids and other compounds with extensive conjugation systems. ^(18, 19)

Another method for quenching singlet oxygen is energy transfer. In this mechanism we assume some cyanine dyes have singlet states ^(20,21), which are spin-allowed to react with singlet O₂ (¹Δ_g) (Figure 4.5).



Figure 4.5 energy transfer mechanism of quenching

In the schematic above, ¹cyanine⁺ is the cyanine dye in the ground state, [O₂-cyanine⁺]^{*} is a transient exciplex and ³cyanine⁺ and O₂ (³Σ_g⁻) are the triplet state of the cyanine dye and the triplet ground state of the oxygen, respectively. ⁽²²⁾

A final method of quenching is called charge transfer. In this mechanism the cyanine dye (cyanine⁺) reacts with singlet oxygen (¹Δ_g) to form a transient charge-transfer complex [O₂^{δ-}-cyanine^{+, δ+}]. The formation of the transient complex relaxes spin restrictions which facilitates energy transfer ^(23, 24) shown in figure 4.6. Note, this pathway quenches excited state oxygen, and not excited state cyanine dyes.

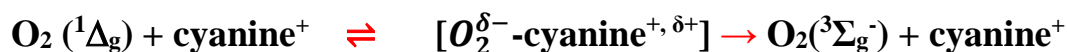


Figure 4.6 cyanine dye quenched through charge and energy transfer.

In a study conducted by Brian *et al.*, ⁽²⁵⁾ it was found that cyanine dyes were quenched through both charge- and energy-transfer mechanisms. It was found that as the ionic strength of aqueous solutions increased, so did the rate constant associated with singlet oxygen quenching with respect to cyanine dyes. ⁽²⁶⁾ It was

hypothesised that an increased ionic strength, and hence polarity of aqueous solution, stabilized the formation of the charge-transfer complex between the singlet oxygen and cyanine dyes. ⁽²⁷⁾

Interestingly, it was found that the rate constant associated with singlet oxygen quenching of various cyanine dyes increased in the presence of deuterium oxide. Behaviour in which the cyanine dyes in aqueous solution formed an aggregate was predicted. ^(28, 29)

An alternative pathway of quenching $^1\text{O}_2$ while also causing dyes to fade is shown in Figure 4.7.

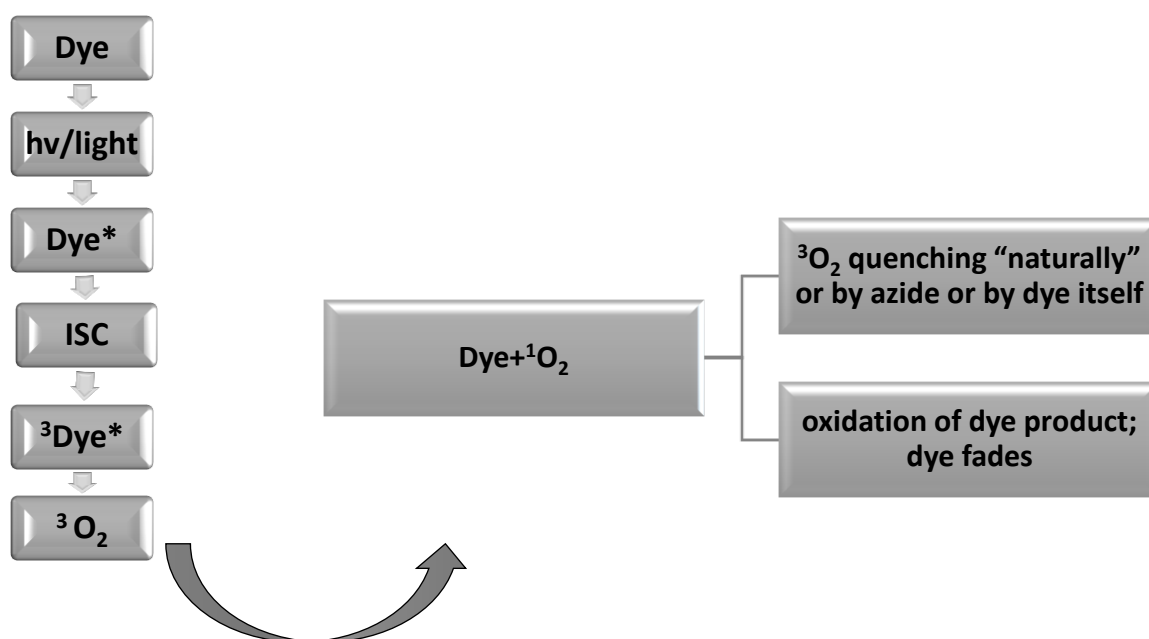


Figure 4.7 Alternative scheme of quenching

4.1.4 Aims and purpose.

Our aims in this Chapter are to study the kinetics of fading for DODC under different conditions. In this chapter we focus on the kinetics of fading of DODC when under different conditions (pH, concentrations of buffer components, buffer additives, temperature) to understand the reaction mechanism when DODC fades upon irradiation in aqueous solutions.

4.2 Results and discussion

4.2.1 Kinetic studies

As discussed in the introduction, DODC is known to fade and we explored the factors that might play a role in controlling the kinetics of the process.

a) light

To confirm that the fading of DODC is driven by light, we stored a solution of DODC in buffer (pH=7, 25 mM MOPS, 50 mM NaCl and 1 mM EDTA), in the dark at 25 °C for 24 hours and we recorded UV-visible spectra (Figure 4.8).

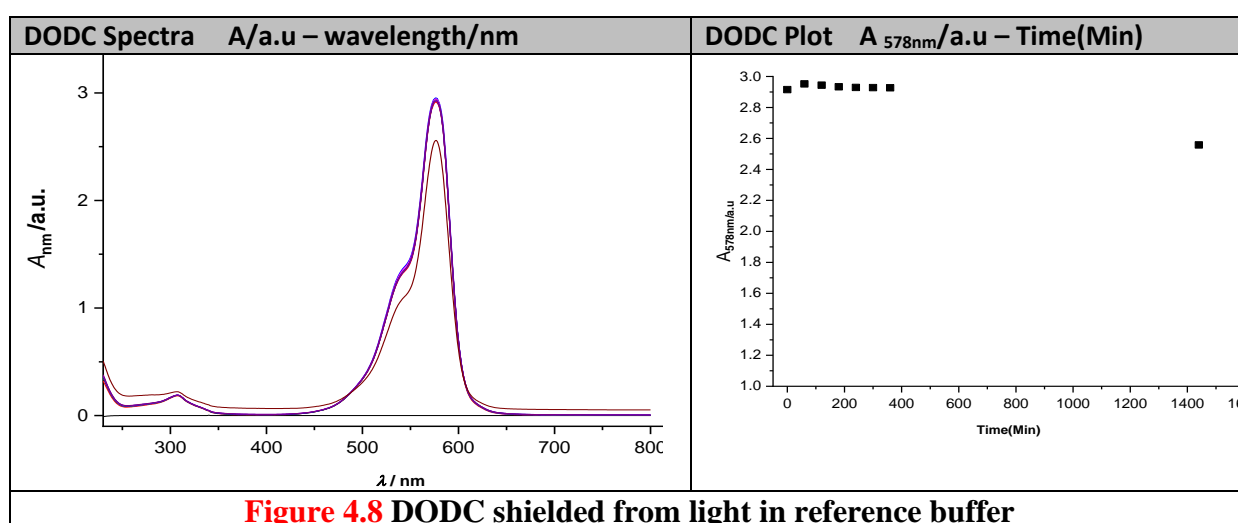


Figure 4.8 shows no change in absorbance at 578 nm as a function of time, in freshly prepared reference buffer (pH=7, 25 mM MOPS, 50 mM NaCl and 1 mM EDTA) in the dark at 25 °C for 24 hours.

We next exposed DODC to the white LED light (using the 4th version of the device as described in Chapter 2) under otherwise identical conditions, i.e. reference buffer (25 mM MOPS, pH 7.0, 50 mM NaCl and 1 mM EDTA) with magnetic stirring at 25°C (Figure 4.9).

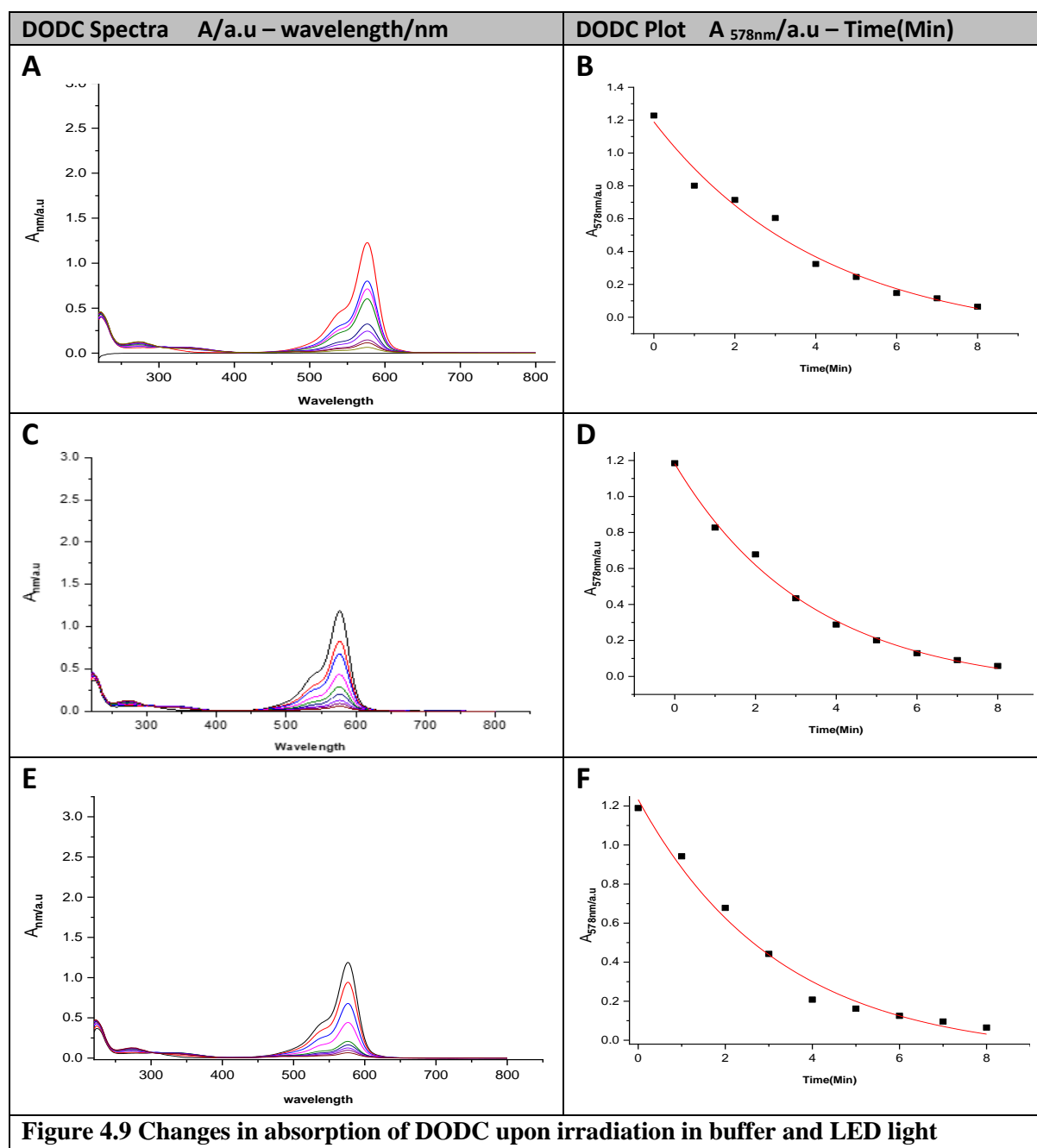


Figure 4.9 shows spectra for DODC exposed to light (A 1st experiment; C 2nd experiment; E 3rd experiment). The changes in absorption at 578 nm upon irradiation are shown in Figure 3 (B, D and F). These graphs show that the decrease in absorbance occurs within less than 10 minutes and results in complete loss of colour. This observation agrees with the results when exposing DODC to ambient light and previous versions of the LED device (version 1 and 2, Chapter 2).

We analysed the absorbance at 578 nm as a function of time in terms of a first order rate law. The resulting rate constants are summarised in Table 2.

Table 2 Rate constants for fading of DODC	
original rate constants	original errors
0.24032 min⁻¹	0.05913
0.29897 min⁻¹	0.04854
0.31087 min⁻¹	0.05235
Average k	Average error
0.283	0.053
standard deviation	% error margin
0.031 min⁻¹	
Experiment number: 25-5-2019	

Table 2 illustrates that reproducible kinetic data for fading DODC can be obtained giving an observed rate constant for fading k of $(0.2833 \pm 0.0533) \text{ min}^{-1}$.

b) Effect of oxygen

We wanted to evaluate the effect of oxygen concentration on fading. We therefore irradiated a solution of DODC in the reference buffer (pH=7, 25 mM MOPS, 50 mM NaCl and 1 mM EDTA) which had been deoxygenated and brought under an N₂ atmosphere at 25 °C with the last version of the LED irradiation device (see Chapter 2).

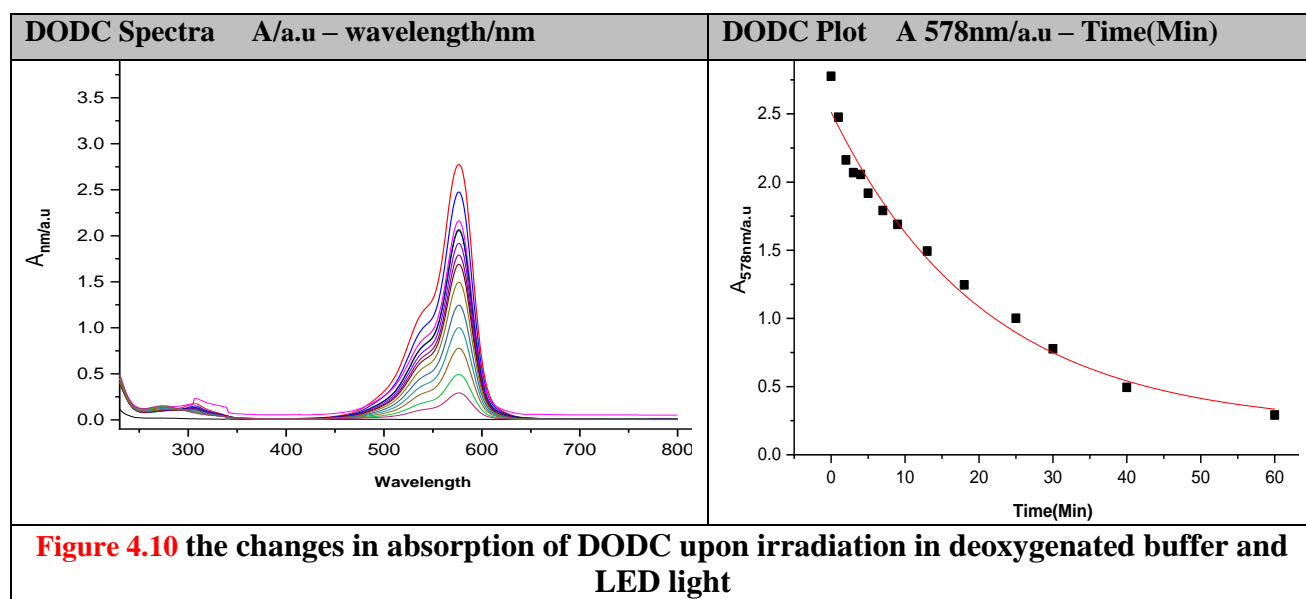


Figure 4.10 illustrates that the fading continued in the normal way but more slowly than usual; it took more than 60 min to complete the fading of the colour of the dye. This observation shows that O₂ is important and that it affects the kinetics. This suggests O₂ plays a role in (or up to) the rate-determining step. The rate constant for fading under deoxygenated conditions is reported in Table 3.

Table 3 Rate constant for fading of DODC in deoxygenated buffer		
original rate constant	original errors	% error margin
0.04831 min⁻¹	0.00782	0.161871248
File 11-9-2019		

We attribute the fact that the reaction still occurs, albeit slowly, to the fact that it is difficult to make the environment of solution inside the cuvette fully deoxygenated. There is probably still limited O₂ available because we used primitive techniques (balloon full of N₂ connected to the interior of the cuvette by a needle, Figure 4.11).



Figure 4.11 balloon full of N₂ to deoxygenate the buffer.

c) effect of pH

We wanted to know the effect of pH of the buffer on the kinetics of fading. Buffers were made at pH 4.3, 7.0 and 10.8 but otherwise identical to the reference buffer (25 mM MOPS, 50 mM NaCl and 1mM EDTA). The new LED after setting (Chapter 2) was used for irradiation with magnetic stirring at 25 °C.

The fading of DODC was followed as a function of time and the data were analysed in terms of a first-order rate law (see Appendix for the plots at the 3 different pH) yielding the rate constants in Table 4.

Table 4 kinetics of fading of DODC at different pH		
	pH	Rate constants (<i>k</i>)
1	4.3	$0.3385 \pm 0.0439 \text{ min}^{-1}$
2	7.0	$0.2834 \pm 0.0467 \text{ min}^{-1}$
3	10.8	$0.1963 \pm 0.0206 \text{ min}^{-1}$

From the results in Table 4, the average k in buffer at pH 4.3 was higher than at pH 7.0 and pH=10.8. Figure 4.12 shows the data.

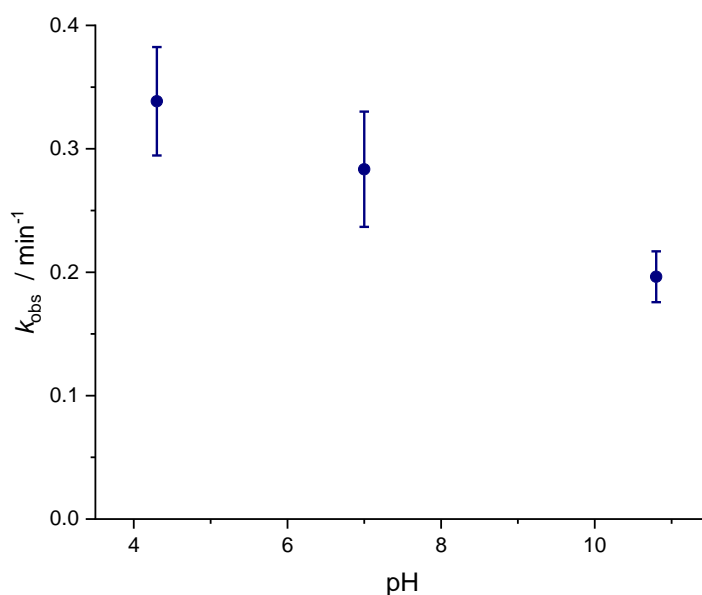


Figure 4.12 Relation between rate constant for fading of DODC with different pH

Figure 4.12 shows a small decrease in k when pH is increased but the decrease is negligible on the log scale. This observation suggests that equilibrium (de)protonation processes do not play a significant role in the reaction up to the rate-determining step. We note that the experiments at pH 4.3 and 10.8 were outside the buffer capacity of the MOPS buffer but, regardless, the difference in observed rate constants is significantly less than an order of magnitude so the conclusion above holds.

d) effect of buffer concentration

We next wanted to study the impact of different concentrations of MOPS in the buffer. The fading of DODC was followed as a function of time and the data were analysed in terms of a first-order rate law (See Appendix for spectra and plots for the reactions) yielding the rate constants in Table 5.

Table 5 Rate constants for fading of DODC in the presence of varying concentration of MOPS				
[MOPs]/mM	average $k_{\text{obs}} / \text{min}^{-1}$	Average error	Standard deviation	Error margin
25 mM	0.2834	0.0467	0.0308	0.0467
50 mM	0.2937	0.0166	0.0086	0.0166
100 mM	0.2339	0.0253	0.0361	0.0361
Concentration of MOPS by millimolar				

The results in Table 5 are graphically represented in Figure 4.13.

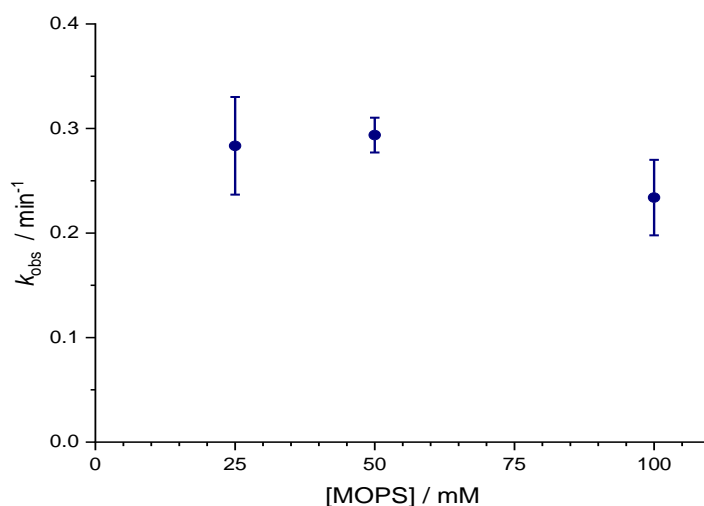


Figure 4.13 Relation between rate constant of fading of DODC with concentration of MOPS.

Figure 4.13 shows that the concentration of MOPS did not significantly affect kinetics. This observation suggests that (de)protonation processes do not play a role in the reaction up to the rate-determining step.

e) Ionic strength

We next studied the impact of ionic strength (by using different NaCl concentrations) of the buffer on the reaction. Fading of DODC was followed as a function of time and the data were analysed in terms of a first-order rate law (See Appendix) yielding the rate constants reported in Table 6.

Table 6 Rate constants for fading of DODC in the presence of varying concentrations of NaCl

Description	average $k_{\text{obs}} / \text{min}^{-1}$	Average error	Standard deviation	Error margin
50 mM	0.2834	0.0467	0.0308	0.0467
100 mM	0.2575	0.0270	0.0162	0.0270
200 mM	0.3354	0.0330	0.0317	0.0330
Concentration of NaCl by millimolar				

The data in Table 6 are shown in Figure 4.14.

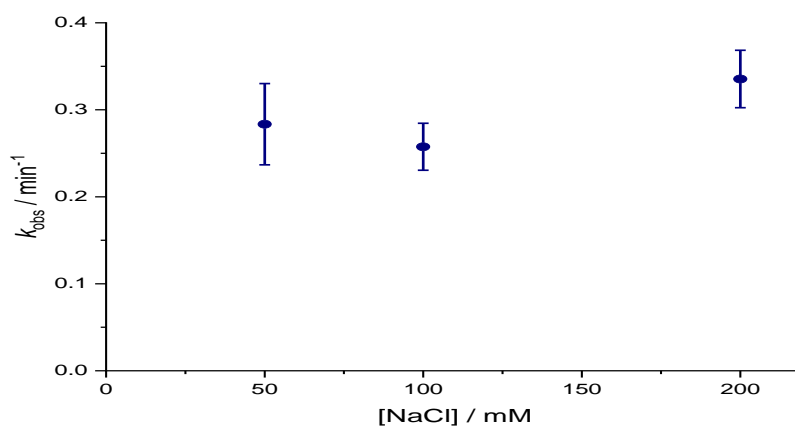


Figure 4.14 Relation between rate constant of fading of DODC with concentration of NaCl in the buffer.

Figure 4.14 shows that different concentrations of NaCl did not affect kinetics. The fact that the observed rate constants show negligible dependence on ionic strength suggests that charge-formation and charge-removal are not important in this reaction under these conditions.

f) Effect of temperature

We next wanted to know the impact of temperatures (25 °C, 35 °C and 50 °C) on the fading of DODC in the reference buffer. The kinetics were followed as before, and the resulting rate constants are reported in Table 7.

Temperature	average $k_{\text{obs}} / \text{min}^{-1}$	Average error	Standard deviation	Error margin
25 °C	0.2834	0.0467	0.0308	0.0467
35 °C	0.2140	0.0170	0.0193	0.0193
50 °C	0.195	0.0168	0.0269	0.0269

Table 7 shows that the k for fading in the reference buffer at 25 °C was higher than k at 35 °C and 50 °C. An Eyring plot was constructed (Figure 4.15).

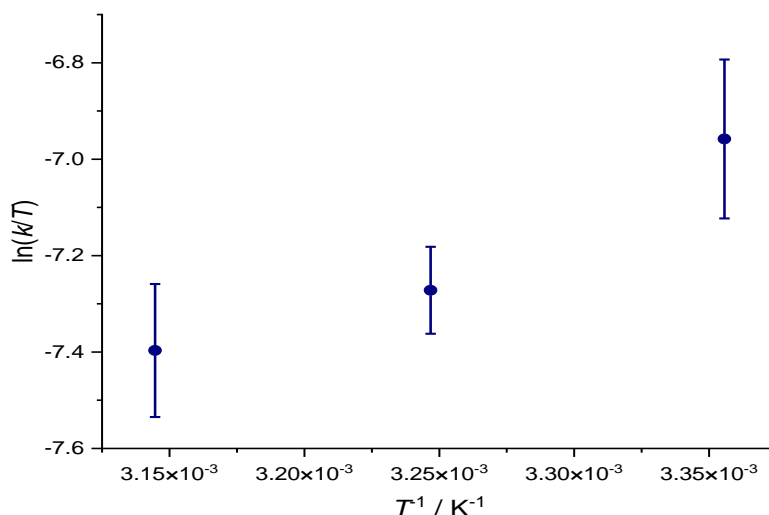


Figure 4.15 Eyring plot for the relation between kinetics of DODC fading and temperature.

Figure 4.15 showed that the change of temperature did not strongly affect the observed kinetics. Surprisingly, the rate constants decrease with increasing temperature, a temperature increase usually increases reaction rate constant. We attribute the decrease in rate constant for fading of DODC to an increase in the rate constant for a competing non-destructive process. As a result, a smaller fraction of the excited state proceeds to react via a pathway resulting in fading and a higher fraction of the excited state returns to the unchanged starting material.

g) Water source

Because the buffer composition did not affect the observed kinetics, we wanted to know whether the reaction proceeds similarly in deionised water. The results of this experiment are shown in Figure 4.16.

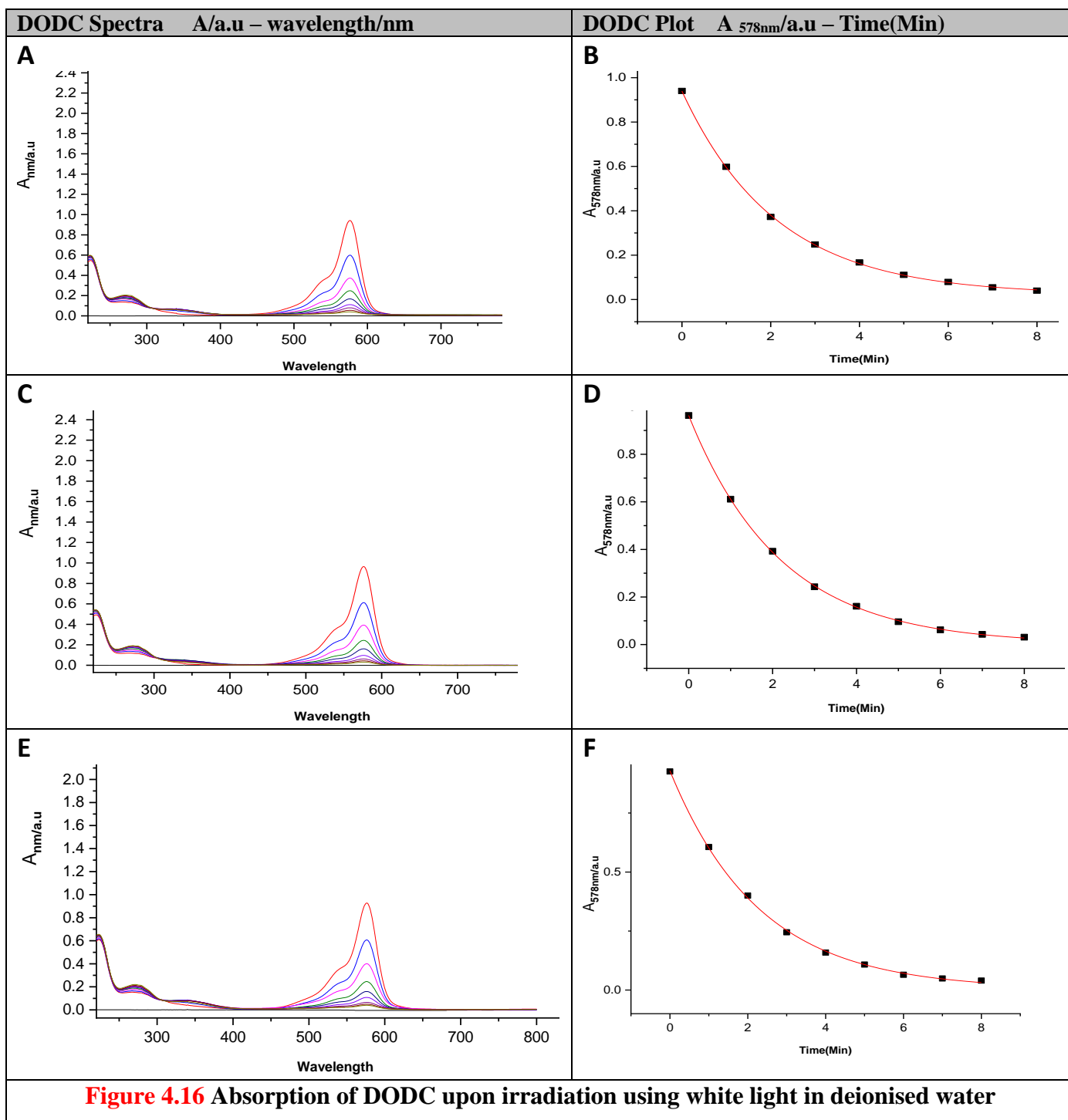


Figure 4.16 Absorption of DODC upon irradiation using white light in deionised water

Figure 4.16 shows spectra for DODC in deionised water exposed to light (1st experiment A; 2nd experiment C; 3rd experiment E).

We plotted the absorbance at 578 nm as a function of time and fitted a first-order curve to the data (Figures 4.20 B, D and F). The resulting rate constants are summarised in Table 8.

Table 8 Rate constant for fading of DODC in deionised water	
original rate constants	original errors
0.47054 min⁻¹	0.0068
0.45677 min⁻¹	0.00524
0.43712 min⁻¹	0.01065
average <i>k</i>	average error
0.455	0.008
standard deviation	
0.014 min⁻¹	
experimental number 22-5-2019	

Table 8 illustrate that reproducible kinetic data for fading DODC in deionised water can be obtained giving a rate constant k of $(0.455 \pm 0.014) \text{ min}^{-1}$. The rate constant in deionised water was therefore higher than the rate constant in the reference buffer. We attribute this observation to a salt effect on the reaction which has levelled off at the high salt concentrations used in the buffer but becomes noticeable at very low salt concentrations. Nevertheless, the effect is rather small so we will not attempt to interpret this here without further experiments carried out a series of low salt concentrations.

h) Solvent kinetic isotope effect (SKIE)

We next used D₂O instead of deionised water to explore whether there is a kinetic isotope effect on the kinetics of fading. The resulting data for experiments in D₂O (not buffered) are shown in Figure 4.17.

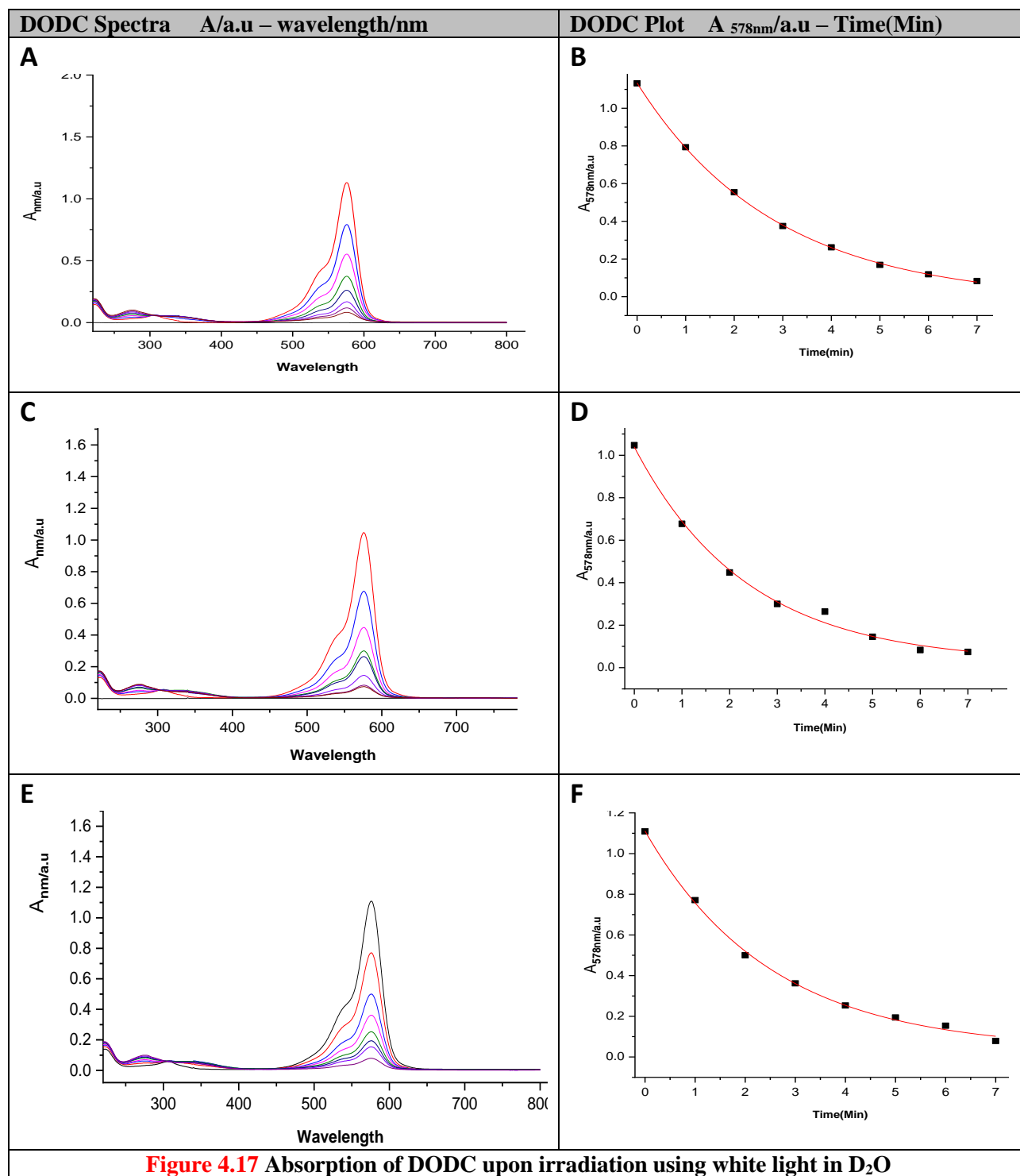


Figure 4.17 shows a significant decrease in absorbance upon exposure to white light within less 8 min and complete loss of colour. We plotted the absorbance at 578 nm as a function of time and fitted a first-order rate law to the data (Figure 4.21, panels B, D and F). The rate constants are summarised in Table 9.

Table 9 Rate constants for fading of DODC in D ₂ O	
original rate constants	original errors
0.35402 min⁻¹	0.0069
0.42383 min⁻¹	0.03946
0.39865 min⁻¹	0.02445
Average <i>k</i>	Average error
0.392 min⁻¹	0.024
standard deviation	
0.029 min⁻¹	
experimental number :24-5-2019	

Table 9 illustrates that reproducible kinetic data for fading of DODC can be obtained in D₂O giving a rate constant k of $(0.392 \pm 0.029) \text{ min}^{-1}$.

The constant rate for fading D₂O is slightly lower than k for fading in deionised water but this constitutes a minimal kinetic isotope effect if any. The absence of an increase in rate constant upon going from H₂O to D₂O suggests that the reaction does not involve singlet oxygen.

i) Fading of DODC in tap water

We finally changed the solution to tap water, in light of proposed potential applications of the fading reaction. The kinetic results for fading of DODC in tap water without additives are shown in Figure 4.18.

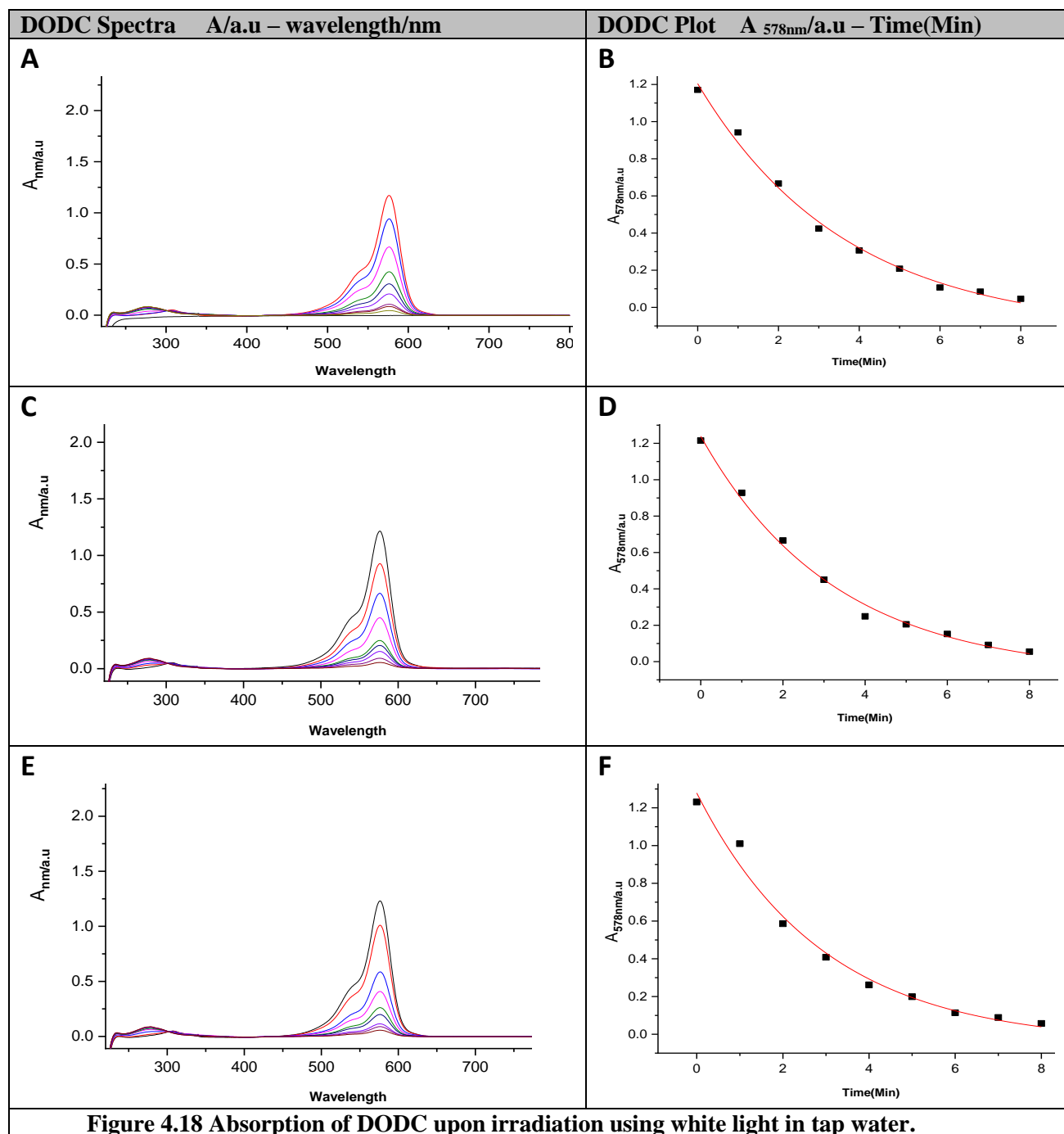


Figure 4.18 shows a significant decrease in absorbance upon exposure to white light. There is a decrease in absorbance within less than 10 min and complete loss of colour.

We plotted the absorbance at 578 nm as a function of time and fitted a first-order rate law to the data. The resulting rate constants are summarised in Table 10.

Table 10 Rate constant for fading of DODC in tap water	
original rate constants	original errors
0.27393 min ⁻¹	0.0318
0.30832 min ⁻¹	0.03166
0.33956 min ⁻¹	0.05097
Average k	Average error
0.307	0.038
standard deviation	
0.027 min ⁻¹	
experimental number : <u>24-5-2019</u>	

Table 10 shows that reproducible kinetic data for fading DODC can be obtained even in tap water. The observed rate constant k is $(0.307 \pm 0.038) \text{ min}^{-1}$.

The rate constant for fading of DODC in tap water is approximately equal to the rate constant in the reference buffer. Table 11 presents an overview of the rate constants in the various solutions.

Table 11 Summary of solutions used with DODC	
description	rate constant (k)
deionised water	$0.4548 \pm 0.0076 \text{ min}^{-1}$
D ₂ O	$0.3922 \pm 0.0236 \text{ min}^{-1}$
tap water	$0.3073 \pm 0.0381 \text{ min}^{-1}$
reference buffer	$0.2834 \pm 0.0467 \text{ min}^{-1}$

j) Effects of buffer choice

To explore the possibility that the amine nitrogen in MOPS acts as sacrificial electron donor, we next changed the buffer from MOPS to phosphate buffer (Na₂HPO₄). Kinetic data are summarised in Table 12 [see in appendix the spectra and plots of phosphate buffer].

Table 12 Rate constants for fading of DODC in Na ₂ HPO ₄ -based buffer	
original rate constants	original errors
0.18757 min ⁻¹	0.01915
0.14918 min ⁻¹	0.01863
0.19684 min ⁻¹	0.0172
Average k	Average error
0.178	0.018
standard deviation	% error margin
0.021 min ⁻¹	11.80%
experimental number <u>3-6-2019</u>	

From the results in Table 13, it is clear that there is a change in average k in phosphate buffer in comparison with MOPS, highlighted in Table 13.

entry	Description	Rate constants (k)
1	Na ₂ HPO ₄ buffer	0.178 ± 0.018 min ⁻¹
2	reference buffer	0.283 ± 0.047 min ⁻¹

Although the reaction is slower in phosphate buffer than in MOPS, the effect is less than a factor of two and the reaction clearly does not stop. This observation suggests that MOPS is not critically involved in the reaction as sacrificial electron donor. This conclusion is also in agreement with the absence of an effect of MOPS concentration on the observed kinetics.

DODC is also known to be an electron donor in its excited state,⁽³⁰⁾ but we did not investigate this effect.

k) Effect of buffer additives

Another compound of which the effect on the kinetics of fading needs to be established is citrate. Sodium citrate is used to stabilise human serum, and when used in regular buffer, we must learn how it affects kinetics.^(31, 32)

Experiments were carried out to discover the effect of added sodium citrate in the buffer on the kinetics of fading. We used buffer (pH=7, 25 mM MOPS, 50 mM NaCl, 1 mM EDTA and 20 mM sodium citrate) for the reaction and the results are summarised in Table 14.

	Description	rate constants (k)
	reference buffer + 20 mM citrate	0.203 ± 0.028 min ⁻¹
	reference buffer	0.283 ± 0.047 min ⁻¹

From Table 14, it is clear that citrate retards the fading by approximately a third.

We next added sodium azide, a singlet-oxygen quencher, to the buffer to discover the effect on kinetics of fading. The addition of sodium azide allows us to evaluate whether singlet oxygen is likely to play a role in the reaction. The results are shown in Table 15.

Table 15 The effect of sodium azide on fading of DODC	
Description	Rate constants (<i>k</i>)
reference buffer	$0.283 \pm 0.047 \text{ min}^{-1}$
reference buffer + 10 mM NaN ₃	$0.410 \pm 0.072 \text{ min}^{-1}$

Table 15, it is clear that there is an increase in average k in comparison with fading in the reference buffer. The absence of a decrease in the observed rate constant is in line with the hypothesis that singlet oxygen is not involved in the reaction based on the absence of an effect of using a deuterated solvent (vide supra). Like in the case of TO (Chapter 3), the effect of azide on DODC kept in the dark was not investigated so we cannot exclude the possibility of a direct reaction between DODC and azide, not involving irradiation.

1) Light intensity

Finally, we wanted to see the effect of changing light intensity on fading of DODC. We used deionised water as the solvent and varied the LED intensity (version 3 of LED - see chapter 2) while stirring at 25 °C. The observed rate constants (see Appendix) were plotted as a function of intensity (Figure 4.19).

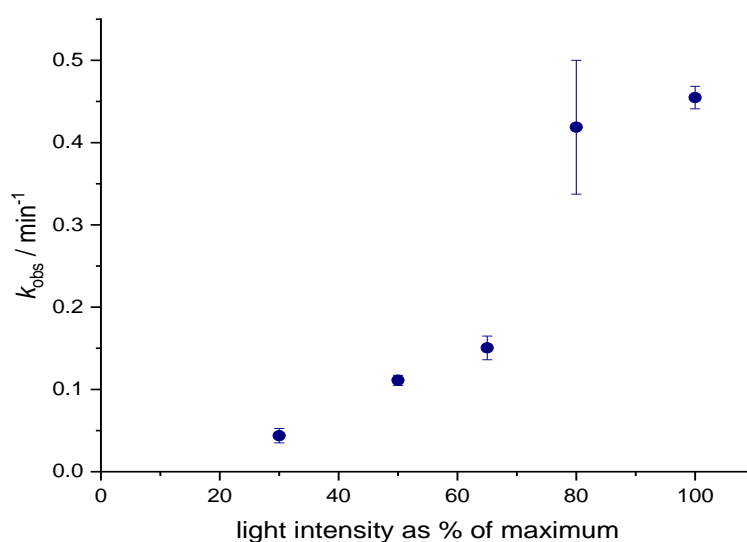


Figure 4.19 Relation between k for fading of DODC and LED intensity as percentage of maximum intensity.

The rate constant clearly increases with increasing light intensity, but the increase is not the linear increase we would have expected. The reason for this may be that deionised water does not allow reproducibility between experiments and this experiment should be repeated in buffered solution. However, this may also be related to the observation that photodisintegration is far more effective from higher excited states, with photodisintegration from S_m states occurring on average after 15 to 30 cycles, rather than after 10^5 cycles from the S_1 state. ⁽³³⁾

4.2.2 product analysis

Mass spectrometry for DODC before and after fading in deionised water was carried out.

Figure 4.20 shows the mass spectrum before fading.

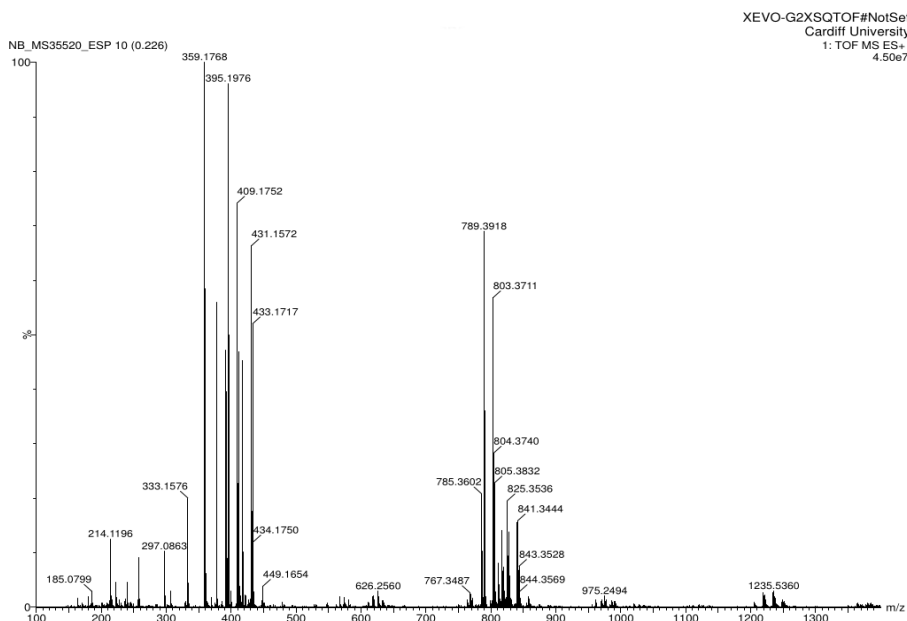


Figure 4.20 mass spectrum for DODC

Figure 4.20 shows more peaks than anticipated for a pure compound. The peak at 359.18 amu/z is the parent cation.

Figure 4.21 shows the mass spectrum after fading.

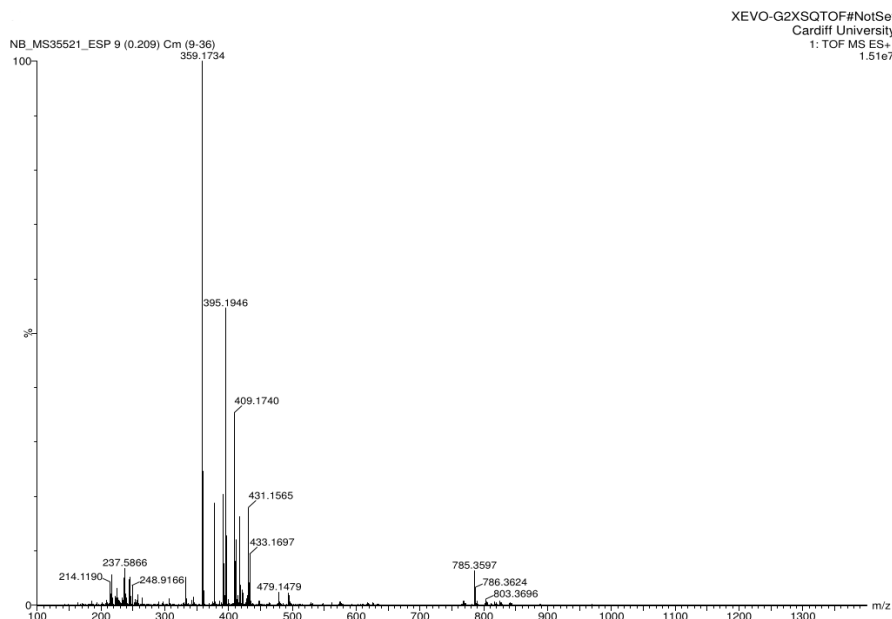


Figure 4.21 mass spectrum for DODC after fading.

Surprisingly, Figure 4.21 still shows a peak at 359.18 amu/z for the parent cation and the biggest difference is that the peaks around 800 amu/z have disappeared. We currently have now interpretation for this observation.

We also studied the reaction using NMR spectroscopy. We first predicted the ^1H NMR spectrum for the DODC cation using Chemdraw (Figure 4.22).

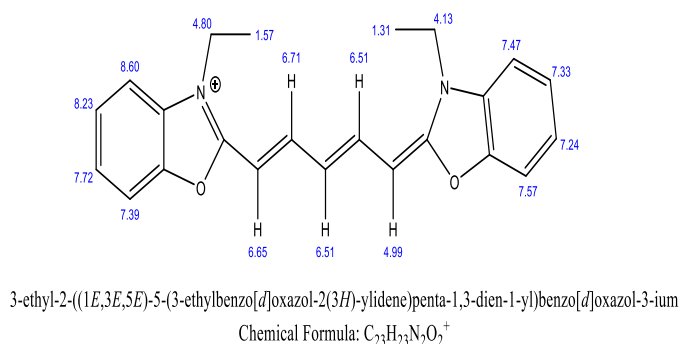
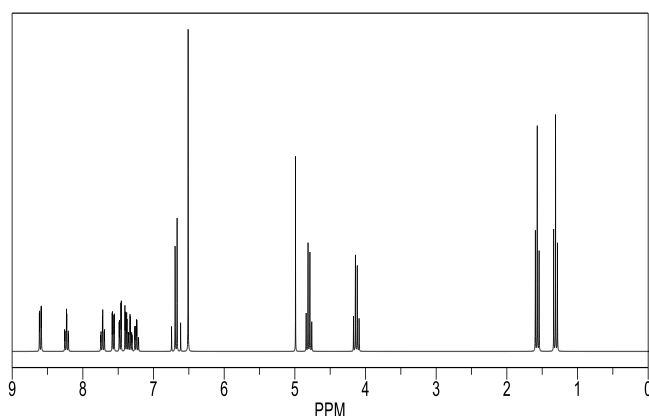


Figure 4.22 Predicted ^1H -NMR spectrum for the DODC cation.

The predicted NMR spectrum in Figure 4.22 is for one of the resonance forms of the DODC cation. The actual spectrum should therefore display half the number of peaks near the average positions for the peaks in Figure 4.22.

The experimental spectrum of DODC before fading in a saturated 50:50 D₂O:DMSO mixture is shown in Figure 4.23.

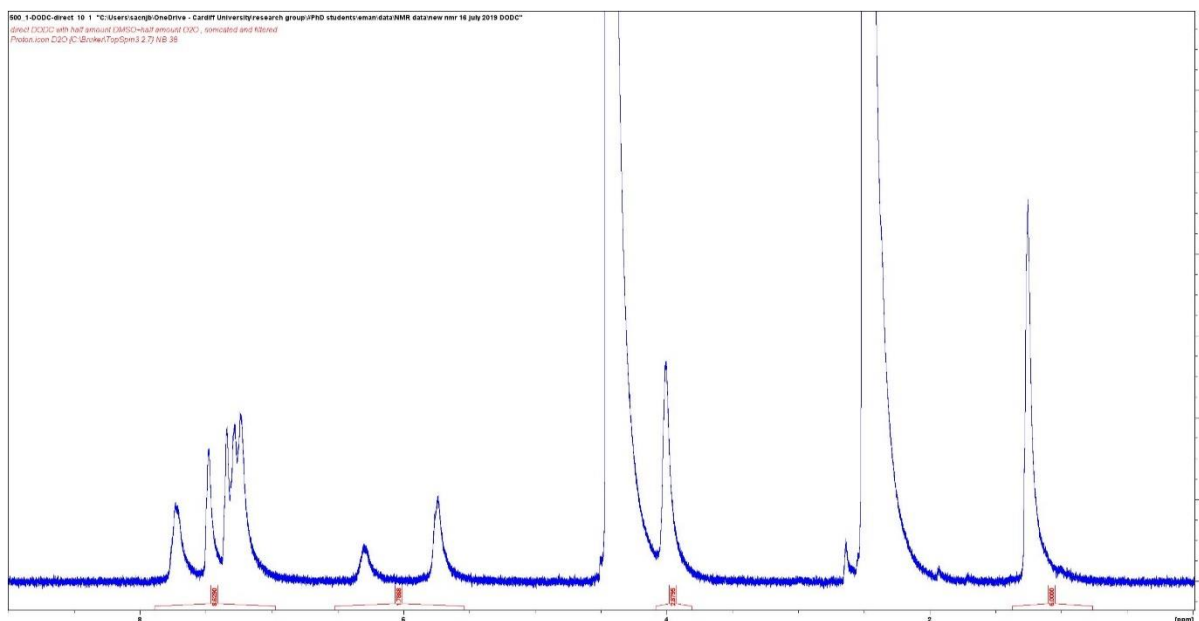


Figure 4.23 spectrum of DODC before fading in a saturated 50:50 D₂O: DMSO mixture (DMSO set to 2.5 ppm).

The peaks in Figure 4.23 are all broad, which we attribute to significant aggregation in the saturated solution. Nevertheless, it is possible to assign the peaks as follows. The peak at 1.3 ppm is assigned to the N-ethyl CH₃s; the peak at 4.0 ppm is assigned to the N-ethyl CH₂s; the two peaks at 5.7 ppm and 6.3 ppm are assigned to the alkene CHs, although we note that the integral is too small; the peaks between 7 and 8 ppm are assigned to the phenyl CHs.

The ^1H NMR spectrum after fading was similarly recorded, but this time for a two-fold diluted solution from saturated, and overlaid on the spectrum of DODC (Figure 4.24).

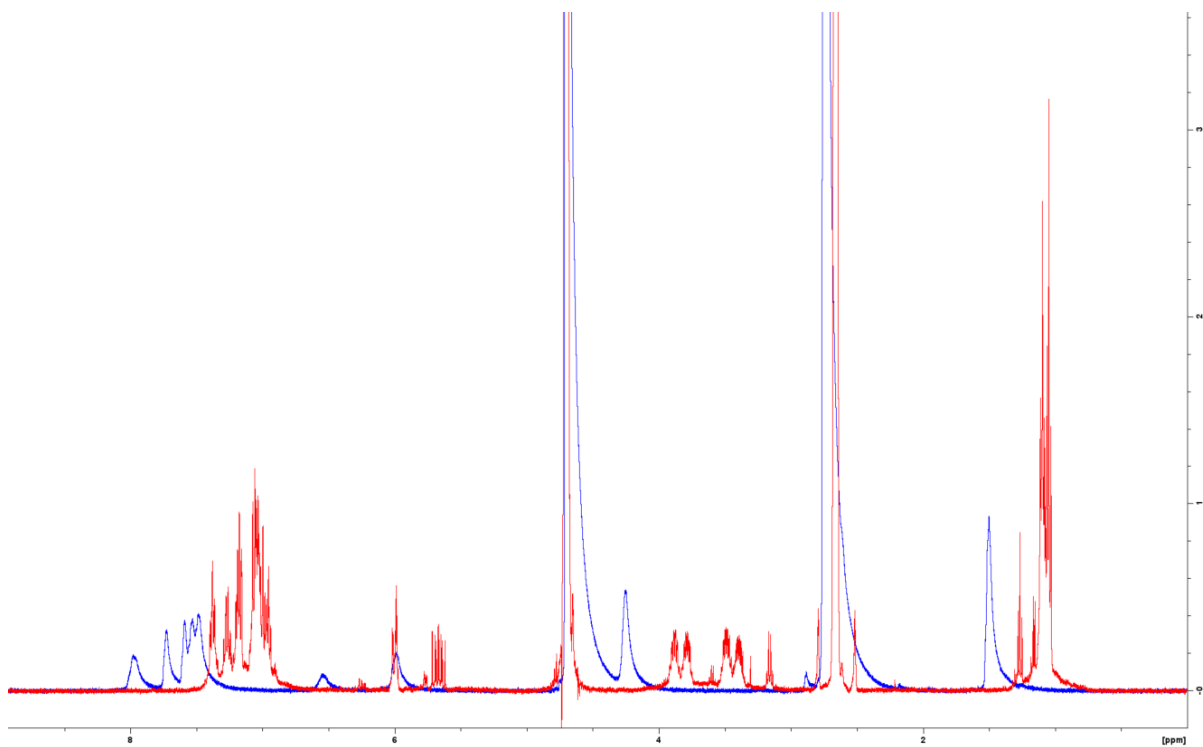


Figure 4.24 NMR spectrum for the fading products resulting from irradiation of DODC in a 50:50 (v/v) D_2O : d_6 -DMSO mixture.

Figure 4.24 shows that the peaks assigned to the alkene CHs have shifted. At the same time, the two $\text{N-CH}_2\text{CH}_3$ appear to have become non-equivalent with surprisingly high multiplicities for the N-CH_2 signals. The aromatic region has shifted. Considering the two $\text{N-CH}_2\text{CH}_3$ appear to have become non-equivalent, one would expect the same to be true for the aromatic CH signals. Somewhat surprisingly, this effect is not immediately obvious from the NMR spectrum. As was the case for the mass spectra, these data don't lend themselves to immediate interpretation.

4.3 Conclusions

The fading of DODC occurs via a mechanism that does not involve proton-transfer processes in the pH range studied. The rate constant increases with light intensity and this increase may be non-linear, in line with photodisintegration being much more efficient from higher excited states. Oxygen is involved in the reaction and it affects the observed rate constant and thus appears to be involved in the rate-determining step. Singlet oxygen does not appear to be involved in the reaction because neither changing from H₂O to D₂O nor addition of azide affects the observed rate constants. The hypothesis that singlet oxygen is not involved is in line with DODC not displaying much intersystem crossing,⁽³⁴⁾ and being a poor singlet oxygen sensitiser.⁽³⁵⁾ Taken together, it may be that the fading of DODC involves a higher order excited state reacting with molecular oxygen in its triplet ground state. An alternative interpretation involves formation of superoxide radicals resulting from electron transfer to oxygen leading to hydroxyl radicals.⁽³⁶⁾

4.4 Experimental

UV-visible spectroscopy

JASCO V630 and V650 UV-visible spectrophotometers as well as a SHIMADZU-UV-1800 were used to monitor reactions by recording absorption spectra after set amounts of time of irradiation using our irradiation device. Both JASCO machines were equipped with a Peltier thermostatted cell holder. Absorption spectra were recorded in 1.00 cm pathlength stoppered quartz cuvettes (Hellma) holding approximately 2.5 cm³ liquid and 1.00 cm of headspace (i.e., under aerobic conditions), at 25 °C unless otherwise stated.

Preparation of DODC solutions for kinetic experiments

A stock solution of DODC was prepared by placing a small amount of DODC in the solvent of interest. The resulting suspension was placed in a sonicator bath and sonicated for 3-6 minutes and then filtered through PTFE syringe filters (Thermo Scientific-0.22 and 0.45 μm). The stock solutions were stored in the dark. For individual experiments, 75-100 μL of the TO stock solution were added to 2425 or 2400 μL of buffer (to generate a total of 2500 μL of solution) in a 1 cm pathlength quartz cuvette (Hellma).

Mass spectroscopy

Approximately 10 mg of DODC was suspended in 7.0 mL deionised water and the resulting mixture was stirred, shielded from light, for two days and subsequently left for 10 days. The resulting suspension was filtered through a 0.22 μm PTFE syringe filter. The filtered solution was diluted two-fold with deionised water to make up a 1 mL samples which was shielded from the light and submitted for MS analysis. A second sample involved 1.5 mL of the filtered solution combined with 1.5 mL of deionised water. This sample was irradiated using our irradiation device and 1 mL was submitted for MS analysis. Mass spectra were recorded on a XEVO-G2XSQTOF.

¹H NMR spectroscopy

Approximately 10 mg of DODC was dissolved in a combination of 1.1 mL d₆-DMSO and 1.1 mL D₂O. The resulting mixture was stirred, shielded from light, for two days and subsequently left for 10 days. The resulting suspension was filtered through a 0.22 μm PTFE syringe filter. Two 1 mL samples were prepared by combining 0.5 mL of this filtered solution with 0.25 mL of d₆-DMSO and 0.25 mL of D₂O. One of these samples was submitted directly for ¹H NMR

spectroscopy, the other sample was first irradiated using our irradiation device and subsequently submitted for ^1H NMR spectroscopy. A further sample of the starting material was obtained by similarly dissolving DODC in a 50:50 mixture of d_6 -DMSO and mL D_2O , filtration and submission of the undiluted (saturated) solution for ^1H NMR spectroscopy.

Software

Graphs were constructed and kinetic data were analysed using OriginLab Origin 2020 software. Wavelengths for analysis were selected through UV-visible time resolved absorption spectra measurement for the reaction (for DODC this was typically 578 nm). All rate constants are expressed as observed first-order rate constants resulting from fitting a first-order rate law to the data at 578 nm using Origin 2020.

Chemicals

All chemicals were commercially available (Acros, Alfa Aesar, Aldrich, Fisher Scientific, ICT, and Maybridge) and used as purchased without further purification. Highly purified H33094 3,3'-Diethyloxadicarbocyanine iodide, 96% from Alfa Aesar was supplied by Thermo Fisher Scientific company. Stock no. H33094.MD (250 mg). Deuterium oxide was from Sigma Aldrich.

Buffer preparation

All experiments were carried out in buffers with different concentration of MOPS and NaCl. Buffers contained 25, 50 or 100 mM MOPS; 50, 100 or 200 mM NaCl and 1 mM EDTA, pH was 4.3, 7.0 or 10.8. Other buffers contained 25 mM Na_2HPO_4 buffer, 50 mM NaCl, 1 mM EDTA, pH 7.0. MOPS was purchased from Melford (CAS 1132-61-2), NaCl was purchased from Fisher Scientific (CAS 7647-14-5), Na_2HPO_4 was purchased from Melford (CAS 7558-79-4), EDTA was purchased from VWR (CAS 6000-4). Buffers were titrated with aqueous NaOH or KOH to the required pH. The pH of aqueous solutions was determined using a Hanna microprocessor pH 113 pH-meter equipped with a VWR 662-1382 glass electrode. Materials were weighed out on a Fisher brand 4-decimal balance. De-ionised water was produced using an ELGA PF3XXXXM1 Water Purification System Type I 2 Lpm for all solutions. Buffers containing 25, 50 or 100 mM MOPS (3-(N-morpholino) propanesulfonic acid) with 50, 100 or 200 mM sodium chloride (NaCl) and 1 mM EDTA were prepared by dissolving the required amounts of MOPS, sodium chloride (NaCl) and EDTA in deionised water and stirring at room temperature until the solids dissolved. A solution of sodium hydroxide (NaOH) was used for adjusting the pH to 7.0 (4.30 – 10.80) and the buffer was made up to 2 litres in a volumetric flask.

Phosphate buffer containing 25 mM Na_2HPO_4 , 50 mM sodium chloride (NaCl) and 1 mM EDTA was prepared by dissolving Na_2HPO_4 , sodium chloride (NaCl) and EDTA in distilled water and stirring at room temperature until the solid dissolved. An aqueous solution of sodium hydroxide (NaOH) was used for adjusting the pH to 7.0 and the buffer was made up to 2 litres in a volumetric flask. NaN_3 -containing buffer was prepared by dissolving the required amount of NaN_3 in 100 mL of the reference buffer. Sodium citrate containing buffer was prepared by dissolving the required amount of sodium citrate in 100 mL of the reference buffer.

Irradiation setup

The LED used was a 4th version of LED (MCWHD3 - 6500 K- LED on Metal-Core PCB) with fan and lenses to increase the intensity. The LED was powered using a T-Cube LEDD1B with a CAB-LEDD1 LED link cable. The irradiation setup was as a 3D-printed device as described in Chapter 2. We used an IKA Big Squid magnetic stirrer placed under our irradiation setup to magnetically stir the solutions during irradiation. For temperature control, the entire setup was placed in a Heidolph unimax 1010 shaker with incubator with temperature control.

4.5 References.

1. National Center for Biotechnology Information (2021). PubChem Compound Summary for CID 2735005. Retrieved January 30, 2021 from <https://pubchem.ncbi.nlm.nih.gov/compound/2735005>. 1.
2. <https://www.sigmaaldrich.com/catalog/product/sial/258091?lang=en®ion=GB>. 67.
3. Marvin-Smith, A. H. Absorption of Carbocyanine Dyes Bound to Quadruplex DNA. (2008).
4. Taniguchi, M., Du, H. & Lindsey, J. S. PhotochemCAD 3: diverse modules for photophysical calculations with multiple spectral databases. *Photochem. Photobiol.* **94**, 277–289 (2018).
5. Aramendia, P. F., Negri, R. M. & Roman, E. S. Temperature dependence of fluorescence and photoisomerization in symmetric carbocyanines. Influence of medium viscosity and molecular structure. *J. Phys. Chem.* **98**, 3165–3173 (1994).
6. Saputra, R. Photoluminescent, Upconversion Luminescent and Nonlinear Optical Metal-organic Frameworks: From Fundamental Photophysics to Potential Applications. *J. Chem. Inf. Model.* **53**, 1689–1699 (2019).
7. Pronkin, P. & Tatikolov, A. Isomerization and properties of isomers of carbocyanine dyes. *Sci* **1**, 5 (2019).
8. Widengren, J. & Schwille, P. Characterization of photoinduced isomerization and back-isomerization of the cyanine dye Cy5 by fluorescence correlation spectroscopy. *J. Phys. Chem. A* **104**, 6416–6428 (2000).
9. Chakrabarty, D., Chakraborty, A., Hazra, P., Seth, D. & Sarkar, N. Dynamics of photoisomerisation and rotational relaxation of 3, 3'-diethyloxadiazocarbocyanine iodide in room temperature ionic liquid and binary mixture of ionic liquid and water. *Chem. Phys. Lett.* **397**, 216–221 (2004).
10. Unsymmetrical Relaxation Paths of the Excited States in Cyanine Dyes Detected by Time-Resolved Fluorescence: Polymethinic and Polyenic Forms. 1–24.
11. Levitus, M. & Ranjit, S. Cyanine dyes in biophysical research: the photophysics of polymethine fluorescent dyes in biomolecular environments. *Q. Rev. Biophys.* **44**, 123 (2011).

12. Improta, R. & Santoro, F. A theoretical study on the factors influencing cyanine photoisomerization: the case of thiacyanine in gas phase and in methanol. *J. Chem. Theory Comput.* **1**, 215–229 (2005).
13. Ghosh, S., Mandal, S., Banerjee, C., Rao, V. G. & Sarkar, N. Photophysics of 3, 3'-diethyloxadicyanine iodide (DODCI) in ionic liquid micelle and binary mixtures of ionic liquids: effect of confinement and viscosity on photoisomerization rate. *J. Phys. Chem. B* **116**, 9482–9491 (2012).
14. Smith, S. & Abdallah, F. B. The Kinetics of the Cis-to-Trans Thermal Isomerization of 4-Anilino-4'- Nitroazobenzene are Highly Influenced by Solvent Polarity. *J. Thermodyn. Catal.* **08**, 4–9 (2017).
15. Garcia-Amorós, J. *et al.* Activation volumes for cis-to-trans isomerisation reactions of azophenols: a clear mechanistic indicator? *Phys. Chem. Chem. Phys.* **20**, 1286–1292 (2018).
16. Henrichs, P. M. & Gross, S. Conformational analysis of carbocyanine dyes with variable-temperature proton Fourier transform nuclear magnetic resonance spectroscopy. *J. Am. Chem. Soc.* **98**, 7169–7175 (1976).
17. Rovnyagina, N. R. *et al.* Fluorescence Lifetime and Intensity of Thioflavin T as Reporters of Different Fibrillation Stages: Insights Obtained from Fluorescence Up-Conversion and Particle Size Distribution Measurements. *Int. J. Mol. Sci.* **21**, 6169 (2020).
18. Foote, C. S., Denny, R. W., Weaver, L., Chang D, Y. & Peters, J. Quenching of singlet oxygen. *Ann. N. Y. Acad. Sci.* **171**, 139–148 (1970).
19. Li, M. Y. *et al.* Quenching of Singlet Molecular Oxygen (1O_2) by Azide Anion in Solvent Mixtures¶. *Photochem. Photobiol.* **74**, 760–764 (2001).
20. Mertsch, A., Letschert, S., Memmel, E., Sauer, M. & Seibel, J. Synthesis and application of water-soluble, photoswitchable cyanine dyes for bioorthogonal labeling of cell-surface carbohydrates. *Zeitschrift für Naturforsch. C* **71**, 347–354 (2016).
21. Turro, N. J., Ramamurthy, V. & Scaiano, J. C. *Modern molecular photochemistry of organic molecules*. (Viva Books University Science Books, Sausalito, 2017).
22. Zheng, Q. *et al.* On the Mechanisms of Cyanine Fluorophore Photostabilization. *J. Phys. Chem. Lett.* **3**, 2200–2203 (2012).
23. Zheng, Q., Jockusch, S., Zhou, Z. & Blanchard, S. C. The contribution of reactive oxygen species to the photobleaching of organic fluorophores. *Photochem. Photobiol.* **90**, 448–454 (2014).

24. Yoshii, H. *et al.* Photo-excitation of carotenoids causes cytotoxicity via singlet oxygen production. *Biochem. Biophys. Res. Commun.* **417**, 640–645 (2012).
25. Sailer, B. L., Nastasi, A. J., Valdez, J. G., Steinkamp, J. A. & Crissman, H. A. Differential effects of deuterium oxide on the fluorescence lifetimes and intensities of dyes with different modes of binding to DNA. *J. Histochem. Cytochem.* **45**, 165–175 (1997).
26. Štacková, L. *et al.* Deciphering the Structure–Property Relations in Substituted Heptamethine Cyanines. *J. Org. Chem.* **85**, 9776–9790 (2020).
27. Zhu, Z. *et al.* Single-walled carbon nanotube as an effective quencher. *Anal. Bioanal. Chem.* **396**, 73–83 (2010).
28. Shank, N. I., Zanotti, K. J., Lanni, F., Berget, P. B. & Armitage, B. A. Enhanced Photostability of Genetically Encodable Fluoromolecules Based on Fluorogenic Cyanine Dyes and a Promiscuous Protein Partner. *J. Am. Chem. Soc.* **131**, 12960–12969 (2009).
29. Lima, E. *et al.* Quinoline-and Benzoselenazole-Derived Unsymmetrical Squaraine Cyanine Dyes: Design, Synthesis, Photophysicochemical Features and Light-Triggerable Antiproliferative Effects against Breast Cancer Cell Lines. *Materials (Basel)*. **13**, 2646 (2020).
30. Doizi, D. & Mialocq, J. C. Photosensitized electron-transfer reaction in the first excited singlet state of the polymethine-cyanine dye DODCI. *J. Phys. Chem.* **91**, 3524–3530 (1987).
31. Goulet, D. R., Knee, K. M. & King, J. A. Inhibition of unfolding and aggregation of lens protein human gamma D crystallin by sodium citrate. *Exp. Eye Res.* **93**, 371–381 (2011).
32. Smith, W. C. & Carroll, R. J. Method of using anticoagulant solution in blood separation. (1996).
33. Reindl, S. & Penzkofer, A. Strong-excitation and weak-excitation photodisintegration of DODCI. *Opt. quantum Electron.* **30**, 49–60 (1998).
34. Reindl, S. & Penzkofer, A. Higher excited-state photoisomerization and singlet to triplet intersystem-crossing in DODCI. *Chem. Phys.* **230**, 83–96 (1998).
35. Kassab, K. Photophysical and photosensitizing properties of selected cyanines. *J. Photochem. Photobiol. B Biol.* **68**, 15–22 (2002).
36. Ochsner, M. Photophysical and photobiological processes in the photodynamic therapy of tumours. *J. Photochem. Photobiol. B Biol.* **39**, 1–18 (1997).

Chapter five

Interaction of TO and DODC with biological samples and the effects on fading

Summary

We have analysed the effects of biomacromolecules and serum on fading of TO and DODC. DNA is found to have little effect of fading of TO but to retard fading of DODC. Serum is found to strongly retard fading of TO and DODC. Similarly, added ethanol and DMSO also strongly retard the kinetics of fading.

5.1 Introduction

Studies of the kinetics of fading of TO and DODC have been described in Chapters 3 and 4, respectively. Both TO and DODC are also known to bind to DNA and other biomacromolecules. This binding may affect fading kinetics which, in turn, might be useful in forensic applications.

5.1.2 Serum, plasma and serum albumins.

The difference between serum and plasma is illustrated in Figure 5.1.⁽²²⁾

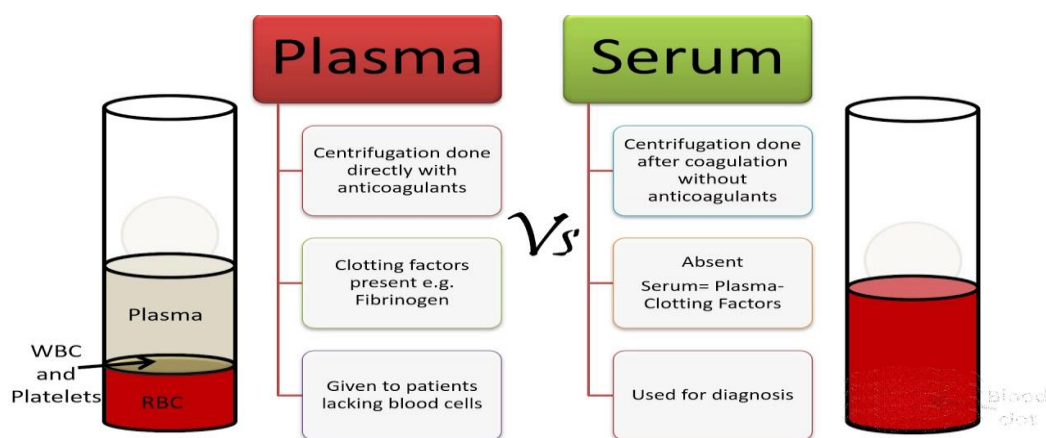


Figure 5.1 The differences between serum and plasma

Human Serum Albumin (HSA) is a single monomeric polypeptide of 585 amino acid residues. HSA is a major protein component of human plasma with a typical concentration of 0.6 mM in the bloodstream, significantly contributing to human serum antioxidant capacity.⁽²³⁾ X-ray crystallography studies have shown that HSA consists of three homologous domains (I-III), and each domain is further divided into subdomains A and B (Figure 5.3). HSA has the ability to bind with a wide range of chemically different endogenous and exogenous ligands in a non-covalent mode.^(24,25)

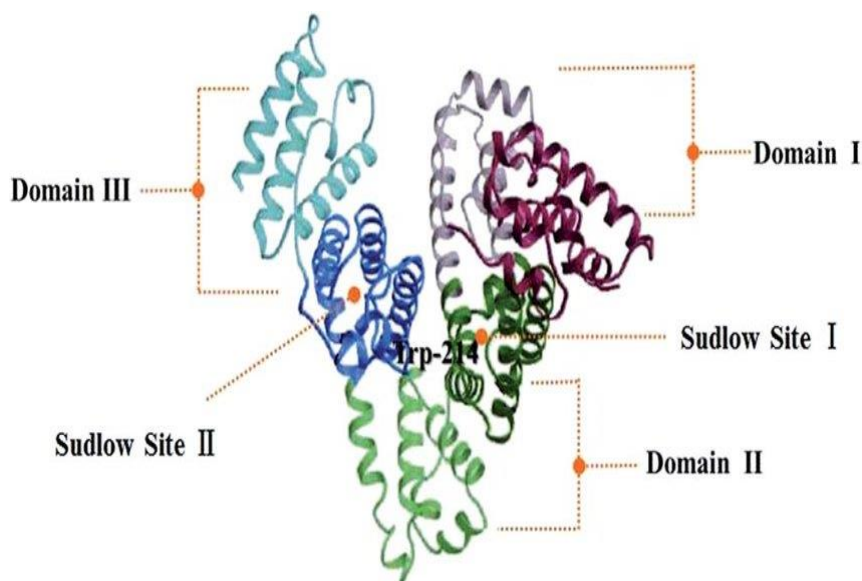


Figure 5.2 The three dimensional structure of HSA. ⁽²⁶⁾

Human serum albumin (HSA) makes up about 60 percent of the protein present in the circulatory system in humans. With a molecular mass of 66,439 Da, a structure that comprises a sequence of 585 amino acids with 17 disulfide bonds, its primary function is to act as the main transporter of exogenous and endogenous materials. ⁽²⁷⁾ HSA is capable of binding several forms of compounds (e.g., ions, fatty acids, bile acids, drugs and their metabolites, etc.). There are many well-researched HSA binding sites: Site 1 of Sudlow (subdomain IIA), a large multi-chamber pocket characterised primarily by a single residue of tryptophan. And Site 2 of Sudlow (subdomain IIIA, shaped similarly to Site 1, but the compounds bound here usually contain a peripherally located negative charge). ^(28, 29)

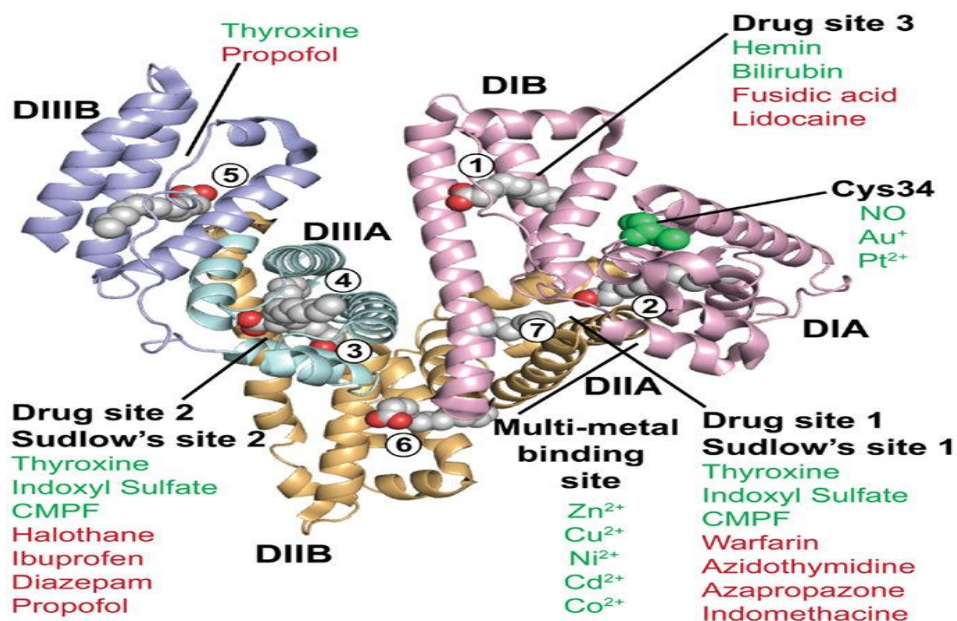


Figure 5.3 Summary of the ligand binding capacity of HSA as defined by crystallographic studies. Ligands are depicted in space filling representation; oxygen atoms are coloured red ⁽³⁰⁾

Bovine Serum Albumin (BSA), is one of the most strongly related proteins to HSA. ⁽³¹⁾ The similarity between HSA and BSA is 76%. Brown elucidated the primary structure of BSA in 1975. BSA contains 607 amino acids, of which twenty-one are tyrosine (Tyr) and two are tryptophan (Trp) located at positions 134 and 212, respectively. These amino acids cause BSA to have intrinsic fluorescence. ⁽³²⁾

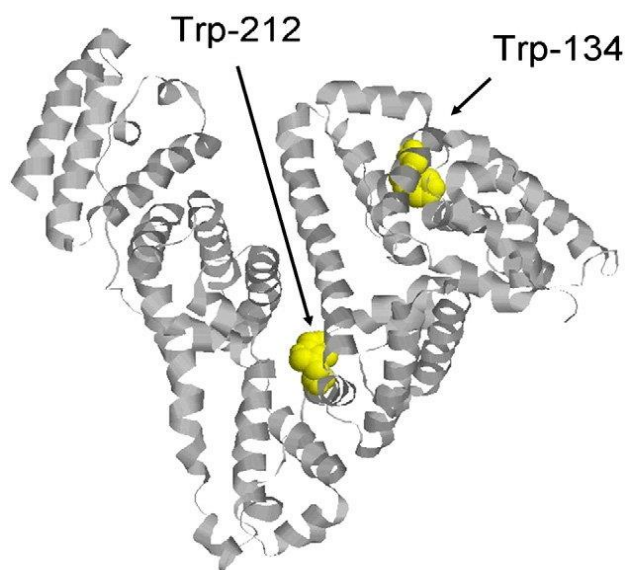


Figure 5.4 Bovine Serum Albumin (BSA) showing the position of Trp residues. ⁽³³⁾

Although there is no substantial difference in function between HSA and BSA (both exist primarily for the attachment and redistribution of small molecules and fatty acids via the bloodstream), there are some variations when it comes to comparing the findings obtained from serum albumins of different organisms.⁽³⁴⁾ HSA and BSA may have entirely different binding sites for the same molecule, as HSA Site I is more flexible and provides more structural adaptability than BSA, which, in contrast, tends to be very rigid. BSA, most importantly, contains two residues of Trp (as opposed to only one in HSA), this second tryptophan (Trp134) is located near to the third binding site in subdomain IB⁽³⁵⁾.

Serum albumin has been, and still is, a model protein in protein science, partly due to its high plasma abundance in humans and other mammals, and also for the study of protein-binder interactions. Serum albumin is the primary transporter in the blood for low-polar compounds and, importantly, this includes many metabolites and drugs.⁽³⁶⁾ Drugs or ligands interact with BSA or HSA to create complexes that may be reversible. Therefore, beyond its role as a model protein, understanding the molecular mechanisms that allow albumin to transport multiple compounds in different organisms is essential.^(37,38)

Compounds' therapeutic efficacies depend on their ability to bind to serum albumin, as well as the mechanism involved in binding. HSA-ligand complexes studied using crystallography show that drug-like compounds mainly interact on the protein subdomains IIA and IIIA with one of the two high-affinity binding sites, which make specific drug delivery possible.⁽³⁹⁾ These different binding sites allow HSA to bind different ligands with an exceptional ability that adds to its biological importance in delivering a variety of drugs in the blood system to their targeting organs / tissues within the human body.⁽⁴⁰⁾ HSA contains a single tryptophan residue (Trp 214) in domain IIA and its fluorescence is extremely sensitive to nearby bound ligands. Fluorescence can therefore be used as a test to elucidate binding properties of HSA drugs.⁽⁴¹⁾

The reversible drug-protein complex formation has attained considerable interest in pharmacokinetics since this formation is by, for example, weaker chemical bonds, hydrogen bonds or Van der Waals forces. The fluorescence approach is used numerous experiments to study the interaction of serum albumin with small molecules, drugs, and toxic chemicals.^(42, 43)

5.1.3 Cyanine dye interaction with serum albumins.

Taking advantage of their brilliant colour changes, the aggregation activity of some cyanine dyes has been used to detect proteins. Therefore, as more colours are being produced for these applications, it is important to obtain information

about their intrinsic absorptive and emissive behaviours and the extent of their affinity for their target proteins. ^(44, 45) Dye aggregation may be beneficial or disadvantageous for the application, depending on the application and the type of detection needed. An increase in the fluorescence signal of the dye after binding with the protein would be useful for sensitive identification in terms of non-covalent labelling. ⁽⁴⁶⁾ Since H-aggregates appear to be weaker in fluorescence than J-aggregates and the dye's monomer form, it would therefore be better to reduce H-aggregation for fluorescence detection. ^(47, 48)

Binding of fluorescent dyes to HSA can occur through hydrophobic interaction. Cyanine dye has received significant interest, when dealing with small hydrophobic molecules binding to HSA. ⁽⁴⁹⁾

5.1.4 Effects of solvents on behaviour of dyes

The kinetics of fading can be affected by the presence of different cosolvents like DMSO. In terms of the Onsager model, the impact of nearby solvent environment on cyanine dye photophysics can be explained by taking into account the effect of the dynamic properties of the DMSO solvation shell on the dye's fluorescence rate constant. ⁽⁵⁰⁾

Solvents can also have effects on aggregation of dyes. According to Chibisov et al. ⁽⁵¹⁾ DMSO is a polar solvent that, in combination with less polar solvents, leads to formation J-aggregates of cyanines. In mixtures with trichloroethylene cyanine dyes can also form H-aggregates, in addition to J-aggregates. The relative yield of J-aggregates depends on the DMSO content and the overall rate of creation. J-aggregates have a fluorescence resonance character. ⁽⁵²⁾

It is commonly accepted for cyanine dyes in polar solutions that trans-cis isomerisation is the primary deactivation mechanism of the excited state of S^1 . DMSO as a solvent can induce attraction between dye molecules and can create aggregates such as dimers. ⁽⁵³⁾ Production of dimers in DMSO microclusters surrounding the dye molecules, i.e. the solvation shells, may cause the excited state to be effectively quenched. ⁽⁵⁴⁾

The split excitonic absorption spectrum of super helical J-aggregates of tetrachlorobenzimidacarbocyanine chromophore obtained in the absence of alcohols was replaced by a 2-fold split spectrum with increased ethanol concentration while the circular dichroism signal usually increases. ⁽⁵⁵⁾ The spectral alterations demonstrate alcohol-induced modifications of the molecular packing of the aggregates. ⁽⁵⁶⁾

5.1.5 Aim and purpose

We want to discover the effect of biological samples on the kinetics of fading of TO and DODC. As biological samples, we used DNA, serum albumin and different types of serum as model systems for materials that may be present in crime scenes. We also tested the effects of cosolvents to identify whether solvents might be used to create false positives or false negatives if TO or DODC were to be used in crime scene investigations.

5.2 Results and discussion

In the following sections, the effects of biomacromolecules on TO and DODC fading are studied. Section 5.2.1 focusses on TO and Section 5.2.2 focusses on DODC.

5.2.1 Effects of biomacromolecules on fading of TO

The effects of various substances on fading of TO were investigated.

5.2.1a Fading of TO in the presence of fish-sperm DNA.

The effect of various concentrations of DNA on fading of TO in reference buffer (25 mM MOPS pH 7.0, 50 mM NaCl and 1 mM EDTA) was studied. An overview of the experiments and results is provided in Table 1. Overlay spectra and extracted kinetic traces can be found in the Appendix.

Table 1 solution preparation and fading kinetics for thiazole orange in the presence of different concentration of DNA ^a					
entry	TO stock amount	[DNA] in stock solution	[DNA] in cuvette	k_{obs}	standard deviation
1	400 μ l	150 μ M	60 μ M	0.352	0.133
2	200 μ l	350 μ M	140 μ M	0.3274	0.08189
3	200 μ l	500 μ M	200 μ M	0.29801	0.00705
4	200 μ l	750 μ M	300 μ M	0.278785	0.058985
5	300 μ l	1000 μ M	400 μ M	0.219985	0.021675
a) pH=7, 25 mM MOPS, 50 mM NaCl and 1 mM EDTA at 25 °C with magnetic stirring.					

Figure 5.10 shows the observed rate constants k_{obs} of fading of TO when in the presence of different concentration of fish-sperm DNA.

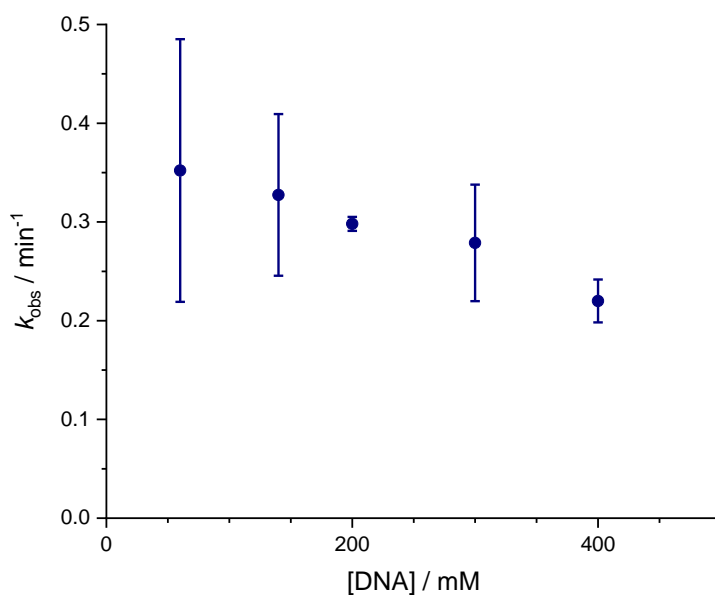
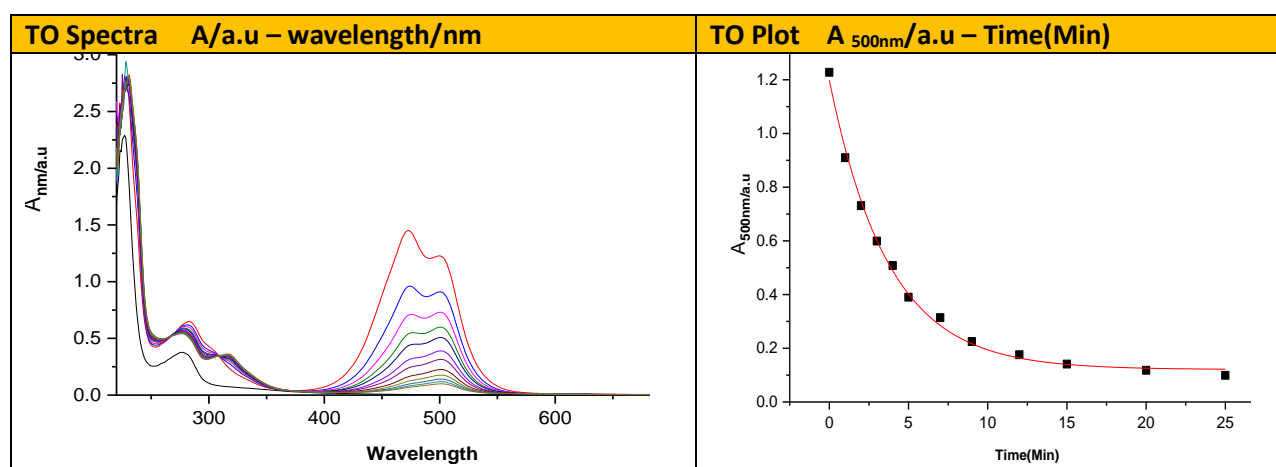


Figure 5.5 Rate constants k for fading of TO with different concentrations of DNA.

Figure 5.5 shows that the k value slowly decreases when the concentration of DNA increases.

5.2.1b Fading of TO in the presence of BSA

Serum albumins are abundant components of blood, so we explored the effect of serum albumins on fading of TO as well (Figure 5.6).



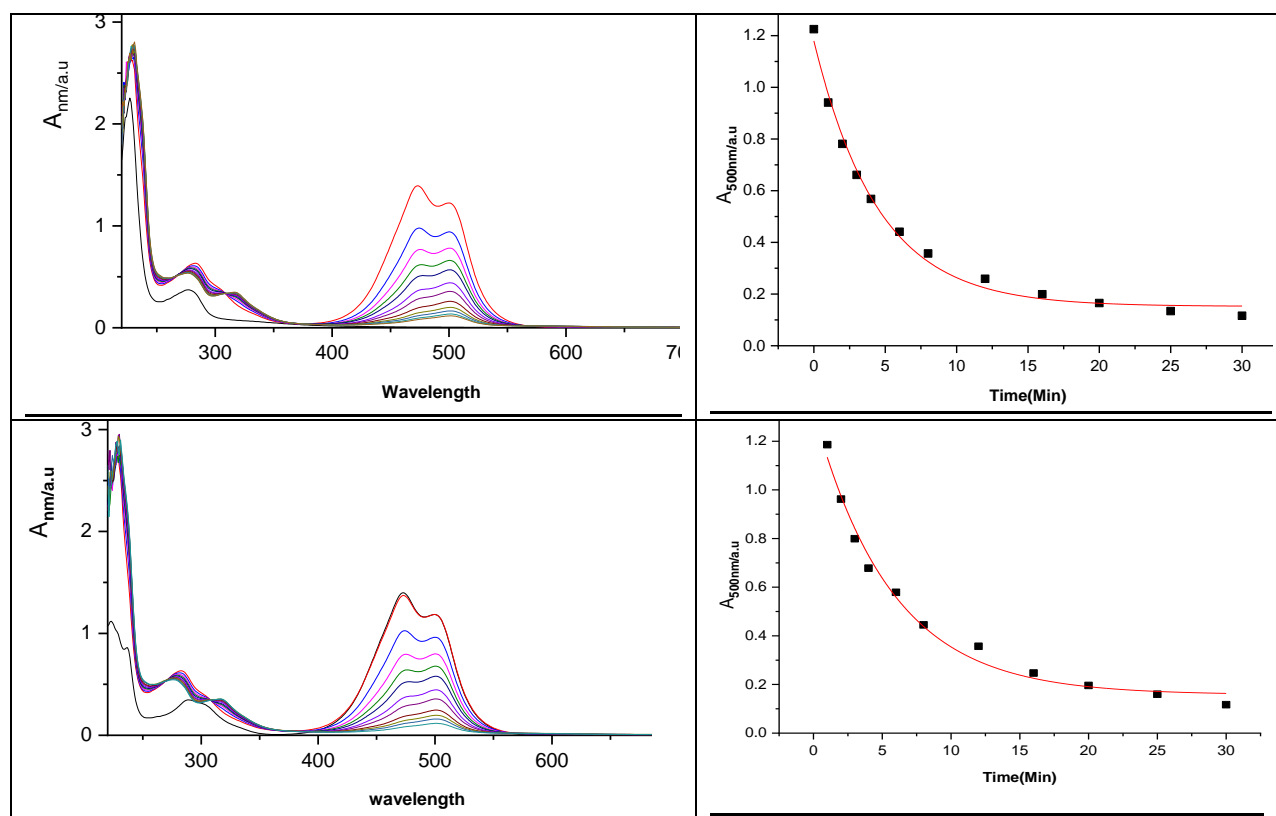


Figure 5.6 spectra and plots for TO fading in the presence of 20 µl of a 1 mM solution of BSA

The resulting rate constants are given in Table 2.

Table 2 Rate constants for fading of TO in solutions containing 20 µl of a 1 mM solution of BSA. ^a	
original rate constants	original errors
0.2687 min⁻¹	0.01203
0.22229 min⁻¹	0.01489
0.17799 min⁻¹	0.01873
Average k	Average error
0.223 min⁻¹	0.015
standard deviation	error margin
0.037	0.037035542
a) 1 mM BSA stock solution in deionised water, sonicated not filtered.	

The rate constant for fading is slightly lower than in the reference buffer. Unfortunately, we only used a very low concentration of BSA in this experiment and didn't carry out further experiments. The role of serum albumin

on fading is therefore not quantifiable from this experiment.

5.2.1c Fading of TO in human serum.

We wanted to evaluate the effect of human serum on the fading of TO. We irradiated a solution of TO in human serum with stirring and at 25 °C.

Figure 5.7 shows the spectra and plot of absorbance of TO at 506 nm when irradiated in human serum under standard conditions.

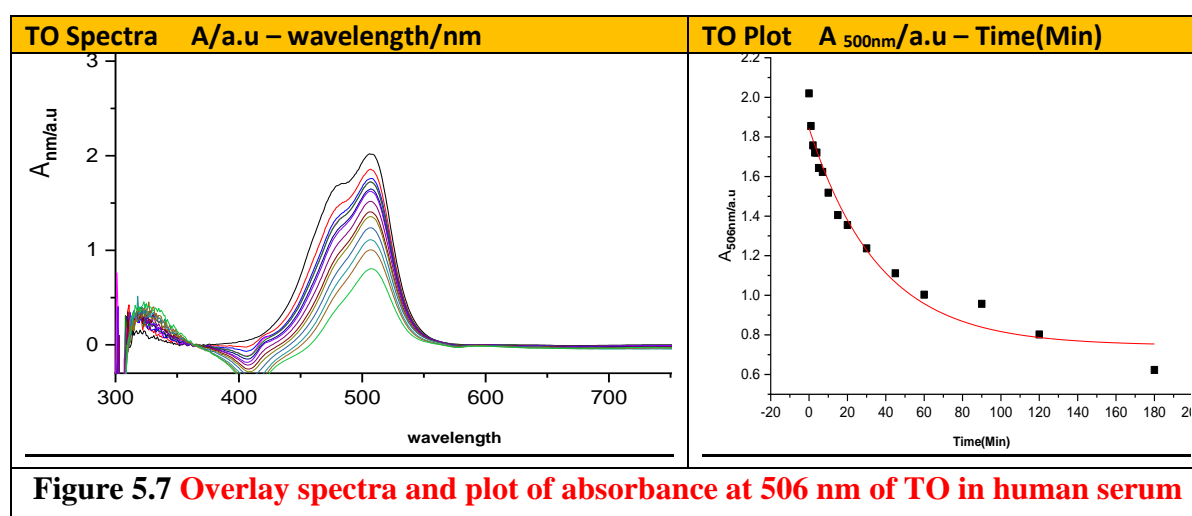


Table 3 shows the k for fading of thiazole orange when in human serum.

Table 3 showed the statistics last experiment (figure 5.13) that was made at 15-6-2019			
A nm/a.u	original rate constants	original errors	% error margin
506 nm	0.027 min ⁻¹	0.005	16.9

Table 3 shows that fading is significantly slower in human serum than in buffer and also significantly slower than in relatively concentrated solutions of DNA. The data also appear to level off at relatively high remaining absorbance so continued fading may be even slower. Serum is typically stabilised using citrate. However, we have shown in Chapter 3 that citrate does not significantly retard fading of TO.

This observation indicates that one (or more) of the components of serum has a significant rate-retarding effect on the fading of TO. We have not yet identified

which component this is, but further experiments involving BSA will allow us to identify whether this component of serum at relevant concentrations might explain the observed retardation of fading of TO.

5.2.1d Fading of TO in calf serum.

We next wanted to compare the effect of serum from different sources and therefore studied the fading of TO in calf serum (Figure 5.8).

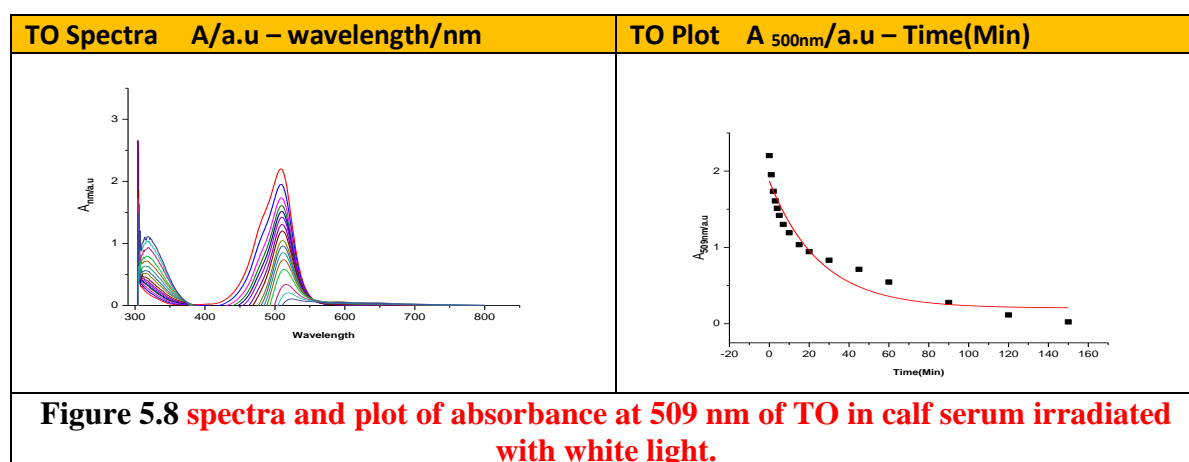


Table 4 gives the observed rate constant k for fading of thiazole orange in calf serum when irradiated with white light while stirring at 25 °C.

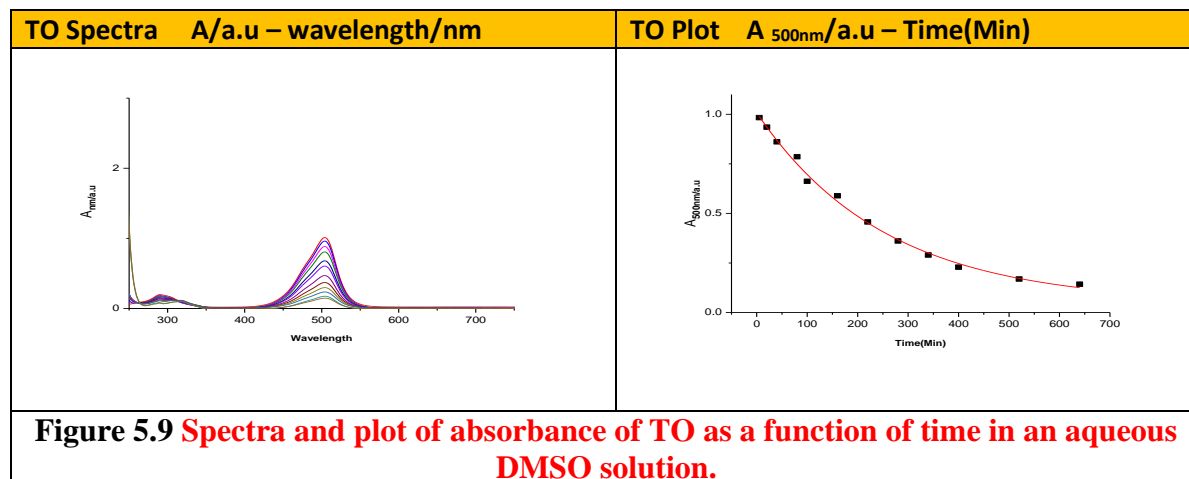
Table 4 showed the statistics of last experiment (figure 5.14) that was made at 16-6-2019			
A nm/a.u	original rate constants	original errors	% error margin
509 nm	0.0396 min ⁻¹	0.0085 min ⁻¹	21.5

Table 4 shows that, like human serum, calf serum strongly retards fading of TO. Because the error margins on the two rate constants overlap, albeit just, we do not feel we can interpret the possible difference in rate constants observed here.

5.2.1e Fading of TO in the presence of DMSO.

Then we wanted to explore reaction medium effects. Reaction medium effects may be informative with respect to the reaction mechanism but can also

highlight the potential effects of compounds that may be used to contaminate crime scenes. We therefore studied the fading of TO in a 50:50 (vol:vol) mixture of deionised water and DMSO (Figure 5.9).



Fitting an exponential rate law to the absorbance at 500 nm as a function of time yielded the data in Table 5.

<p>Table 5 Rate constant for fading of TO in 50-50 (vol-vol) DMSO deionised water.</p>		
original rate constants	original errors	% error margin
0.0039 min ⁻¹	0.0003 min ⁻¹	8.2

Table 5 shows clearly that the presence of DMSO has a very significant effect on fading of TO.

5.2.1f Fading of TO in the presence of ethanol.

We similarly studied the effect of ethanol on fading of TO (Figure 5.10).

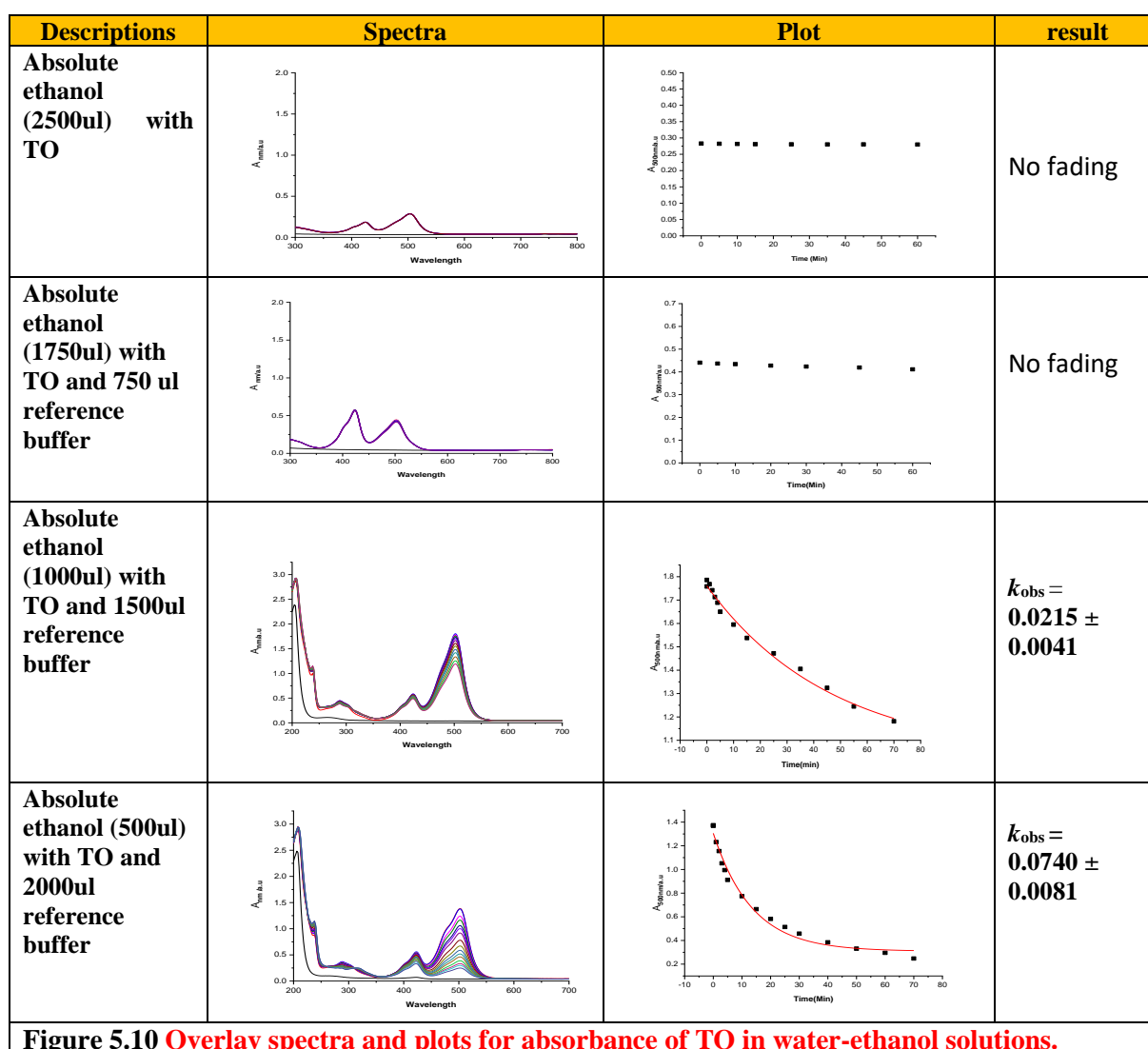


Figure 5.10 Overlay spectra and plots for absorbance of TO in water-ethanol solutions.

From Figure 5.10 it is clear that added ethanol protects TO from fading with higher fractions of ethanol stopping fading completely.

5.2.2 Effects of biomacromolecules on fading of DODC.

5.2.2a Fading of DODC in the presence of fish-sperm DNA.

The kinetics of fading of DODC was followed in the presence of fish-sperm DNA under otherwise standard conditions (Table 6).

Table 6 shows the statistics related to different concentration of DNA and DODC

entry	[DNA] in stock solution	[DNA] in cuvette	k_{obs}	error margin	standard deviation	error margin
1	0 μM	0 μM	0.2834	0.0467	0.0308	0.0467
2	150 μM	60 μM	0.1723	0.0168	0.0225	0.0225
3	350 μM	140 μM	0.0552	0.0178	0.0030	0.0178
4	500 μM	200 μM	0.0758	0.0186	0.0062	0.0186
5	750 μM	300 μM	0.0459	0.0132	0.0034	0.0132
6	1000 μM	400 μM	0.0873	0.0152	0.0043	0.0152

Table 6 illustrates that the k value decreases when the concentration of DNA increases. Figure 5.11 shows the k of fading of DODC when interacting with different concentration of fish-sperm DNA.

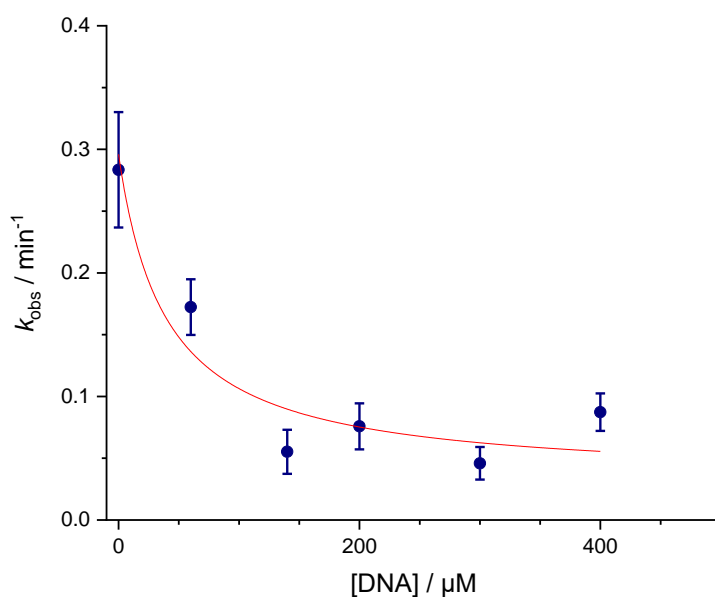


Figure 5.11 k in relation with different concentration of DNA.

Figure 5.16 shows that added DNA retards fading, as expected. In order to analyse the data, we developed a kinetic model. There are two potential models to describe the kinetic data. The first model using a mass-action model to describe binding of DODC to DNA. This model becomes complex in this case because the concentration of DODC changes during the experiment. The alternative model is a pseudophase model in which the DNA is described as a pseudophase with DODC partitioning over bulk water and the DNA

pseudophase.⁽⁹⁰⁾ The DODC concentration was estimated from the typical initial absorbance of 2 which, using an extinction coefficient of $270\,000\text{ M}^{-1}\text{ cm}^{-1}$ at 582 nm,⁽⁸⁴⁾ gives a DODC concentration of $7.4\ \mu\text{M}$. This means that at all DNA concentrations in Figure 5.17 the concentration of binding sites (estimated to be $[\text{DNA}]_{\text{tot}}/3$, based on a binding site size of three basepairs) exceeds the DODC concentration. This suggests the pseudophase model should be applicable because under these conditions binding of DODC to DNA is not limited by availability of DNA binding sites; DNA can therefore be considered similar to a pseudophase.

In the pseudophase approximation, the observed rate constant k_{obs} can be described by Equation 1,

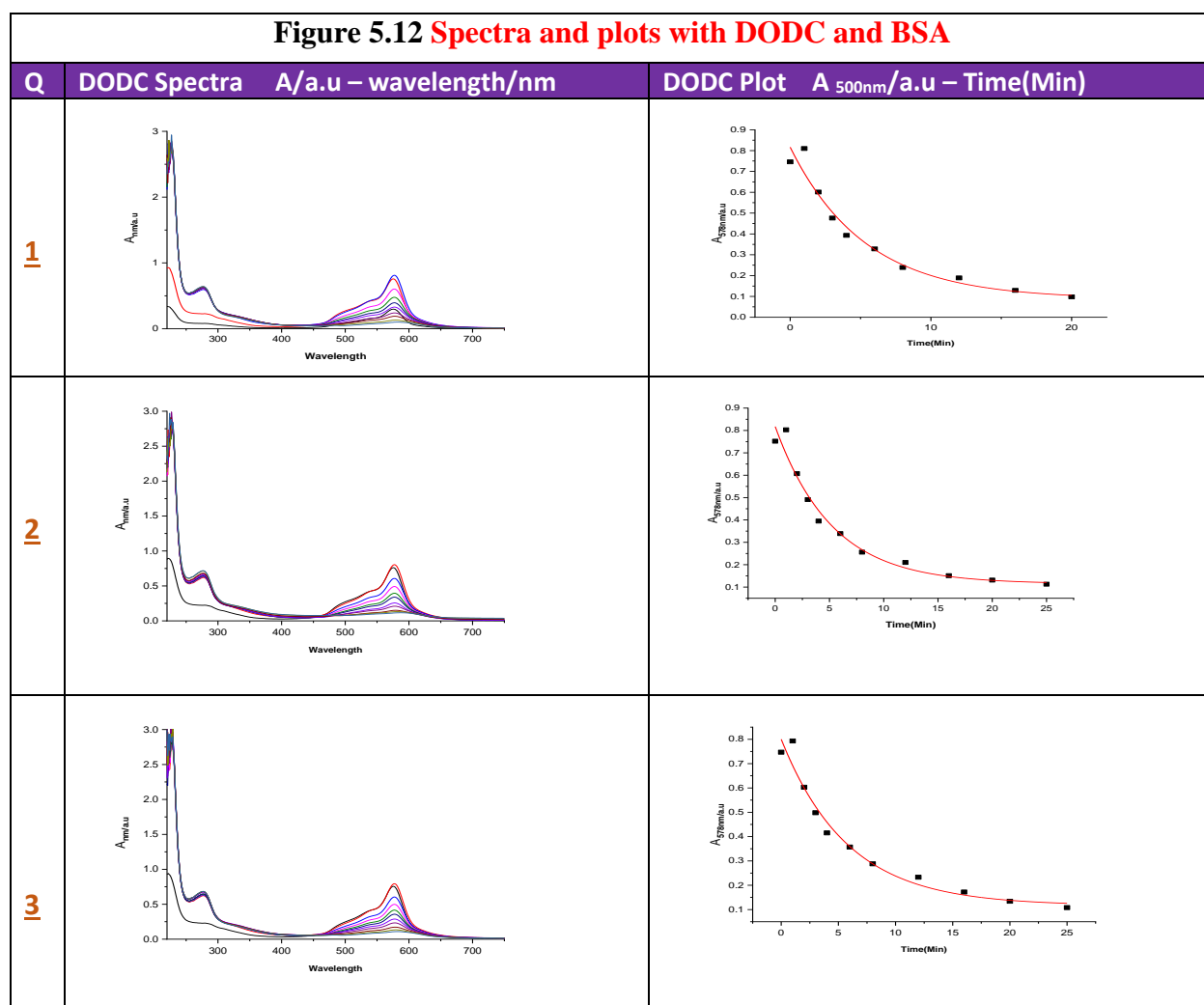
$$k_{\text{obs}} = \frac{k_w + k_{\text{DNA}} \times K_{\text{DNA}} \times \frac{[\text{DNA}]}{n}}{1 + K_{\text{DNA}} \times \frac{[\text{DNA}]}{n}}$$

where k_w is the rate constant in water or buffer, k_{DNA} is the rate constant when bound to DNA. K_{DNA} is the affinity constant for the DNA pseudophase and n is the number of basepairs that form a “unit of pseudophase”, in this case a binding site in the traditional sense.

Analysis of the data in Figure 5.16 in terms of this model yields k_w of $(0.296 \pm 0.094)\text{ min}^{-1}$, k_{DNA} of $(0.032 \pm 0.040)\text{ min}^{-1}$ and K_{DNA} of $(7 \times 10^4 \pm 8 \times 10^4)\text{ M}^{-1}$ for a binding site size restricted to 3 basepairs.

5.2.2b Fading of DODC in the presence of BSA.

We next studied the effect of addition of $20\ \mu\text{l}$ of a $1\ \text{mM}$ solution of BSA bovine serum albumin on fading of DODC (Figure 5.12).



Fitting of the absorbance of DODC as a function of time yielded the rate constants for the process (Table 7).

Table 7 Rate constants for fading of DODC in the presence of BSA	
original rate constants	original errors
0.18649	0.03982
0.19111	0.03241
0.17271	0.02954
Average k	Average error
0.183436667	0.033923333
standard deviation	% error margin
0.00781589	0.034
Experiment of 5-2-2019	

The rate constants in Table 9 for fading are slightly lower than in the reference buffer. Unfortunately, we only used a very low concentration of BSA in this experiment and didn't carry out further experiments. The role of serum albumin on fading is therefore not quantifiable from this experiment.

5.2.2c Fading of DODC in human serum.

We wanted to evaluate the effect of human serum on the fading of DODC. We irradiated a solution of DODC in human serum with stirring and at 25 °C (Figure 5.13).

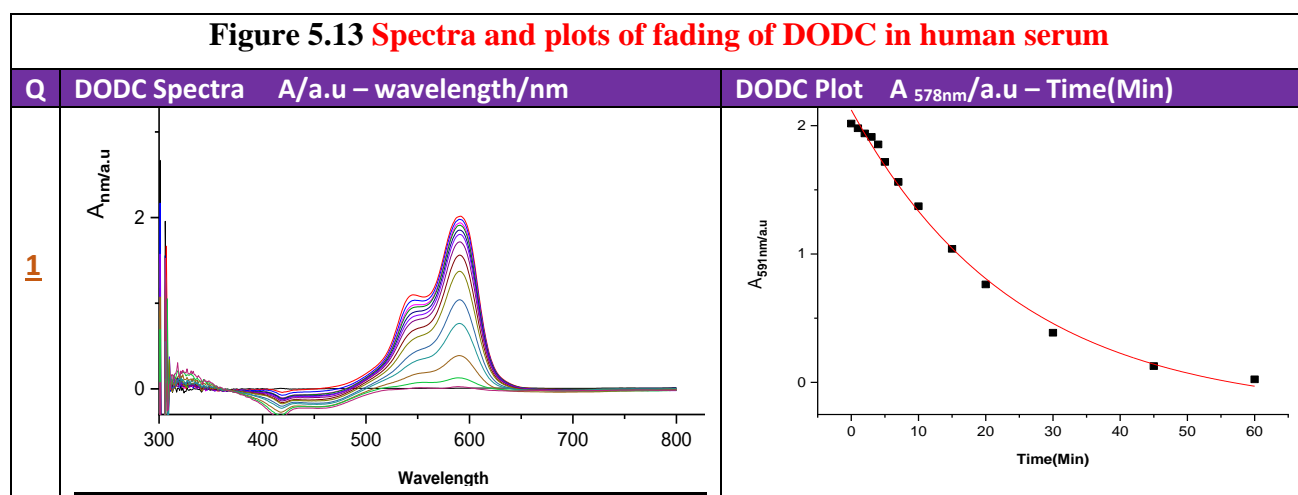


Table 8 showed the statistics of last experiments (5.18) that were made at 14-6-2019.

original rate constants	original errors	% error margin
0.04077 min⁻¹	0.00393	0.096394408

Table 8 illustrates that the *k* value decreases significantly for reaction in human serum.

5.2.2d Fading of DODC in calf serum.

We wanted to compare the effect of human serum with the effect of calf serum on the fading of DODC. We irradiated a solution of DODC in calf serum with stirring and at 25 °C (Figure 5.14).

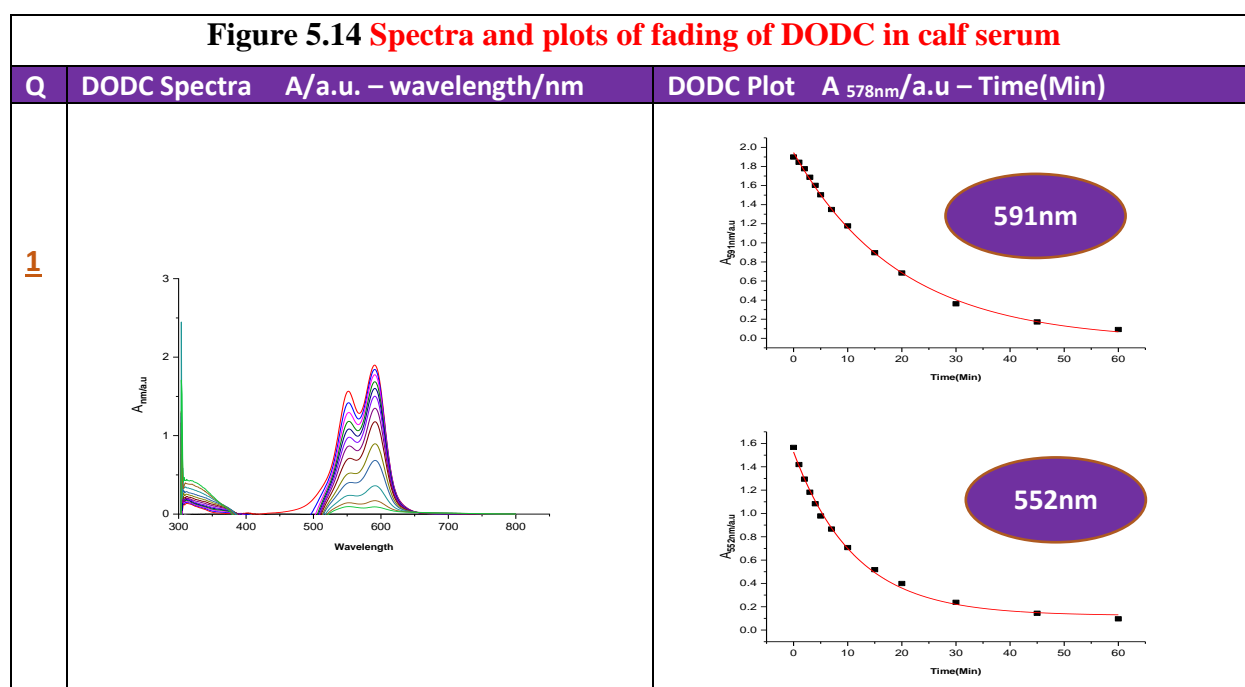
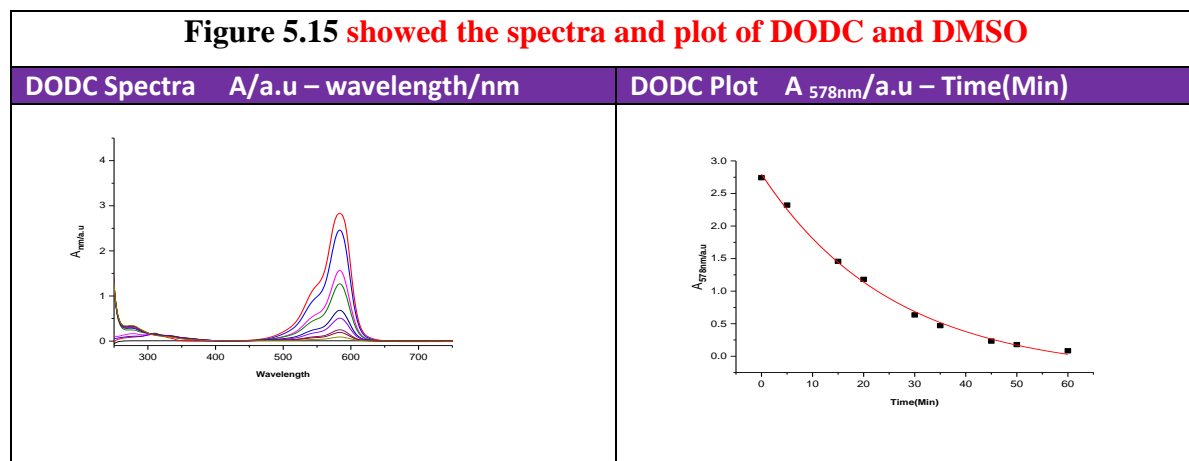


Table 9 Rate constants for fading of DODC in calf serum.			
	original rate constants	original errors	% error margin
591nm	0.05088 min⁻¹	0.00196	0.038522013
552nm	0.08908 min⁻¹	0.00422	0.047373148
15-6-2019			

Table 9 shows that the k value decreases in calf serum. Surprisingly, the rate constants for fading at different wavelengths are not the same within error margins.

5.2.2e Fading of DODC in the presence of DMSO.

We next wanted to explore reaction medium effects, as we did for TO (vide supra). We studied the fading of DODC in a 50:50 (vol:vol) mixture of deionised water and DMSO (Figure 5.15).



Fitting an exponential rate law to the absorbance at 578 nm as a function of time yielded the data in Table 10.

Table 10 illustrate Rate constant for fading of DODC in a 50:50 (v:v) mixture of water and DMSO		
original rate constant	original errors	% error margin
0.0389 min⁻¹	0.0029	0.074550129
30-5-2019		

Table 10 shows clearly that the presence of DMSO has a very significant effect on fading of DODC.

5.2.3 Effect of TO and DODC on integrity of DNA samples

We wanted to explore whether TO and DODC under fading conditions damage DNA. We therefore irradiated TO in the presence of a known plasmid and ran gel electrophoresis before and after irradiation (Figure 5.16).

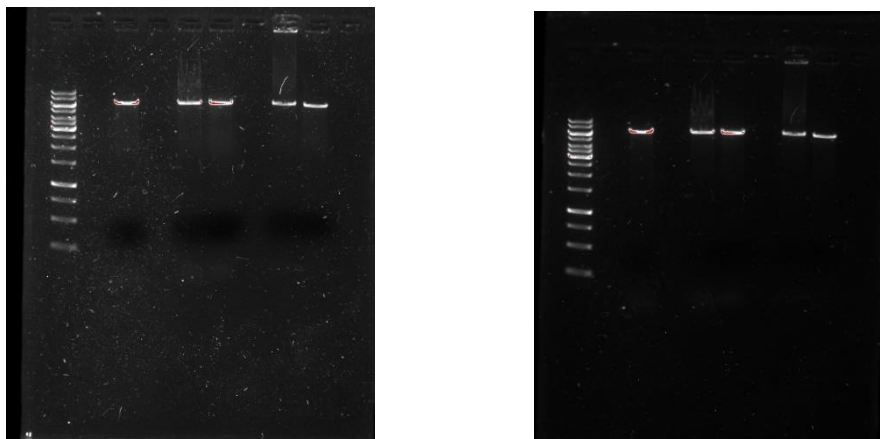


Figure 5.21 electrophoresis of plasmid DNA before and after irradiation in the presence of TO (and DODC).

Figure 5.16 shows that there was no degradation and separation of plasmid through its migration. This means that TO (and DODC, *vide infra*) do not affect the plasmid DNA during fading. This finding is in agreement with the dimer of thiazole orange, TOTO, causing single-strand cleavage less efficiently than the dimer of oxazole yellow (YOYO) with double-strand cleavage only happening upon continued single-strand cleavage based on the statistics of multiple single-strand breaks being close to each other.^(91,92) If strand cleavage is required, cyanine dyes can be substituted with heavy atoms to increase intersystem crossing to generate more efficient strand-breaking dyes generating singlet oxygen and hydroxyl radicals.⁽⁹³⁾

5.3 Experimental

Buffer preparation

All experiments were carried out in MOPS buffer. The reference buffer contained 25 mM MOPS, 50 mM NaCl and 1 mM EDTA, pH 7.0.

MOPS was purchased from Melford (CAS 1132-61-2), NaCl was purchased from Fisher Scientific (CAS 7647-14-5), EDTA was purchased from VWR (CAS 60-00-4). The required amounts were placed in distilled water and stirred at room temperature until the solids dissolved. A solution of sodium hydroxide (NaOH) was used for adjusting the pH to 7.0 and the buffer was made up to 2 litres in a volumetric flask.

The pH of aqueous solutions was determined using a Hanna microprocessor pH-meter equipped with a VWR 662-1382 glass electrode. Materials were weighed out on a Fisher brand 4-decimal balance. De-ionised water was produced using an ELGA water purifier for all solutions.

DNA preparation

Fish sperm DNA was purchased from Acros Organics (CAS 68938-01-2). The stock solution of fish sperm DNA was prepared by dissolving the DNA in buffer and then sonicating the suspension of FS-DNA for about 10 minutes to get a homogeneous solution. All DNA solutions were dialysed against buffer. The dialysis process for the DNA solution was carried out by taking the DNA solution and placing it into the dialysis tube of appropriate pore size (3.5 kDa MWCO). The dialysis tube was suspended for 24 hours inside a beaker that contains the MOPS buffer until the impurities were completely diffused out. The DNA concentrations were determined from the absorbance using the extinction coefficient of FSDNA of $12800 \text{ M}^{-1} \text{ cm}^{-1}$ in terms of base pair molarity as recorded using UV-visible spectroscopy at 260 nm.

Thiazole orange (TO)

We used a batch of TO which was 80-90% pure obtained from ChemCruz. We then used another new version of TO which was 98% pure from Insight Biotechnology (MCE MedChemExpress). This version was stored at 4°C, protect from light.

TO with fish DNA

We wanted to explore the effect of DNA on the fading of TO. We prepared a solution of thiazole orange (TO – 98% pure from Insight Biotechnology) in the reference buffer (pH = 7, 25 mM MOPS, 50 mM NaCl and 1 mM EDTA). The solution was sonicated and filtered through 13 mm 0.22 micron filter. A fish-sperm DNA (Acros Organics (CAS 68938-01-2) see details in experimental section) stock solution with a concentration of 23 mM was prepared and kept in a refrigerator. For individual experiments, the required volume of a stock solution of fish-sperm DNA was combined with the required volume of the stock solution of TO and made up to 2.5 mL using buffer. Spectra were recorded as a function of time, with the sample being irradiated using the last version of LED (see chapter 2) with magnetic stirring at 25 °C.

TO fading with bovine serum albumin (BSA)

We prepared our solution from a stock solution of thiazole orange (98%) in reference buffer (pH=7, 25 mM MOPS, 50 mM NaCl and 1 mM EDTA) which had been sonicated and filtered. We then prepared a bovine serum albumin solution (BSA - 1 mM). This solution was not filtered and kept it in refrigerator. In the experiments 20 ul of this BSA solution was added to the cuvette which was otherwise prepared as for the other experiments.

TO fading in human serum

Two approaches were followed for the preparation of thiazole orange solutions in human serum.

Thiazole orange was suspended in human serum and the mixture was sonicated and filtered.

We prepared a solution of thiazole orange in reference buffer (pH= 7, 25 mM MOPS, 50 mM NaCl and 1 mM EDTA) as before. We took 500 µl and added this to 2000 µl human serum (Sigma, H 3667-100ml) inside cuvette without further dilution or filtration.

All kinetic experiments used the last version of LED (see Chapter 2) with magnetic stirring.

TO with Calf serum

A stock solution of thiazole orange in the reference buffer at (pH=7, 25 mM MOPS, 50 mM NaCl and 1 mM EDTA) was prepared by sonication and filtration. A cuvette was filled with 2000 μ l calf serum from (Sigma-N4762-500ml) and 350 μ l of the thiazole orange stock solution. Irradiation was carried out using the last version of LED (see Chapter 2) with magnetic stirring.

TO in the presence of DMSO

We studied the fading of TO in a 50:50 (vol: vol) mixture of deionised water and DMSO. TO was suspended in deionised water, sonicated and filtered. We then took 50% of the total volume of solution required in the cuvette. An equal volume of DMSO was added directly to the cuvette with TO solution.

TO in the presence of ethanol

A solution of TO in reference buffer prepared as described before was mixed with the required amount of ethanol ranging from 500 μ l to 2500 μ l.

DODC with Fish DNA

We prepared a solution of DODC (3,3'-Diethyloxadicarbocyanine iodide, 96% dye from Alfa Aesar company) in the reference buffer (pH= 7, 25 mM MOPS, 50 mM NaCl and 1 mM EDTA) by sonication and filtration. This solution was stored in the dark. A 23 mM fish sperm DNA (Acros Organics, CAS 68938-01-2) solution was prepared and kept in the refrigerator until use. These solutions were mixed with buffer as required for the experiment. For irradiation, we used the last version of LED (see chapter 2) with magnetic stirring.

DODC fading in the presence of human serum.

We prepared our solution of DODC (3,3'-diethyloxadicarbocyanine iodide, 96% dye from Alfa Aesar company) in reference buffer (pH= 7, 25 mM MOPS, 50 mM NaCl and 1 mM EDTA), sonicated and filtered at 25 °C. We used 200 μ l to add to the serum. There was 2300 μ l human serum (Sigma, H 3667-100ml) inside cuvette without dilution. We used the last version of LED (see Chapter 2) for irradiation with magnetic stirring.

DODC fading in the presence of calf serum.

We prepared our solution of DODC (3,3'-diethyloxadicyanone iodide, 96% dye from Alfa Aesar company) in reference buffer (pH= 7, 25 mM MOPS, 50 mM NaCl and 1 mM EDTA), sonicated and filtered at 25 °C. We used 300 µl to add to the serum. There was 2200 µl calf serum from (Sigma-N4762-500ml) inside cuvette without dilution. We used the last version of LED (see Chapter 2) for irradiation with magnetic stirring.

DODC with BSA

We prepared our solution from a stock solution of DODC in reference buffer (pH=7, 25 mM MOPS, 50 mM NaCl and 1 mM EDTA) which had been sonicated and filtered. We then prepared a bovine serum albumin solution (BSA - 1 mM). This solution was not filtered and kept it in refrigerator. In the experiments 20 µl of this BSA solution and 100 µl of the DODC solution was added to the cuvette containing buffer.

DODC with DMSO

We studied the fading of DODC in a 50:50 (vol:vol) mixture of deionised water and DMSO. DODC dissolved with deionised water, sonicated and filtered at 25 °C. Equal volumes of this stock solution and of DMSO were then placed in the cuvette and the mixture exposed to irradiation.

Gel electrophoresis technique

A stock solution of a pET28a derived plasmid (40 µL, 6251 bp) was mixed with FastDigest Clear buffer (ThermoFisher, 4 µL, 10 x) and FastDigest XhoI (ThermoFisher, 1 µL) was added. The mixture was incubated at 37 degrees for 30 minutes, then split into aliquots (5 x 8 µL). One was kept aside as a control, and two of the others were mixed with each of DODC and TO. One of each of the two dye-containing Eppendorfs was covered in aluminium foil and the others were illuminated for 11 minutes, which was sufficient to decolourise the dye solutions. Each aliquot was then mixed with gel loading buffer (2 µL, containing glycerol and bromophenol blue) and loaded into a 1% agarose gel alongside a ladder (ThermoFisher GeneRuler 1 kbp) and subjected to

electrophoreses (100 mA, 45 minutes).

The gel was then imaged with a ChemiDoc MP using a variety of filters. Plasmid Sequence (see in Appendix).

Filters for solutions

PTFE syringe filters (Thermo Scientific Titan 3 and Target 2 syringe filters) with 0.22 μm and 0.45 μm membranes were used for filtration of aqueous solutions.

UV-visible spectroscopy

JASCO V630 and V650 UV-visible spectrophotometers as well as a SHIMADZU-UV-1800 were used to monitor reactions by recording absorption spectra after set amounts of time of irradiation using our irradiation device. Both JASCO machines were equipped with a Peltier thermostatted cell holder. Absorption spectra were recorded in 1.00 cm pathlength stoppered quartz cuvettes (Hellma) holding approximately 2.5 cm^3 liquid and 1.00 cm of headspace (i.e., under aerobic conditions), at 25°C unless otherwise stated.

Water Purification System

Water was purified using an ELGA PF3XXXXM1 Water Purification System Type I 2 Lpm.

Irradiation setup

The LED used was a 4th version of LED (MCWHD3 - 6500 K- LED on Metal-Core PCB) with fan and lenses to increase the intensity. The LED was powered using a T-Cube LEDD1B with a CAB-LEDD1 LED link cable. The irradiation setup was as a 3D-printed device as described in Chapter 2. We used an IKA Big Squid magnetic stirrer placed under our irradiation setup to magnetically stir the solutions during irradiation. For temperature control, the entire setup was placed in a Heidolph unimax 1010 shaker with incubator with temperature control.

Software

Graphs were constructed and kinetic data were analysed using OriginLab Origin 2020 software. Wavelengths for analysis were selected through UV-visible time resolved absorption spectra measurement for the reaction (for DODC this was typically 578 nm). All rate constants are expressed as observed first-order rate constants resulting from fitting a first-order rate law to the data at 578 nm using Origin 2020.

Molarity Calculator - GraphPad Prism

We used GraphPad Prism to calculate the molarity (Molar), volume (Milliliter) and formula weight (daltons - g/mol).

<https://www.graphpad.com/quickcalcs/molarityform.cfm>

5.4 References

1. Garoff, R. A., Litzinger, E. A., Connor, R. E., Fishman, I. & Armitage, B. A. Helical aggregation of cyanine dyes on DNA templates: Effect of dye structure on formation of homo- and heteroaggregates. *Langmuir* **18**, 6330–6337 (2002).
2. Timcheva, I. I. *et al.* Fluorescence spectral characteristics of novel asymmetric monomethine cyanine dyes in nucleic acid solutions. *FEBS Lett.* **405**, 141–144 (1997).
3. Karlsson, H. *et al.* Groove-binding unsymmetrical cyanine dyes for staining of DNA: syntheses and characterization of the DNA-binding. *Nucleic Acids Res.* **31**, 6227–6234 (2003).
4. West, W. & Pearce, S. The dimeric state of cyanine dyes. *J. Phys. Chem.* **69**, 1894–1903 (1965).
5. Zanotti, K. J. *Creating Genetically Encodable Biosensors Based on Fluorogenic Dyes and Proteins.* (2011).
6. Biver, T. *et al.* Influence of cyanine dye structure on self-aggregation and interaction with nucleic acids: a kinetic approach to TO and BO binding. *Arch. Biochem. Biophys.* **465**, 90–100 (2007).
7. Nygren, J., Svanvik, N. & Kubista, M. The interactions between the fluorescent dye thiazole orange and DNA. *Biopolym. Orig. Res. Biomol.* **46**, 39–51 (1998).
8. Silva, G. L., Ediz, V., Yaron, D. & Armitage, B. A. Experimental and computational investigation of unsymmetrical cyanine dyes: understanding torsionally responsive fluorogenic dyes. *J. Am. Chem. Soc.* **129**, 5710–5718 (2007).
9. Guo, Y. *et al.* Label-free DNA-based biosensors using structure-selective light-up dyes. *Analyst* **141**, 6481–6489 (2016).
10. Lakowicz, J. R. *Principles of fluorescence spectroscopy.* (Springer science & business media, 2013).
11. Patonay, G., Salon, J., Sowell, J. & Streckowski, L. Noncovalent labeling of biomolecules with red and near-infrared dyes. *Molecules* **9**, 40–49 (2004).

12. Sovenyhazy, K. M., Bordelon, J. A. & Petty, J. T. Spectroscopic studies of the multiple binding modes of a trimethine-bridged cyanine dye with DNA. *Nucleic Acids Res.* **31**, 2561–2569 (2003).
13. Rye, H. S. *et al.* Stable fluorescent complexes of double-stranded DNA with bis-intercalating asymmetric cyanine dyes: properties and applications. *Nucleic Acids Res.* **20**, 2803–2812 (1992).
14. Haugland, R. P. *Handbook of fluorescent probes and research chemicals.* (Molecular Probes, 1992).
15. Deligeorgiev, T. G. Molecular probes based on cyanine dyes for nucleic acid research. in *Near-Infrared Dyes for High Technology Applications* 125–139 (Springer, 1998).
16. Goodwin, P. M. *et al.* Rapid sizing of individual fluorescently stained DNA fragments by flow cytometry. *Nucleic Acids Res.* **21**, 803–806 (1993).
17. Gurrieri, S., Wells, K. S., Johnson, I. D. & Bustamante, C. Direct visualization of individual DNA molecules by fluorescence microscopy: Characterization of the factors affecting signal/background and optimization of imaging conditions using YOYO. *Anal. Biochem.* (1997) doi:10.1006/abio.1997.2102.
18. Clegg, R. M. *et al.* Fluorescence resonance energy transfer analysis of the structure of the four-way DNA junction. *Biochemistry* **31**, 4846–4856 (1992).
19. Mortensen, B. & Chui, M. Fluorescein-cyanine 5 as a fluorescence resonance energy transfer pair. (2002).
20. Biver, T., De Biasi, A., Secco, F., Venturini, M. & Yarmoluk, S. Cyanine dyes as intercalating agents: kinetic and thermodynamic studies on the DNA/Cyan40 and DNA/CCyan2 systems. *Biophys. J.* **89**, 374–383 (2005).
21. Armitage, B. A. Cyanine Dye–Nucleic Acid Interactions. 11–29 (2008) doi:10.1007/7081_2007_109.
22. Liu, L. *et al.* Differences in metabolite profile between blood plasma and serum. *Anal. Biochem.* **406**, 105–112 (2010).
23. Steele, W. H., Lawrence, J. R., Stuart, J. F. B. & McNeill, C. A. The

- protein binding of methotrexate in the serum of patients with neoplastic disease. *Cancer Chemother. Pharmacol.* **7**, 61–64 (1981).
24. Alsamamra, H., Kh, K., Darwish, S. & Abuteir, M. Analysis of Aspirin-Human serum albumin complex interaction using various spectroscopic methods. *J. Med. Physiol. Biophys.* **49**, 1–8 (2018).
 25. He, X. M. & Carter, D. C. Atomic structure and chemistry of human serum albumin. *Nature* **358**, 209–215 (1992).
 26. Chen, Z. *et al.* Spectroscopy study of the interaction between endocrine disruptor 4-OH-2,2',3,4'-BDE and human serum albumin. *Anal. Methods* **9**, 3338–3346 (2017).
 27. ZIMMERMAN, L. E. Serum albumin and globulin determinations. *Med. Techn. Bull.* **1**, 1–5 (1950).
 28. Sun, H. *et al.* A colorimetric and fluorometric dual-modal supramolecular chemosensor and its application for HSA detection. *Analyst* **139**, 581–584 (2013).
 29. Vaneková, Z. *et al.* Analysis of Binding Interactions of Ramipril and Quercetin on Human Serum Albumin: A Novel Method in Affinity Evaluation. *Molecules* **25**, 547 (2020).
 30. Sakhaei, N. Effect of urea on warfarin-human serum albumin complex: fluorescence study. (2011).
 31. Steinhardt, J., Krijn, J. & Leidy, J. G. Differences between bovine and human serum albumins. Binding isotherms, optical rotatory dispersion, viscosity, hydrogen ion titration, and fluorescence effects. *Biochemistry* **10**, 4005–4015 (1971).
 32. Peters Jr, T. Serum albumin. in *Advances in protein chemistry* vol. 37 161–245 (Elsevier, 1985).
 33. Zhao, X., Liu, R., Teng, Y. & Liu, X. The interaction between Ag⁺ and bovine serum albumin: a spectroscopic investigation. *Sci. Total Environ.* **409**, 892–897 (2011).
 34. Joshi, R., Jadhao, M., Kumar, H. & Ghosh, S. K. Is the Sudlow site I of human serum albumin more generous to adopt prospective anti-cancer bioorganic compound than that of bovine: A combined spectroscopic and docking simulation approach. *Bioorg. Chem.* **75**, 332–346 (2017).

35. Banerjee, M., Pal, U., Subudhhi, A., Chakrabarti, A. & Basu, S. Interaction of Merocyanine 540 with serum albumins: photophysical and binding studies. *J. Photochem. Photobiol. B Biol.* **108**, 23–33 (2012).
36. Hamann, F. M. *et al.* Controlled modulation of serum protein binding and biodistribution of asymmetric cyanine dyes by variation of the number of sulfonate groups. *Mol. Imaging* **10**, 258–269 (2011).
37. Larsen, M. T., Kuhlmann, M., Hvam, M. L. & Howard, K. A. Albumin-based drug delivery: harnessing nature to cure disease. *Mol. Cell. Ther.* **4**, 1–12 (2016).
38. Karimi, M. *et al.* Albumin nanostructures as advanced drug delivery systems. *Expert Opin. Drug Deliv.* **13**, 1609–1623 (2016).
39. Fasano, M. *et al.* The extraordinary ligand binding properties of human serum albumin. *IUBMB Life* **57**, 787–796 (2005).
40. Yang, F., Zhang, Y. & Liang, H. Interactive association of drugs binding to human serum albumin. *Int. J. Mol. Sci.* **15**, 3580–3595 (2014).
41. Roy, S. Review on interaction of serum albumin with drug molecules. *Res. Rev. J. Pharmacol. Toxicol. Stud.* **4**, 7–16 (2016).
42. Patterson, J. E. & Geller, D. M. Bovine microsomal albumin: amino terminal sequence of bovine proalbumin. *Biochem. Biophys. Res. Commun.* **74**, 1220–1226 (1977).
43. Alsamamra, H. iMedPub Journals Biophysical Interaction of Propylthiouracil with Human and Bovine Serum Albumins Materials and Samples Preparation. *iMedPub Journals* **8**, 1–7 (2019).
44. Guralchuk, G. Y. *et al.* Anomalous surfactant-induced enhancement of luminescence quantum yield of cyanine dye J-aggregates. *J. Phys. Chem. C* **112**, 14762–14768 (2008).
45. Losytskyy, M. Y. *et al.* Fluorescent properties of pentamethine cyanine dyes with cyclopentene and cyclohexene group in presence of biological molecules. *J. Fluoresc.* **15**, 849–857 (2005).
46. Behera, G. B., Behera, P. K. & Mishra, B. K. Cyanine dyes : Self aggregation and behaviour in surfactants: A review. *J. Surf. Sci. Technol.* **23**, 1–31 (2007).

47. Lewis, E. ScholarWorks @ Georgia State University Spectroscopic Studies of Cyanine Dyes and Serum Albumins for Bioanalytical Applications. (2015).
48. Saikiran, M., Sato, D., Pandey, S. S. & Kato, T. Photophysical investigations of squaraine and cyanine dyes and their interaction with bovine serum albumin. *J. Phys. Conf. Ser.* **704**, (2016).
49. Zhang, X. *et al.* Study on the interaction of a cyanine dye with human serum transferrin. *Luminescence* **30**, 1176–1183 (2015).
50. Petrov, N. K., Gulakov, M. N., Alfimov, M. V, Busse, G. & Techert, S. Solvation-shell effect on the cyanine-dye fluorescence in binary liquid mixtures. *Zeitschrift für Phys. Chemie* **221**, 537–547 (2007).
51. Chibisov, A. K., Slavnova, T. D. & Görner, H. J-aggregation of N-sulfobutyl oxacarbocyanine in binary mixtures of organic solvents. *Chem. Phys. Lett.* **498**, 63–66 (2010).
52. Harazi, S., Kapon, O., Sharoni, A. & Tischler, Y. R. Direct Formation of Carbocyanine J-Aggregates in Organic Solvent. *J. Phys. Chem. C* **123**, 19087–19093 (2019).
53. Pronkin, P. & Tatikolov, A. Isomerization and properties of isomers of carbocyanine dyes. *Sci* **1**, 5 (2019).
54. Kalra, A. P. *et al.* Behavior of α , β tubulin in DMSO-containing electrolytes. *Nanoscale Adv.* **1**, 3364–3371 (2019).
55. Von Berlepsch, H. *et al.* Supramolecular structures of J-aggregates of carbocyanine dyes in solution. *J. Phys. Chem. B* **104**, 5255–5262 (2000).
56. Shindy, H. A. Structure and solvent effects on the electronic transitions of some novel furo/pyrazole cyanine dyes. *Dye. Pigment.* **149**, 783–788 (2018).
57. Lee, L. G., Chen, C. & Chiu, L. A. Thiazole orange: a new dye for reticulocyte analysis. *Cytom. J. Int. Soc. Anal. Cytol.* **7**, 508–517 (1986).
58. Oomoto, I. *et al.* ECHO-liveFISH: in vivo RNA labeling reveals dynamic regulation of nuclear RNA foci in living tissues. *Nucleic Acids Res.* **43**, e126–e126 (2015).
59. Krichevsky, O. & Bonnet, G. Fluorescence correlation spectroscopy: The

- technique and its applications. *Reports Prog. Phys.* (2002)
doi:10.1088/0034-4885/65/2/203.
60. Moreira, B. G., You, Y., Behlke, M. A. & Owczarzy, R. Effects of fluorescent dyes, quenchers, and dangling ends on DNA duplex stability. *Biochem. Biophys. Res. Commun.* (2005) doi:10.1016/j.bbrc.2004.12.035.
 61. Pei, R., Rothman, J., Xie, Y. & Stojanovic, M. N. Light-up properties of complexes between thiazole orange-small molecule conjugates and aptamers. *Nucleic Acids Res.* **37**, e59–e59 (2009).
 62. Prodhomme, S. *et al.* A theoretical and experimental study of two thiazole orange derivatives with single- and double-stranded oligonucleotides, polydeoxyribonucleotides and DNA. *J. Photochem. Photobiol. B Biol.* **53**, 60–69 (1999).
 63. Boger, D. L. & Winston, C. T. Thiazole orange as the fluorescent intercalator in a high resolution fid assay for determining DNA binding affinity and sequence selectivity of small molecules. *Bioorg. Med. Chem.* **9**, 2511–2518 (2001).
 64. Kovalska, V. B., Losytsky, M. Y. & Yarmoluk, S. M. Luminescence spectroscopic studies of trimethinecyanines substituted in polymethine chain with nucleic acids and proteins. *Spectrochim. Acta - Part A Mol. Biomol. Spectrosc.* **60**, 129–136 (2004).
 65. Jarikote, D. V., Krebs, N., Tannert, S., Röder, B. & Seitz, O. Exploring base-pair-specific optical properties of the DNA stain thiazole orange. *Chem. - A Eur. J.* **13**, 300–310 (2007).
 66. Svanvik, N., Westman, G., Wang, D. & Kubista, M. Light-Up Probes: Thiazole Orange-Conjugated Peptide Nucleic Acid for Detection of Target Nucleic Acid in Homogeneous Solution. *Anal. Biochem.* **281**, 26–35 (2000).
 67. Pellestor, F. & Paulasova, P. The peptide nucleic acids (PNAs), powerful tools for molecular genetics and cytogenetics. *Eur. J. Hum. Genet.* **12**, 694–700 (2004).
 68. Liang, M. *et al.* A convenient thiazole orange fluorescence assay for the evaluation of DNA duplex hybridization stability. *Mol. Imaging Biol.* **11**, 439 (2009).

69. Bordelon, J. A., Feierabend, K. J., Siddiqui, S. A., Wright, L. L. & Petty, J. T. Viscometry and atomic force microscopy studies of the interactions of a dimeric cyanine dye with DNA. *J. Phys. Chem. B* **106**, 4838–4843 (2002).
70. Zipper, H., Brunner, H., Bernhagen, J. & Vitzthum, F. Investigations on DNA intercalation and surface binding by SYBR Green I, its structure determination and methodological implications. *Nucleic Acids Res.* **32**, e103–e103 (2004).
71. Nanjunda, R. & Wilson, W. D. Binding to the DNA Minor Groove by Heterocyclic Dications: From AT-Specific Monomers to GC Recognition with Dimers. *Curr. Protoc. nucleic acid Chem.* **51**, 8 (2012).
72. Fang, W.-J. *et al.* A DNA minor groove binder shows high effectiveness as a quencher for FRET probes. *Bioorg. Med. Chem. Lett.* **24**, 3956–3960 (2014).
73. Monchaud, D., Allain, C. & Teulade-Fichou, M.-P. Thiazole orange: a useful probe for fluorescence sensing of G-quadruplex–ligand interactions. *Nucleosides, Nucleotides, and Nucleic Acids* **26**, 1585–1588 (2007).
74. Tran, P. L. T., Largy, E., Hamon, F., Teulade-Fichou, M.-P. & Mergny, J.-L. Fluorescence intercalator displacement assay for screening G4 ligands towards a variety of G-quadruplex structures. *Biochimie* **93**, 1288–1296 (2011).
75. Murat, P., Singh, Y. & Defrancq, E. Methods for investigating G-quadruplex DNA/ligand interactions. *Chem. Soc. Rev.* **40**, 5293–5307 (2011).
76. Ida, J. *et al.* G-quadruplexes as an alternative recognition element in disease-related target sensing. *Molecules* **24**, 1079 (2019).
77. Cao, R., Venezia, C. F. & Armitage, B. A. Investigation of DNA binding modes for a symmetrical cyanine dye trication: effect of DNA sequence and structure. *J. Biomol. Struct. Dyn.* **18**, 844–857 (2001).
78. Almaqwashi, A. A., Paramanathan, T., Rouzina, I. & Williams, M. C. Mechanisms of small molecule–DNA interactions probed by single-molecule force spectroscopy. *Nucleic Acids Res.* **44**, 3971–3988 (2016).

79. Tao, M., Zhang, G., Pan, J. & Xiong, C. Deciphering the groove binding modes of tau-fluvalinate and flumethrin with calf thymus DNA. *Spectrochim. Acta Part A Mol. Biomol. Spectrosc.* **155**, 28–37 (2016).
80. Benveniste, A. L. *et al.* Fluorescent DNA nanotags: supramolecular fluorescent labels based on intercalating dye arrays assembled on nanostructured DNA templates. *J. Am. Chem. Soc.* **129**, 2025–2034 (2007).
81. Hannah, K. C. & Armitage, B. A. DNA-templated assembly of helical cyanine dye aggregates: a supramolecular chain polymerization. *Acc. Chem. Res.* **37**, 845–853 (2004).
82. Heikaus, C. C., Pandit, J. & Klevit, R. E. Cyclic nucleotide binding GAF domains from phosphodiesterases: structural and mechanistic insights. *Structure* **17**, 1551–1557 (2009).
83. Lu, L., Jones, R. M., McBranch, D. & Whitten, D. Surface-enhanced superquenching of cyanine dyes as J-aggregates on Laponite clay nanoparticles. *Langmuir* **18**, 7706–7713 (2002).
84. Paramasivan, S. & Bolton, P. H. Mix and measure fluorescence screening for selective quadruplex binders. *Nucleic Acids Res.* **36**, e106–e106 (2008).
85. Xiong, Y.-X., Huang, Z.-S. & Tan, J.-H. Targeting G-quadruplex nucleic acids with heterocyclic alkaloids and their derivatives. *Eur. J. Med. Chem.* **97**, 538–551 (2015).
86. Chen, Q., Kuntz, I. D. & Shafer, R. H. Spectroscopic recognition of guanine dimeric hairpin quadruplexes by a carbocyanine dye. *Proc. Natl. Acad. Sci.* **93**, 2635–2639 (1996).
87. Mullice, L. A., Laye, R. H., Harding, L. P., Buurma, N. J. & Pope, S. J. A. Rhenium complexes of chromophore-appended dipicolylamine ligands: syntheses, spectroscopic properties, DNA binding and X-ray crystal structure. *New J. Chem.* **32**, 2140–2149 (2008).
88. Yao, Y., Wang, Q., Hao, Y. & Tan, Z. An exonuclease I hydrolysis assay for evaluating G-quadruplex stabilization by small molecules. *Nucleic Acids Res.* **35**, e68 (2007).

89. Ma, D.-L. *et al.* Discovery of a natural product-like c-myc G-quadruplex DNA groove-binder by molecular docking. *PLoS One* **7**, e43278 (2012).
90. Buurma, N. J. Kinetic medium effects on organic reactions in aqueous colloidal solutions. *Adv. Phys. Org. Chem.* **43**, 1–37 (2009).
91. Gurrieri, S., Smith, S. B., Wells, K. S., Johnson, I. D. & Bustamante, C. Real-time imaging of the reorientation mechanisms of YOYO-labelled DNA molecules during 90 and 120 pulsed field gel electrophoresis. *Nucleic Acids Res.* **24**, 4759–4767 (1996).
92. Kanony, C., Åkerman, B. & Tuite, E. Photobleaching of asymmetric cyanines used for fluorescence imaging of single DNA molecules. *J. Am. Chem. Soc.* **123**, 7985–7995 (2001).
93. Mapp, C. T., Owens, E. A., Henary, M. & Grant, K. B. Oxidative cleavage of DNA by pentamethine carbocyanine dyes irradiated with long-wavelength visible light. *Bioorg. Med. Chem. Lett.* **24**, 214–219 (2014).

Chapter six

Preliminary forensics, overall conclusions, future work and outlook

Summary

This chapter presents the result from preliminary forensic experiments. We created a mock crime scene with limited materials (ethics limits the work we could carry out). We show that we can identify the location of DNA left on a piece of paper using our dyes.

We then present an overview of our results and conclusions and finish with future plans. These future plans include application of our idea in a real crime scene through a strong collaboration with the internal ministry and the police office or with the criminology department in a university. This step will allow us to understand the kinetics of fading under uncontrolled conditions as they occur in crime scenes.

6. Introduction

6.1 DNA Forensics in Criminal Cases

As discussed in Chapter 1, there are multiple systems for identifying trace evidence in crime scenes. The most famous is luminol, whose chemiluminescence is accountable for lightstick-like glow. Crime scene investigators use the response to detect blood traces at crime scenes. Luminol powder is mixed in a spray bottle with hydrogen peroxide (H_2O_2) and a hydroxide (e.g., KOH). Where blood can be discovered, the luminol solution is sprayed. The haemoglobin iron in the blood acts as a catalyst for the chemiluminescence response that causes luminol to shine. As a result, a blue glow is generated when the solution is sprayed in a location where there is blood to catalyse the reaction. Only a small amount of iron is required so the technique is very sensitive. The faint blue glow lasts about 30 seconds before it disappears, which is enough time to take pictures of the darkened crime scene and then the photos can be more carefully researched.

6.2 Preliminary studies of forensic applications – results and discussion

Our preliminary studies were restricted in scope to experiments for which we do not require ethical approval.

6.2.1 Visual changes in solution when adding DNA

In the previous Chapters, spectroscopic changes were followed using UV-visible spectroscopy but here we want to establish whether the changes are also visible to the naked eye.

In the first experiment, we combined the reference buffer buffer (1000 ul) TO dissolved in the same buffer (filtered and sonicated, 500 ul) and a stock solution of fish sperm DNA (1000 ul).

First of all, the presence of DNA changes the colour of the solution from orange to pink (Figure 1).



Figure 1 Thiazole orange with DNA under normal day light.*

The solutions were then exposed to normal day light of relatively low intensity (on a cloudy and rainy day). Fading of the colour happens within 50 min, which is slower than fading without DNA. This experiment shows that our approach provides potential naked eye detection of DNA using TO.

We carried out the analogous experiment with DODC using reference buffer (pH= 7, 25 mM MOPS, 50 mM NaCl and 1 mM EDTA) (1450ul) with DODC dissolved in same buffer (filtered and sonicated, 50 ul) and then adding 1000ul of a solution of fish sperm DNA. Exposure to normal day light of low intensity (cloudy and rainy) resulted in colour changes (Figure 2).

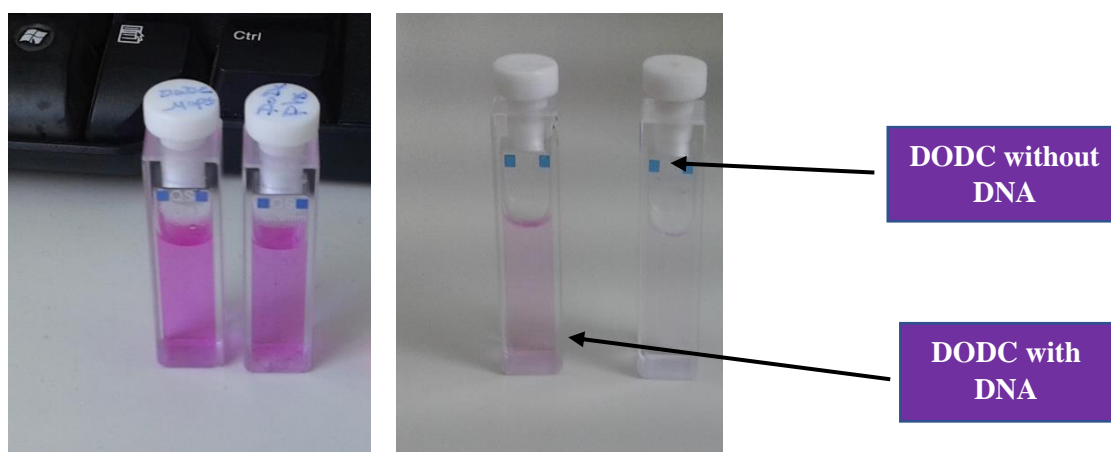


Figure 2 showed the DODC with DNA and without DNA

It is clear from Figure 5 that the DODC didn't change the colour after adding DNA. Different fading in the absence and presence of DNA did occur, however.

6.4.2 Visually detected colour changes when spraying or swabbing the dyes

We next wanted to explore whether DODC and TO can be used on surfaces rather than in solution. To explore this, we spread solutions containing DNA, BSA and simple buffers on paper and sprayed the paper with the dye solutions using a domestic sprayer (Figure 3).

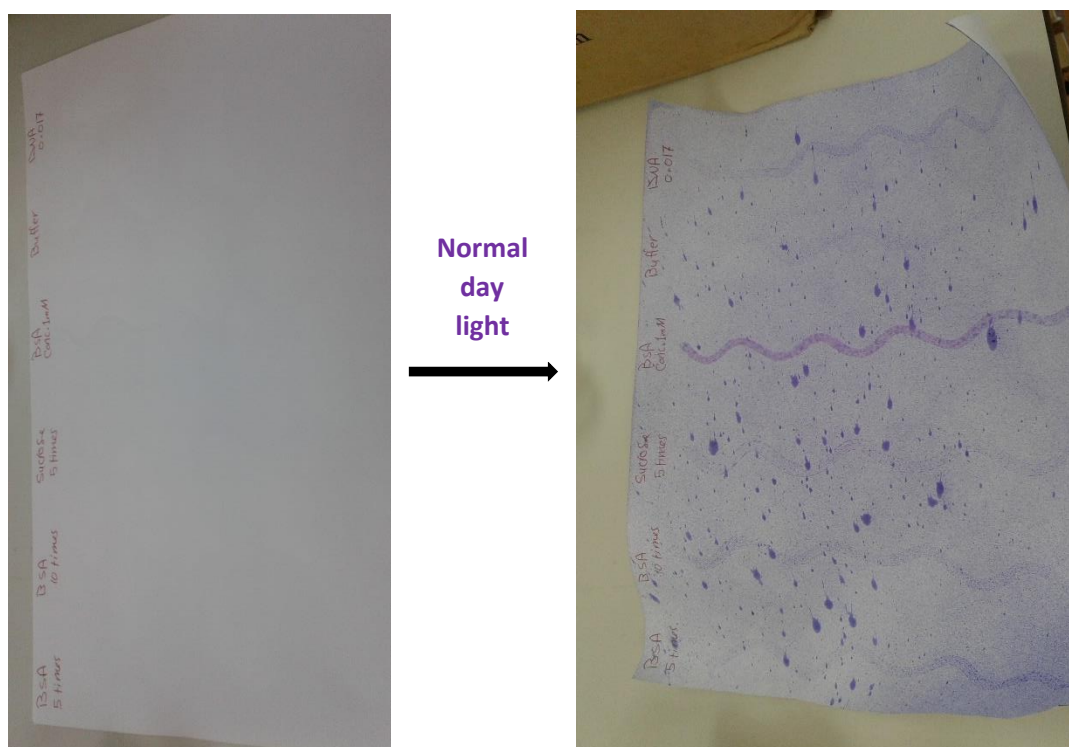


Figure 3 showed the DODC when sprayed it with N.B, BSA(1 mM), DNA(0.17mM) and sucrose under normal day light.

From Figure 3, it is clear that DODC interacts with all samples except buffer and keeps its colour for longer when interacting.

We similarly explored the sensitivity of using DODC solutions to visualise DNA on swabs (Figure 4).



Figure 4 A) illustrate when we took 3 swabs and immerse them on stock DNA, Buffer and BSA then sprayed by DODC. B) showed the effect of normal day light after 2 hours.

From Figure 4, it is clear that under ambient conditions (normal day light and oxygen) DODC fades but that the colour stay longer with DNA and BSA than with buffer.

Out of curiosity, we also used different types of quadruplex DNA and duplex DNA of known sequence with TO. Again, the samples were left out with normal day light (Figure 5).

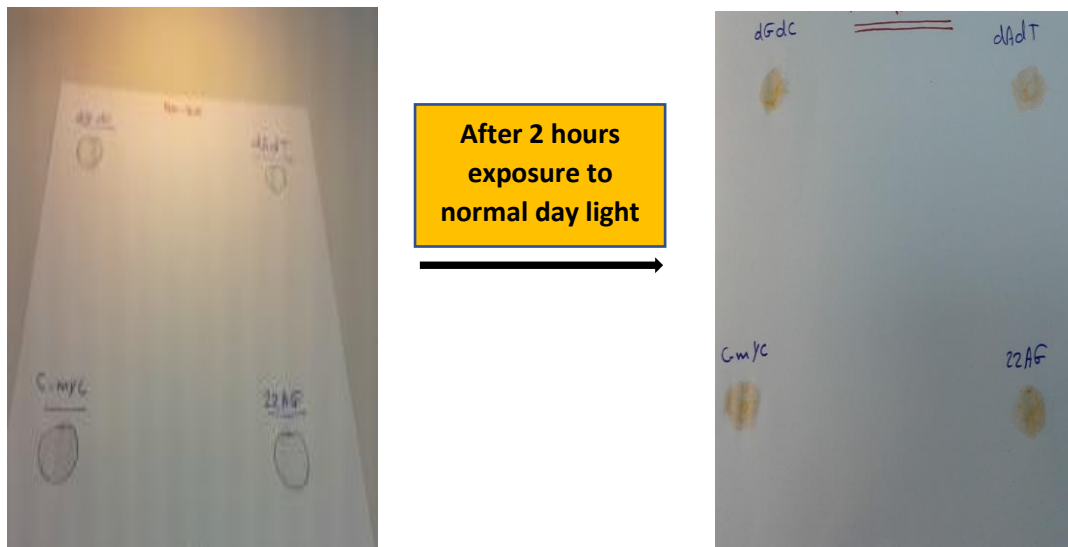


Figure 5 A) illustrate when we took 4 swabs and immerse them on stock quardplex then put it on white paper B) showed the effect of normal day light after 2 hours.

From Figure 5, it is clear that normal day light and oxygen effect fading of TO but the colour stays longer with the quadruplex and duplex DNA sequences than with buffer or water.

These preliminary experiments give us a simple proof that fading happens with DNA or even with other biological materials, but the time to lose the colour is different, although we couldn't specify it with these limited experiments. To further prove these experiments as a practical idea, it needs many experiments with fewer limitations.

6.3 Experimental

Buffers were prepared as in previous chapters. Spray bottles were from superdrug (Figure 6 A). TO and DODC were from Alfa Aesar and MCE MedChemExpress (Figure 6 B and 6 C).

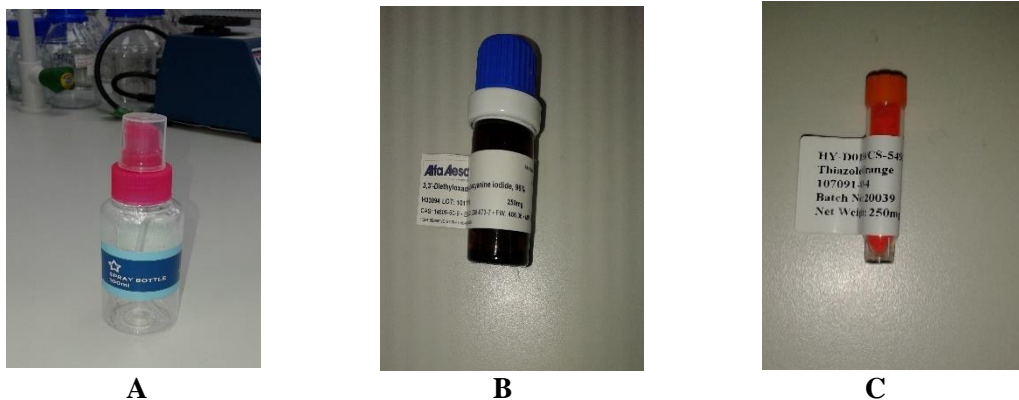


Figure 6 A) show the spray bottle that we used in our experiment. B) shows the 3,3'-Diethyloxadicarbocyanine iodide,96% dye from Alfa Aesar company. C) shows the thiazole orange dye from MCE MedChemExpress that we used.

Cotton buds and paper were typical products for domestic use. Experiments requiring spraying of a dye solution were carried out inside a fish tank which was placed inside a fumehood (Figure 7).

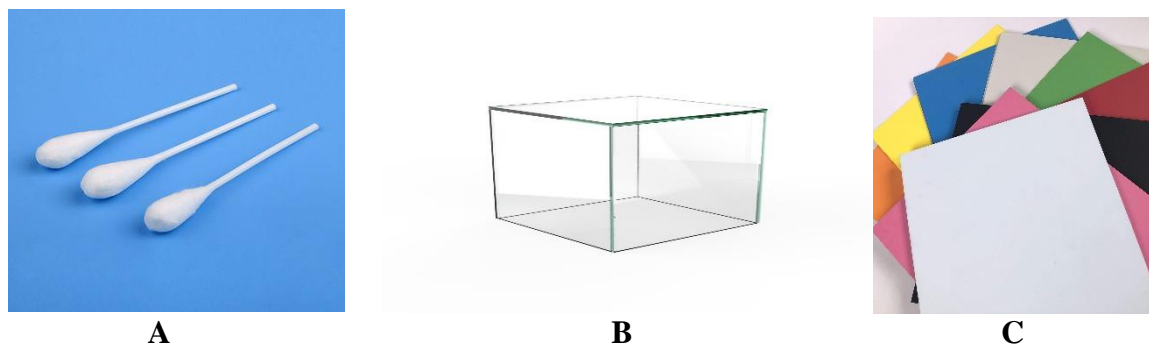


Figure 7 A) shows the ear cotton pads. B) shows the glass box that used inside the chemical hood in laboratory. C) shows the colour thick papers that used in our experiments.

General conclusions

The main objective of this project was to explore and advance photochemically active cyanine dyes for use as a detector to identify the biological samples in potential crime scenes.

The first purpose achieved was development of a LED device. Through 4 version of LED and its additives such as lens, fan, filters, magnetic stirrer and new LED, we produced a version of a LED device that give us reproducible results in our chemical reaction.

Through Chapters 3 and 4 the first-order light-driven fading reactions of TO and DODC in many solutions like buffers, deionised water, D₂O and others under different circumstances from temperature, pH, different molar of MOPs, different concentrations of NaCl, absence or presence of light, availability of O₂ or not, and others was studied. Both DODC and thiazole orange showed fading when exposed to light in presence of O₂.

The final chapter (5) presented the results of both dyes when reacting in the presence of biological samples under the exposure of LED light. The rate constants of fading in the presence of fish sperm DNA, human serum, calf serum and bovine serum albumin under the same circumstances are lower than in buffer alone. The results show that fading in the presence of biological materials may take a longer time than the absence of these materials. This practical result pushed us to experiment with both dyes in a mock crime scene (Chapter 6). The results that we extracted from forensic experiments which were made on papers and surfaces are promising but we need more experiments in real crime scenes.

Suggestions for future work

To confirm and enrich the results we need to repeat all the experiments under the last version LED and strict circumstances (mean not change anything from UV-spectrometer, incubator, shaker, buffers until the intensity of LED). we need to use laser flash photolysis laser and Ivan module device * to improve our studies and see the difference between excitation and emission of light on cyanine dye.

For the cyanine dye family, we need to develop experiments related to other DNA binders to enhance selectivity and sensitivity to DNA. Still, we also need to focus on our dyes (TO and DODC) to continue previous experiments with DNA, serum, and other biological samples.

For the forensic part, we should create a mock crime scene inside the lab, in order to spray the dyes on the scene with biological materials. Then we need to take pictures to analyse the reaction when the dye solutions have been sprayed and exposed to ambient light. We need to make a comparison with the old compounds which are used in crime scenes, like luminol.

* Ivan Lesnianski. (2019). The Construction of an inexpensive, compact and modular 3D-printed UV-vis spectrometer for the measurement of absorption, emission and kinetics of photo driven reactions. Cardiff university, chemistry school. Master thesis.

Other experiments with 2nd version LED and 1st version TO

- Sonicated and not filtered TO only with Distilled water (D.W)-24/7/2018+20/6/2018
- Sonicated and not filtered TO only with N.B at 35C-30/5/2018
- Sonicated and not filtered TO only half amount of ethanol-30/5/2018+16/3/2018
- Sonicated and not filtered TO only with 500 ul ethanol -20/3/2018+16/3/2018
- Sonicated and not filtered TO only with ethanol 1000uL-12/6/2018
- Sonicated and not filtered TO only with absolute ethanol-30/5/2018
- Sonicated and not filtered TO only with DMSO+D2O-13/6/2018
- Sonicated and filtered TO only with N.B at 25C put 24hours in dark then start-10-18/5/2018
- Sonicated and not filtered TO only with N.B and filters-18,17/4/2018
- Sonicated and not filtered TO only with phosphate buffer-29/4/2018+27/4/2018
- Sonicated and not filtered TO only with normal buffer /NaCl 200mM-29/4/2018
- Sonicated and filtered TO only with N.B at 45C-29/7/2018
- Not Sonicated and filtered TO only with N.B at 25C/ without oxygen-28/2/2018-9/3/2018
- Not Sonicated and filtered TO only with N.B at 35C and 25C/50,100mM MOPS-22/3/2018
- Sonicated and not filtered TO only with N.B in glass cuvette-30/5/2018

Other experiments with 3rd version LED and 2nd version TO

- Thiazole orange TO 90% sonicated and filtered with normal buffer pH=7 without 24 hours overnight at 25C. 19-10-2018
- Thiazole orange TO 90% sonicated and filtered with D.W.and DNA (17.929uM) at 25C. 27-10-2018 purified TO with D.W.and DNA
- Thiazole orange TO 90% sonicated and filtered with Tap water and DNA (17.929uM) at 25C. 1-11-2018 TO with tap water and DNA
- Thiazole orange TO 90% sonicated only with N.B (pH=7, 25mM MOPs, 50mM NaCl and 1mM EDTA) and DNA at 25C. 24-9-2017 sonicated TO with and without DNA
- Thiazole orange TO 90% sonicated and filtered with Tap. Water at 25C.20-10-2018

Other experiments with 3rd version LED and 3rd version TO

- Thiazole orange 98% sonicated and filtered with Normal buffer pH=10.80 (25mM MOPs, 50mM NaCl and 1mM EDTA)- N.B-eman 3-2-2019
- Thiazole orange 98% sonicated and filtered with Normal buffer pH=4.30 (25mM MOPs, 50mM NaCl and 1mM EDTA)- N.B-eman 4-2-2019
- Thiazole orange 98% sonicated and filtered with Normal buffer (D2O instead D.W) (25mM MOPs, 50mM NaCl and 1mM EDTA)- 9-11-2018 D₂O instead buffer in N.B
- Thiazole orange 98% sonicated and filtered with Normal buffer pH=7(NaCl 100mM, 25mM MOPs and 1mM EDTA) at 25°C. 11-11-2018 with N.B (100mM NaCl)
- Thiazole orange 98% sonicated and filtered with Normal buffer pH=7(NaCl 200mM, 25mM MOPs and 1mM EDTA) at 25°C. 12-11-2018 with N.B(200 mM) NaCl
- Thiazole orange 98% sonicated and filtered with Normal buffer pH=7 (25mM MOPs, 50mM NaCl and 1mM EDTA) and BSA (1mM)- N.B-eman 6-2-2019
- Thiazole orange 98% sonicated and filtered with Normal buffer pH=7 (25mM MOPs, 50mM NaCl and 1mM EDTA) at 25°C. 2-3-2019
- Thiazole orange 98% sonicated and filtered with Normal buffer pH=7 (25mM MOPs, 50mM NaCl and 1mM EDTA) at 35 °C. 28-2-2019
- Thiazole orange 98% sonicated and filtered with Normal buffer pH=7 (25mM MOPs, 50mM NaCl and 1mM EDTA) at 45 °C. 27-2-2019

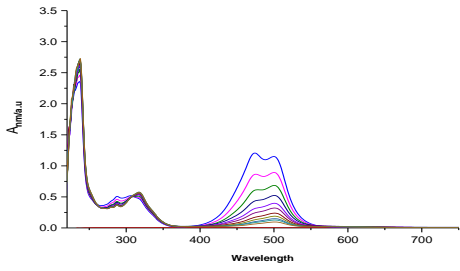
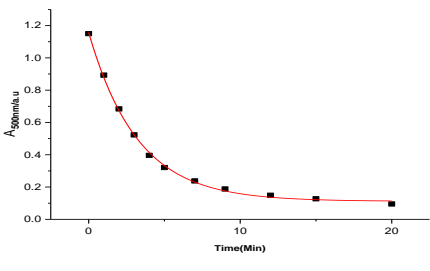
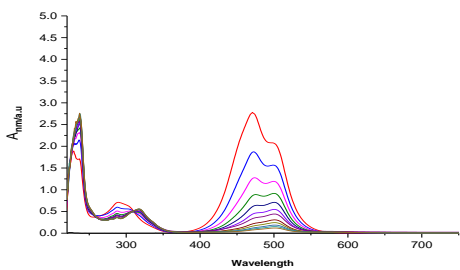
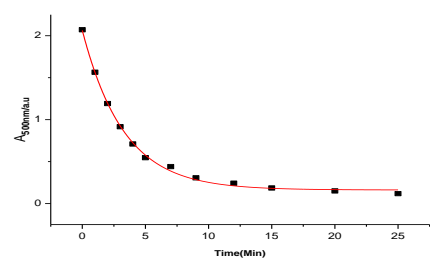
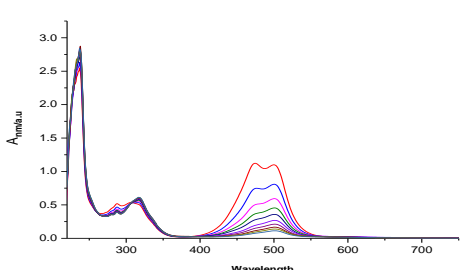
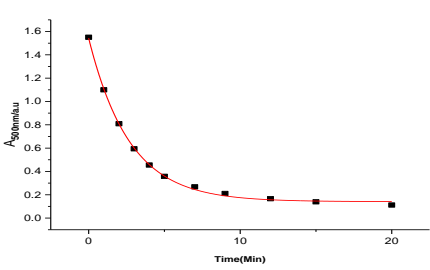
Other experiments with 4th version LED before setting

- 16-3-2019 D2O instead D.W.in N.B with TO 98%.
- 17-3-2019 D.W with TO 98% (65-75% LED intensity)
- 17-3-2019 D.W with TO 98% (55-45% LED intensity)
- 17-3-2019 TO with D.W (less 100% LED-75-85%)
(Controlled by power supplier)

All other experiments made by 4th version LED after setting which listed in other chapters and the results were reducible for calculating and data.

Appendix

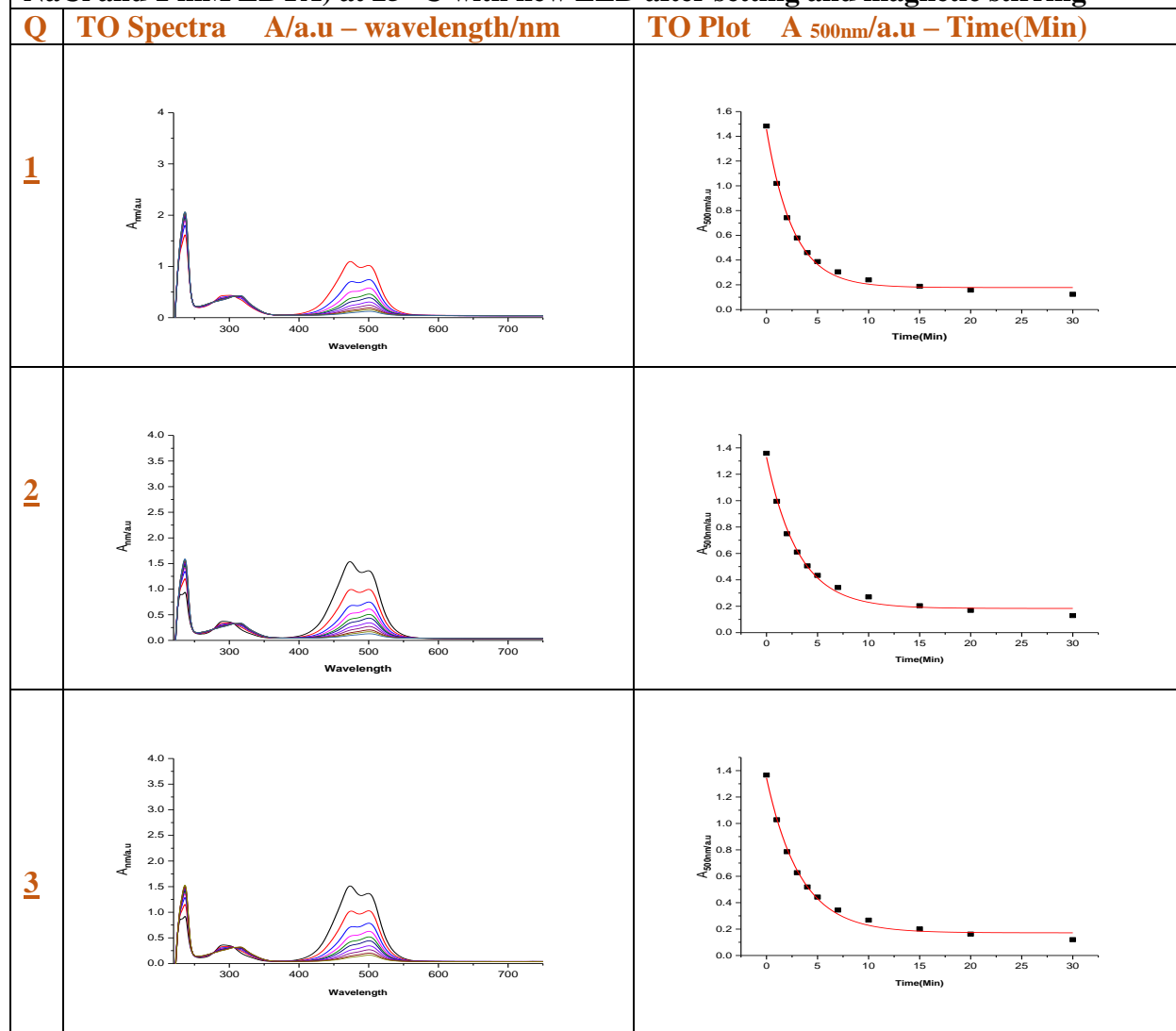
Thiazole orange 98% sonicated and filtered in buffer pH=10.80 (25 mM MOPS, 50 mM NaCl and 1 mM EDTA) at 25 °C with new LED after setting and magnetic stirring

Q	TO Spectra A/a.u – wavelength/nm	TO Plot A _{500nm} /a.u – Time(Min)
1		
2		
3		

File name: 9-4-2019/ pH=10.80

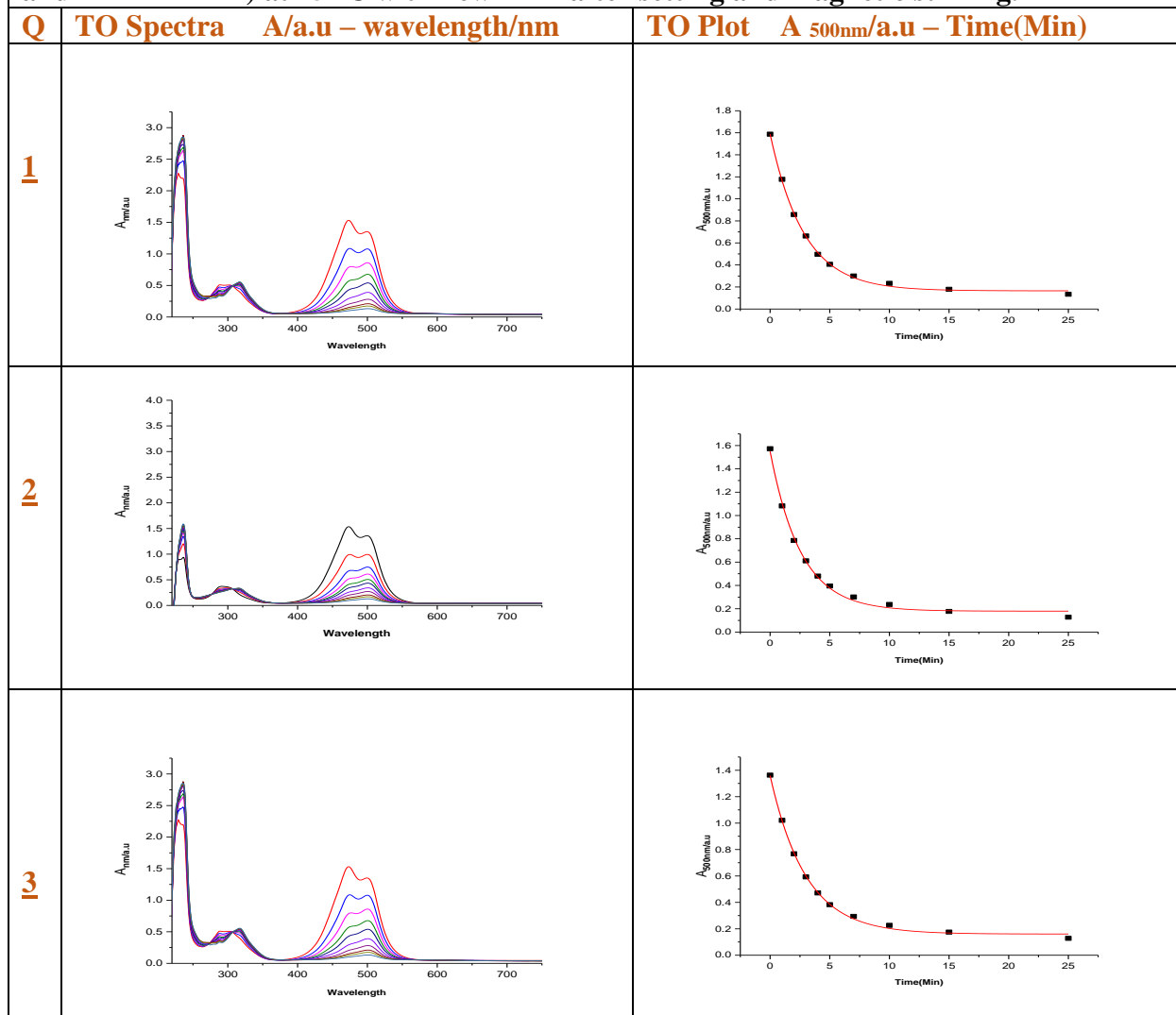
	original rate constants	original errors
1	0.31036 min⁻¹	0.00927
2	0.304429699 min⁻¹	0.009852545
3	0.371036872 min⁻¹	0.009443899
	Average k	Average error
	0.328608857	0.009522148
	standard deviation	Average error %
	0.030098665 min⁻¹	0.028977149

Thiazole orange 98% sonicated and filtered in buffer pH=4.30 (25 mM MOPS, 50 mM NaCl and 1 mM EDTA) at 25 °C with new LED after setting and magnetic stirring



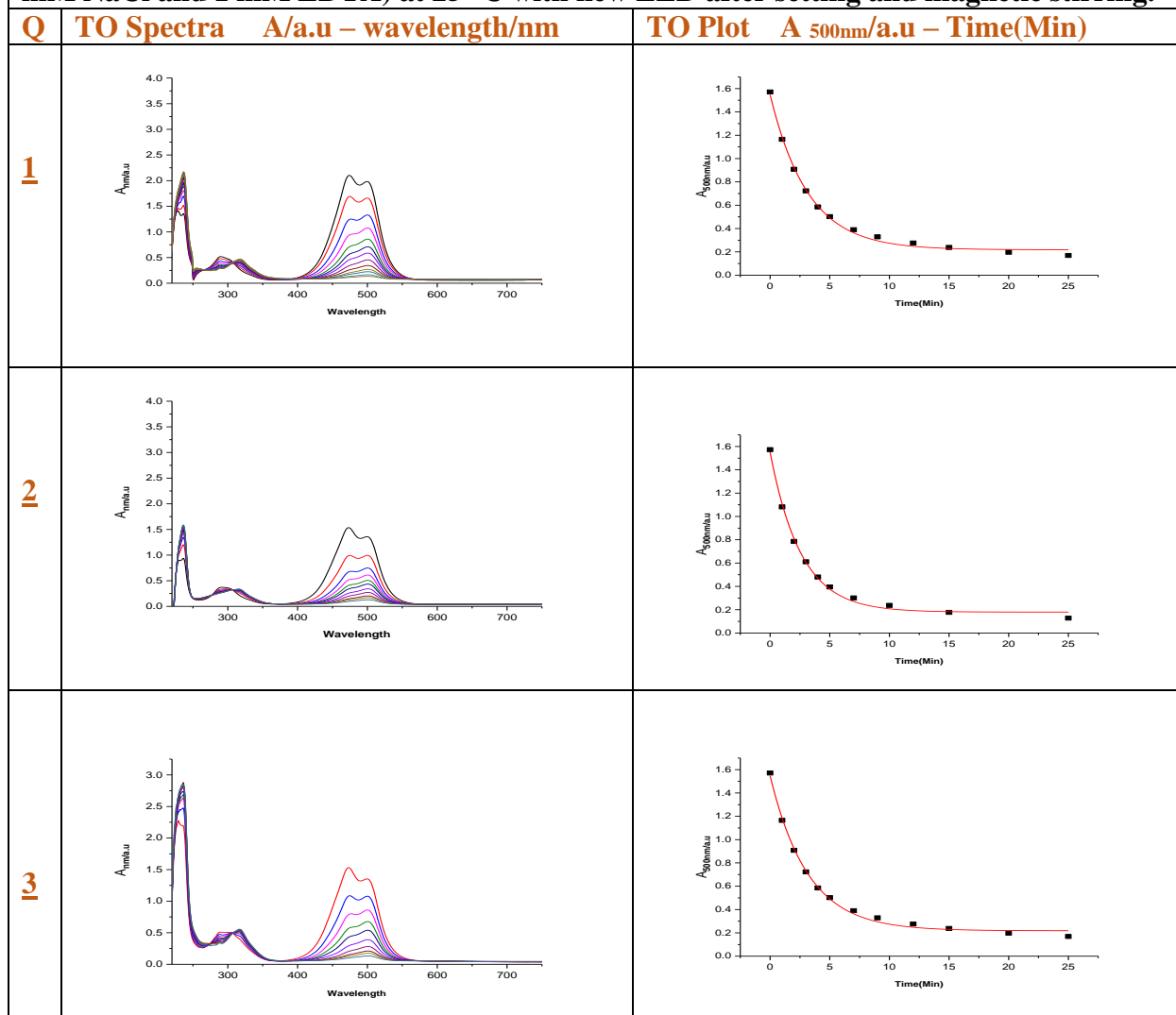
File name: <u>17-4-2019/</u> pH=4.30		
	original rate constants	original errors
1	0.38436 min ⁻¹	0.02153
2	0.32028 min ⁻¹	0.02042
3	0.30266 min ⁻¹	0.01652
	Average k	Average error
	0.335766667	0.01949
	standard deviation	Average error %
	0.035105556 min ⁻¹	0.058046262

Thiazole orange 98% sonicated and filtered in buffer pH=7 (50 mM MOPS, 50 mM NaCl and 1 mM EDTA) at 25 °C with new LED after setting and magnetic stirring.



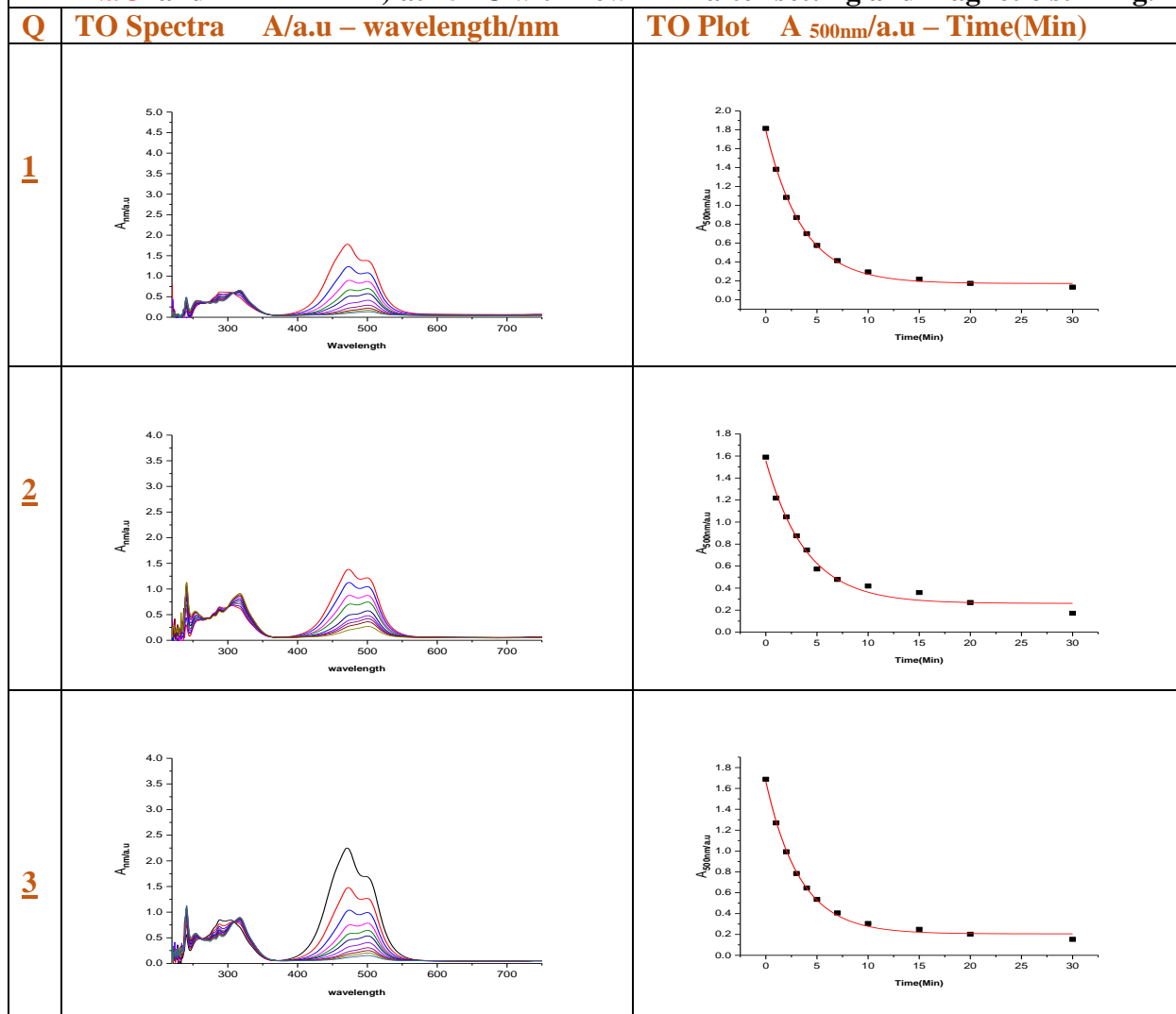
<u>2-5-2019/ (50 mM MOPS)</u>		
	original rate constants	original errors
1	0.35256 min⁻¹	0.01026
2	0.38711 min⁻¹	0.01963
3	0.33411 min⁻¹	0.01088
	Average k	Average error
	0.357926667	0.01359
	standard deviation	% error margin
	0.021967413 min⁻¹	0.037968671

Thiazole orange 98% sonicated and filtered in Normal buffer pH=7 (100 mM MOPS, 50 mM NaCl and 1 mM EDTA) at 25 °C with new LED after setting and magnetic stirring.



2-5-2019/100 mM MOPS		
	original rate constants	original errors
1	0.34686 min⁻¹	0.01656
2	0.34954 min⁻¹	0.01974
3	0.31282 min⁻¹	0.00794
	Average k	Average error
	0.336406667	0.014746667
	standard deviation	% error margin
	0.01671414 min⁻¹	0.043835834

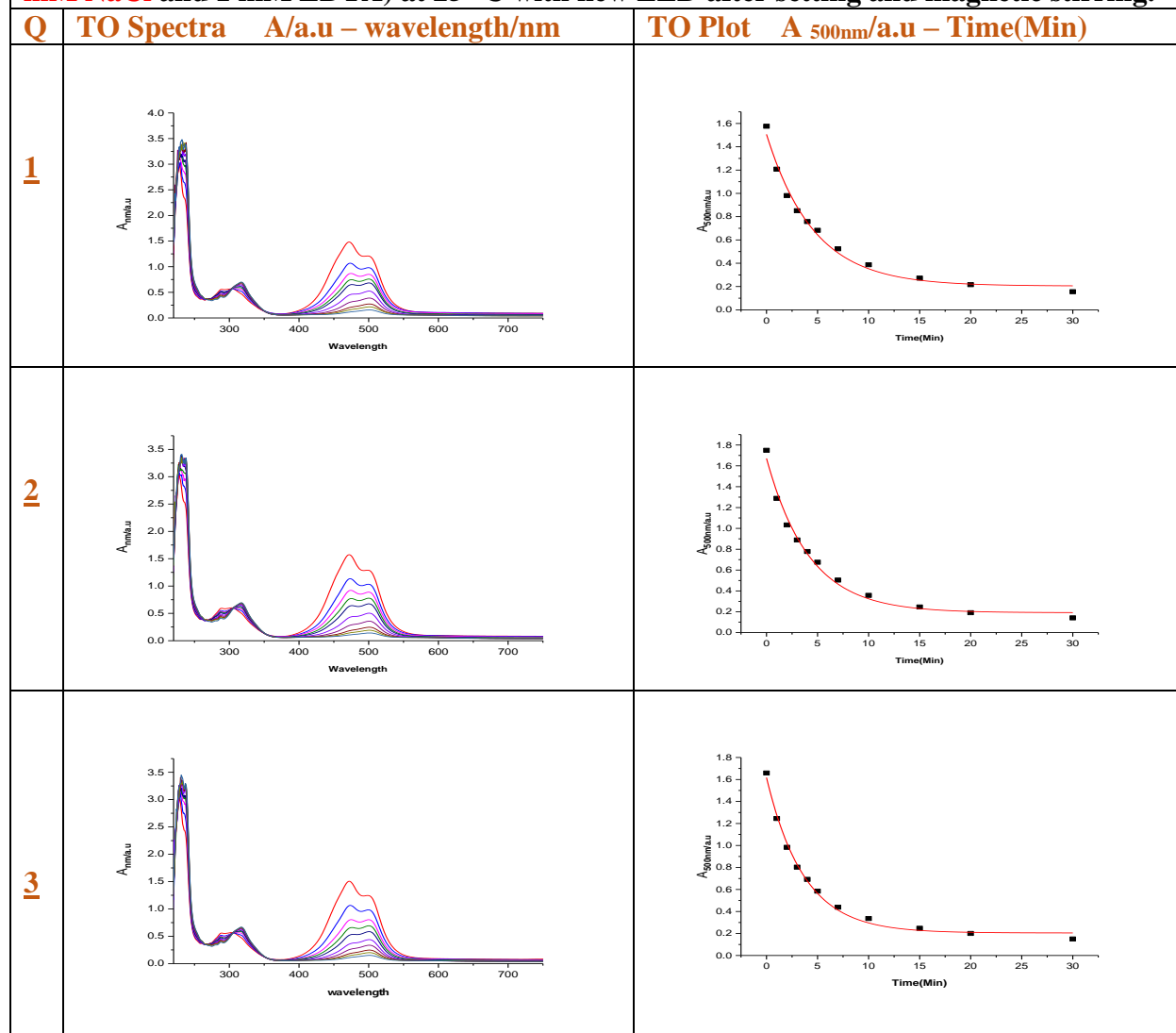
Thiazole orange 98% sonicated and filtered in Normal buffer pH=7 (25 mM MOPS, 100 mM NaCl and 1 mM EDTA) at 25 °C with new LED after setting and magnetic stirring.



File : 7-5-2019/ 100 mM NaCl

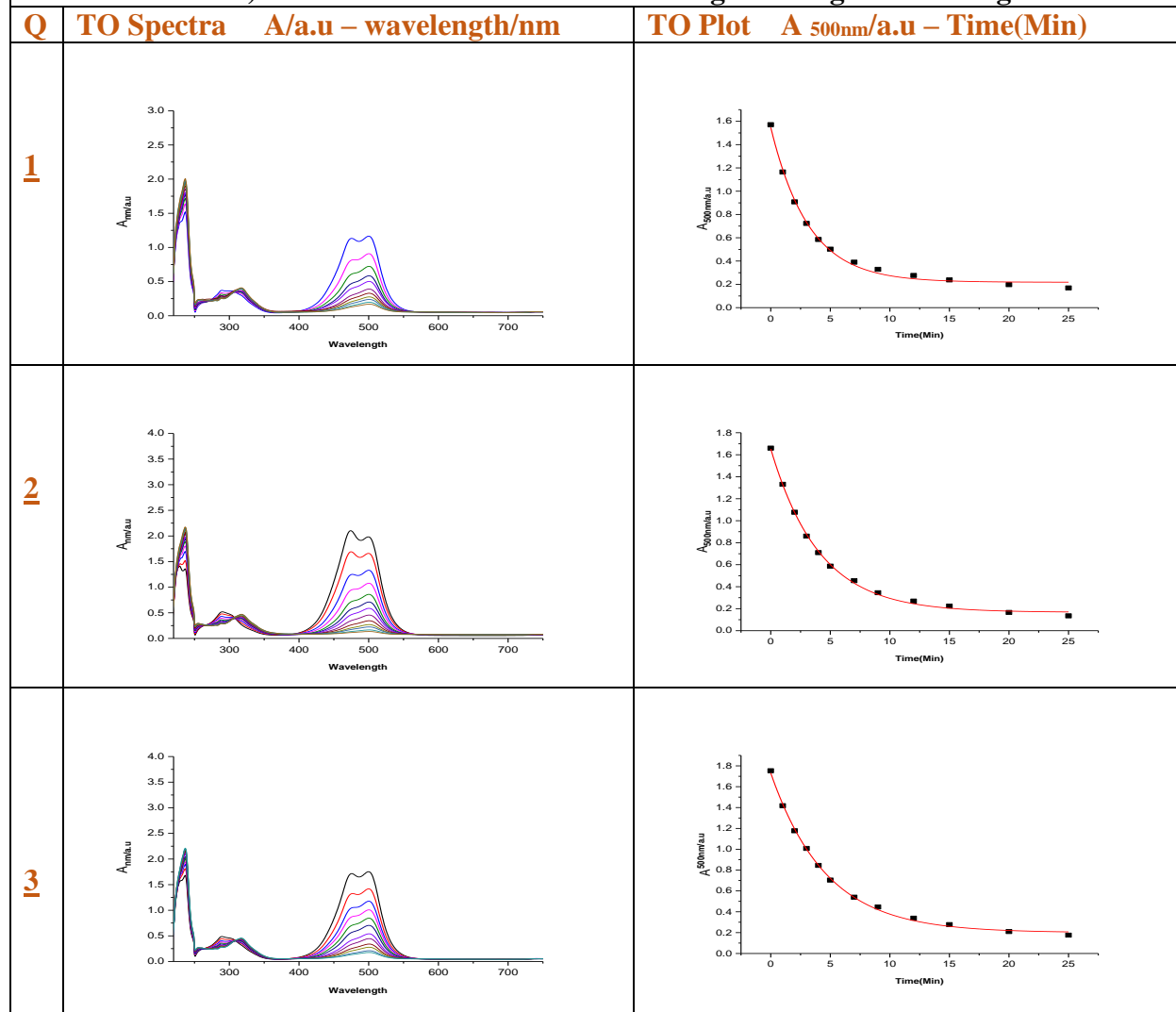
	original rate constants	original errors
1	0.28015 min⁻¹	0.00787
2	0.25439 min⁻¹	0.02241
3	0.30121 min⁻¹	0.01193
	Average k	Average error
	0.278583333	0.01407
	standard deviation	Average error %
	0.01914626 min⁻¹	0.05050534

Thiazole orange 98% sonicated and filtered in Normal buffer pH=7 (25 mM MOPS, 200 mM NaCl and 1 mM EDTA) at 25 °C with new LED after setting and magnetic stirring.



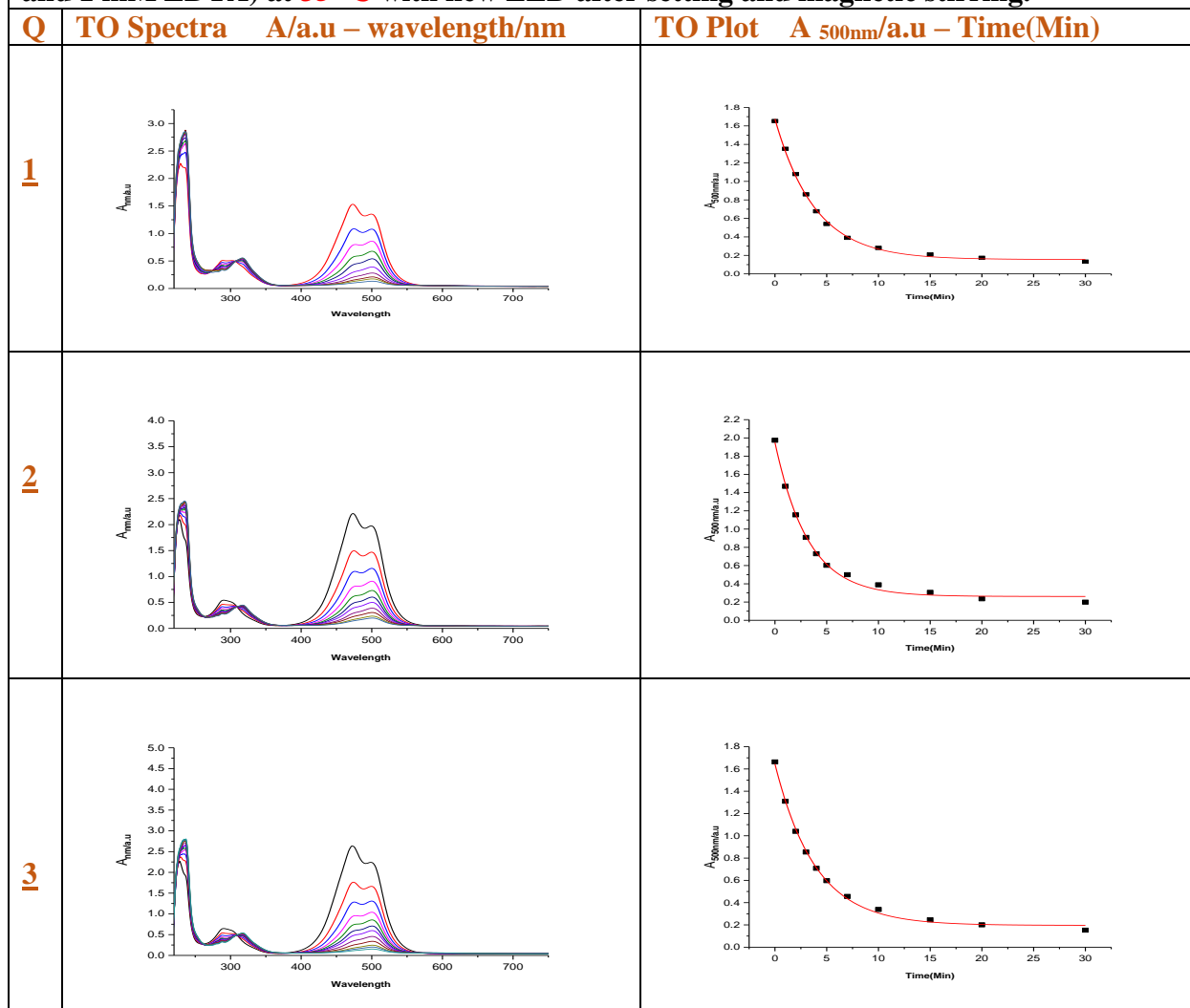
File: <u>16-4-2019/ 200 mM NaCl</u>		
	original rate constants	original errors
1	0.217029425 min⁻¹	0.018134172
2	0.24063 min⁻¹	0.01929
3	0.273629484 min⁻¹	0.015576932
	Average k	Average error
	0.24376297	0.017667035
	standard deviation	Average error %
	0.023212831 min⁻¹	0.072476286

Thiazole orange 98% sonicated and filtered in buffer pH=7 (25 mM MOPS, 50 mM NaCl and 1 mM EDTA) at 45 °C with new LED after setting and magnetic stirring.

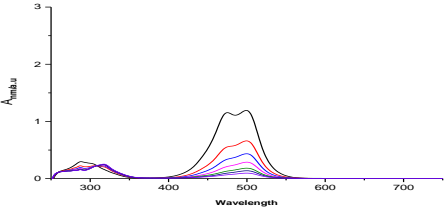
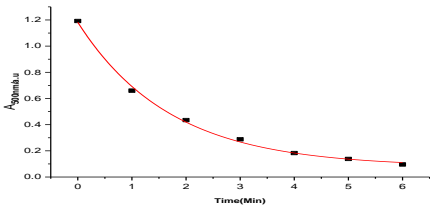
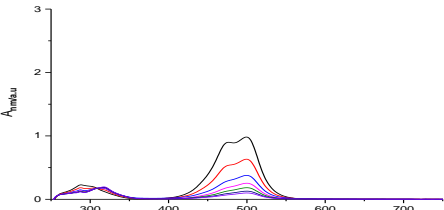
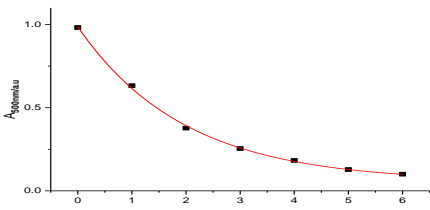
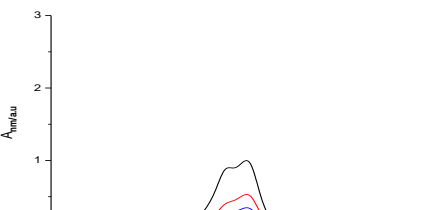
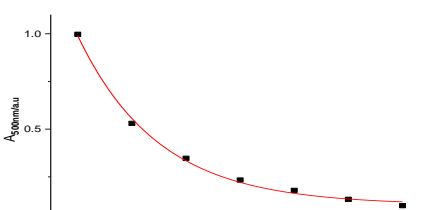


File name: 10-4-2019/ 45 °C		
	original rate constants	original errors
1	0.3159 min⁻¹	0.01409
2	0.245997101 min⁻¹	0.007403642
3	0.215457052 min⁻¹	0.006639721
	Average k	Average error
	0.259118051	0.009377787
	standard deviation	Average error %
	0.042042169 min⁻¹	0.036191178

Thiazole orange 98% sonicated and filtered in buffer pH=7 (25 mM MOPS, 50 mM NaCl and 1 mM EDTA) at 35 °C with new LED after setting and magnetic stirring.

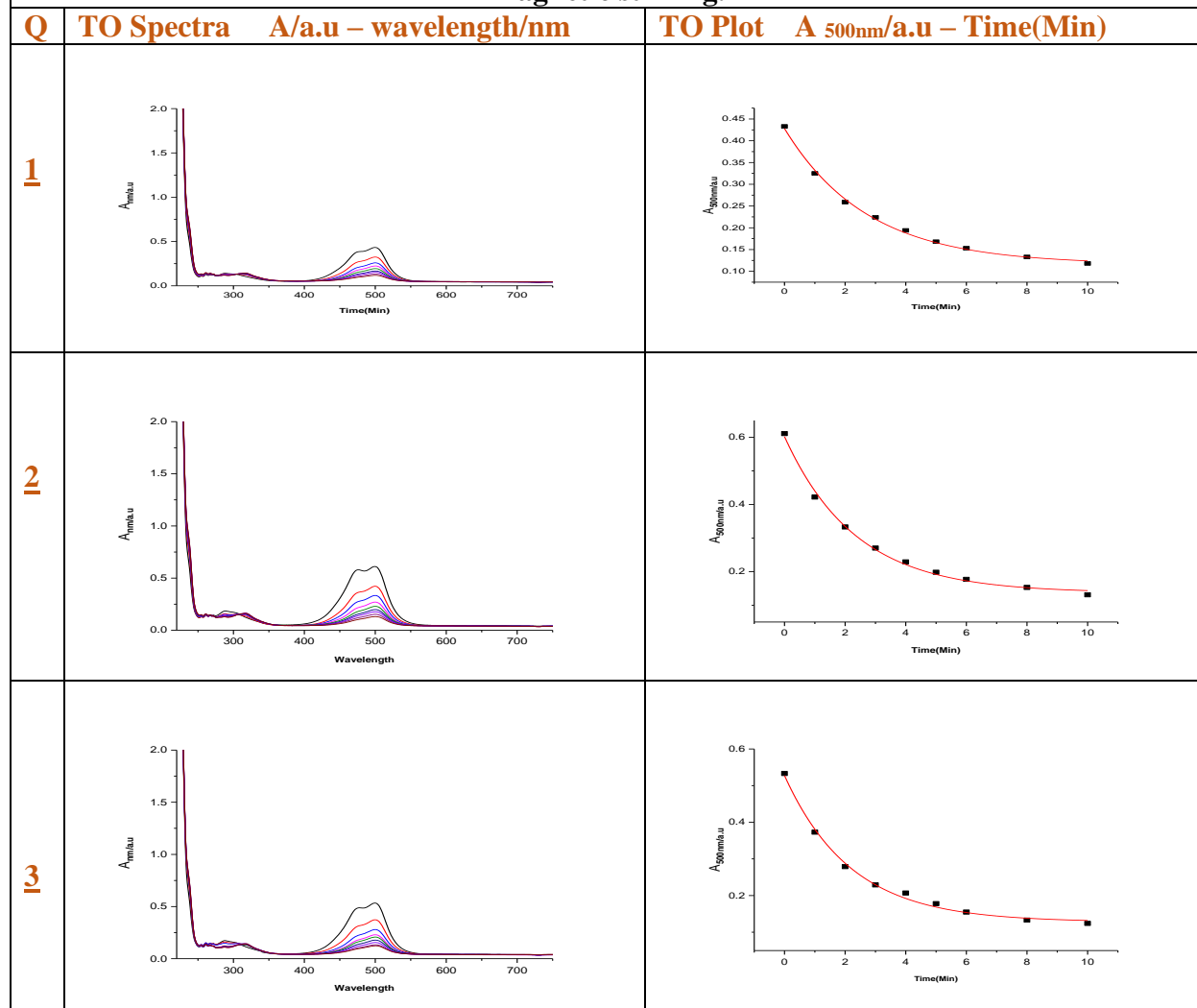


File name: <u>17-4-2019/ 35 °C</u>		
	original rate constants	original errors
1	0.26011 min ⁻¹	0.0085
2	0.3135 min ⁻¹	0.01565
3	0.25723 min ⁻¹	0.00936
	Average k	Average error
	0.276946667	0.01117
	standard deviation	Average error %
	0.025873838 min ⁻¹	0.040332675

Thiazole orange 98% sonicated and filtered in D_2O only at $25\text{ }^\circ\text{C}$ with new LED after setting and magnetic stirring.		
Q	TO Spectra A/a.u – wavelength/nm	TO Plot A _{500nm} /a.u – Time(Min)
1		
2		
3		

File name: <u>10-4-2019/</u> D_2O only		
	original rate constants	original errors
1	0.58726 min⁻¹	0.0388
2	0.50817 min⁻¹	0.02336
3	0.67231 min⁻¹	0.04772
	Average k	Average error
	0.589246667	0.036626667
	standard deviation	Average error %
	0.067024598 min⁻¹	0.062158462

Thiazole orange 98% sonicated and filtered buffer in **D₂O- based reference buffer** (25 mM MOPS, 50 mM NaCl and 1 mM EDTA) at 25 °C with new LED after setting and magnetic stirring.

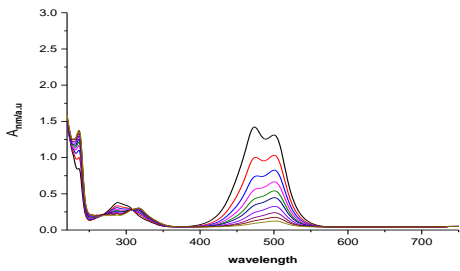
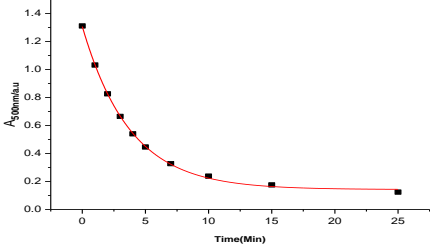
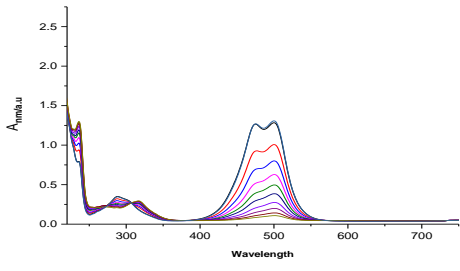
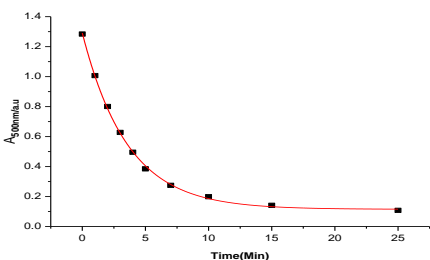
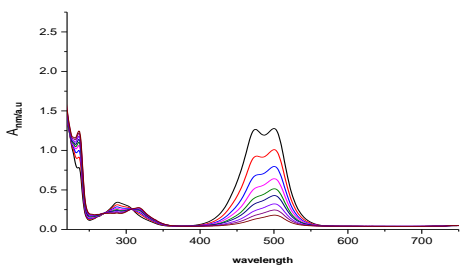
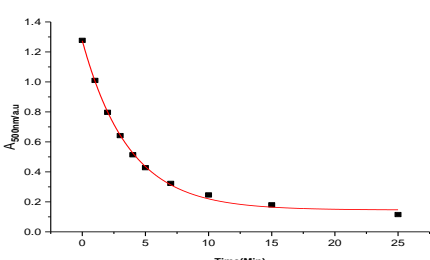


10-4-2019/D₂O- based reference buffer		
	original rate constants	original errors
1	0.36675 min⁻¹	0.02098
2	0.42793 min⁻¹	0.02731
3	0.45654 min⁻¹	0.03005
	Average k	Average error
	0.417073333	0.026113333
	standard deviation	Average error %
	0.037451848 min⁻¹	0.062610892

Thiazole orange 98% sonicated and filtered in deionised water only at 25 °C with new LED after setting and magnetic stirring		
Q	TO Spectra A/a.u – wavelength/nm	TO Plot A _{500nm} /a.u – Time(Min)
1		
2		
3		

11-4-2019/ deionised water		
	original rate constants	original errors
1	0.204364839 min⁻¹	0.005521467
2	0.21124 min⁻¹	0.00237
3	0.27868 min⁻¹	0.0111
	Average k	Average error
	0.23142828	0.006330489
	standard deviation	Average error %
	0.033529696 min⁻¹	0.027354

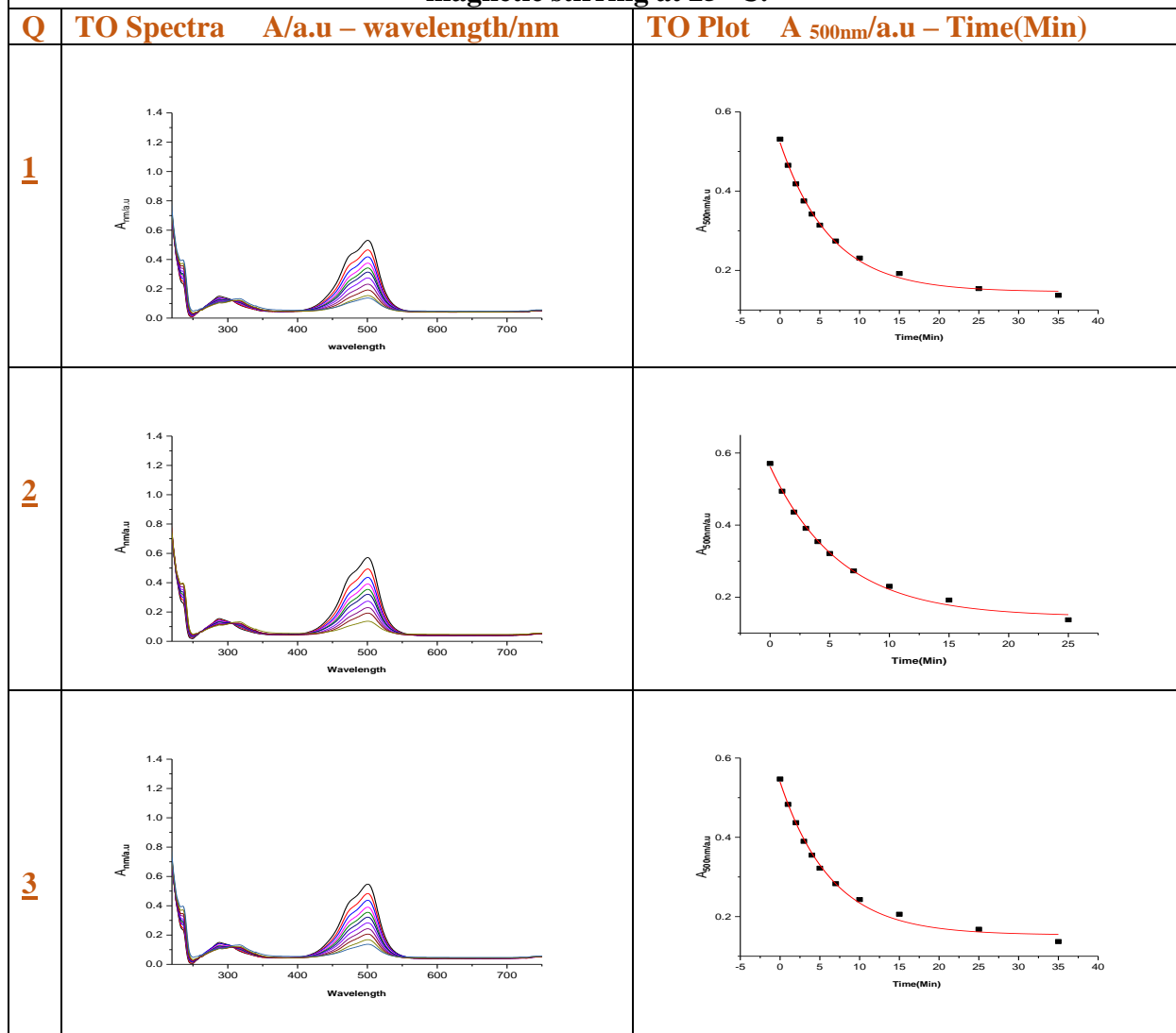
Thiazole orange 98% sonicated and filtered in **reference buffer prepared using tap water** with new LED after setting and magnetic stirring at 25 °C.

Q	TO Spectra A/a.u – wavelength/nm	TO Plot A _{500nm} /a.u – Time(Min)
1		
2		
3		

File name: **29-4-2019/ Tap water**
in reference buffer

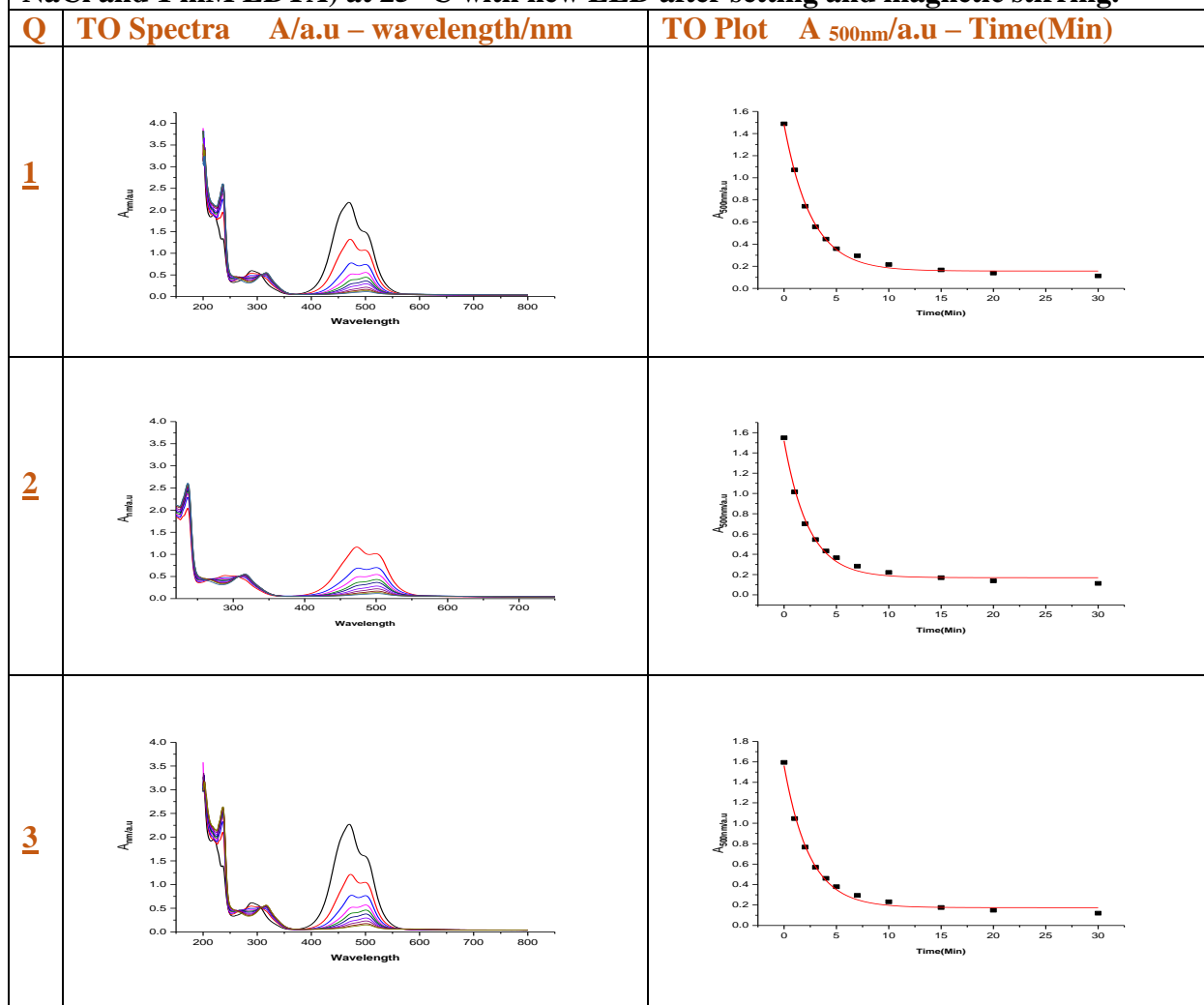
	original rate constants	original errors
1	0.26598 min⁻¹	0.00564
2	0.27984 min⁻¹	0.00665
3	0.27215 min⁻¹	0.00998
	Average k	Average error
	0.272656667	0.007423333
	standard deviation	Average error %
	0.005669652 min⁻¹	0.027225937

Thiazole orange 98% sonicated and filtered in **tap water only**, new LED after setting and magnetic stirring at 25 °C.



File: 29-4-2019/ Tap water only		
	original rate constants	original errors
1	0.15723 min⁻¹	0.00714
2	0.17019 min⁻¹	0.01037
3	0.15629 min⁻¹	0.0098
	Average k	Average error
	0.161236667	0.009103333
	standard deviation	% error margin
	0.006342583 min⁻¹	0.056459449

Thiazole orange 98% sonicated and filtered in buffer pH=7 (25 mM phosphate, 200 mM NaCl and 1 mM EDTA) at 25 °C with new LED after setting and magnetic stirring.

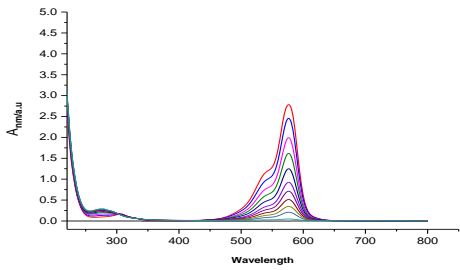
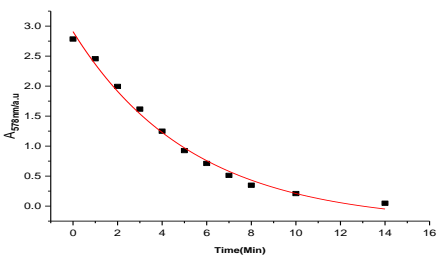
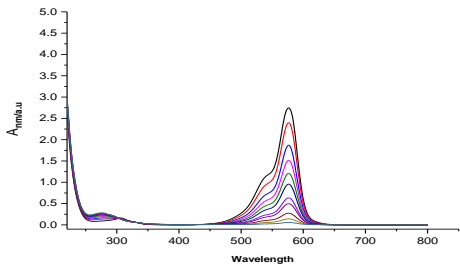
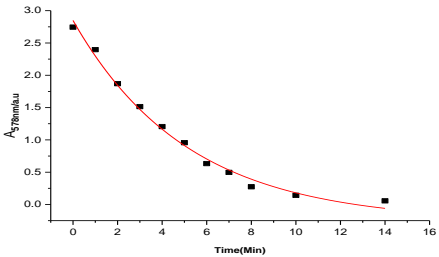
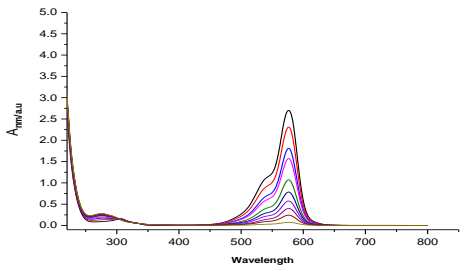
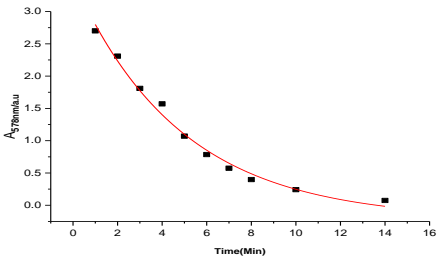


File: **8-5-2019** /phosphate buffer

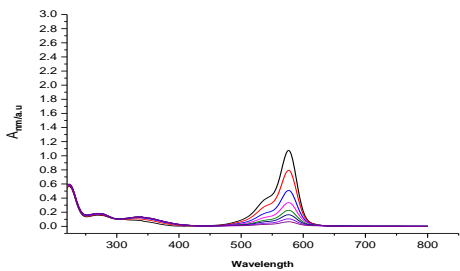
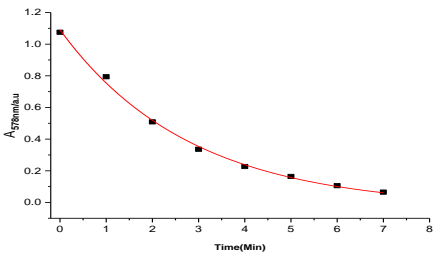
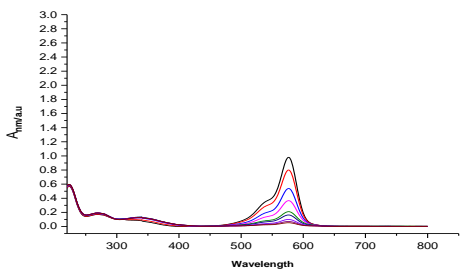
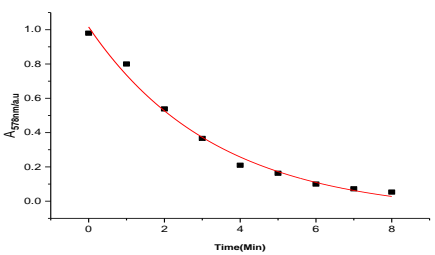
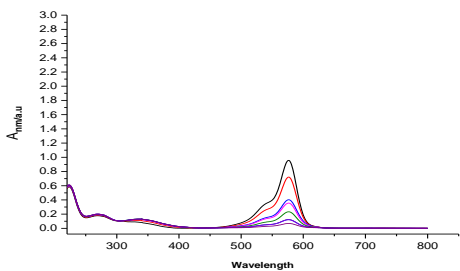
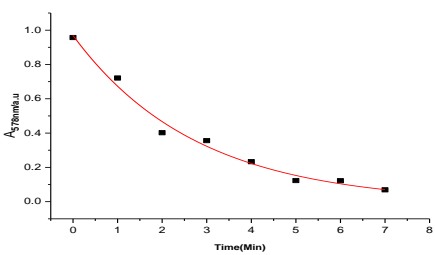
	original rate constants	original errors
1	0.38362 min⁻¹	0.01797
2	0.42836 min⁻¹	0.02698
3	0.41243 min⁻¹	0.02368
	Average k	Average error
	0.408136667	0.022876667
	standard deviation	% error margin
	0.018515605 min⁻¹	0.056051486

File name: <u>20-6-2019</u>		
	original rate constants	original errors
1	0.36337 min⁻¹	0.01416
2	0.32968 min⁻¹	0.00834
3	0.37899 min⁻¹	0.01762
	Average k	Average error
	0.357346667	0.013373333
	standard deviation	% error margin
	0.020576353 min⁻¹	0.037423977
<p>Thiazole orange 98% sonicated and filtered in reference buffer pH=7 with added citrate (25 mM MOPS, 50 mM NaCl, 1 mM EDTA and 20 mM sodium citrate) at 25°C with new LED after setting and magnetic stirring.</p>		

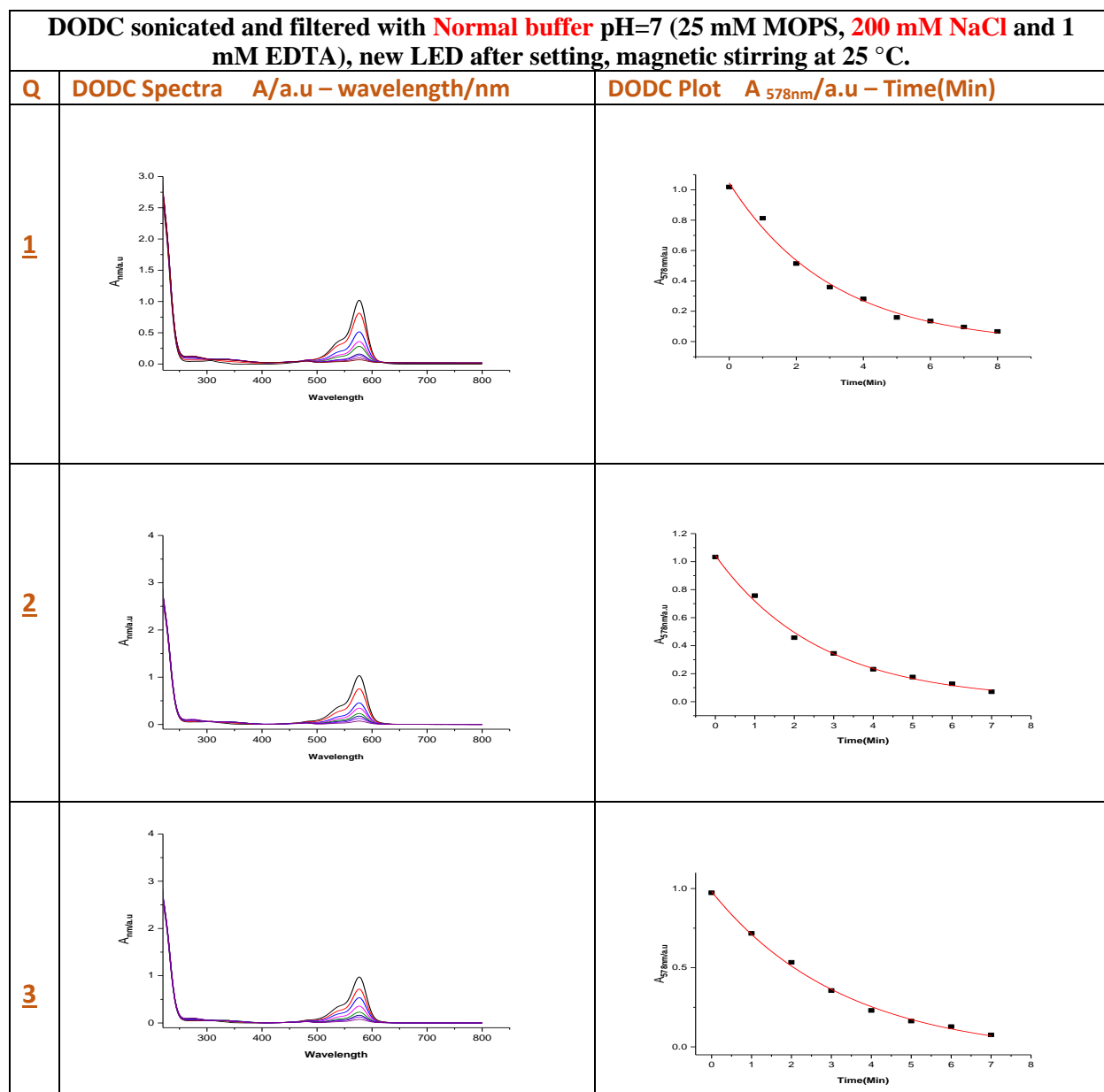
Appendix

DODC sonicated and filtered with Normal buffer pH=10.80 (25 mM MOPS, 50 mM NaCl and 1 mM EDTA), new LED after setting, magnetic bar at 25 °C.		
Q	DODC Spectra A/a.u – wavelength/nm	DODC Plot A _{578nm} /a.u – Time(Min)
1		
2		
3		

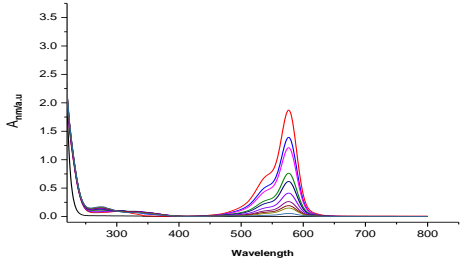
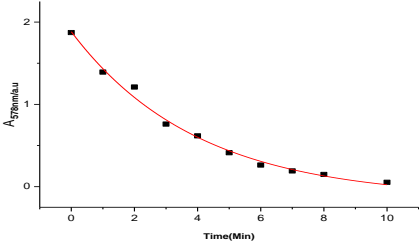
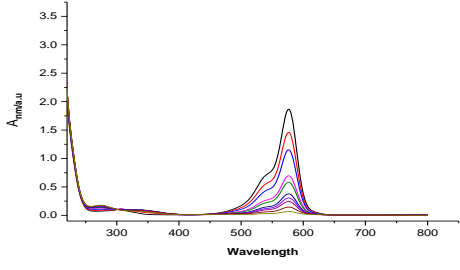
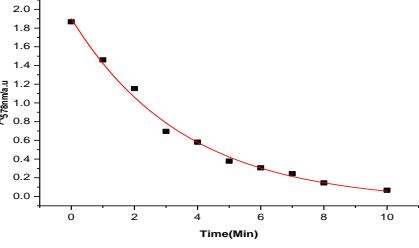
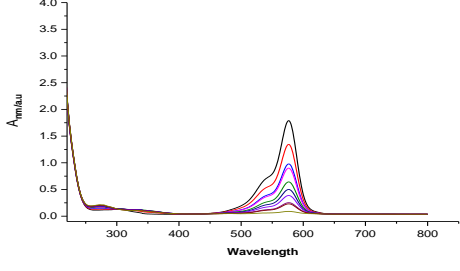
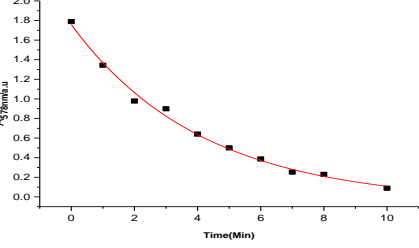
File name: 25-5-2019/ pH=10.80		
	original rate constants	original errors
1	0.20712 min⁻¹	0.02458
2	0.19467 min⁻¹	0.0188
3	0.18722 min⁻¹	0.01828
	Average k	Average error
	0.196336667	0.020553333
	standard deviation	% error margin
	0.008209175 min⁻¹	0.020553333

DODC sonicated and filtered with Normal buffer pH=4.30 (25 mM MOPS, 50 mM NaCl and 1 mM EDTA), new LED after setting, magnetic bar at 25 °C.		
Q	DODC Spectra A/a.u – wavelength/nm	DODC Plot A _{578nm} /a.u – Time(Min)
1		
2		
3		

File name: 25-5-2019 / pH=4.30		
	original rate constants	original errors
1	0.35623 min⁻¹	0.02799
2	0.29828 min⁻¹	0.04192
3	0.36097 min⁻¹	0.06192
	Average k	Average error
	0.338493333	0.043943333
	standard deviation	% error margin
	0.028500889 min⁻¹	0.043943333

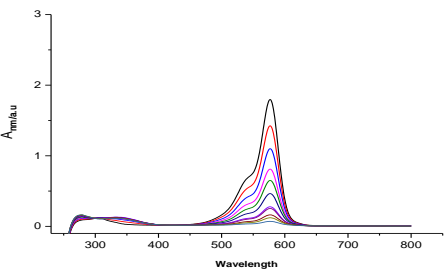
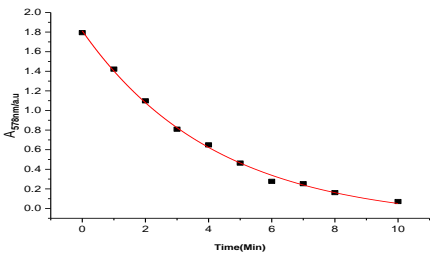
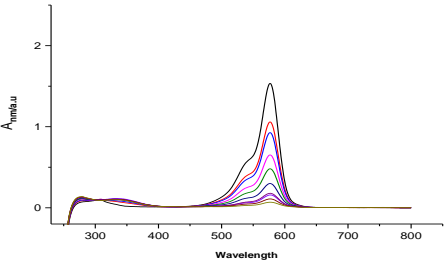
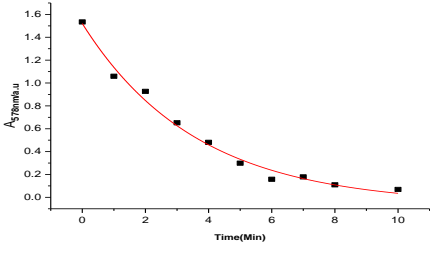
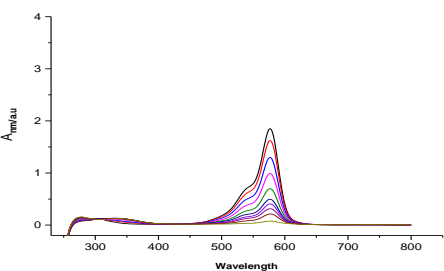
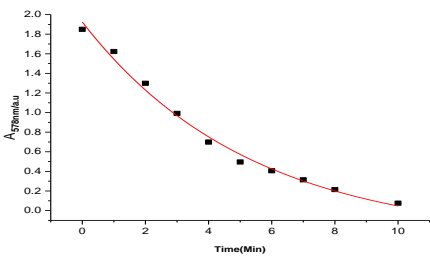


File name: 25-5-2019/200mM NaCl		
	original rate constants	original errors
1	0.32545 min⁻¹	0.03808
2	0.37823 min⁻¹	0.03655
3	0.30258 min⁻¹	0.0245
	Average k	Average error
	0.33542	0.033043333
	standard deviation	% error margin
	0.031678397 min⁻¹	0.033043333

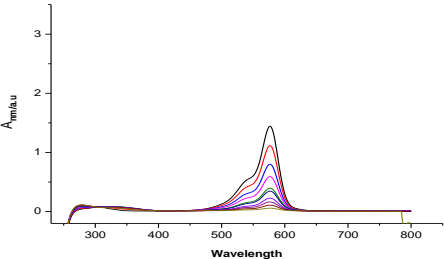
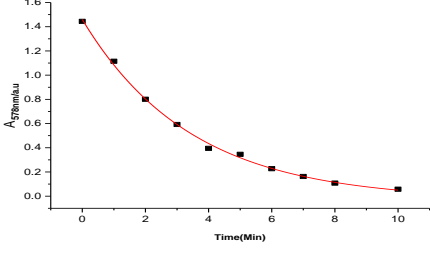
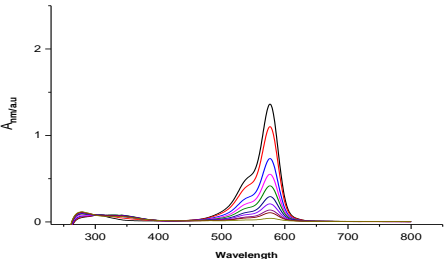
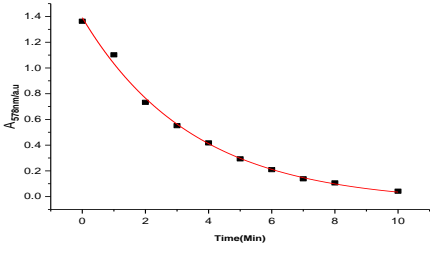
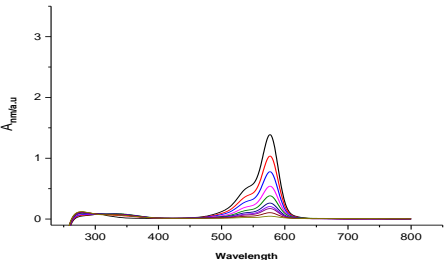
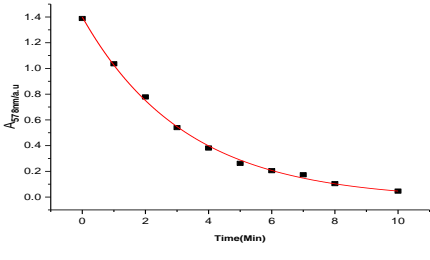
DODC sonicated and filtered with Normal buffer pH=7 (25 mM MOPS, 100 mM NaCl and 1 mM EDTA), new LED after setting, magnetic stirring at 25 °C.		
Q	DODC Spectra A/a.u – wavelength/nm	DODC Plot A _{578nm} /a.u – Time(Min)
1		
2		
3		

File name: 25-5-2019/100mM NaCl		
	original rate constants	original errors
1	0.25101 min⁻¹	0.02795
2	0.27972 min⁻¹	0.02763
3	0.24179 min⁻¹	0.02535
	Average k	Average error
	0.257506667	0.026976667
	standard deviation	% error margin
	0.016151909 min⁻¹	0.026976667

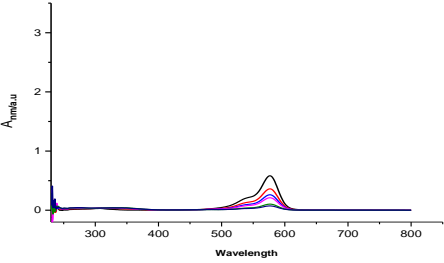
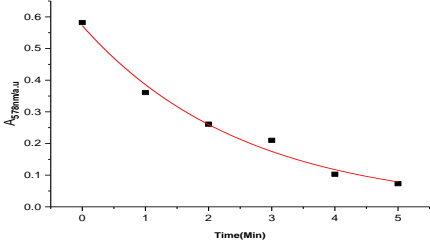
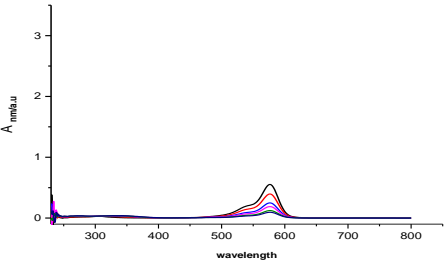
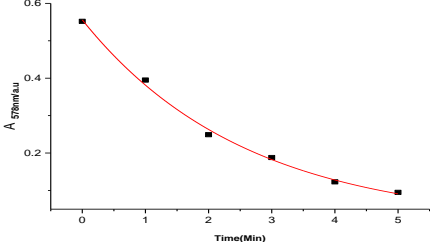
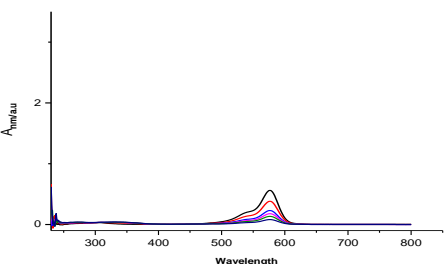
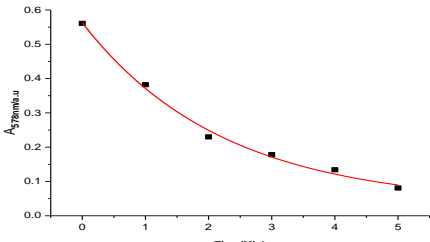
Appendix
Chapter 4

DODC sonicated and filtered with Normal buffer pH=7 (100 mM MOPS, 50 mM NaCl and 1 mM EDTA), new LED after setting, magnetic stirring at 25 °C.		
Q	DODC Spectra A/a.u – wavelength/nm	DODC Plot A _{578nm} /a.u – Time(Min)
1		
2		
3		

File name: 26-5-2019 /100mM MOPS		
	original rate constants	original errors
1	0.23645 min⁻¹	0.01457
2	0.27679 min⁻¹	0.03446
3	0.18844 min⁻¹	0.02683
	Average k	Average error
	0.233893333	0.025286667
	standard deviation	% error margin
	0.036114014 min⁻¹	0.036114014

DODC sonicated and filtered with Normal buffer pH=7 (50 mM MOPS, 50 mM NaCl and 1 mM EDTA) , new LED after setting, magnetic stirring at 25 °C.		
Q	DODC Spectra A/a.u – wavelength/nm	DODC Plot A _{578nm} /a.u – Time(Min)
1		
2		
3		

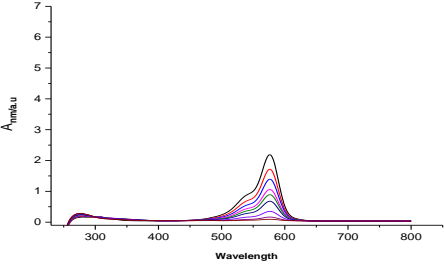
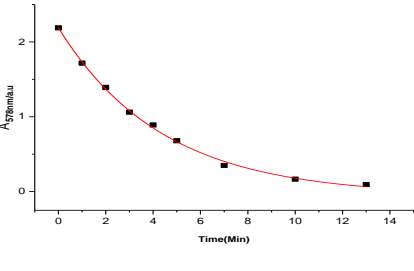
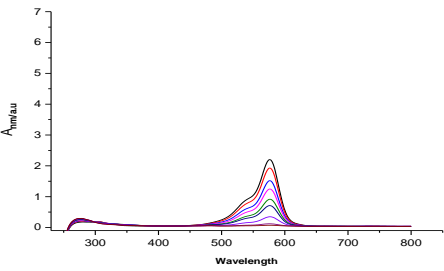
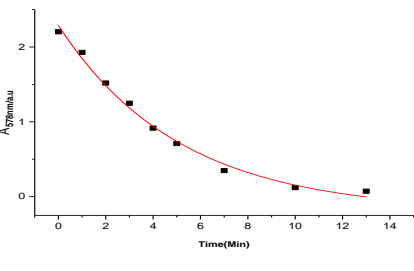
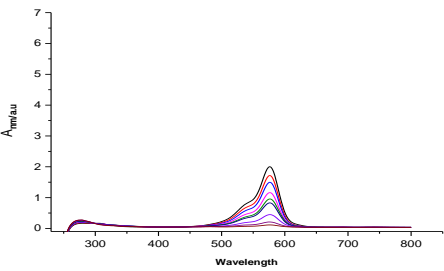
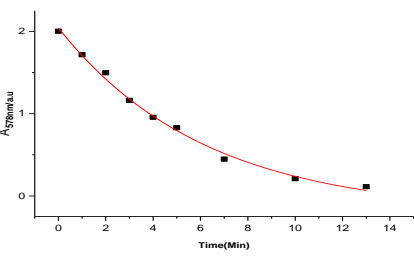
File name: 26-5-2019/50mM MOPS		
	original rate constants	original errors
1	0.2904 min⁻¹	0.01509
2	0.28527 min⁻¹	0.02107
3	0.30545 min⁻¹	0.01362
	Average k	Average error
	0.293706667	0.016593333
	standard deviation	% error margin
	0.008563824 min⁻¹	0.016593333

DODC sonicated and filtered with Normal buffer pH=7 (25 mM MOPS, 50 mM NaCl and 1 mM EDTA+NaN3 10 mM), new LED after setting, magnetic stirring at 25 °C.		
Q	DODC Spectra A/a.u – wavelength/nm	DODC Plot A _{578nm} /a.u – Time(Min)
1		
2		
3		

File name: <u>26-5-2019/ NaN3 10 mM</u>		
	original rate constants	original errors
1	0.39251 min⁻¹	0.10196
2	0.38745 min⁻¹	0.0498
3	0.449176178 min⁻¹	0.065296337
	Average k	Average error
	0.409712059	0.072352112
	standard deviation	% error margin
	0.027981701 min⁻¹	0.072352112

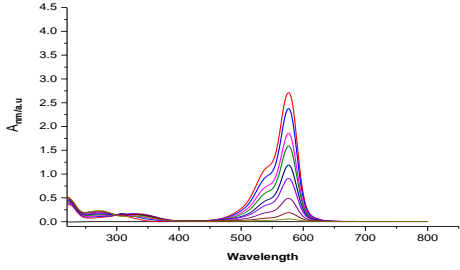
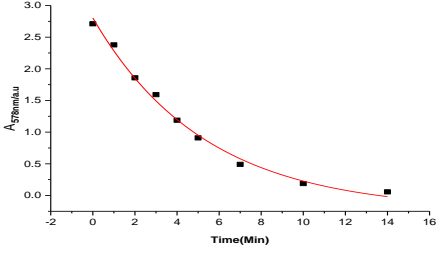
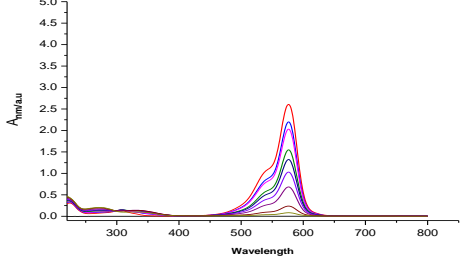
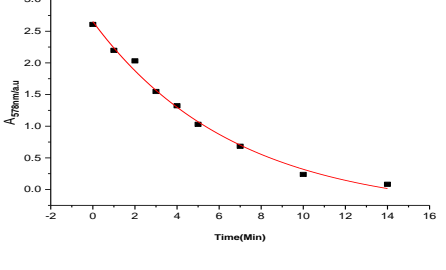
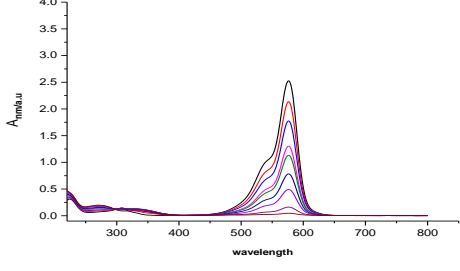
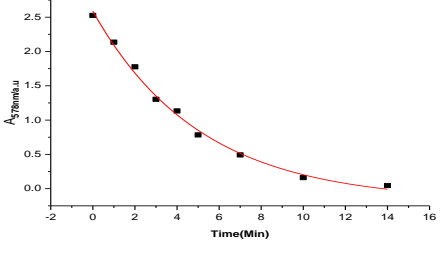
DODC sonicated and filtered with Normal buffer pH=7 (25 mM MOPS, 50 mM NaCl and 1 mM EDTA), new LED after setting, magnetic stirring at 35 °C .		
Q	DODC Spectra A/a.u – wavelength/nm	DODC Plot A _{578nm} /a.u – Time(Min)
1		
2		
3		

File name: 29-5-2019 / at 35 °C .		
	original rate constants	original errors
1	0.19464 min⁻¹	0.01615
2	0.2071 min⁻¹	0.01697
3	0.24036 min⁻¹	0.01786
	Average k	Average error
	0.214033333	0.016993333
	standard deviation	% error margin
	0.019298237 min⁻¹	0.019298237

DODC sonicated and filtered with Normal buffer pH=7 (25 mM MOPS, 50 mM NaCl and 1 mM EDTA), new LED after setting, magnetic stirring at 50 °C .		
Q	DODC Spectra A/a.u – wavelength/nm	DODC Plot A _{578nm} /a.u – Time(Min)
1		
2		
3		

File name: 29-5-2019/ at 50 °C .		
	original rate constants	original errors
1	0.22787 min⁻¹	0.01124
2	0.19522 min⁻¹	0.02205
3	0.16191 min⁻¹	0.017
	Average k	Average error
	0.195	0.016763333
	standard deviation	% error margin
	0.026928507 min⁻¹	0.026928507

DODC sonicated and filtered with **phosphate buffer** pH=7 (25 mM **Na₂Hpo₄**, 50 mM NaCl and 1 mM EDTA), new LED after setting, magnetic stirring at 25 °C.

Q	DODC Spectra A/a.u – wavelength/nm	DODC Plot A _{578nm} /a.u – Time(Min)
1		
2		
3		

File 3-6-2019/ phosphate buffer		
	original rate constants	original errors
1	0.18757 min⁻¹	0.01915
2	0.14918 min⁻¹	0.01863
3	0.19684 min⁻¹	0.0172
	Average k	Average error
	0.177863333	0.018326667
	standard deviation	% error margin
	0.020632231 min⁻¹	0.020632

DODC sonicated and filtered with Normal buffer pH=7 (25 mM MOPS, 50 mM NaCl, 1 mM EDTA and 20mM sodium citrate) at 25 °C wth new LED after setting and magnetic stirring.		
Q	DODC Spectra A/a.u – wavelength/nm	DODC Plot A _{578nm} /a.u – Time(Min)
1		
2		
3		

21-6-2019/ 20mM sodium citrate		
	original rate constants	original errors
1	0.20874 min⁻¹	0.03187
2	0.20315 min⁻¹	0.01769
3	0.19708 min⁻¹	0.03502
	Average k	Average error
	0.20299	0.028193333
	standard deviation	% error margin
	0.004761519 min⁻¹	0.028193333

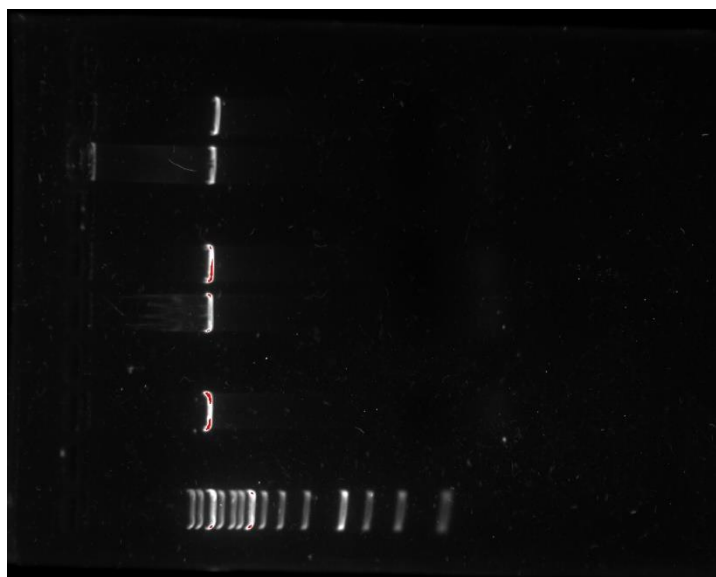
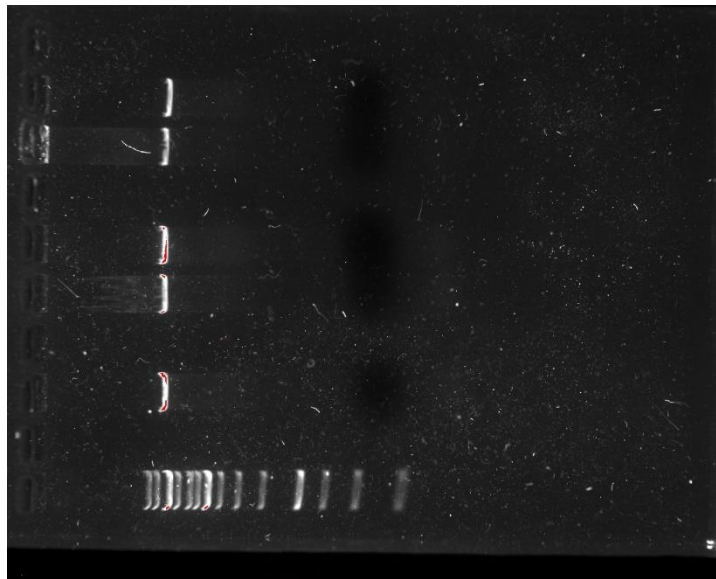
Appendix 5.A.9 - plasmid sequences

agggttccacagggtagccagcagcatcctgcgatgcagatccggaacataatggtgcagggcgctgactccgcgttccagactttacgaaacacggaacc
gaagaccattcatgttctcaggtcgagacgtttgcagcagcagctcctcagctcgcgtatcggtagtcattctcctaaccagtaaggcaaccccgc
cagcctagccggctcctcaacgacaggagcacgatcatgcgaccctggggcccatgcccggcgataatggcctgcttcgcccgaacgttggggcgg
gaccagtacgaaggctgagcaggcgtgcaagattccgaataccgcaagcgacaggccgatcatcgcgctccagcgaagcgctctcggcga
tgaccagagcgtgcccggcacctgcctacgagtgcagataaagaagacagtcataagtggcgacgatagtcacccccgcccaccggaaggagct
gactgggtgaaggctcctcaaggcctcagctgagatccccggctcctaatgagtgagtaacttacattaattgctgctcactgcccgttccagtcgggaa
acctgctgctccagctgcattaatgaatggccaacgcggggagaggcgggttgcgtattgggcccaggggtgtttctttccaccagtgcagggcaaca
gctgattgccctcaccgctggcctgagagagttgcagcaagcgctccacgtggtttccccagcagggcaaaatcctggttgatggtgtaacggcgggat
ataacatgagctgtcttggtatcgtcgtatcccactaccgagatataccgaccaacgcgagccccgactcggtaatggcgccattgcccagcgccatctga
tcgttggcaaccagcatgcagtggaacgatccccctcattcagcattgcatggtttgtaaaaccggacatggcactccagtcgcttcccgttccgctatcggc
tgaattgattgcgagtgagatattatgccagccagccagcagcagcgcggagacagaacttaattggcccgtaacagcgcgatttgcgtgacccaatg
cgaccagatgctccacgcccagtcgctgaccgtctcctcatgggagaaaataactgttgatgggtgctggtcagagacatcaagaataacgccgaacattagt
gcaggcagctccacagcaatggcatcctggtcatccagcggatgtaatgatagccactgacgcttgcgagagaagattgtgaccgccgctttacaggct
tcgacccgcttcttaccatcgaccaccacgctggcaccagttgatcggcgcgagatttaatcgccgcgacaattgacgagcgcgctgagggccaga
ctggaggtggcaacgcaatcagcaacgactgtttgcccgccagtgtgtggccacgcggttgggaatgtaattcagctccgcatcgcgcttccacttttcccgc
gttttcgcagaacgtggctggcctggttaccacgcgggaacggtctgataagacaccggcactactctgcgacatgataacgttactggtttcacattcac
caccctgaattgactcttccggcgctatcatgccataccgcgaaaggtttgcgcccattgatggttccgggatctcgacgctctcctttagcactcctgact
aggaaagcagcccagtagtaggtgagggctgagcaccgcgcgcaaggatggtgatgcaaggagatggcggcaacagtcccccggccacggggcc
tgccaccataccacgcccgaacaagcgtcatgagcccgaagtggcgagccgatctccccatcggtgatgctggcgatagggccagcaaccgcacct
gtggcggcgggtgatgccggccacgatgcgtccggcgtagagatcgagatctgatcccggcaaaataatacgaactactataggggaattgtgagcggataac
aattcccctctagaataaattttgtaactttaagaaggagatatacCATGGGCAGCAGCCATCATCATCATCACACTTACA
AATTAATCCTTAATGGTAAAACATTGAAAGGCGAAACAACACTACTGAAGCTGTTGATGCTGCTACTG
CAGAAAAAGTCTTCAAACAATACGTAACATGACAACCGTGTGACGGTGAATGGACTTACGACTAGT
CGGACTAAGACTTTACAGTTACTGAACTATGAAAACCTGTATTTTTAGTGGCAGACTTTTACG
GCTAGCTCAGCCCTAAGTATTATGCTAGCTACTAGAGAAAGAGGAGAAAAACTAGTATGGTTAGC
AAAGGCGAGGAGctgATTAAGGAGAATATGCACATGAAACTGTACATGGAAGGCACCGTGAACAA
CCACCACTTCAAGTGCACCAGCGAGGGTGAAGGCAAACCGTATGAAGGCACCCAGACCATGCGTA
TCAAAGTGGTTGAGGGTGGCCCGCTGCCGTTTCGCGTTTGATATTCTGGCGACCAGCTTCATGTACG
GTAGCCGTACCTTTATCAACCACACCCAGGGCATTCCGGATTTCTTTAAACAGAGCTTCCCGGAAG
GTTTTACCTGGGAGCGTGTGACCACCTACGAAGACGGTGGCGTTCTGACCGCGACCCAGGACACC
AGCCTGCAAGATGGCTGCCTGATCTATAACGTGAAGATTTCGTGGTGTAACTTTCCGAGCAACGGC
CCGGTGATGCAGAAGAAAACCCTGGGTTGGGAGGCGAACACCGAAATGCTGTATCCGGCGGATGG
TGGCCTGGAGGGCCGTAGCGACATGGCGCTGAAGCTGGTTGGTGGCGGTACCTGATCTGCAACTT
CAAAACCACCTATCGTAGCAAGAAACCGGCGAAGAACCTGAAAATGCCGGTGTGTACTATGTTG
ATCACCGTCTGGAGCGTATTAAGGAAGCGGACAAAGAGACCTACGTTGAGCAACACGAAGTGGCG
GTTGCGCGTTATTGCGATCTGCCGAGCAAGCTGGGTACAAACTGAACTAGCGGTCTCCTGATAAC
tcgagcaccaccaccaccactgagatccggctgtaacaagcccgaaggagctgagttggctgctccaccgctgagcaataactagcataaccctt
ggggcctctaacggctctgagggtttttgctgaaggaggaactataccggattggcgaatgggacgcgcctgtagcggcgcaataagcgcggcgggtg
tgggtggtacgcagcgtgaccgtacacttgcagcgccttagcggcctcttctccttctccttctccttccgacggtcggcgttcccccgcaagct
ctaaatcgggggctcccttagggttccgatttagctttacggcacctcgacccccaaaaactgattaggggtgatggttcacgtagtgggccatcgccctgatag
acgggttttcgccccttagcgtggagtcacgctttaaagtggactctgttccaaactggaacaactcaacctatcctggtctattctttgattataagggaatt
tgccgatttcggcctattggttaaaaaatgagctgatttaacaaaaatlaacgcgaatttaacaaaataftaacgtttacaatttcagggtggcacttttcgggaaatgt
gcgcggaaccctattgttttctaaatacattcaaatatgatccgctcatgaattaattcttagaaaaactcagcagcatcaaatgaaactgcaatttattcatat
caggattatcaatacattttgaaaagccgttctgtaatgaaggagaaaactaccgagggcagttccatagatggcaagatcctggtatcggctcgcgattcc
gactgtccaacatcaataacctaatttcccctgtaaaaaataaggttatcaagtgagaataccatgagtgacgactgaatccggtgagaaatggcaaaaag
ttatgcatcttctccagactgttcaacagccagccattacgctcgtcatcaaaatcactcgcataccaaaccgttattcattcgtgattgcgctgagcagagc
aaatacgcgatcgtttaaaggacaattacaacaggaatcgaatgcaaccggcgcaggaactccagcgcatacaaatfttccactgaaatcagatata
tctctaataactggaaatgctgttttccgggagtcgagtggtgagtaacctatcatcagagtagcgataaaaatgctgattggtcggaaaggcataaatcc
gtcagccagtttagtctgacctcactctgaacatcattgcaacgctacctttcagatgttttcagaacaactctggcgatcgggcttccatcaatcagatatt
gtcgcacctgattcccacattatcgcgagcccttataccatataatcagcatccattggaatttaacgcggcctagagcaagcgttcccgttgaaatg
gtcataacacccttcttactgtttatgtaagcagacagtttattgttcatgacaaaatccctaacgtgattttcgttccactgagcgtcagaccctgtagaaaa
gatcaaaagatcttctgagatcctttttctgcgctaatctctgctctgcaaaacaaaaaacaccgctaccagcgggtgttgggttccgggatcaagagctacca
ctcttttccgaaggtaactgcttcagcagagcgcagatacacaatactgctctctagtgtagccgtgattaggccaccactcaagaactctgtagaccgcctac
atacctcgtctgtaactctgttaccagtggctgctccagtgccgataagtcgtgtcttaccgggttgactcaagacgatagttaccggataagcgcagcggg
cgggctgaaacggggggtctgacacagcccagctggagcgaacgacctaccgaactgagatacctacagcgtgagctatgagaagcggccacgcttc

**Appendix
Chapter 5**

cgaaggagaaaaggcggacaggtatccggtaagcggcagggcgggaacaggagagcgcacgaggagctccaggggaaacgcctggtatctttatagtc
ctgtcgggttcgccacctctgacttgagcgtcgtatgttgatgctcgtcagggggggcggagcctatggaaaaacgccagcaacggccttttacggctctgg
ccttttgctggccttttgctcatatgttcttctgcgttatcccctgattctgtggataaccgtattaccgctttgagtgagctgataccgctcggcagccgaacgac
cgagcgcagcgagtcagtgagcgaagcgggaagagcgcctgatcgggtatgttctccttacgcatctgtgcgggtatttcacaccgcatatattggtgactctca
gtacaatctgctctgatccgcatagtaagccagtafacactccgctatcgtctacgtgactgggtcatggctgcgccccgacaccgccaacaccgctgacgg
ccctgacgggctgtctgctcccggcatccgcttacagacaagctgtgaccgtctccgggagctgcatgtgtcagaggtttaccgtcataccgaaacgcgcga
ggcagctcgggtaaagctcatcagcgtggtcgtgaagcattcacagatgtctgctgttcacccgctccagctcgtgagtttctccagaagcgttaagtctggc
ttctgataaacggggccatgtaaggcgggtttttcctgtttggtcactgatccctccgtgaagggggatttctgttcattgggggtaatgataccgatgaacgaga
gaggatgctcagatacgggttactgatgatgaacatgcccggtactggaacgtgtgagggtaaacaactggcgggtatggatgcggcgggaccagagaaaaa
tcactcagggtcaatgccagcgtctcgttaatacagatgt

Pictures took from the gel electrophoresis related Camera.



Appendix
Chapter 5

